UNIVERSITY OF TERAMO

FACULTY OF BIOSCIENCE AND TECHNOLOGY FOR FOOD, AGRICULTURE AND ENVIRONMENT

PhD in Food Science

XXXII CYCLE

Novel nanomaterials for lab on chip devices development: application to food system and their effect on the oxidative stress in cell cultures

CHIM01-CHIMICA ANALITICA

PhD Candidate

José Daniel Rojas Tizón

Tutor

Michele Del Carlo

PhD Coordinator

Dario Compagnone

Tutor

Jesús Alberto Escarpa Miguel

RepEat project Coordinator

Barbara Barboni

Novel nanomaterials for lab on chip devices development: application to food system and their effect on the oxidative stress in cell cultures

A dissertation presented by

José Daniel Rojas Tizón

ESR n. 2

In partial fulfillment of the requirements for the degree of Doctor of Philosophy in the subject of Food Technology from University of Teramo and Chemistry from the University of Acalá

October 2020

I declare that myself have composed the thesis and that the work has not be submitted for any other degree or professional qualification. I confirm that the work submitted is my own, except where work which has formed part of jointly authored publications has been included.

The work presented in Chapter III has been published in the journal Microchimica Acta as *Nanohybrid carbon black-molybdenum disulfide transducers for preconcentration-free voltammetric detection of the olive oil o-diphenols hydroxytyrosol and oleuropein* by **Daniel Rojas**, Flavio Della Pelle, Michele Del Carlo, Emiliano Fratini, Alberto Escarpa and Dario Compagnone. Article can be found at 10.1007/s00604-019-3418-5.

The work presented in Chapter IV has been published in the journal Sensors and actuators B: Chemical as *High-performance carbon black/molybdenum disulfide nanohybrid sensor for cocoa catechins determination using an extraction-free approach* by Flavio Della Pelle, **Daniel Rojas**, Annalisa Scroccarello, Michele Del Carlo, Giovanni Ferraro, Carla Di Mattia, Maria Martuscelli, Alberto Escarpa and Dario Compagnone. Article can be found at 10.1007/s00604-019-3418-5.

The work presented in Chapter V has been published in the journal Microchimica Acta as *Class-selective voltammetric determination of hydroxycinnamic acids structural analogs by using a WS_2/catechin-capped AuNPs/carbon black-based nanocomposite sensor* by Flavio Della Pelle, **Daniel Rojas**, Filippo Silveri, Giovanni Ferraro, Emiliano Fratini, Annalisa Scroccarello, Alberto Escarpa and Dario Compagnone. Article can be found at 10.1007/s00604-020-04281-z.

The work presented in Chapter VI has been published in the journal Electrochemistry Communications as *Group VI transition metal dichalcogenides as antifouling transducers for electrochemical oxidation of catechol-containing structures* by **Daniel Rojas**, Flavio Della Pelle, Michele Del Carlo, Dario Compagnone and Alberto Escarpa. Article can be found at 10.1016/j.elecom.2020.106718.

The work presented in Chapter VII has been published in the journal Sensors and actuators B: Chemical as *Electrodeposited Prussian Blue on carbon black modified*

disposable electrodes for direct enzyme-free H_2O_2 sensing in a Parkinson's disease in vitro model by **Daniel Rojas**, Flavio Della Pelle, Michele Del Carlo, Michele d'Angelo, Reyes Dominguez-Benot, Annamaria Cimini, Dario Compagnone and Alberto Escarpa. Article can be found at 10.1016/j.snb.2018.08.040.

The work presented in Chapter VIII has been accepted for publication in the journal Biosensors and Bioelectronics as *Oxidative Stress on-chip: Prussian blue-based electrode array for in situ detection of H_2O_2 from cell populations* by **Daniel Rojas**, Juan Francisco Hernández Flavio Della Pelle, Michele Del Carlo, Dario Compagnone and Alberto Escarpa. Article in press.

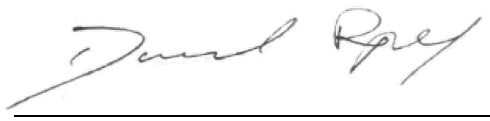

Sig. José Daniel Rojas Tizón

Acknowledgements

Acknowledgements

It is hard to realize how important acknowledgments are in a doctoral thesis until you write it. At that point, you can look back and realize how much you have changed and grown personally and professionally. But especially, you realize that it could not be possible without the people who have helped and supported you during that period. So, it is time to apply the Spanish idiom *es de bien nacidos ser agradecidos*.

Firstly, I would like to acknowledge all the institutions enrolled in the RepEat project, MSCA (Marie Skłodowska-Curie actions) supported by the EC H2020 programme, Region of Abruzzo and the University of Teramo (UNITE) for given me the opportunity to fund this PhD program. Secondly, to the University of Alcalá (UAH) to embrace me during my secondment period and allow me to enroll in a joint PhD program between UNITE and UAH.

Thanks to Prof. Del Carlo, for trusting me and giving me the opportunity to carry out this project. But also, to Prof. Compagnone for advising, supporting me in all my research, and more importantly for listening and considering each and all my ideas.

I also want to make a special mention to Alberto Escarpa. Thank you very much for transmitting to me that tireless passion for science that you already knew how to transmit to us in your classes. Thank you very much for having believed in me from the beginning and for taking out the scientist that we all have inside. But above all, thank you very much for teaching me so much and taught me the rigor and know-how that is needed in science.

Quiero hacer también una mención especial a Alberto Escarpa. Muchas gracias por transmitirme esa incansable pasión por la ciencia que ya sabías transmitirnos en tus clases. Muchas gracias por haber creído en mí desde el inicio y haberme sacado el científico que todos llevamos dentro. Pero, sobre todo, muchas gracias por haberme enseñado tanto y transmitirme el rigor y saber hacer que se necesita en ciencia.

To all my colleagues from the Teramo research group for embracing me from the first day as if I belong to the group from always. For all the dinners we have enjoyed and for taught me the Italian culture in the best way, living it! Thanks to Flavio for supporting and helping me in this period in my research. Thanks also to Annalisa, Sara Gaggiotti, Sara Palmieri, Filippo, Federico, Alessia and Prof. Manuel Sergi for all the good moments inside and outside the lab. *Grazie mille a tutti!*

But also, I would like to acknowledge all the people who accompanied me during the secondment in Alcalá.

También me gustaría agradecer a toda la gente que me ha acompañado durante mi etapa en Alcalá. Por todas esas horas que hemos pasado juntos en el lab y fuera han dado para tantas historias y cotilleos que nos han alegrado el tiempo. Gracias Laura, por ayudarme en mis primeros pasos en la investigación. A Tania y a Rocío, por tantos años y etapas juntos. A Roberto, Águeda y Marimore por todos esos buenos ratos. También con los que compartí menos tiempo con ellos, pero me acogieron con los brazos abiertos en el laboratorio y fuera de él Víctor, Silvia, Marta y Kaisong muchas gracias. A Juanfran por todo lo que me has enseñado, pero, sobre todo, muchas gracias por haberme ayudado tanto en este último período. Espero haberos dado algo de vuelta por lo que me habéis aportado en todo este tiempo. Agradecer también a Beatriz, Juan Víctor y Agustín por vuestro apoyo.

To all the RepEat people, but especially to the Mediterranean family. Thanks to Vivi for being the best neighbor and for all the energy and happiness. Bu also to all our little family in Teramo, Juliana, Rodri, Natalia, Sandra, and Marina. To the italian guys, Giancarlo, Matteo and Angelo, thanks a lot to teach the Italian and Abruzzo culture!

Por último, pero no menos importante, a mi familia, aunque a veces les fuese difícil entender todo lo que contaba sobre la tesis siempre han estado ahí. Gracias a mis padres por haberme demostrado, predicando con el ejemplo, la importancia del trabajo, esfuerzo y la constancia. A mi hermano, primos, tíos y abuelos por todo vuestro apoyo y por haber creído en mí en todo este proceso. Quiero mencionar especialmente a mis tíos Juan Andrés y Ester, por haberme ayudando tanto en mi formación y apoyarme en el camino que ha hecho que hoy pueda escribir estos

agradecimientos. Vosotros también habéis puesto vuestro granito de arena en esta tesis. Por último, no puede faltar agradecer especialmente a esa persona que ha vivido esta tesis tan intensamente como yo, Sofía, gracias por estar siempre ahí, y nunca dejar de apoyarme y creer en mí.

Summary

Summary

Over the last decade nanotechnology have been substantially developed allowing the discovery of new downsized scale-based materials with different properties compared to their bulk counterparts. The evolution in the synthesis, preparation and application of new nano and microscale nanomaterials has opened new opportunities for the creation of new analytical devices with improved properties.

Carbon nanomaterials are widely used in electrochemistry due to their chemical inertness, relatively wide potential window, low background current, and suitability for different types of electroanalysis. Among carbon nanomaterials, carbon black has been recognized as an electrode material with comparable heterogeneous electron-transfer rate (HET) to other more *noble* carbon nanomaterials such as graphene or carbon nanotubes (CNTs), with the advantage of a much simpler manufacturing and lower costs.

Transition metal dichalcogenides (TMDs) are a family of compounds with MX_2 formula, where M is a transition metal element, typically from groups IV (Ti, Zr, Hf), V (V, Nb or Ta) and VI (Mo and W), and X is a chalcogen (S, Se or Te). These materials possess a layered structure. The atoms in of the MX_2 formula are strongly held together by covalent bonds, whereas each triatomic layer is only linked to its neighbors by weak Van der Waals interactions, forming layered materials. These properties allow a top-down approach for producing nanosheets of these compounds by using intercalation chemistry or by liquid phase exfoliation allowing individual sheets to be separated from each other forming 2D materials very easily. These features had led to an exponential growth in the research interest in the last five years. However, even though there is growing interest in these materials just few applications for sensing purposes has been developed. TMDs-based nanocomposites and hybrid nanoarchitectures are the most widespread. These strategies avoid restacking and expand the narrow potential window and low conductivity of TMDs, improving the general electrochemical performance. While TMDs have been widely explored as supercapacitors and catalyst for the hydrogen evolution reaction (HER), very little research has been carried out regarding their capabilities as sensing element, especially in the food analysis.

Summary

Detection of hydrogen peroxide is still of the paramount significance and it is conventionally carried out using platinum-based electrochemical sensors. Poor selectivity of the latter towards hydrogen peroxide reduction (due to reduction of oxygen at same potentials) requires detection by its oxidation at high anodic potential causing oxidation of easily oxidizable compounds worsen the selectivity. Another problem of platinum-based electrocatalysts is poisoning of their surface limiting, for example, analysis of sweat. Prussian blue-based electrodes solve these drawbacks. Prussian blue is selective to H_2O_2 reduction allowing its detection at low potential in the presence of oxygen. This almost completely avoids the problem of reductants. Prussian blue is insensitive to compounds poisoning platinum thus, for example, allowing analysis in cell culture media. For all these reasons, PB stands out as the best choice for measuring H_2O_2 in cell culture as marker of oxidative stress.

On the other hand, microfluidic systems and lab-on-a-chip (LOC) technologies offer excellent features to improve the analytical performance by reducing analysis time, decreasing extremely the consumption of sample and reagents, integrating multiplexed analysis, and provide the possibility of development of analysis integrated in cell culture. Electrochemical detection provides high sensitivity, allows miniaturization, and it is highly compatible with micro and nanotechnologies due to the simplicity of the instrumentation required. Nevertheless, the surface characteristics of nanomaterials can further improve the sensitivity as well as other important characteristics such as antifouling properties. Up to now the fabrication of these devices relied on clean-room-based fabrication method, which are not available for most laboratories. While clean room manufacturing may still provide powerful research-scale solutions, many clinical and biological applications have obviated some of the need for the ultrafine resolution of photolithographic techniques and hence are very suitable for being fabricated employing alternative manufacturing methods. Low-cost fabrication techniques (3D printing, laser cutting or xurography) and electrochemical detection create a powerful combination for the fabrication of ultra-low-cost disposable devices to perform (bio)-chemical assays.

Therefore, this exciting hybrid area of research is expected to make important contributions to diverse fields, leading to new capabilities that are currently beyond our reach and bringing major benefits to our quality of life.

In this doctoral thesis, different nano- and micromaterials such as carbon black (CB), transition metal dichalcogenides (TMDs) and Prussian Blue (PB), have been employed in the development of new (LOC-based) miniaturized strategies by exploiting their unique and improved electrochemical properties in two well-defined sensing topics:

1. Improved detection and determination of antioxidants in food samples.
2. Reliable detection of hydrogen peroxide as marker of oxidative stress (OS) in living cells.

To this end, this Doctoral Thesis has three defined objectives:

1. To synthetize and characterize novel TMDs-based nanomaterials.
2. To develop hybrid novel CB/TMDs-based electrochemical sensors for antioxidant determination in food samples.
3. To study oxidative stress in living cells and functional food protection on cell culture employing a PB-based electrochemical chip.

To achieve these objectives, the main milestones have been set as follow:

1. Study the exfoliation of group VI TMDs (MoS_2, WS_2, $MoSe_2$ and WSe_2) using different organic solvents and mix of water-surfactants.

2. Characterization of the exfoliated nanomaterials by scanning electron microscopy (SEM), UV-Vis spectroscopy and Raman spectroscopy.

3. Design, characterization, and evaluation of TMDs-based electrochemical transducers.

4. Evaluation of CB/TMDs hybrid transducers for PPs electrochemical determination in complex food environments.

5. Design, characterization, and development of PB-based electrochemical sensors able to detect H_2O_2 released from living cells as oxidative stress (OS) marker.

6. Design, characterization, and development of a PB-based electrochemical chip for real-time detection of H_2O_2 released from living cells as oxidative stress (OS) marker.

After a discussed background about the topics covered along this doctoral thesis in Chapter II, the results of this Doctoral Thesis have been divided in chapters III to IX. Finally, general conclusions and concluding remarks regarding this doctoral thesis are collected in chapter IX.

Chapter III deals with the synthesis, characterization, and applications of MoS_2, as representative TMDs, that in combination with CB have been investigated. While MoS_2 exhibited remarkable antifouling properties towards olive oil PPs but low sensitivity, CB present a high sensitivity with a poor fouling resistance. Interestingly, CB-MoS_2 nanohybrids combines the best properties of each individual nanomaterial with a higher sensitivity than CB and retained antifouling properties of MoS_2. The developed electroanalytical platform has been employed in the analysis of o-diphenolic content in olive oil and related products showing an impressive correlation without significant statically differences with a well-establish HPLC-UV method.

In Chapter IV, the developed CB-MoS_2 electrochemical sensor is applied to catechins determination in cocoa-samples. Again, the ability to merge CB ability to enhance the electrochemical response and the MoS_2 antifouling property was found. In fact, catechins can attach to carbon and CB modified electrodes by forming an electroactive product, which is totally hindered in the case of MoS_2 and CB-MoS_2 electrodes. Moreover, a fast extraction procedure to achieve fast and eco-friendly PPs evaluation is studied. The developed method results highly correlated with well-established methods for PPs content and antioxidant activity.

Chapter V is related to the development of a new electroanalytical platform based on other Group VI TMD, WS_2 and its combination with catechin-capped gold nanoparticles (WS_2/AuNP-CT) into a CB network. The nanomaterial-based synergistic effect of the sensor results in enhanced selectivity, sensitivity, and reproducibility in the simultaneous determination of three-hydroxycinnamic acid (hCN), caffeic, sinapic, and *p*-coumaric acids and their structural analogs in food samples. The assembly of WS_2/AuNP-CT into CB network exhibited a further conductivity enhancement without loss of antifouling performance. The nanomaterial-based synergistic effect of the sensor results in enhanced selectivity and sensitivity.

Chapter VI presents a comprehensive study comparing the electrochemical performance of Group VI TMDs (MoS_2, WS_2, $MoSe_2$ and WSe_2). Their electrochemical properties have been studied revealing a superior performance of the selenides versus the sulfides. This trend is also observed for catechol-containing flavonoids but also an enhanced antifouling propertied is observed for TMDs compared to carbon electrodes. More importantly, in this chapter an explanation to the mechanism involved in their antifouling properties is highlighted, giving a deeper response to findings found and discussed in the previous chapters.

In Chapter VII the combination of Carbon Black (CB) and electrodeposited Prussian Blue (PB) covered with a Nafion layer on Screen-Printed electrodes (CB/PB-SPE) was used for non-enzymatic H_2O_2 sensing in Neuroblastoma cell line (SH-SY5Y) challenged with 6-hidroxidopamine (6-OHDA) for modelling Parkinson's disease. CB was demonstrated to play a key role in the electrodeposition and further electrochemical performance of the developed device. The sensor showed detection limit in the nanomolar range and excellent selectivity in a complex environment such as the culture medium used, allowing the selective determination of very low amounts of H_2O_2 without interferences. In addition, in this work H_2O_2 was quantified not just detected upon the instantaneous release from cells challenged to a stressor as usually reported in literature.

In Chapter VIII an innovative electrochemical multiwell chip is designed to monitor the real-time release of H_2O_2 by HeLa cells. The chips are composed by a set 8 of electrochemical sensors and produced employing a benchtop microfabrication technology allowing their ultra-low-cost production. Electrodes were characterized, in terms of inherent electroactivity and stability. Electrochemical sensing of H_2O_2 was carried out at -100 mV vs Ag|AgCl, with a LOD of 0.1 μM and linear range between 1 and 1000 μM. These features allow the interference-free real-time detection of H_2O_2 in HeLa cell culture, which are directly cultured in the electrochemical chips enabling high-throughput analysis. As proof of the developed chips, cocoa extracts were employed to test their ability to decrease the H_2O_2 production from HeLa cells demonstrating a dose-dependent decrease.

The main and transversal conclusion of this Doctoral Thesis is the demonstration of the potential of miniaturized nanomaterial-based electrochemistry in two sensing relevant applications: the potential of TMD in the analysis of relevant PPs in food samples together with the ability of PB-based sensors to detect and quantify oxidative stress in different cell lines. Hence, the main conclusions derived from this Doctoral Thesis are:

1. The incorporation of TMD to other nanomaterials in electrochemical sensor technology has been demonstrated to be highly relevant, resulting in a synergistic approach that combines the unique physical and chemical properties of TMD with the intrinsic benefits of carbon nanomaterials. Even though the relatively low intrinsic conductivity and narrow electrochemical window of TMD, their hybridization with other nanomaterials has allowed improving their inherent properties. Two enhanced properties have been identified:

    - Apparent electrocatalysis towards catechol containing PPs.
    - Impressive antifouling properties during the oxidation of the catechol containing PPs compounds. These findings have also been demonstrated for the other compounds of the group VI TMDs; $MoSe_2$ and WSe_2. The mechanism underlying their antifouling properties has also been proposed for the first time.

2. PB-based sensors have demonstrated its potential in the evaluation of oxidative stress in cell lines. The incorporation of PB-based sensors in LoC devices have permitted the culturing of cells and direct *in-situ* evaluation of their oxidative stress status and the effect of food functional PPs on it.

- PB-based electrochemical sensors have enabled a reliable detection of oxidative stress (OS) in living cells towards hydrogen peroxide monitorization in two different cell cultures SH-SY5Y and HeLa.
- The sensors have been PB-based electrochemical sensors integrated in a LoC device have enabled the detection of the produced H_2O_2 in the culturing of HeLa cells. The device was able to effectively detect a decrease in the H_2O_2 production response of HeLa cells treated with cocoa extracts in a dose-dependent-way

.

Table of Contents

Table of Contents

I. Hypothesis, objectives, and milestones

Over the last decade nanotechnology have been substantially developed allowing the discovery of new downsized scale-based materials with different properties compared to their bulk counterparts. The evolution in the synthesis, preparation and application of new nano and microscale nanomaterials has opened new opportunities for the creation of new analytical devices with improved properties.

Carbon nanomaterials are widely used in electrochemistry due to their chemical inertness, relatively wide potential window, low background current, and suitability for different types of electroanalysis. Among carbon nanomaterials, carbon black has been recognized as an electrode material with comparable heterogeneous electron-transfer rate (HET) to other more *noble* carbon nanomaterials such as graphene or carbon nanotubes (CNTs), with the advantage of a much simpler manufacturing and lower costs.

Transition metal dichalcogenides (TMDs) are a family of compounds with MX_2 formula, where M is a transition metal element, typically from groups IV (Ti, Zr, Hf), V (V, Nb or Ta) and VI (Mo and W), and X is a chalcogen (S, Se or Te). The atoms in of the MX_2 formula are strongly held together by covalent bonds, whereas each triatomic layer is only linked to its neighbors by weak Van der Waals interactions, forming layered materials. These properties allow a top-down approach for producing nanosheets of these compounds by using intercalation chemistry or by liquid phase exfoliation allowing individual sheets to be separated from each other forming 2D materials very easily. These features had led to an exponential growth in the research interest in the last five years. However, even though there is growing interest in these materials just few applications for sensing purposes has been developed. TMDs-based nanocomposites and hybrid nanoarchitectures are the most widespread. These strategies avoid restacking and expand the narrow potential window and low conductivity of TMDs, improving the general electrochemical performance. While TMDs have been widely explored as supercapacitors and catalyst for the hydrogen evolution reaction (HER), very little research has been carried out regarding their capabilities as sensing element, especially in the food analysis.

Detection of hydrogen peroxide still of paramount significance and it is conventionally carried out using platinum-based electrochemical sensors. Poor selectivity of the latter towards hydrogen peroxide reduction (due to reduction of oxygen at same potentials) requires detection by its oxidation at high anodic potential causing oxidation of easily oxidizable compounds worsen the selectivity. Another problem of platinum-based electrocatalysts is poisoning of their surface limiting the use on complex matrices. Prussian blue-based electrodes solve most of these drawbacks. Prussian blue (PB) is selective to H_2O_2 reduction allowing its detection at low potential in the presence of oxygen. PB is also insensitive to compounds found in biological matrices like ascorbate, lactate, or glucose. These features allow its application for the analysis of living cells. For all these reasons, PB stands out as the best choice for measuring H_2O_2 in cell culture as marker of oxidative stress.

On the other hand, microfluidic systems and lab-on-a-chip (LOC) technologies offer excellent features to improve the analytical performance by reducing analysis time, decreasing extremely the consumption of sample and reagents, integrating multiplexed analysis, and provide the possibility of development of analysis integrated in cell culture. Electrochemical detection provides high sensitivity, allows miniaturization, and it is highly compatible with micro and nanotechnologies due to the simplicity of the instrumentation required. Nevertheless, the surface characteristics of nanomaterials can further improve the sensitivity as well as other important characteristics such as antifouling properties. Up to now the fabrication of these devices relied on clean-room-based fabrication method, which are not available for most laboratories. While clean room manufacturing may still provide powerful research-scale solutions, many clinical and biological applications have obviated some of the need for the ultrafine resolution of photolithographic techniques and hence are very suitable for being fabricated employing alternative manufacturing methods. Low-cost fabrication techniques (3D printing, laser cutting or xurography) and electrochemical detection create a powerful combination for the fabrication of ultra-low-cost disposable devices to perform (bio)-chemical assays.

Therefore, this exciting multidisciplinary area of research is expected to make important contributions to diverse fields, leading to new capabilities that are currently beyond our reach and bringing major benefits to our quality of life.

In this Doctoral Thesis, different nano- and micromaterials such as carbon black (CB), transition metal dichalcogenides (TMDs) and Prussian Blue (PB), have been employed in the development of new (LOC-based) miniaturized strategies by exploiting their unique and improved electrochemical properties in two well-defined sensing topics:

1. Improved detection and determination of antioxidants in food samples.
2. Reliable detection of hydrogen peroxide as marker of oxidative stress (OS) in living cells.

To this end, this Doctoral Thesis has three defined objectives:

1. To synthetize and characterize novel TMDs-based nanomaterials.
2. To develop hybrid novel CB/TMDs-based electrochemical sensors for antioxidant determination in food samples.
3. To study oxidative stress in living cells and functional food protection on cell culture employing a PB-based electrochemical chip.

In order to achieve these objectives, the main milestones have been set as follow:

1. Study the exfoliation of group VI TMDs (MoS_2, WS_2, $MoSe_2$ and WSe_2) using different organic solvents and mix of water-surfactants.
2. Characterization of the exfoliated nanomaterials by scanning electron microscopy (SEM), UV-Vis spectroscopy and Raman spectroscopy.
3. Design, characterization, and evaluation of TMDs-based electrochemical transducers.
4. Evaluation of CB/TMDs hybrid transducers for PPs electrochemical determination in complex food environments.

5. Design, characterization, and development of PB-based electrochemical sensors able to detect H_2O_2 released from living cells as oxidative stress (OS) marker.
6. Design, characterization, and development of a PB-based electrochemical chip for real-time detection of H_2O_2 released from living cells as oxidative stress (OS) marker.

II. Introduction

II.1. Nanomaterials-based electrochemical sensors

A chemical sensor is a device able to transform chemical properties of certain molecules into an analytical useful signal. This signal can be the presence or not of a certain chemical (qualitative analysis) or the quantity (quantitative analysis). Chemical sensors are classified into two main criteria: the nature of the recognition element or the transduction mechanism. Electrochemical sensors can be divided in chemosensors and biosensors depending on the nature of the recognition element (i.e. ionophores for chemical enzymes and antibodies for biosensors). For the case of the transduction mechanism, the classification regards the nature of the physical magnitude, being optical (absorbance, fluorescence, luminescence…), magnetic, thermometric, radiometric, and electrochemical (amperometric, potentiometric, or impedimetric).

Electrochemical sensors are able to sense analytes directly, when electroactive species are analyzed, or indirectly via a recognition element or an enzymatic reaction. An electrical signal is produced, dependent on the analyte concentration. Different electrochemical techniques can be employed to measure the analyte concentration [2]. Potentiometry measures the change in the open-circuit potential (OCP), with no current flow between two electrodes, working (WE) and reference (RE). They measure the potential change according to the analyte concentration; one example of these kind of sensors is the pH meter. Amperometry and voltammetry requires a third electrode, the counter electrode (CE), which ensures no drift in the potential applied between WE and RE due to the ohmic drop across the solution. In amperometry, a constant potential is applied, and the current is recorded in the WE, which can be considered as the sensing electrode. The recorded current arising from the oxidation or reduction of electroactive analytes is proportional to their concentration. Voltammetry involves recording the current while the potential is changed. This change can be carried out linearly, cyclically or by pulses giving the linear sweep voltammetry (LSV), cyclic voltammetry (CV) and differential or square wave voltammetry (DPV and SWV) respectively. Finally, impedance spectroscopy (EIS) measurements involve the use of a sinusoidal potential waveform along a range of frequencies. This powerful technique

allows to study the interfacial properties of the electrode by the extraction of parameters such as capacitance, resistance to charge transfer and so on.

The choice of the electrode material is crucial when designing the electrochemical sensor since it will determine sensitivity, selectivity, and stability. Commonly used materials are noble metals (Au, Pt, Au), semiconducting materials (ZnO, In_2O_3, Sn) or carbon-based, including glassy-carbon electrodes (GCE), boron-doped diamond (BDE) or ink-based. These base materials could be modified with a wide range of compounds to enhance their sensing properties. Nanomaterials are playing a key role in this sense since their enhanced physico-chemical properties [1]. Modification with metal nanoparticles, carbon-based materials such as carbon nanotubes (CNTs) and graphene, metallorganic frameworks (MOF), conducting polymers (polypyrrole, polyaniline) and their hybrid nanocomposites have demonstrated improved electrocatalytic properties and enhanced sensitivity and selectivity as will be explained in section I.2.

II.1.1. Nanomaterials

Nanomaterial (NM) can be defined as a material with at least one dimension in the nanoscale (1 nm = 10^{-9} m). In 2011, the European Commission released a specific recommendation on the definition of a nanomaterial:

"A natural, incidental or manufactured material containing particles, in an unbound state or as an aggregate or as an agglomerate and where, for 50 % or more of the particles in the number size distribution, one or more external dimensions is in the size range 1 nm-100 nm".

Some researchers have suggested to consider "nano" as a different state together with solid, liquid, gas and plasma. In fact, given nanomaterial exhibits very different physical and chemical properties than the bulk counterpart due to surface and quantum effects that appears with decrease in size. On one hand, surface effects are related to an increased fraction of atoms at the nanomaterial surface compared to the bulk. On the other hand, quantum effects rely on the confinement of electrons in the very small materials, which results in quantized behavior. These features result in an enhanced thermal, mechanical, optical, electrical, magnetic and biological properties, which are

size dependent and can be tuned by simply adjusting the size, shape and extent of agglomeration [3].

NMs are usually classified according to their dimensionality. NM with all dimensions in the nanoscale is classified as zero-dimensional material (0D), as nanoparticles and quantum dots. One-dimensional nanomaterials (1D) present two dimensions in the nanoscale while the third one is usually at the microscale. Some examples of 1D nanomaterials are nanowires, nanotubes, nanorods and nanofibers. Two-dimensional nanomaterials (2D) have only one dimension at the nanoscale. Thin films, nanocoatings, nanoplates and nanosheets are common examples of 2D nanomaterials. Lastly, 3D nanomaterials present internal nanoscale features while no external dimension at the nanoscale is present. This category includes nanocomposites, porous and nanostructured materials. The implementation of nanomaterials in the analytical sciences is a fast-growing research field. A plethora of nanostructures has been investigated to exploit their potentialities for being applied in the sensors and biosensors field. In this thesis three nanomaterials have been employed: Carbon Black, Prussian Blue, and Transition Metal Dichalcogenides. These NM will be introduced in the following sections.

II.1.2. Carbon Black

The huge impact of carbon nanomaterials in electroanalysis has been well documented in the literature [4–6]. However, in the last years a cost-effective, already known material, carbon black (CB), has been re-discovered. CB exhibits excellent electrical conductivity, dispersibility in a wide range of solvents; facile functionalization and fast electron transfer kinetics [7]. Moreover, CB is a very low-cost nanomaterial (c.a. 1 € Kg^{-1}), which represent a key advantage in the development of new low-cost electrochemical devices.

CB consists of aggregated spheroid primary particles, carbon combined into an extended network which can form agglomerates [8] (See **Figure II-1**). Features of CB can vary its physicochemical properties, including the degree of crystallinity, the size of the primary particles (15-100 nm), the number of aggregated particles, and the amount and nature of functional groups on the surface of the particles [9]. CB is a

material produced by the incomplete combustion of heavy petroleum products; it is commonly employed as reinforcing filler used in rubber compounds and also used as black pigment. In the IUPAC compendium of chemical terminology is defined as: *An industrial manufactured colloidal carbon material in the form of spheres and of their fused aggregates with size below 1000nm* [10].

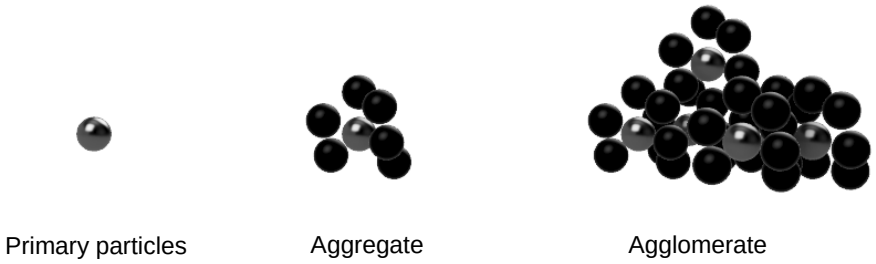

Figure II-1: Illustration of CB structure.

Until few years ago, the main applications in electrochemistry for CB were related to energy applications in fuel cells and batteries [7]. Several works have also focused on the comparison of the CB properties with other more widely employed carbon and carbon-NM based electrodes such as multiwall carbon nanotubes (MWCNTs), thermally reduced graphene oxide (tRGO), GC and edge plane pyrolytic graphite. In these works, the electrochemical properties of CB have been highlighted because of the faster or comparable electrochemical performance and heterogeneous electron transfer rate (HET) with the advantage of low cost and ease of use [11–13]. All these features open new gates for the employment of this outstanding nanomaterial an its combination in the development of new electrochemical sensors.

II.1.3. Prussian Blue

Prussian Blue (PB) is considered the first coordination compound discovered in XVIII century; it took a long time to discover the properties as electroactive film in the late 70s [14]. PB is a mixed valence compound, where iron atoms in different oxidation states (Fe^{II}/Fe^{III}) are present in face-centered cubic (FCC) lattice with a unit cell dimensions of 10.2 Å [15]. The high-spin iron atoms are linked by the nitrogen atoms in an octahedral environment, low-spin iron atoms are surrounded by carbon atoms.

The stoichiometry of 3 to 4 from Fe^{II} to Fe^{III} causes a 25% vacancy of $[Fe(CN)_6]^{4-}$ anions [16]. The result is a structure with a three-dimensional lattice with channels and cavities of 3.2 Å. These dimensions and chemical environment enable a certain selectivity since the size exclusion of several biomolecules is possible.

The cyclic voltammogram of PB is presented in **Figure II-2**. At around 0.10 V (vs Ag|AgCl) two sets of peaks corresponding to the oxidation of PB and its reduction to another polycrystal known as Prussian White (PW) occur; the reduction is accompanied with the loss of its characteristic blue color. The transfer of electrons is compensated by the entrapment of cations in the crystalline lattice. This reaction is presented in the equation **Eq.I.1.**

$$\mathbf{Fe_4^{III}[Fe^{II}(CN_6)_3] + 4e^- \leftrightarrow K_4Fe_4^{II}[Fe^{II}(CN_6)_3]} \qquad \text{Eq.I.1}$$

PB *PW*

PB can be fully oxidized at higher anodic potentials as can be seen from the set of peaks at around 0.75 V. The fully oxidized state is known as Berlin Green (BG), and the reaction follows the equation **Eq.I.2.**

$$\mathbf{Fe_4^{III}[Fe^{III}(CN_6)_3]A_3 + 3e^- \leftrightarrow Fe_4^{III}[Fe^{II}(CN_6)_3] + 3A^-} \qquad \text{Eq.I.2}$$

PB *BG*

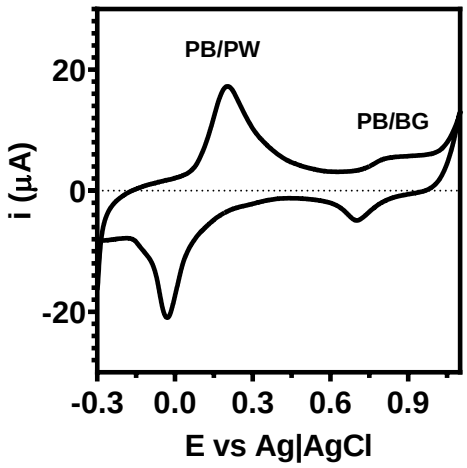

Figure II-2: Typical cyclic voltammogram of Prussian Blue.

Prussian blue-based electrodes have found utility as energy storage devices, due to their ability of entrap cations in their structure [17]. However, PB is particularly famous for the catalytic properties towards the reduction of H_2O_2. Prussian Blue is an outstanding catalyst in the reduction of H_2O_2, beating metallic-based electrodes, but even the natural peroxidase enzyme [18], yet the other key point is the selectivity. PB is able to selectively detect H_2O_2 at around 0 V (vs Ag/AgCl) in the presence of O_2, catalytic currents are 400-600 times bigger in the case of H_2O_2 than O_2; for this reason, is known as the "*artificial peroxidase*" [18–20].

These properties have made it very appealing for application in electrochemical sensors for H_2O_2 and peroxidase-based biosensors for a plethora of analytes [21]. H_2O_2 itself is used for disinfection of water pools, food, and beverage packages, thus determination of the residual concentration is important. Additionally, is a product of oxidases, the enzymes, which are employed as recognition element in most of the existing enzyme-based biosensors and analytical kits. Another more recent application is the sensing of H_2O_2 in cell cultures as a marker of oxidative stress, this aspect will be reviewed in more detail in section I.3.

II.1.4. Transition Metal Dichalcogenides

2D nanomaterials are crystalline solids with a high ratio between their lateral size (1-10^4 μm) and thickness (<1 nm) [22]. The layered structure of the bulk crystals is due to the strong intralayer covalent interaction and the weaker Van der Waals (VdW) interlayer interaction, which facilitates the exfoliation of nanosheets from the bulk materials. The discovery of graphene boosted a scientific revolution allowing the discovery of a plethora of 2D materials. These include materials like phosphorene, germanene, hexagonal boron nitride (hBN) and Transition Metal Dichalcogenides (TMDs) to name a few [23]. The latter were of special interest since were studied for analytical purposes in this Doctoral Thesis.

TMDs are a large family of layered crystals with MX_2 formula, where M is a transition metal element; typically, from group IV to VI and X is a chalcogen (S, Se or Te). Monolayer of TMDs are comprised of an X-M-X sandwich configuration while these monolayers are held by weak VdW forces (See **Figure II-3**).

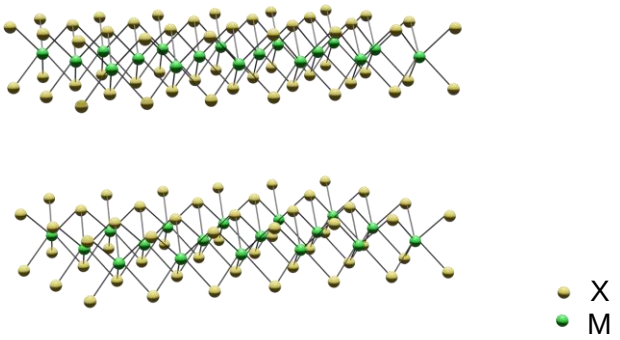

Figure II-3: General crystalline structure of Group VI MX_2 TMDs

TMDs from group IV and VI are semiconductors while those from group V are metallic. Molybdenum disulfide (MoS_2) is the most widely studied in the electrochemical field, especially for energy storage and conversion purposes [24–27]. However, the interesting features showed together with intrinsically behavior of a 2D material such as the high surface-to-volume ratio are directly exploitable in electrochemistry and provide an extreme sensitivity to environment [28]. One of the most common methods to produce nanosheets of these NM is ultrasonication-assisted liquid phase exfoliation (LPE). This method is a top-down technique, which produces a high amount of thin nanosheets dispersed in a solvent by breaking the VdW interaction between individual layers [29,30]. LPE methods offer several advantages in comparison with other exfoliation methods since their scalability and simple instrumentation required. In fact, these features perfectly match for their applications in catalysis, sensors, or energy applications where a comprised material quality it is not an issue [31,32]. This have encouraged analytical chemist to explore their capabilities for analytical purposes [33,34]. MoS_2 is the most studied TMDs and has been used as material for electrochemical devices fabrication for hydrogen evolution reaction (HER) [35,36] and energy storage [37,38]. Layered transition-metal dichalcogenides, in particular WS_2 and MoS_2, have attracted increasing attention even in the field of sensors [39–42], for their unique chemical, physical and electrochemical properties, low cost, stability and excellent electrocatalytic properties [43–46]. The use of MoS_2 in electrochemical sensing is a growing field and holds great promise in sensors and biosensors development. MoS_2 is composed of three atom layers: a Mo layer sandwiched between two S layers; it has low conductivity and the (three atom layers) sheets tend to restack

during the deposition/modification [47]. Consequently, in the last years MoS_2-based nanocomposites have attracted researchers' attention [48]; some MoS_2 hybrid materials have shown great versatility as advanced electrode modifier, showing unique and sometimes unexpected sensing properties and catalytic activity [49–57]. Indeed, it is widely known that functionalization or hybridization of transition-metal dichalcogenides with conductive NMs is a consolidated and effective way to improve the catalytic properties of individual materials. The integration of carbon-based NMs [52–55] and metal or metal oxide nanoparticles [51] in MoS_2 structures have shown synergistic effects, exploitable in electrochemical sensing. These nanocomposites allow tuning of two or more materials in a plethora of combinations and conformations. Functionalizing MoS_2 with carbonaceous nanomaterials is a recognized way to overcome shortcomings of individual components, overcoming restacking problems, broadening the working potential window, increasing at the same time the fouling resistance.

II.2. Oxidative Stress

Redox homeostasis plays a key role in cell physiology; in normal conditions cells can maintain this status through the interaction and interconversion of redox active molecules. The most representative groups of molecules involved in the process are the Reactive Oxygen Species (ROS) and Reactive Nitrogen Species (RNS). ROS are produced intracellularly during aerobic metabolism and includes species like superoxide ($O_2^{\cdot-}$), hydrogen peroxide (H_2O_2) and hydroxyl radical ($OH^{\cdot}$). RNS comprises nitric oxide ($NO^{\cdot}$) and related compounds like peroxynitrite ($ONOO^-$) and nitrite (NO_2^-). Low concentrations have been proved to stimulate the maintenance of the redox balance in cellular processes whereas high concentrations are able to cause the so-called oxidative stress [58,59]. Oxidative stress is a very general concept that has been defined by Sies [60]:

"An imbalance between oxidants and antioxidants in favor of the oxidants, leading to a disruption of redox signaling and control and/or molecular damage"

Aerobic cells are known to continuously produce superoxide ions during aerobic metabolism as a side product during their normal metabolism. This molecule is highly

reactive, and it is readily eliminated by fast disproportionation into H_2O_2 and O_2, with an estimated half-life of 5 s at physiological pH [61]. However, the high intracellular activity of the superoxide dismutase (SOD) keeps the physiological concentrations of superoxide in the range of few pM [62]. SOD can convert superoxide into H_2O_2, a much more stable product. In fact, it is considered as more powerful cytotoxic agent since its extended half-life allow them to diffuse along the whole cell and extracellular space, acting as source of hydroxyl radical's trough the Fenton Reaction (FR). Hydroxyl radicals are among the most powerful hydrogen acceptors, being able to damage cellular components. Living cells also possess the ability to scavenge H_2O_2 by catalase (CAT), which catalyzes its disproportionation into O_2 and H_2O. This mechanism allows to maintain a steady state concentration of H_2O_2 in the range of few nM [59]. However, CAT suffers from substrate inhibition, which make it quite efficient in the physiological levels but leave cells unprotected when H_2O_2 concentrations raises [62]. Cells can change its normal metabolism under xenobiotics exposure to produce high quantities of $O_2^{\cdot-}$ by NADPH oxidase activation. This physiological response is also accompanied by the activation NO-synthases which are able to produce NO, which can react with O_2 to form NO_2^-, but also with the other primary molecule $O_2^{\cdot-}$ to form another highly oxidant specie, peroxynitrite ($ONOO^-$). The latter can also decompose to the conjugated acid and into NO_3^- and NO_2^- through a first and second order decomposition reactions, respectively [63,64]. These few lines serve to give a general overview of the complexity of interconnected pathways from the primary production of $O_2^{\cdot-}$ and NO by the cells justifying why the nature, levels and roles of ROS remains a real challenge for the scientific community. For the sake of clarity, **Figure II-4** has been added for a general overview of the reactions involved in oxidative stress.

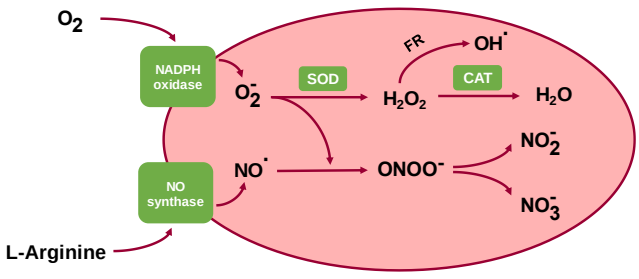

Figure II-4: Relationship between ROS/RNS and their cross-reactivity in biological media.

The levels of these molecules are very important due to *two-faced* character of oxidative stress (see **Figure II-5**). On one hand, low levels of oxidant species are essential for life due to their key role in redox signaling; this has been termed as *oxidative eustress*. On the other hand, excessive oxidant challenge causes damage to biomolecules and in the long term can trigger several diseases; in this case this situation is named *oxidative distress* [60]. The interest in the cellular responses linked to oxidative stress (oxidative distress) mechanism is fundamental for understanding physiological and pathological process since it has been related to several pathological conditions such as cancer, ischemia, atherosclerosis, Parkinson's and Alzheimer's disease [65–68].

Figure II-5: Schematic representation of oxidative stress and its relationship with health and disease evolution.

However, understanding the limits between eustress and distress remains a current challenge in redox biology as the development of new analytical methods to define them**.** Great efforts have been made in the development of analytical methods able to fulfill the challenging requirements exposed above. Most of the classical methods are based on fluorescence, chemiluminescence, colorimetric assays, electron paramagnetic resonance (EPR) or electrochemical methods [69]. Some methods are also based on the detection of oxidation products formed in the presence or ROS and RNS, however this is not a direct measurement and make challenging the real time detection [70].

EPR techniques are recognized to be the most specific; however, the equipment is hard to use and expensive which hinders their use [71]. Fluorescence-based probes are the most used in biology labs and usually employed coupled to fluorescence

microscopy or flow cytometry. The most popular probe is the cell-permeant diclorodihydrofluorescein diacetate (DCFH-DA), which can cross the cell membrane where it is decarboxylated to DCFH and trapped inside the cells. DCF is oxidized to form the fluorescent product DCF. However, several compounds can oxidize DCFH as well as several intracellular peroxidases [72]. Fluorescent probes are easy to use, able to cross cell membranes and the equipment is usually available in biochemical labs, thus their use is widespread [73]. However, the specificity of these methods is discussed, and some molecules, able to form secondary species by redox cycling, can give artifacts or even being toxic to the cells [74].

Electrochemical methods offer several advantages, the advances in microelectronics allowed the extreme miniaturization of electrochemical systems and instrumentation required, which allows the in-situ and real time detection in biological systems [75].

NM-based sensors can improve selectivity and sensitivity due to their exceptional chemical and physical properties while the miniaturized systems are able to confine sensors as close as possible to the production site of ROS/RNS [76]. Additionally, the hybridization of these transduction techniques with microdevices is highlighted as a promising tool for coupling on-line measurements in living cells [77,78].

II.3. Food polyphenols

Polyphenols (PPs) are the most widely known group of food antioxidants, being present in diet in form of fruits, vegetables and their derived food and drinks. PPs are compounds that possess one or more aromatic ring with one or more hydroxyl groups. PPs can be classified in several subgroups according to their structure: phenolic acids, flavonoids, and non-flavonoids. Phenolics acids are hydroxyl derivatives of aromatic carboxylic acids that can be divided in benzoic and cinnamic acid depending on their structure. According to the substitution in the aromatic ring of the benzoic or cinnamic acid skeleton, several compounds can be obtained. Flavonoids is a vast group of PPs which consists of two phenyl rings (A and C) and a heterocyclic ring (B). Depending on how B and C ring are linked can be classified in isoflavones when is linked in position 3 (see **Figure II-6**). When linked in position 2 it can be divided in several classes depending on the functionalization of rings C and B. These subgroups are:

flavonols, flavones, flavanols, isoflavones and flavanones. The non-flavonoid class is divided in two classes stilbenes and lignans. For an exhaustive classification of PPs reader is referred to very useful database website phenolexplorer.eu but a general classification with some representative structures is presented in **Figure II-6**.

The highly conjugated aromatic system together with multiple hydroxyl groups make these compounds highly antioxidants owing to their ability to donate electrons or hydrogen atoms. Hence, they can react with free radicals breaking the chain reaction of free-radicals generation. Their ability of chelating transition metals, especially iron, is also involved in the inhibition of generation of hydroxyl radicals via the FR [79].

There is a strong correlation between the PP chemical structure and their radical scavenging, reducing power and metal chelating activity. In a nutshell, the antioxidant potential of a particular PP depends on the number and position of hydroxyl groups. Hydroxyl groups in *para*- or *ortho*- have demonstrated higher antioxidant power compared with other positions or monosubstituted [80,81]. An increase in the number of hydroxyl aromatic rings has shown higher antioxidant activity (AA). For example, flavonoids display higher AA compared to phenolic acids [82]. But this strong antioxidant power can be a double-edge sword, when a phenolic compound is oxidized (i.e. act as a reducing agent), loses one electron becoming a radical itself. So, the intermediates (semiquinones) and oxidation products (quinones) can become harmful at high concentrations [83].

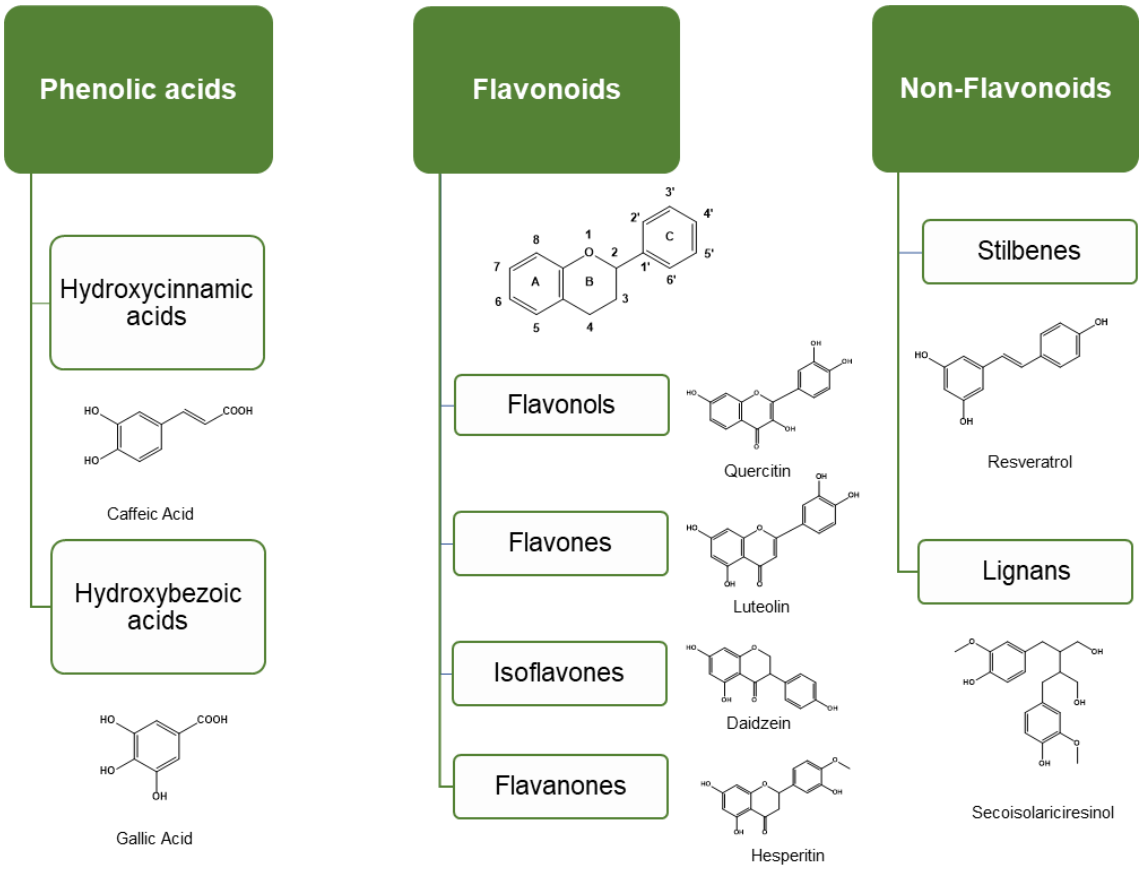

Figure II-6: General classification of food polyphenols in their main classes and some representative compounds

Studies regarding AA have been assessed using the chemical standards of selected PP and phenolic extracts from selected plants and foodstuffs. These *classical* analytical methods can test the antioxidant power by ferric reducing antioxidant power (FRAP) and cupric reducing antioxidant capacity (CUPRAC) tests. But also, the radical scavenging activity by the scavenging of colored radical species such as 2,2'-azino-bis(3-ethylbenzothiazoline-6-sulfonic acid) (ABTS), 2,2-diphenyl-1-picrylhydrazyl (DPPH) and oxygen radical absorbance capacity (ORAC) has been employed as screening tools for antioxidant capacity [84]. Due to their low bioavailability, the physiological concentrations of PP or their metabolites is too low to be detected with these kinds of assays. In addition, the hydrophobic benzenoid rings and hydrogen bonding ability of the hydroxyl groups made them able to inhibit some enzymes involved in radical generation such as lipoxygenases, cyclooxygenase, and xanthine

oxidase [85]. PP also enhances the activity of antioxidant enzymes and suppresses OS by reducing inflammatory responses [86, 87].

PPs consumption through diet has been linked to lowered risk of most common degenerative and chronic diseases that are known to be caused by oxidative stress [88]. In fact, in the last years some PPs rich foodstuffs like olive oil, tea or cocoa has emerged as functional food science [89]. The highest PPs antioxidant activity is generally attributed to structures containing o-diphenolic structures [80,81]. Indeed, these compounds have also been reported to play an important role against oxidative stress damage in biological systems [88]. In the case of olive oil PPs, hydroxytyrosol and oleuropein derivatives have been tested in *in vitro* studies showing positive potential effects preventing degenerative diseases [90]. Green and black tea PPs demonstrated its ability to modulate the antioxidant capacity of individuals, reducing the oxidative stress damage [91]. Even cocoa extracts have demonstrated beneficial effects on oxidative stress-related diseases [92–94].

II.4. References

[1] N.J. Ronkainen, H.B. Halsall, W.R. Heineman, Electrochemical biosensors, Chem. Soc. Rev. 39 (2010) 1747–1763. doi:10.1039/b714449k.

[2] K. Izutsu, Overview of Electrochemical Techniques, in: Electrochem. Nonaqueous Solut., Wiley-VCH Verlag GmbH & Co. KGaA, 2003: pp. 107–165. doi:10.1002/3527600655.ch5.

[3] P.I. Dolez, Nanomaterials Definitions, Classifications, and Applications, in: Nanoengineering, Elsevier, 2015: pp. 3–40. doi:10.1016/B978-0-444-62747-6.00001-4.

[4] M. Pumera, The Electrochemistry of Carbon Nanotubes: Fundamentals and Applications, Chem. - A Eur. J. 15 (2009) 4970–4978. doi:10.1002/chem.200900421.

[5] A. Martín, A. Escarpa, Graphene: The cutting–edge interaction between chemistry and electrochemistry, TrAC Trends Anal. Chem. 56 (2014) 13–26. doi:10.1016/J.TRAC.2013.12.008.

[6] M. Pumera, Electrochemistry of graphene, graphene oxide and other graphenoids: Review, Electrochem. Commun. 36 (2013) 14–18. doi:10.1016/J.ELECOM.2013.08.028.

[7] V. Mazzaracchio, M.R. Tomei, I. Cacciotti, A. Chiodoni, C. Novara, M. Castellino, G. Scordo, A. Amine, D. Moscone, F. Arduini, Inside the different types of carbon black as nanomodifiers for screen-printed electrodes, Electrochim. Acta. 317 (2019) 673–683. doi:10.1016/J.ELECTACTA.2019.05.117.

[8] A.I. Medalia, F.A. Heckman, Morphology of aggregates—II. Size and shape factors of carbon black aggregates from electron microscopy, Carbon N. Y. 7 (1969) 567–582. doi:10.1016/0008-6223(69)90029-3.

[9] F. Arduini, S. Cinti, V. Mazzaracchio, V. Scognamiglio, A. Amine, D. Moscone, Carbon black as an outstanding and affordable nanomaterial for electrochemical (bio)sensor design, Biosens. Bioelectron. 156 (2020) 112033. doi:10.1016/J.BIOS.2020.112033.

[10] G. Book, IUPAC Gold Book, n.d.

[11] C.H. An Wong, A. Ambrosi, M. Pumera, Thermally reduced graphenes exhibiting a close relationship to amorphous carbon, Nanoscale. 4 (2012) 4972–4977. doi:10.1039/c2nr30989k.

[12] T.W.B. Lo, L. Aldous, R.G. Compton, The use of nano-carbon as an alternative to multi-walled carbon nanotubes in modified electrodes for adsorptive stripping voltammetry, Sensors Actuators B Chem. 162 (2012) 361–368. doi:10.1016/J.SNB.2011.12.104.

[13] F.C. Vicentini, A.E. Ravanini, L.C.S. Figueiredo-Filho, J. Iniesta, C.E. Banks, O. Fatibello-Filho, Imparting improvements in electrochemical sensors: evaluation of different carbon blacks that give rise to significant improvement in the performance of electroanalytical sensing platforms, Electrochim. Acta. 157 (2015) 125–133. doi:10.1016/J.ELECTACTA.2014.11.204.

[14] V.D. Neff, Electrochemical Oxidation and Reduction of Thin Films of Prussian Blue, J. Electrochem. Soc. 125 (1978) 886. doi:10.1149/1.2131575.

[15] A. Paolella, C. Faure, V. Timoshevskii, S. Marras, G. Bertoni, A. Guerfi, A. Vijh, M. Armand, K. Zaghib, A review on hexacyanoferrate-based materials for energy storage and smart windows: Challenges and perspectives, J. Mater. Chem. A. 5 (2017) 18919–18932. doi:10.1039/c7ta05121b.

[16] B. Wang, Y. Han, X. Wang, N. Bahlawane, H. Pan, M. Yan, Y. Jiang, Prussian Blue Analogs for Rechargeable Batteries, IScience. 3 (2018) 110–133. doi:10.1016/J.ISCI.2018.04.008.

[17] L. Wang, Y. Han, X. Feng, J. Zhou, P. Qi, B. Wang, Metal–organic frameworks for energy storage: Batteries and supercapacitors, Coord. Chem. Rev. 307 (2016) 361–381. doi:10.1016/J.CCR.2015.09.002.

[18] M.A. Komkova, A.A. Zarochintsev, E.E. Karyakina, A.A. Karyakin, Electrochemical and sensing properties of Prussian Blue based nanozymes “artificial peroxidase,” J. Electroanal. Chem. (2020) 114048. doi:10.1016/j.jelechem.2020.114048.

[19] A.A. Karyakin, E.E. Karyakina, Prussian blue-based “artificial peroxidase” as a transducer for hydrogen peroxide detection. Application to biosensors, Sensors Actuators, B Chem. 57 (1999) 268–273. doi:10.1016/S0925-4005(99)00154-9.

[20] Y. Matos-Peralta, M. Antuch, Review—Prussian Blue and Its Analogs as Appealing Materials for Electrochemical Sensing and Biosensing, J. Electrochem. Soc. 167 (2020) 037510. doi:10.1149/2.0102003jes.

[21] A.A. Karyakin, Advances of Prussian blue and its analogues in (bio)sensors, Curr. Opin. Electrochem. (2017). doi:10.1016/j.coelec.2017.07.006.

[22] K.S. Novoselov, V.I. Fal9ko, L. Colombo, P.R. Gellert, M.G. Schwab, & K. Kim, A roadmap for graphene, Nature. 490 (2012). doi:10.1038/nature11458.

[23] X. Chia, M. Pumera, Layered transition metal dichalcogenide electrochemistry: journey across the periodic table, Chem. Soc. Rev. 47 (2018) 5602–5613. doi:10.1039/C7CS00846E.

[24] A. Sajedi-Moghaddam, E. Saievar-Iranizad, M. Pumera, Two-dimensional transition metal dichalcogenide/conducting polymer composites: synthesis and applications, Nanoscale. 9 (2017) 8052–8065. doi:10.1039/C7NR02022H.

[25] S.M. Tan, Z. Sofer, J. Luxa, M. Pumera, Aromatic-Exfoliated Transition Metal Dichalcogenides: Implications for Inherent Electrochemistry and Hydrogen Evolution, ACS Catal. 6 (2016) 4594–4607. doi:10.1021/acscatal.6b00761.

[26] A. Sajedi-Moghaddam, C.C. Mayorga-Martinez, E. Saievar-Iranizad, Z. Sofer, M. Pumera, Exfoliated transition metal dichalcogenide (MX_2; M = Mo, W; X = S, Se, Te) nanosheets and their composites with polyaniline nanofibers for electrochemical capacitors, Appl. Mater. Today. 16 (2019) 280–289. doi:10.1016/J.APMT.2019.06.002.

[27] W. Choi, N. Choudhary, G.H. Han, J. Park, D. Akinwande, Y.H. Lee, Recent Development of Two--Dimensional Transition Metal Dichalcogenides and Their Applications, Mater. Today. 20 (2017) 116–130. doi:10.1016/j.mattod.2016.10.002.

[28] M. Velický, P.S. Toth, From two-dimensional materials to their heterostructures: An electrochemist's perspective, Appl. Mater. Today. 8 (2017) 68–103. doi:10.1016/J.APMT.2017.05.003.

[29] C. Backes, T.M. Higgins, A. Kelly, C. Boland, A. Harvey, D. Hanlon, J.N. Coleman, Guidelines for Exfoliation, Characterization and Processing of Layered Materials Produced by Liquid Exfoliation, Chem. Mater. 29 (2017) 243–255. doi:10.1021/acs.chemmater.6b03335.

[30] Z. Gholamvand, D. McAteer, C. Backes, N. McEvoy, A. Harvey, N.C. Berner, D. Hanlon, C. Bradley, I. Godwin, A. Rovetta, M.E.G. Lyons, G.S. Duesberg, J.N. Coleman, Comparison of liquid exfoliated transition metal dichalcogenides reveals MoSe 2 to be the most effective hydrogen evolution catalyst, Nanoscale. 8 (2016) 5737–5749. doi:10.1039/C5NR08553E.

[31] S. Wu, Z. Zeng, Q. He, Z. Wang, S.J. Wang, Y. Du, Z. Yin, X. Sun, W. Chen, H. Zhang, Electrochemically Reduced Single-Layer MoS2 Nanosheets: Characterization, Properties, and Sensing Applications, Small. 8 (2012) 2264–2270. doi:10.1002/smll.201200044.

[32] F. Bonaccorso, A. Bartolotta, J.N. Coleman, C. Backes, 2D-Crystal-Based Functional Inks, Adv. Mater. 28 (2016) 6136–6166. doi:10.1002/adma.201506410.

[33] K. Kalantar-Zadeh, J.Z. Ou, Biosensors Based on Two-Dimensional MoS2, ACS Sensors. 1 (2016) 5–16. doi:10.1021/acssensors.5b00142.

[34] A. Sinha, Dhanjai, B. Tan, Y. Huang, H. Zhao, X. Dang, J. Chen, R. Jain, MoS2 nanostructures for electrochemical sensing of multidisciplinary targets: A review, TrAC Trends Anal. Chem. 102 (2018) 75–90. doi:10.1016/J.TRAC.2018.01.008.

[35] M.A. Lukowski, A.S. Daniel, F. Meng, A. Forticaux, L. Li, S. Jin, Enhanced hydrogen evolution catalysis from chemically exfoliated metallic MoS2 nanosheets, J. Am. Chem. Soc. 135 (2013) 10274–10277. doi:10.1021/ja404523s.

[36] Y. Lin, X. Chen, Y. Lin, Q. Zhou, D. Tang, Non-enzymatic sensing of hydrogen peroxide using a glassy carbon electrode modified with a nanocomposite made from

carbon nanotubes and molybdenum disulfide, Microchim. Acta. 182 (2015) 1803–1809. doi:10.1007/s00604-015-1517-5.

[37] N. Lingappan, N.H. Van, S. Lee, D.J. Kang, Growth of three dimensional flower-like molybdenum disulfide hierarchical structures on graphene/carbon nanotube network: An advanced heterostructure for energy storage devices, J. Power Sources. 280 (2015) 39–46. doi:10.1016/j.jpowsour.2015.01.064.

[38] K.J. Huang, L. Wang, J.Z. Zhang, L.L. Wang, Y.P. Mo, One-step preparation of layered molybdenum disulfide/multi-walled carbon nanotube composites for enhanced performance supercapacitor, Energy. 67 (2014) 234–240. doi:10.1016/j.energy.2013.12.051.

[39] A. Sinha, Dhanjai, B. Tan, Y. Huang, H. Zhao, X. Dang, J. Chen, R. Jain, MoS2 nanostructures for electrochemical sensing of multidisciplinary targets: A review, TrAC - Trends Anal. Chem. 102 (2018) 75–90. doi:10.1016/j.trac.2018.01.008.

[40] T. Wang, H. Zhu, J. Zhuo, Z. Zhu, P. Papakonstantinou, G. Lubarsky, J. Lin, M. Li, Biosensor based on ultrasmall MoS2 nanoparticles for electrochemical detection of H2O2 released by cells at the nanomolar level, Anal. Chem. 85 (2013) 10289–10295. doi:10.1021/ac402114c.

[41] X. Wang, F. Nan, J. Zhao, T. Yang, T. Ge, K. Jiao, A label-free ultrasensitive electrochemical DNA sensor based on thin-layer MoS_2 nanosheets with high electrochemical activity, Biosens. Bioelectron. 64 (2014) 386–391. doi:10.1016/j.bios.2014.09.030.

[42] M. Pumera, A.H. Loo, Layered transition-metal dichalcogenides (MoS2and WS2) for sensing and biosensing, TrAC - Trends Anal. Chem. 61 (2014) 49–53. doi:10.1016/j.trac.2014.05.009.

[43] J. Hong, Z. Hu, M. Probert, K. Li, D. Lv, X. Yang, L. Gu, N. Mao, Q. Feng, L. Xie, J. Zhang, D. Wu, Z. Zhang, C. Jin, W. Ji, X. Zhang, J. Yuan, Z. Zhang, Exploring atomic defects in molybdenum disulphide monolayers, Nat. Commun. 6 (2015) 1–8. doi:10.1038/ncomms7293.

[44] K.J. Huang, L. Wang, J. Li, Y.M. Liu, Electrochemical sensing based on layered MoS_2-graphene composites, Sensors Actuators, B Chem. 178 (2013) 671–677. doi:10.1016/j.snb.2013.01.028.

[45] F. Arduini, A. Amine, C. Majorani, F. Di Giorgio, D. De Felicis, F. Cataldo, D. Moscone, G. Palleschi, High performance electrochemical sensor based on modified screen-printed electrodes with cost-effective dispersion of nanostructured carbon black, Electrochem. Commun. 12 (2010) 346–350. doi:10.1016/j.elecom.2009.12.028.

[46] X. Chia, A.Y.S. Eng, A. Ambrosi, S.M. Tan, M. Pumera, Electrochemistry of Nanostructured Layered Transition-Metal Dichalcogenides, Chem. Rev. 115 (2015) 11941–11966. doi:10.1021/acs.chemrev.5b00287.

[47] V. Mani, M. Govindasamy, S.-M.M. Chen, R. Karthik, S.-T.T. Huang, Determination of dopamine using a glassy carbon electrode modified with a graphene and carbon nanotube hybrid decorated with molybdenum disulfide flowers, Microchim. Acta. 183 (2016) 2267–2275. doi:10.1007/s00604-016-1864-x.

[48] W. Zhang, P. Zhang, Z. Su, G. Wei, Synthesis and sensor applications of MoS_2 -based nanocomposites, Nanoscale. 7 (2015) 18364–18378. doi:10.1039/C5NR06121K.

[49] H. Sun, J. Chao, X. Zuo, S. Su, X. Liu, L. Yuwen, C. Fan, L. Wang, Gold nanoparticle-decorated MoS2 nanosheets for simultaneous detection of ascorbic acid, dopamine and uric acid, RSC Adv. 4 (2014) 27625. doi:10.1039/c4ra04046e.

[50] X. Li, X. Du, Molybdenum disulfide nanosheets supported Au-Pd bimetallic nanoparticles for non-enzymatic electrochemical sensing of hydrogen peroxide and glucose, Sensors Actuators, B Chem. 239 (2017) 536–543. doi:10.1016/j.snb.2016.08.048.

[51] S. Ji, Z. Yang, C. Zhang, Y.E. Miao, W.W. Tjiu, J. Pan, T. Liu, Nonenzymatic sensor for glucose based on a glassy carbon electrode modified with Ni(OH)2nanoparticles grown on a film of molybdenum sulfide, Microchim. Acta. 180 (2013) 1127–1134. doi:10.1007/s00604-013-1035-2.

[52] N.A. Kumar, M.A. Dar, R. Gul, J.B. Baek, Graphene and molybdenum disulfide hybrids: Synthesis and applications, Mater. Today. 18 (2015) 286–298. doi:10.1016/j.mattod.2015.01.016.

[53] H. Huang, J. Zhang, M. Cheng, K. Liu, X. Wang, Amperometric sensing of hydroquinone using a glassy carbon electrode modified with a composite consisting of graphene and molybdenum disulfide, Microchim. Acta. 184 (2017) 4803–4808. doi:10.1007/s00604-017-2531-6.

[54] K.J. Huang, Y.J. Liu, H.B. Wang, Y.Y. Wang, Y.M. Liu, Sub-femtomolar DNA detection based on layered molybdenum disulfide/multi-walled carbon nanotube composites, au nanoparticle and enzyme multiple signal amplification, Biosens. Bioelectron. 55 (2014) 195–202. doi:10.1016/j.bios.2013.11.061.

[55] I. Vasilescu, S.A.V. Eremia, M. Kusko, A. Radoi, E. Vasile, G.-L. Radu, Molybdenum disulphide and graphene quantum dots as electrode modifiers for laccase biosensor, Biosens. Bioelectron. 75 (2016) 232–237. doi:10.1016/J.BIOS.2015.08.051.

[56] K.J. Huang, J.Z. Zhang, Y.J. Liu, L.L. Wang, Novel electrochemical sensing platform based on molybdenum disulfide nanosheets-polyaniline composites and Au nanoparticles, Sensors Actuators, B Chem. 194 (2014) 303–310. doi:10.1016/j.snb.2013.12.106.

[57] K.J. Huang, Y.J. Liu, Y.M. Liu, L.L. Wang, Molybdenum disulfide nanoflower-chitosan-au nanoparticles composites based electrochemical sensing platform for bisphenol a determination, J. Hazard. Mater. 276 (2014) 207–215. doi:10.1016/j.jhazmat.2014.05.037.

[58] H. Sies, Oxidative stress: a concept in redox biology and medicine, Redox Biol. 4 (2015) 180–183. doi:10.1016/j.redox.2015.01.002.

[59] H. Sies, Hydrogen peroxide as a central redox signaling molecule in physiological oxidative stress: Oxidative eustress, Redox Biol. 11 (2017). doi:10.1016/j.redox.2016.12.035.

[60] H. Sies, C. Berndt, D.P. Jones, Oxidative Stress, Annu. Rev. Biochem. 86 (2017) 715–748. doi:10.1146/annurev-biochem-061516-045037.

[61] S. Marklund, Spectrophotometric study of spontaneous disproportionation of superoxide anion radical and sensitive direct assay for superoxide dismutase, J. Biol. Chem. 251 (1976) 7504–7507.

[62] B. Chance, H. Sies, A. Boveris, Hydroperoxide metabolism in mammalian organs, Physiol. Rev. 59 (1979) 527–605. doi:10.1152/physrev.1979.59.3.527.

[63] P.C. Ford, D.A. Wink, D.M. Stanbury, Autoxidation kinetics of aqueous nitric oxide, FEBS Lett. 326 (1993) 1–3. doi:10.1016/0014-5793(93)81748-O.

[64] C. Molina, R. Kissner, W.H. Koppenol, Decomposition kinetics of peroxynitrite: Influence of pH and buffer, Dalt. Trans. 42 (2013) 9898–9905. doi:10.1039/c3dt50945a.

[65] A.J. Kattoor, N.V.K. Pothineni, D. Palagiri, J.L. Mehta, Oxidative Stress in Atherosclerosis, Curr. Atheroscler. Rep. 19 (2017). doi:10.1007/s11883-017-0678-6.

[66] S.I. Liochev, Reactive oxygen species and the free radical theory of aging, Free Radic. Biol. Med. 60 (2013) 1–4. doi:10.1016/j.freeradbiomed.2013.02.011.

[67] W. Vessey, A. Perez-Miranda, R. Macfarquhar, A. Agarwal, S. Homa, Reactive oxygen species in human semen: Validation and qualification of a chemiluminescence assay, Fertil. Steril. 102 (2014) 1576–1583. doi:10.1016/j.fertnstert.2014.09.009.

[68] C.W. Olanow, An introduction to the free radical hypothesis in Parkinson's disease, Ann. Neurol. 32 (1992) S2–S9. doi:10.1002/ana.410320703.

[69] Y. Zhang, M. Dai, Z. Yuan, Methods for the detection of reactive oxygen species, Anal. Methods. 10 (2018) 4625–4638. doi:10.1039/c8ay01339j.

[70] P.G. Winyard, C.M. Spickett, H.R. Griffiths, Analysis of radicals and radical reaction products in cell signalling and biomolecular damage: The long hard road to gold-standard measures, Biochem. Soc. Trans. 39 (2011) 1217–1220. doi:10.1042/BST0391217.

[71] M. Kopáni, P. Celec, L. Danišovič, P. Michalka, C. Biró, Oxidative stress and electron spin resonance, Clin. Chim. Acta. 364 (2006) 61–66. doi:10.1016/J.CCA.2005.05.016.

[72] M. Whiteman, Y. Dogra, P.G. Winyard, J.S. Armstrong, Detection and measurement of reactive oxygen intermediates in mitochondria and cells, Methods Mol. Biol. 476 (2008) 29–50. doi:10.1007/978-1-59745-129-1_3.

[73] X. Jiao, Y. Li, J. Niu, X. Xie, X. Wang, B. Tang, Small-Molecule Fluorescent Probes for Imaging and Detection of Reactive Oxygen, Nitrogen, and Sulfur Species in Biological Systems, Anal. Chem. (2017) acs.analchem.7b04234. doi:10.1021/acs.analchem.7b04234.

[74] P. Wardman, Fluorescent and luminescent probes for measurement of oxidative and nitrosative species in cells and tissues: Progress, pitfalls, and prospects, Free Radic. Biol. Med. 43 (2007) 995–1022. doi:10.1016/j.freeradbiomed.2007.06.026.

[75] C. Calas-Blanchard, G. Catanante, T. Noguer, Electrochemical Sensor and Biosensor Strategies for ROS/RNS Detection in Biological Systems, Electroanalysis. 26 (2014) 1277–1286. doi:10.1002/elan.201400083.

[76] F.S. Ligler, H.S. White, Nanomaterials in analytical chemistry, Anal. Chem. 85 (2013) 11161–11162. doi:10.1021/ac403331m.

[77] P. Ortiz, X. Munoz-Berbel, J. Gonzalo-Ruiz, Microfluidics for Monitoring Oxidative Stress and Antioxidant Capacity, Curr. Anal. Chem. 8 (2012) 456–471. doi:10.2174/157341112803216708.

[78] J. Kieninger, A. Weltin, H. Flamm, G.A. Urban, Microsensor systems for cell metabolism - from 2D culture to organ-on-chip., Lab Chip. 18 (2018) 1274–1291. doi:10.1039/c7lc00942a.

[79] S.A. Cherrak, N. Mokhtari-Soulimane, F. Berroukeche, B. Bensenane, A. Cherbonnel, H. Merzouk, M. Elhabiri, In vitro antioxidant versus metal ion chelating properties of flavonoids: A structure-activity investigation, PLoS One. 11 (2016). doi:10.1371/journal.pone.0165575.

[80] E. Bendary, R.R. Francis, H.M.G. Ali, M.I. Sarwat, S. El Hady, Antioxidant and structure–activity relationships (SARs) of some phenolic and anilines compounds, Ann. Agric. Sci. 58 (2013) 173–181. doi:10.1016/J.AOAS.2013.07.002.

[81] F. Della Pelle, A. Scroccarello, M. Sergi, M. Mascini, M. Del Carlo, D. Compagnone, Simple and rapid silver nanoparticles based antioxidant capacity assays: Reactivity study for phenolic compounds, Food Chem. 256 (2018). doi:10.1016/j.foodchem.2018.02.141.

[82] E. Guardado, E. Molina, M. Joo, E. Uriarte, Antioxidant and Pro-Oxidant Effects of Polyphenolic Compounds and Structure-Activity Relationship Evidence, in: Nutr. Well-Being Heal., InTech, 2012. doi:10.5772/29471.

[83] B. Halliwell, Free radicals and antioxidants: Updating a personal view, Nutr. Rev. 70 (2012) 257–265. doi:10.1111/j.1753-4887.2012.00476.x.

[84] M. Antolovich, P.D. Prenzler, E. Patsalides, S. McDonald, K. Robards, Methods for testing antioxidant activity, Analyst. 127 (2002) 183–198. doi:10.1039/b009171p.

[85] D.M. Pereira, P. Valentão, J.A. Pereira, P.B. Andrade, Phenolics: From Chemistry to Biology, (2009) 2202–2211. doi:10.3390/molecules14062202.

[86] E. Kansanen, S.M. Kuosmanen, H. Leinonen, A.L. Levonenn, The Keap1-Nrf2 pathway: Mechanisms of activation and dysregulation in cancer, Redox Biol. 1 (2013) 45–49. doi:10.1016/j.redox.2012.10.001.

[87] C.-C. Chuang, M.K. McIntosh, Potential Mechanisms by Which Polyphenol-Rich Grapes Prevent Obesity-Mediated Inflammation and Metabolic Diseases, Annu. Rev. Nutr. 31 (2011) 155–176. doi:10.1146/annurev-nutr-072610-145149.

[88] H. Zhang, R. Tsao, Dietary polyphenols, oxidative stress and antioxidant and anti-inflammatory effects, Curr. Opin. Food Sci. 8 (2016) 33–42. doi:10.1016/J.COFS.2016.02.002.

[89] I. Hassen, H. Casabianca, K. Hosni, Biological activities of the natural antioxidant oleuropein: Exceeding the expectation – A mini-review, J. Funct. Foods. 18 (2015) 926–940. doi:10.1016/J.JFF.2014.09.001.

[90] C. Angeloni, M. Malaguti, M. Barbalace, S. Hrelia, Bioactivity of Olive Oil Phenols in Neuroprotection, Int. J. Mol. Sci. 18 (2017) 2230. doi:10.3390/ijms18112230.

[91] I. Peluso, M. Serafini, Antioxidants from black and green tea: from dietary modulation of oxidative stress to pharmacological mechanisms, Br. J. Pharmacol. 174 (2017) 1195–1208. doi:10.1111/bph.13649.

[92] M. Serafini, I. Peluso, Functional Foods for Health: The Interrelated Antioxidant and Anti-Inflammatory Role of Fruits, Vegetables, Herbs, Spices and Cocoa in Humans., Curr. Pharm. Des. 22 (2016). doi:10.2174/1381612823666161123094235.

[93] M. Serafini, E. Jirillo, Editorial: Chocolate and Health: Friend or Foe?, Front. Nutr. 4 (2017) 67. doi:10.3389/fnut.2017.00067.

[94] F. Ioannone, G. Sacchetti, M. Serafini, Effect of Dark Chocolate Extracts on Phorbol 12-Myristate 13-Acetate-Induced Oxidative Burst in Leukocytes Isolated by Normo-Weight and Overweight/Obese Subjects, Front. Nutr. 4 (2017) 23. doi:10.3389/fnut.2017.00023.Nanohybrid carbon black-molybdenum disulfide transducers for preconcentration-free voltammetric detection of the olive oil o-diphenols hydroxytyrosol and oleuropein

III. Nanohybrid carbon black-molybdenum disulfide transducers for preconcentration-free voltammetric detection of the olive oil o-diphenols hydroxytyrosol and oleuropein

III.1. Introduction and objectives

CB has been recognized as a full-fledged carbonaceous nanomaterial becoming widely employed in the sensors field. Its features stimulated intense research interest; indeed, CB nanospheres possess high surface area, high electrical conductivity, low cost and high dispersibility in a wide range of solvents. For these reasons, CB nanospheres have been used to build sensors and biosensors employed in several applications [1–6]. On the other hand, two-dimensional TMDs have become new attractive 2D nanomaterials for electrochemical applications [7]. MoS_2 is the most representative TMD and has been intensively explored as material in the fabrication of electrochemical devices for energy storage and in HER [8]. On the contrary, the use of MoS_2 in electrochemical sensing is just a growing field and holds great promise in sensors and biosensors development [9]. In fact, some MoS_2 hybrid materials have shown great versatility as advanced electrode transducers, showing unique and sometimes unexpected sensing properties and catalytic activity. The integration of carbon-based nanomaterials [10,11], metallic [12,13] or metal oxide nanoparticles [14] in MoS_2 structures has been reported to have synergistic effects, exploitable in electrochemical sensing.

Extra virgin olive oil (EVOO) has emerged as functional food due to the demonstrated health benefits which are attributed to the fatty acid profile and PPs content [15]. Interestingly, the highest PPs antioxidant activity is generally attributed to o-diphenolic structures [16]. The most abundant EVOO ortho-diphenols are hydroxytyrosol (HYT) and oleuropein (OLEU) which are the major contributors to the antioxidant capacity of EVOO. Indeed, these compounds have also been reported to play an important role against oxidative stress damage in biological systems showing positive potential effects in the prevention of degenerative diseases [17].

The development of analytical methods for the selective detection of the antioxidants fraction bearing o-diphenol functionalities is, thus, relevant for the evaluation of food quality, including nutritional value. Several assays have been proposed in recent years, using many different analytical approaches, to evaluate antioxidant capacity/PPs content in food samples [18–21]. The most commonly used assays are based on spectrophotometry, such as the classical determination of total phenolic content with

the Folin Ciocalteu (FC) method [22]. Several electrochemical methods have been developed for PPs analysis exploiting the electrochemical behavior of the samples for determining total reducing capacity or even individual PPs. However, electrode fouling represents a classical limitation of direct electrochemical detection of PPs. This is due to polymerization of oxidation products, resulting in an insulating film layer deposition onto the electrode surface [23]. Even in this case, nanomaterials can help to overcome or reduce this drawback.

In this Chapter, we report for the first-time hybrid MoS_2-CB transducers and demonstrate their sensing ability towards o-diphenols. These transducers have been used to build an SPE electrochemical sensor for the determination of EVOO o-diphenols in complex EVOO and related samples.

III.2. Material and methods

III.2.1. Reagents and apparatus

Catechol, OLEU, HTYR, disodium hydrogen phosphate anhydrous, sodium dihydrogen phosphate hydrate, potassium ferrocyanide, potassium ferricyanide, potassium chloride, N, N-dimethylformamide and MoS_2 were purchased from Sigma Aldrich (St. Louis, Mo, USA). CB N220 was obtained from Cabot Corporation (Ravenna, Italy). Electrochemical measurements were carried out in Autolab PGSTAT 12 potentiostat from Metrohm (Utrecht, The Netherlands), SPEs were purchased from Dropsens S.L. (Oviedo, Spain). Stock solutions of PPs standards were prepared in methanol at a concentration of 10 mM and stored at -20 ºC in the dark.

III.2.2. Building of CB-MoS_2 based SPE

CB and MoS_2 dispersions were prepared in DMF-H_2O 1:1 (v/v) at 1.0 mg mL^{-1} in a bath sonicator (3000683 Ultrasons Selecta, Barcelona, Spain) for 6 h keeping the temperature below 25 °C. CB-MoS_2 solutions at different ratios (25-75, 50-50, 75-25 v/v) were prepared by mixing different volumes of CB and MoS_2, previously dispersed for 1 h, followed by a further 5h of sonication after mixing. SPEs modification was performed via drop casting onto the working electrode surface in ten steps for a total of 10 µL (1 µL each) of CB, MoS_2 and 25-75, 50-50, 75-25 v/v CB-MoS_2 mixed solutions, respectively.

III.2.3. Electrochemical Characterization

SPEs CB-MoS_2 nanohybrids were investigated using cyclic voltammetry CV and EIS using a solution containing 5 mM $[Fe(CN)_6]^{3-/4-}$ and 0.1 M KCl. CV experiment were carried out at a scan rate of 50 mV s^{-1}. EIS experiment used a sinusoidal wave of 5 mV amplitude in the 10^5 to 10^{-1} Hz frequency range at open circuit potential.

III.2.4. Microstructure and elemental characterization

CB-MoS_2 SPEs microstructure and homogeneity were investigated by field-emission scanning microscopy (FE-SEM) coupled with energy-dispersive X-ray spectroscopy (EDS). Images were obtained using a ΣIGMA scanning electron microscope (Carl Zeiss) based on the GEMINI® column featuring a high brightness Schottky field

emission source, beam booster, and in-lens secondary electron detector. Measurements were conducted in low acceleration potential mode (i.e. 2 kV) with a working distance of about 4 mm thus allowing the use of uncoated samples. EDS was performed using a silicon-drift detector (Oxford Instruments), directly coupled with FE-SEM working at an optimal distance of 8.5 mm with an accelerating voltage up to 20 kV and sampling areas of about 6 mm^2.

III.2.5. CV and DPV o-diphenols measurements

The SPEs CB-MoS_2 electrodes response was investigated toward catechol, OLEU and HYT using CV and DPV in phosphate buffer (50 mM, pH 7.0) containing 0.1M KCl. CV was carried out with a scan rate of 50 mV s^{-1}. The DPV parameters were pulse amplitude of 25 mV and scan rate of 50 mV s^{-1}.

III.2.6. Sample preparation

EVOO samples were obtained from different batches of mixed varieties including Dritta, Coratina, Leccino, and Tortiglione. The samples were cultivated and milled in the Abruzzo region (Italy). Sampling was carried out in the year 2017 and three representative samples were selected and stored at room temperature in darkened glass bottles. Extraction of Phenolic fraction was carried out following the procedure previously used by our group [23]. Commercially available octadecyl C18 cartridges (1 g, 6 mL) (International Sorbent Technology, UK) were used for the extraction of the phenolic fraction according to the following protocol: 1 g of EVOO was dissolved in 5 mL of hexane, and the solution was loaded onto a column previously conditioned with 2x5 mL of methanol and 2x5 mL of hexane. The column was eluted with 2x5 mL of hexane to eliminate all the lipophilic fraction; the retained polar compounds were recovered by eluting with 2x10 mL of methanol. The elute was then placed in a conical flask and evaporated to dryness at room temperature (30 ºC, 150 RPM) in a rotary evaporator. The extract was recovered with 0.5 mL of methanol and stored at -20 ºC, in the dark. Commercial olive leaf extracts were donated by Oleafit srl, (Teramo, Italy). OLEU dietary supplement (PienaVita) was treated as follows; 100 mg were extracted using 4 mL of 60:40 (v/v) methanol-water solution under stirring for ten minutes in the

dark at room temperature, sample was then centrifuged for 10 minutes (5000 rpm) and supernatant was collected and stored in the dark at -20 °C.

III.2.7. Sample analysis

The electrochemical determination was carried out using DPV (section 2.5). Before analysis, samples were diluted in phosphate buffer as appropriate to fit the calibration linear range. The results obtained using the CB-MoS_2 sensor, have been expressed as mg Kg^{-1} of OLEU equivalents. OLEU was chosen as reference compounds because in all the samples resulted to be the most abundant phenol found (by HPLC analysis, data not shown). The chromatographic analysis of phenolic compounds was carried out using a Perkin Elmer Series 200 HPLC-UV/Vis according to Pirisi et al [24] with some modifications. The chromatographic separation was carried out using a Kinetex C18 column (4.6 mm diameter, 250 mm length, size of particles 5 microns), a guard column was also included. The mobile phases were ultrapure water with 0.1% HCOOH (phase A) and acetonitrile (phase B). The solvent gradient was obtained changing the amount of phase A as follows: min 0-95% A, min 20-84% A, min 30-70% A, min 40-70% A, min 50-65% A, min 60-60% A; min 70-30% A; min 80-5% A. The flow of the mobile phase was set at a 1 mL/minute. The wavelength was set at 280 nm and quantification of the single PPs was performed by external calibration of the individual PPs. All samples were prepared and analyzed in triplicate.

III.3. Results and Discussion

III.3.1. Characterization of CB-MoS_2 transducers

Group VI TMDs, particularly MoS_2, have not been yet intensively explored in the development of electrochemical sensors. As 2D material, they offer a potential improved performance in their exfoliated form due to the high-surface and catalytic properties. Despite their low conductivity, their use in conjunction with other highly conductive nanomaterials for the realization of nanohybrid surfaces constitutes an interesting novel avenue for the development of electrochemical sensors.

In this chapter, nanohybrid CB-MoS_2-based electrochemical sensors are built by drop casting at different ratios of each nanomaterial. The charge transfer process at the electrode surface was studied by CV and EIS using $[Fe(CN)_6]^{3-/4-}$as redox probe. EIS data were plotted in the Nyquist plot where the diameter of the semi-circle corresponds to the charge transfer resistance value and the linear part correspond to the diffusion-controlled region. Impedance data were fitted considering the Randless equivalent circuit, shown in the inset of **Figure III-1A** and **B**, where R_s, R_{CT}, C_{DL}, and Z_W represents solution resistance, charge-transfer resistance, double layer capacitance and Warburg impedance, respectively. Firstly, different ratios of CB-MoS_2-based electrodes were investigated in **Figure III-1** obtaining decreasing ΔE_p by increasing the CB ratio in the mixture. Values of 130 mV, 100 mV and 94 mV for 25-75, 50-50 and 75-25 (v/v). The same trend is also observed for the increased peak current intensity. As expected, as the amount of CB in the hybrid material increase, a progressive decrease in the R_{CT} is observed (172 Ω and 111 Ω for 25-75, 50-50). Interestingly, CB-MoS_2 (75-25) electrodes showed an R_{CT} comparable to pure CB (79 Ω and 82 Ω respectively) (See **Figure III-1B)**.

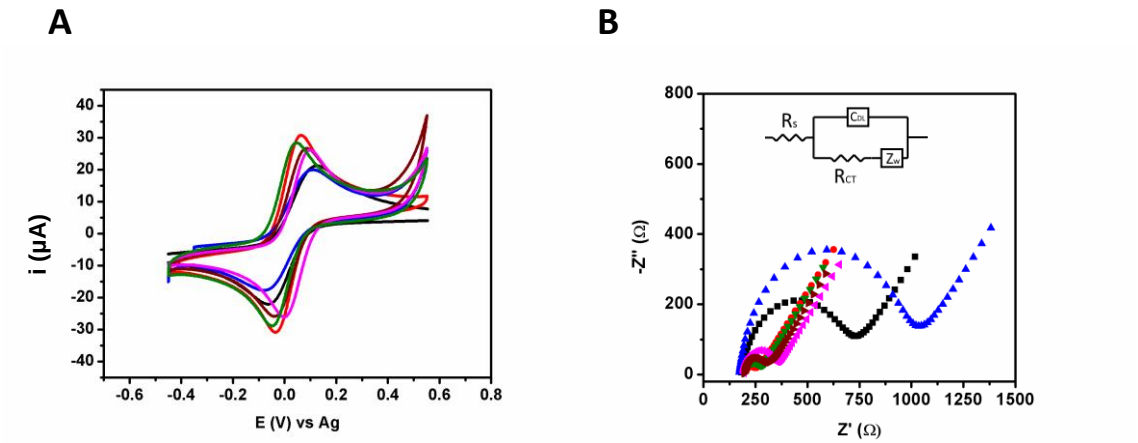

Figure III-1: Electrochemical characterization using A) cyclic voltammetry and B) EIS spectroscopy using $[Fe(CN)_6]^{3-/4-}$ redox probe for SPE (black), CB (red), MoS_2 (blue) MoS_2-CB 25:75 (magenta), MoS_2-CB 50:50 (wine) and MoS_2-CB 75:25 (green).

Then, individual materials were investigated. **Figure III-2A** reports the CV of the different nanomaterials. Highest peak-to-peak separation, and the lowest peak current were found for bare SPE and MoS_2 electrode, while the peak current intensity slightly decreased in the case of MoS_2. This behavior had previously been observed by other researchers [11,25]. It was attributed to the repulsion between the negatively charged surface of MoS_2 and the negatively charged redox probe and, probably, for the low conductivity of the material. The electrode modification with the pure CB results in lower ΔE_p, (90 mV) and an increase in the peak current intensity. Interestingly, all nanohybrids proportions showed improved behavior compared to pure MoS_2, being comparable to the highly conductive CB. **Figure III-1B** shows the impedance data obtained for each electrode, where mixed kinetic and diffusion control reaction is observed in the range of frequencies studied. The highest values in R_{CT} were found in the case of MoS_2 (824 Ω) and bare electrode (514 Ω), the increase in the R_{CT} can be attributed to the repulsion between the MoS_2 surface and the redox probe [26]. The charge-transfer properties of MoS_2 results to be highly improved by the addition of the CB, showing a comparable behavior CB itself with very high conductivity. These results are in accordance with data reported in the literature for TMDs hybrid electrodes; conductive materials as metal nanoparticles or carbonaceous nanomaterials enhance the charge-transfer properties of MoS_2 [12,14,26].

Therefore, CB-MoS_2 hybrid structures provide a high-performance electrochemical platform for sensors development.

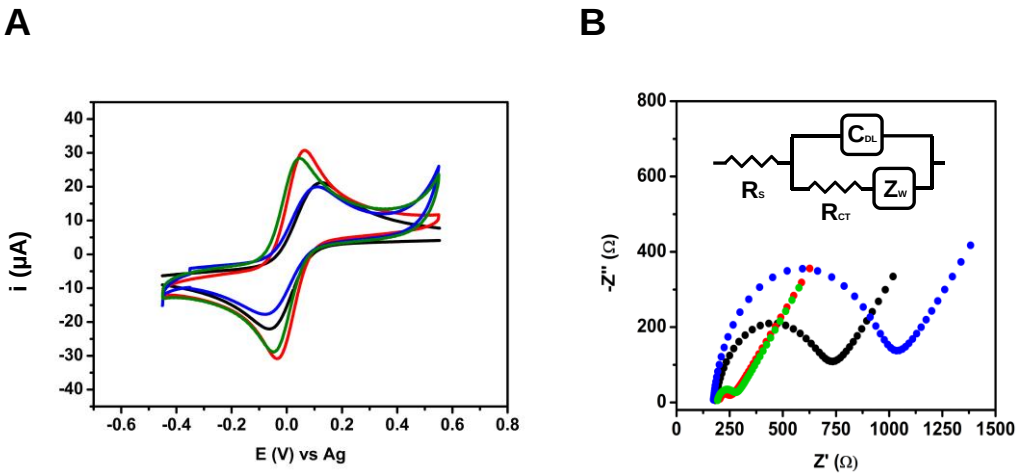

Figure III-2: Electrochemical characterization employing A) CV and B) EIS of 5 mM $[Fe(CN)_6]^{3-/4-}$ in 0.1 M KCl using SPE (black), CB (red), MoS_2 (blue) and MoS_2-CB 75-25 (green). CV sweep rate 50 mV s^{-1}. EIS performed using a sinusoidal wave of 5 mV amplitude in the 10^5 to 10^{-1} Hz frequency range at open circuit potential

The morphological characterization of the CB-MoS_2-based electrochemical sensors was carried out by FE-SEM and the elemental composition by EDS analysis. **Figure III-3** reports some representative micrographs of SPEs prepared with exfoliated MoS_2, CB and the 75:25 CB-MoS_2 mixture, respectively. In the case of **Figure III-3A** the surface morphology evidences a quite compact and homogeneous layer of MoS_2 only. The MoS_2 flakes are quite polydisperse in shape and size, their dimensions spanning from few tenths of nm up to few tenths of microns. Considering **Figure III-3B**, a nanostructured surface is evident where the characteristic globular unit of the carbon black can be easily appreciated. The average dimension of these units is about 20-30 nm, in agreement with data reported in the literature for similar carbonaceous materials [27]. **Figure III-3C** correspond to the case were the SPE surface is modified using 75% of carbon black and 25% of MoS_2. The morphology, in this case, agrees with a solid mixture of the two starting powders where the MoS_2 is embedded in the CB. Even in this case, the surface homogeneity of the final hybrid is quite good.

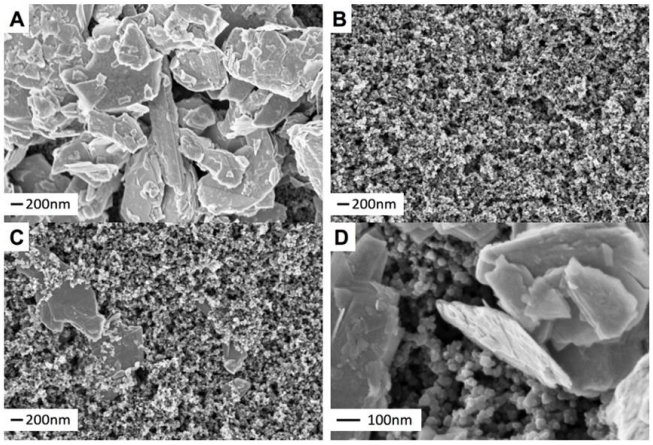

Figure III-3: SEM micrographs of A) exfoliated MoS2, B) CB, C) and D) CB-MoS2 hybrid at 75:25 ratio with magnification of 50 kX and 200 kX, respectively.

The presence of the MoS_2 in the SPE has been also confirmed by EDS. The EDS spectra reported in **Figure III-4** clearly show the K line for S and the L line for Mo both in the MoS_2 and in the CB-MoS_2 cases.

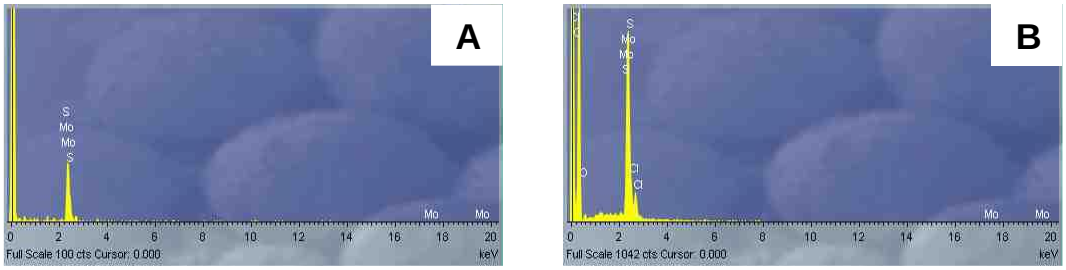

Figure III-4: EDS spectra of SPEs modified with A) Exfoliated MoS_2 B) CB-MoS_2 composite at 75:25. The small peak of Cl is associated with external contamination.

The homogeneity of each SPE can be appreciated in the low magnification micrographs reported in **Figure III-5A-C**. Interestingly. We can observe that the layered structure of MoS_2 flakes is retained in all samples even after deposition as shown in **Figure III-5D**.

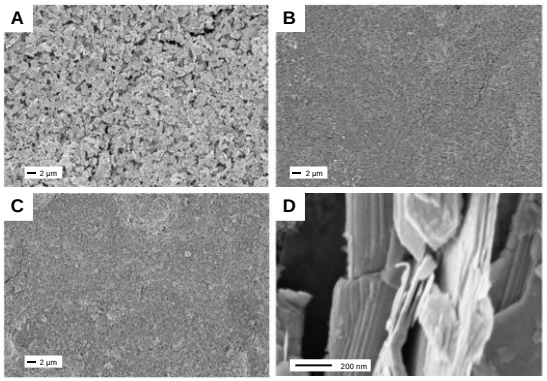

Figure III-5: SEM micrographs of A) Exfoliated MoS_2 B) CB C) CB-MoS_2 composite at 75:25 ratio with magnification of 5 kX. Panel D) Detail of case a) Exfoliated MoS_2 with magnification 200 kX.

III.3.2. Electrochemical behavior of o-diphenols at CB-MoS_2

The electrochemical performance was tested using catechol as a representative molecule of o-diphenols. Interestingly, as shown in **Figure III-6**, the improved performance, exhibited by CB-MoS_2, was evident in terms of reversibility and sensitivity, not only with respect to the bare SPE but also with respect to the electrodes modified with the individual nanomaterials (CB and MoS_2). A progressive decrease in the peak-to-peak separation is also observed from the bare electrode (ΔE_p=280 mV) to CB (ΔE_p=185 mV), MoS_2 (ΔE_p=177 mV) and CB-MoS_2 (ΔE_p=130 mV). Furthermore, the peak intensity increases 1.38 times for MoS_2, 1.69 for CB and 2.14 for CB-MoS_2 with respect to bare SPE. These results suggest the electrocatalytic effect of each nanomaterial, CB or MoS_2, towards catechol oxidation since both are able to increase the current due to catechol oxidation and decrease the peak-to-peak separation. In addition, a synergistic effect was markedly exhibited by CB-MoS_2 in comparison with each nanomaterial individually, revealing for the first time the electroanalytical capabilities of these nanohybrid transducers. These results are in accordance with literature, where CB has been already described as an effective nanomaterial for PPs sensing [28]. In addition, MoS_2 together with noble metal nanoparticles was used for improving catechol sensing [29]. Furthermore, the ability of Mo(VI) salts to form complexes with o-diphenols has been previously exploited by our group for selective voltammetric o-diphenols sensing [30]. This interaction between Mo and o-diphenols may explain the improvement in the signal towards o-diphenols oxidation.

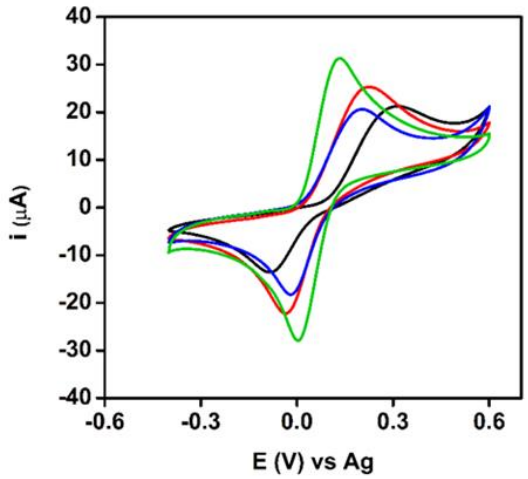

Figure III-6: CV of 1 mM Catechol in Phosphate Buffer (50 mM, 0.1 M KCl, pH=7) at SPE (black), CB (red), MoS_2 (blue) and CB-MoS_2 (green). Scan rate 50 mV s^{-1}.

III.3.3. Analytical performance and sample analysis at CB-MoS_2: determination of o-diphenols in EVOO and related samples

The CB-MoS_2 transducers were then used for the determination of the target analytes with o-diphenols function, as commonly found in natural products and foods. To this aim, Differential Pulse Voltammetry (DPV) was used for the determination of o-diphenols in EVOO and related samples. The highest signal was again observed for the CB-MoS_2 electrodes (see **Figure III-7A** and **Figure III-7C** for OLEU and HYT respectively). According to these results, CB-MoS_2-based electrochemical sensors appears to be optimal for sensing PPs with o-diphenols functions. Furthermore, as fouling is one of the drawbacks in the electrochemical sensing of PPs, the fouling resistance ability of the different electrodes was tested towards OLEU, the EVOO o-diphenol with the highest fouling effect. Measurements using DPV were performed in order to evaluate the effect of repetitive measurements on peak intensity. As shown in **Figure III-7B**, the retained signal was 86% for CB-MoS_2 after 10 measurements, demonstrating a very good fouling resistance (RSD<8%, n=10). This retained signal was higher than in the case of CB (53%) and bare electrodes (38%). Interestingly, the values obtained in the hybrid nanomaterial are close to those of MoS_2 itself (84%), demonstrating the key role of this material in the antifouling properties.

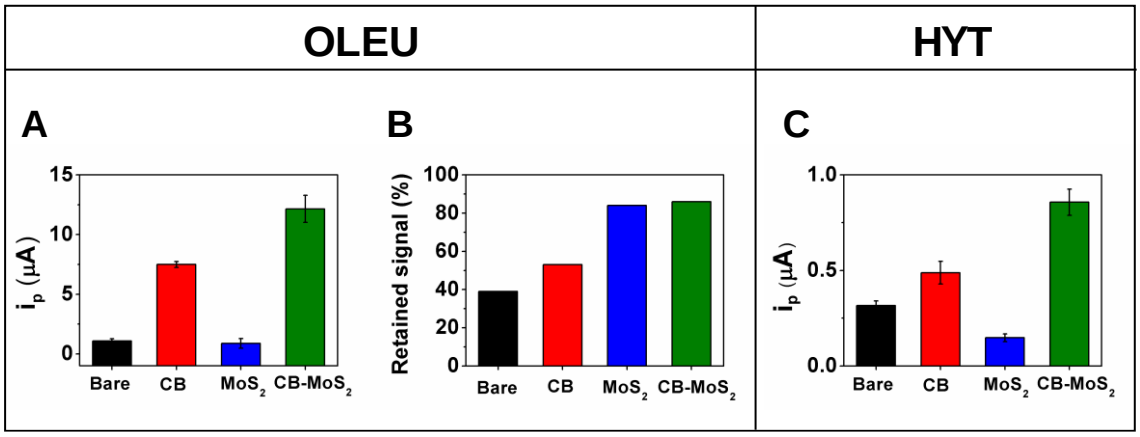

Figure III-7: A) DPV peak current intensities for OLEU B) fouling resistance of each SPE (n=10 consecutive measurements of OLEU) and C) DPV peak current intensities for HYT. Experiments carried out in Phosphate Buffer (50 mM, 0.1M KCl, pH=7) containing 10 and 5 µM of OLEU and HYT respectively with pulse amplitude of 25 mV and a scan rate of 50 mV s^{-1}.

CB-MoS_2 were then used for the determination of the target analytes in EVOO and related samples. **Figure III-8** shows the DPV calibration voltammograms (and the corresponding calibration linear plot in the inset) of OLEU and HYT at CB-MoS_2 electrodes obtained for each concentration assayed. Peak current intensities for building the calibration plot are obtained at 55 mV and 59 mV for HYT and OLEU, respectively. The linear range is obtained in the 0.30-30 and 2-100 µM range for OLEU and HYT, respectively. The linear regression equations are ip(µA)=-0.05(±0.02)+1.33(±0.02) [OLEU] (µM) and ip(µA)=0.041(±0.007)+0.151(±0.002)[HYT] (µM). The LODs (S/N=3) are 0.1 and 1.0 µM for OLEU and HYT respectively. Inter-electrode reproducibility for OLEU and HYT was also evaluated and values of 9% and 8% (n=5) were respectively obtained.

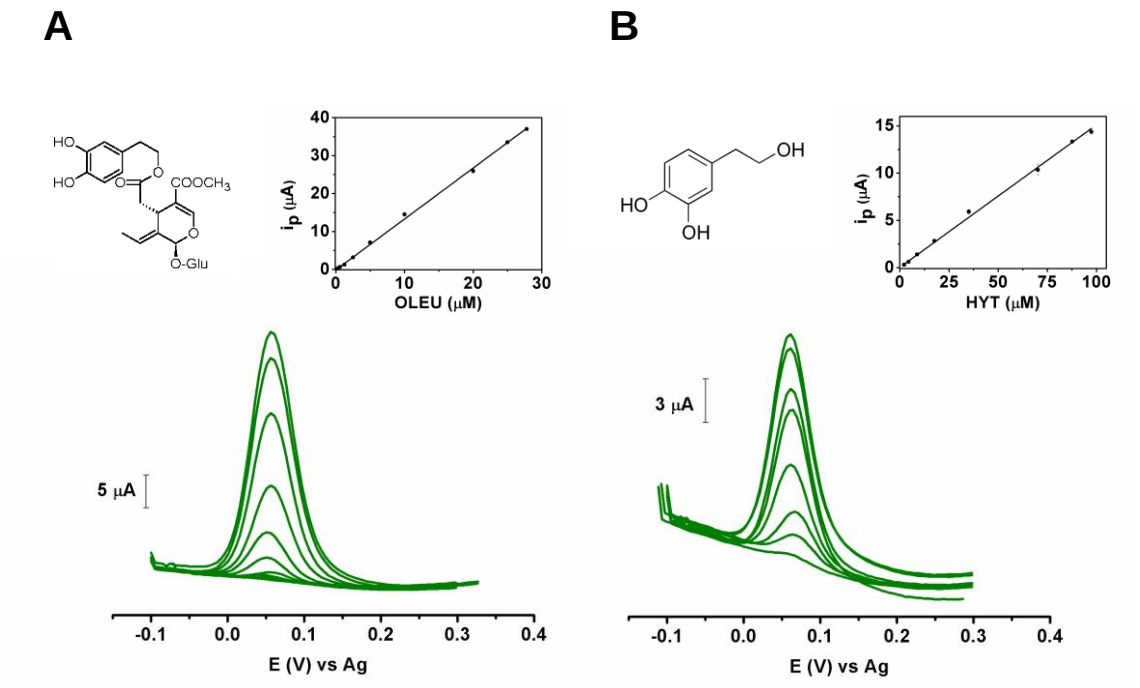

Figure III-8: DP voltammograms for calibration concentrations of a) OLEU and b) HYT in Phosphate Buffer (50 mM, 0.1M KCl, pH=7). Inset shows the corresponding calibration plot. The DPV parameters were pulse amplitude of 25 mV and a scan rate of 50 mV s^{-1}.

For comparison, **Table III-1** shows recently reported electrochemical sensors for OLEU and HYT determination. In most of the cases, a stripping step is required which is time-consuming. The proposed method shows the advantage of faster analysis time by avoiding stripping step maintaining comparable analytical performance. In addition, the lower oxidation potential for the o-diphenols oxidation is a further confirmation of the electrocatalytic behavior of the hybrid nanomaterial.

Table III-1: Nanomaterial-based electrochemical sensors for determination of OLEU and HYT

Nanomaterial	Technique	Detection potential	Linear range (µM)		LOD (µM)		Analytical remarks	Ref
			OLEU	HYT	OLEU	HYT		
CB	DPV	133 mV vs Ag/AgCl	-	10–75	-	6	High fouling resistance (RSD_{HTYR}<12%, n=28) Analysis of EVOO samples	[31]
GCE/MWCNTs	AdSWV	540 mV vs Ag/AgCl (sat. KCl)	0.01–0.70	-	0.003	-	15 min accumulation time Analysis of Olive Leaf extracts Comparison with LC-MS/MS method	[32]
LGH-GOPGE	AdDPV	Not reported	0.10 – 37	-	0.030	-	Analysis of Olive Leaf extract	[33]
DNA-coated CHIT/CPE	AdDPV	210 mV vs Ag/AgCl	0.3-12	-	0.090	-	10 min accumulation time Analysis of Olive Leaf and serum	[34]
CB-MoS2	DPV	55 and 59 mV vs Ag for HYT and OLEU respectively	0.3-30	2-100	0.1	1	High fouling resistance (RSD_{OLEU}<8%, n=10) Analysis of EVOO and related samples High correlation with HPLC (r=0.995) High agreement in quantitative levels obtained by HPLC	Present work

Finally, the results obtained for the quantitative determination of o-diphenols in EVOO and related samples using CB-MoS_2-based electrochemical sensors and an HPLC-UV method are listed in **Table III-2**. The methods were highly correlated (r=0.995), with a slope of 1.03±0.04 and intercept of 21±83, expressed as $a \pm ts_a$ and $b \pm ts_b$, ($p<0.05$), respectively. Since intercept confidence interval contained 0 and slope confidence interval contained 1, both methods did not show significant statistically differences ($p<0.05$). These results indicate that although the CB-MoS_2 sensors are not able to selectively differentiate among HYT and OLEU, the results for total o-diphenols content were highly in agreement with those reported by HPLC-UV method.

Table III-2: Quantitative determination of o-diphenols in EVOO and related samples using CB-MoS_2-based electrochemical sensor and HPLC[a]

	CB-MoS_2-electrochemical sensor[b]		**HPLC-UV**[c]	
Sample	**OLEU eq.** (mg Kg^{-1})	**RSD** (%)	**o-diphenols** (mg Kg^{-1})	**RSD** (%)
Dietary Supplement	5708±562	10	5534±277	5
Olive Leaf 1	1286±55	4	1302±91	7
Olive Leaf 2	1193±97	8	1007±50	5
EVOO 1	129±16	13	115±2	2
EVOO 2	156±15	12	164±18	11
EVOO 3	45±3	7	36±6	15

[a]Results expressed as mean value ± standard deviation (n=3), RSD=Relative Standard deviation.
[b]Expressed as OLEU equivalents.
[c]Expressed as sum of each individual OLEU and HYT.

III.4. Conclusions

Hybrid CB-MoS_2 transducers have shown an enhanced electrochemical (improved charge-transfer ability, low charge-transfer resistance, high electrical conductivity, enhanced electrocatalysis) and analytical (stripping-free fast and sensitive voltammetric detection, and remarkably reduced fouling) performances compared to individual nanomaterials. Furthermore, the comparison between the CB-MoS_2-based electrochemical sensor and HPLC-UV method have demonstrated that both methods were not only highly correlated ($r=0.995$), but they did not show significant statistically differences ($p<0.05$). This demonstrates the reliability of CB-MoS_2 sensors for the determination of target o-diphenols in the analysis of complex EVOO and related samples. These results open new perspectives for hybrid carbon/transition metal dichalcogenides based nanomaterials for on-site and decentralized sensing in fields of miscellanea significance.

III.5. References

[1] T.A. Silva, F.C. Moraes, B.C. Janegitz, O. Fatibello-Filho, Electrochemical Biosensors Based on Nanostructured Carbon Black: A Review, J. Nanomater. 2017 (2017) 1–14. doi:10.1155/2017/4571614.

[2] F. Della Pelle, C. Angelini, M. Sergi, M. Del, A. Pepe, D. Compagnone, M. Del Carlo, A. Pepe, D. Compagnone, Nano carbon black-based screen printed sensor for carbofuran, isoprocarb, carbaryl and fenobucarb detection: application to grain samples, Talanta. 186 (2018) 389–396. doi:10.1016/j.talanta.2018.04.082.

[3] D. Rojas, F. Della Pelle, M. Del Carlo, M. d'Angelo, R. Dominguez-Benot, A. Cimini, A. Escarpa, D. Compagnone, Electrodeposited Prussian Blue on carbon black modified disposable electrodes for direct enzyme-free H2O2 sensing in a Parkinson's disease in vitro model, Sensors Actuators B Chem. 275 (2018) 402–408. doi:10.1016/J.SNB.2018.08.040.

[4] S. Cinti, N. Colozza, I. Cacciotti, D. Moscone, M. Polomoshnov, E. Sowade, R.R. Baumann, F. Arduini, Electroanalysis moves towards paper-based printed electronics: carbon black nanomodified inkjet-printed sensor for ascorbic acid detection as a case study, Sensors Actuators B Chem. 265 (2018) 155–160. doi:10.1016/J.SNB.2018.03.006.

[5] F. Della Pelle, L. Vázquez, M. Del Carlo, M. Sergi, D. Compagnone, A. Escarpa, Press-Printed Conductive Carbon Black Nanoparticle Films for Molecular Detection at the Microscale, Chem. - A Eur. J. 22 (2016) 12761–12766. doi:10.1002/chem.201601743.

[6] F. Della Pelle, M. Del Carlo, M. Sergi, D. Compagnone, A. Escarpa, Press-transferred carbon black nanoparticles on board of microfluidic chips for rapid and sensitive amperometric determination of phenyl carbamate pesticides in environmental samples, Microchim. Acta. 183 (2016) 3143–3149. doi:10.1007/s00604-016-1964-7.

[7] M. Pumera, A.H. Loo, Layered transition-metal dichalcogenides (MoS_2 and WS_2) for sensing and biosensing, TrAC Trends Anal. Chem. 61 (2014) 49–53. doi:10.1016/J.TRAC.2014.05.009.

[8] A. Hirsch, F. Hauke, Post-Graphene 2D Chemistry: The Emerging Field of Molybdenum Disulfide and Black Phosphorus Functionalization, Angew. Chemie - Int. Ed. 57 (2018) 4338–4354. doi:10.1002/anie.201708211.

[9] A. Sinha, Dhanjai, B. Tan, Y. Huang, H. Zhao, X. Dang, J. Chen, R. Jain, MoS2 nanostructures for electrochemical sensing of multidisciplinary targets: A review, TrAC Trends Anal. Chem. 102 (2018) 75–90. doi:10.1016/J.TRAC.2018.01.008.

[10] V. Mani, M. Govindasamy, S.-M.M. Chen, R. Karthik, S.-T.T. Huang, Determination of dopamine using a glassy carbon electrode modified with a graphene and carbon nanotube hybrid decorated with molybdenum disulfide flowers, Microchim. Acta. 183 (2016) 2267–2275. doi:10.1007/s00604-016-1864-x.

[11] I. Vasilescu, S.A.V. Eremia, M. Kusko, A. Radoi, E. Vasile, G.-L. Radu, Molybdenum disulphide and graphene quantum dots as electrode modifiers for laccase biosensor, Biosens. Bioelectron. 75 (2016) 232–237. doi:10.1016/J.BIOS.2015.08.051.

[12] K.J. Huang, J.Z. Zhang, Y.J. Liu, L.L. Wang, Novel electrochemical sensing platform based on molybdenum disulfide nanosheets-polyaniline composites and Au nanoparticles, Sensors Actuators, B Chem. 194 (2014) 303–310. doi:10.1016/j.snb.2013.12.106.

[13] X. Li, X. Du, Molybdenum disulfide nanosheets supported Au-Pd bimetallic nanoparticles for non-enzymatic electrochemical sensing of hydrogen peroxide and glucose, Sensors Actuators, B Chem. 239 (2017) 536–543. doi:10.1016/j.snb.2016.08.048.

[14] S. Ji, Z. Yang, C. Zhang, Y.E. Miao, W.W. Tjiu, J. Pan, T. Liu, Nonenzymatic sensor for glucose based on a glassy carbon electrode modified with $Ni(OH)_2$ nanoparticles grown on a film of molybdenum sulfide, Microchim. Acta. 180 (2013) 1127–1134. doi:10.1007/s00604-013-1035-2.

[15] I. Hassen, H. Casabianca, K. Hosni, Biological activities of the natural antioxidant oleuropein: Exceeding the expectation – A mini-review, J. Funct. Foods. 18 (2015) 926–940. doi:10.1016/J.JFF.2014.09.001.

[16] F. Della Pelle, A. Scroccarello, M. Sergi, M. Mascini, M. Del Carlo, D. Compagnone, Simple and rapid silver nanoparticles based antioxidant capacity assays: Reactivity study for phenolic compounds, Food Chem. 256 (2018) 342–349. doi:10.1016/j.foodchem.2018.02.141.

[17] C. Angeloni, M. Malaguti, M.C. Barbalace, S. Hrelia, C. Angeloni, M. Malaguti, M.C. Barbalace, S. Hrelia, Bioactivity of Olive Oil Phenols in Neuroprotection, Int. J. Mol. Sci. 18 (2017) 2230. doi:10.3390/ijms18112230.

[18] F. Della Pelle, D. Compagnone, Nanomaterial-Based Sensing and Biosensing of Phenolic Compounds and Related Antioxidant Capacity in Food, Sensors. 18 (2018) 462. doi:10.3390/s18020462.

[19] A. Scroccarello, F. Della Pelle, L. Neri, P. Pittia, D. Compagnone, Silver and gold nanoparticles based colorimetric assays for the determination of sugars and polyphenols in apples, Food Res. Int. 119 (2019) 359–368. doi: 10.1016/j.foodres.2019.02.006.

[20] F. Della Pelle, M.C.M.C.M.C. González, M. Sergi, M. Del Carlo, D. Compagnone, A. Escarpa, Gold Nanoparticles-based Extraction-Free Colorimetric Assay in Organic Media: An Optical Index for Determination of Total Polyphenols in Fat-Rich Samples, Anal. Chem. 87 (2015) 6905–6911. doi:10.1021/acs.analchem.5b01489.

[21] I. Ignat, I. Volf, V.I. Popa, A critical review of methods for characterisation of polyphenolic compounds in fruits and vegetables, Food Chem. 126 (2011) 1821–1835. doi:10.1016/J.FOODCHEM.2010.12.026.

[22] T.A. Enache, A.M. Oliveira-brett, Phenol and para -substituted phenols electrochemical oxidation pathways, J. Electroanal. Chem. 655 (2011) 9–16. doi:10.1016/j.jelechem.2011.02.022.

[23] F. Della Pelle, D. Vilela, M.C. González, C. Lo Sterzo, D. Compagnone, M. Del Carlo, A. Escarpa, Antioxidant capacity index based on gold nanoparticles formation. Application to extra virgin olive oil samples, Food Chem. 178 (2015) 70–75. doi:10.1016/j.foodchem.2015.01.045.

[24] F.M. Pirisi, P. Cabras, C.F. Cao, M. Migliorini, M. Muggelli, Phenolic Compounds in Virgin Olive Oil. 2. Reappraisal of the Extraction, HPLC Separation, and Quantification Procedures, J. Agric. Food Chem. 48 (2000) 1191–1196. doi:10.1021/jf991137f.

[25] M.D. Petit-Domínguez, C. Quintana, L. Vázquez, M. del Pozo, I. Cuadrado, A.M. Parra-Alfambra, E. Casero, Synergistic effect of MoS2 and diamond nanoparticles in electrochemical sensors: determination of the anticonvulsant drug valproic acid, Microchim. Acta. 185 (2018) 334. doi:10.1007/s00604-018-2793-7.

[26] H. Huang, J. Zhang, M. Cheng, K. Liu, X. Wang, Amperometric sensing of hydroquinone using a glassy carbon electrode modified with a composite consisting of graphene and molybdenum disulfide, Microchim. Acta. 184 (2017) 4803–4808. doi:10.1007/s00604-017-2531-6.

[27] G. Ferraro, E. Fratini, R. Rausa, P. Fiaschi, P. Baglioni, Multiscale Characterization of Some Commercial Carbon Blacks and Diesel Engine Soot, Energy & Fuels. 30 (2016) 9859–9866. doi:10.1021/acs.energyfuels.6b01740.

[28] D. Talarico, F. Arduini, A. Constantino, M. Del Carlo, D. Compagnone, D. Moscone, G. Palleschi, Carbon black as successful screen-printed electrode modifier for phenolic compound detection, Electrochem. Commun. 60 (2015) 78–82. doi:10.1016/J.ELECOM.2015.08.010.

[29] S. Su, W. Cao, C. Zhang, X. Han, H. Yu, D. Zhu, J. Chao, C. Fan, L. Wang, Improving performance of MoS2-based electrochemical sensors by decorating noble metallic nanoparticles on the surface of MoS2 nanosheet, RSC Adv. 6 (2016) 76614–76620. doi:10.1039/c6ra12401a.

[30] M. Del Carlo, A. Amine, M. Haddam, F. Della Pelle, G.C. Fusella, D. Compagnone, Selective voltammetric analysis of o-diphenols from olive oil using Na2MoO4 as electrochemical mediator, Electroanalysis. 24 (2012) 889–896. doi:10.1002/elan.201100603.

[31] F. Della, R. Di, L. Vázquez, F.J. Palomares, M. Del, M. Sergi, D. Compagnone, A. Escarpa, Press-transferred carbon black nanoparticles for class-selective antioxidant electrochemical detection, Appl. Mater. Today. 9 (2017) 29–36. doi:10.1016/j.apmt.2017.04.012.

[32] M. Cittan, S. Koçak, A. Çelik, K. Dost, Determination of oleuropein using multiwalled carbon nanotube modified glassy carbon electrode by adsorptive stripping square wave voltammetry, Talanta. 159 (2016) 148–154. doi:10.1016/J.TALANTA.2016.06.021.

[33] F.J. V. Gomez, A. Spisso, M. Fernanda Silva, Pencil graphite electrodes for improved electrochemical detection of oleuropein by the combination of Natural Deep Eutectic Solvents and graphene oxide, Electrophoresis. 38 (2017) 2704–2711. doi:10.1002/elps.201700173.

[34] M. Mohamadi, A. Mostafavi, M. Torkzadeh-Mahani, Electrochemical determination of biophenol oleuropein using a simple label-free DNA biosensor, Bioelectrochemistry. 101 (2015) 52–57. doi:10.1016/j.bioelechem.2014.07.003.

IV. High-performance carbon black/molybdenum disulfide nanohybrid sensor for cocoa catechins determination using an extraction-free approach

IV.1. Introduction and objectives

Recent trends in food science suggest that cocoa and cocoa-products present multiple-benefits which are becoming subject of increased scientific research, mainly because of their phytochemical composition [1,2]. In fact, the high PPs content of cocoa has generated a renewed interest for nutritional and health viewpoints [3], and thanks to these properties, the global demand for cocoa is increasing [4]. In the cocoa-based products market, the cocoa content results to be an added value, influencing price and the organoleptic properties [5]. Cocoa is rich in flavanols and proanthocyanidins, strong antioxidants, which have been associated with several potential health benefits [1,3]. Moreover, they also affect the cocoa fat resistance towards oxidation, during the production process and conservation [3,6–8]. In fact, the final content of antioxidant compounds in cocoa-based products is a function of several variables related to the raw material and others related to processing and formulation [3,6–8].

Cocoa catechins contents and their antioxidant capacity evaluation still challenging, for the complexity of the matrix. Indeed, the extraction step is necessary to remove the possible interfering compounds, separate the PPs from the lipids, but can lead to low recovery, resulting in consumption of solvents and time [9]. The cocoa polyphenolic extracts classically are analyzed with spectrophotometric assays or chromatographic methods [2,3,10–14]; the latter can provide identification of the constituents and amount, but do not returns direct information on the antioxidant capacity of PPs [15]. Classical spectrophotometric methods are simple but can present some disadvantages as the use of expensive reagents, not environmentally friendly undefined reaction time, long sample pretreatment, and low precision, selectivity, and sensitivity [16]. Several other methods have been proposed for PPs cocoa analysis, as e.g. capillary electrophoresis [17], NIR [18] and FT-IR spectroscopy [19], and only few methods do not require sample preparation and extraction [9].

Electrochemical sensors represent a valuable alternative approach to the detection of PPs and antioxidant capacity [15,16] and different electrochemical approaches for the direct sensing using several electrodes/transducers types and configurations have been proposed [15,16,20–22]. However, direct electrochemical oxidation of PPs onto

classical unmodified carbon-based materials is affected by the typical drawback of fouling [15,23]. This phenomenon is particularly relevant for flavanols structures [24]. In fact, the redox behavior of catechins onto carbon electrodes, despite being initially apparently reversible, results in an electrode surface irreversible passivation [25]. The passivation is caused by adsorption and polymerization of oxidation products onto the working electrode surface [15,23]. Nanomaterials (NMs) have attracted attention since they can reduce the passivation of the electrode area, potentially also improving sensitivity and selectivity [15,26–30]. Different NMs have been used for catechins direct sensing purposes, as nanotubes [31], graphene [32,33], and nanoparticles based. [24,34–38]. However, the catechins by-products of oxidation tendency to interact with the electrode surface is strong and this does not allow reproducible and accurate analysis. In fact, very often the electrochemical behavior of the catechins is studied as proof of concept, without a deep study of both passivation and exploitability using complex samples [15]. This drawback and the need of an extraction step have limited the use of electrochemical sensors in this field, for example, as very few applications of sensors on cocoa samples are reported in literature [35,38].

In the last years, carbon black (CB) has been widely employed for building electrochemical platforms. Its particular features stimulated intense research efforts; in fact, CB nanospheres possess high surface area, high electrical conductivity, low cost, and high dispersibility and can be easily prepared for the realization of electrochemical sensors [15,39–42]. On the other hand, transition Metal Dichalcogenides (TMDs) materials have become an attractive alternative for electrochemical applications [43]. Layered transition-metal dichalcogenides WS_2 and MoS_2, have attracted increasing interest as modifiers of working surfaces for HER [44,45] and energy storage [46–48]. The use of MoS_2 in electrochemical sensing is a growing field and holds great promise in sensors and biosensors development [49–51]. However, despite the carbon black have been used for the construction of some electrodes for the direct PPs detection [15,52], even in foods matrices as olive oil[53], the potential of the use of MoS_2 in the direct detection of PPs has not been yet exploited; just a paper reported on the MoS_2 as electrode modifier for laccase biosensor used for red wine PPs indirect estimation [54].

In the last years MoS_2-based nanocomposites have attracted researchers' attention [49]; since some MoS_2 hybrid materials have shown great versatility as advanced electrode modifier, showing unique and sometimes unexpected sensing properties and catalytic activity [51,55,56]. The integration of carbon-based NMs [54,57], metal [58] or metal oxide nanoparticles [56] in MoS_2 structures has been reported to have synergistic effects, exploitable in the electrochemical sensing.

In the present chapter we aim to explore catechins determination ability on a new CB/MoS_2 nanohybrid electrode (SPE CB-MoS_2) and to test the regenerability and antifouling properties of the sensor. The developed sensor was then applied to the assessment of the catechins content of 59 cocoa powder samples. The results obtained for the 59 cocoa powder samples are compared with classical methods as FC, ABTS and gold nanoparticles based (AuNPs) assay.

IV.2. Materials and methods

IV.2.1. Reagents and stock solutions

MoS_2, Epicatechin, catechin, epigallocatechin, cetyltrimethylammonium chloride (CTAC; 25% in water), hydrogen tetracholoroaurate ($HAuCl_4 \cdot 3H_2O$, 99.9%), 2,2-azino-bis(3- ethylbenzothiazoline-6-sulphonic acid) (ABTS), sodium carbonate (Na_2CO_3), Folin & Ciocalteu's phenol reagent, sodium phosphate monobasic monohydrate ACS reagent ($NaH_2PO_4 \cdot H_2O$) sodium phosphate dibasic anhydrous (Na_2HPO_4), potassium ferrocyanide, potassium ferricyanide, potassium chloride, methanol, N, N-dimethylformamide, dimethyl sulfoxide (DMSO), acetonitrile, acetic acid, sodium acetate, formic acid were purchased from Sigma Aldrich (St Louis, MO, USA). CB N220 was obtained from Cabot Corporation (Ravenna, Italy). PPs stock solutions were prepared in methanol at a concentration of 1.0×10^{-2} mol L^{-1} and stored in the dark at - 20 °C. Milli-Q water (18.2 MΩ) was employed for all the experiments.

IV.2.2. Apparatus

Electrochemical measurements were carried out using an Autolab PGSTAT 12 potentiostat from Metrohm (Utrecht, Netherlands), screen-printed electrodes (SPE) were purchased from Dropsens S.L. (ref. DS110). Samples were shaken and centrifuged with an SSL1 orbital shaker from Stuart equipment (Belfast, UK) and an ALC4237R refrigerated centrifuge (ALC Intl., Cologno Monzese, Italy), respectively. For the gold nanoparticles assay, the reaction was performed in a water bath using a 720 D thermostat digital group (Asal, Italy). Absorbance was recorded using a JENWAY 6400 spectrophotometer from Barlworld Scientific (Staffordshire, UK,).

IV.2.3. Samples

A large number (59) of commercially available cocoa powder samples were analyzed. The investigated samples, coming from different varieties of cocoa and subjected to different production processes, were codified with numbers from 1 to 59 for reasons of corporate confidentiality. The samples were stored in plastic bags with pressure closure and kept in a cool, dry and dark place to avoid degradation phenomena.

In order to speed up the analysis, cocoa catechins were directly solubilized in DMSO, according to Della Pelle et al. 2015 [9], with some modifications. Briefly, 0.1 g of cocoa powder were weighted and solubilized in 1.5 mL of DMSO. The dispersion was vortexed for 1 min and sonicated in an ultrasonic bath for 5 min at a temperature of 20°C. Subsequently, the dispersion was centrifuged at 12000 rpm for 5 minutes at a temperature of + 4 °C for 10 min. The resulting supernatant was recovered and stored at – 20°C in the dark until analysis. In order to prove the effectiveness, of the proposed sample pretreatment, the samples have been extracted even according to Gu et al. [59], in this case, the defatting step [8] is followed by a solid-liquid extraction [59]. Both extracts, prior to each further analysis, were diluted to the appropriate dilution in 0.01 mol L^{-1} (pH 7.0) phosphate buffer (PB).

IV.2.4. Preparation of the SPE-CB/MoS_2

CB and MoS_2 dispersion volume, ratio/concentration and solvent were optimized in order to obtain the most effective electrodes in terms of sensitivity and reproducibility. The CB and MoS_2 dispersions (1 mg mL^{-1}) were separately prepared in DMF-H20 1:1 (v/v) using a bath sonicator (3000683 Ultrasons Selecta, Barcelona, Spain) for 5 h at a temperature below 20 °C. The CB-MoS_2 75:25 (v/v) dispersion was prepared by mixing CB and MoS_2 dispersions, the mix was further sonicated for 1h. If dispersion is not directly used, requires 1h of sonication prior to use. This solution was employed for the SPEs modification, performed via drop casting onto the working electrode surface in five steps, for a total of 10 µL allowing drying and solvent evaporation after each deposition, the latter process was sped up thanks to a warm light lamp. Before use, the electrodes were pretreated using CV (10 scans) in 0.1 mmol L^{-1} PB (pH 7) in 0.1 mol L^{-1} KCl, in the -0.30 V / +0.7 V potential range (vs. pseudo-Ag), using a scan rate of 0.5 V s^{-1}. This procedure was also employed for the electrode surface regeneration, after the measurement of catechins standards or samples.

IV.2.5. Morphological characterization

Field Emission Scanning Electron Microscopy (FE-SEM) was used to investigate the morphology of the SPE-CB/MoS_2 sensors. All experiments were performed with a ΣIGMA high-resolution scanning electron microscope (Carl Zeiss Microscopy GmbH, Germany). Measurements were conducted on uncoated samples with an acceleration potential of 2 kV and at a working distance of about 4 mm. All the micrographs were analysed with an image processing software (ImageJ, v.1.49.p) [60] in order to evaluate the mean dimension of the MoS_2 crystals and the CB particles, together with the homogeneity of surface coverage and the relative percentage of MoS_2 and CB in the SPE-CB/MoS_2 electrode.

IV.2.6. Electrochemical measurements (CV, EIS, and DPV)

SPEs electrochemical behavior was investigated using CV and DPV. CVs of analytes were carried out using a scan rate of 50 mV s^{-1} in the potential range −0.20 V / +0.70 V (vs. pseudo Ag/AgCl) at different pHs: 4.0 and 5.0 in acetate buffer (0.01 mol L^{-1}) and pH 6.0, 7.0, 8.0 ,9.0 and 10.0 in phosphate buffer (0.01 mol L^{-1}). The electrode passivation, after catechins analysis, was further assessed by EIS using 5 mmol L^{-1} $[Fe(CN)_6]^{4-/3-}$ in 0.1M KCl. A sinusoidal wave with an amplitude of ± 10 mV was employed, in a frequency scan range 10^{-2}–10^5 Hz at open circuit potential, the results were analyzed by Nyquist plot (−Zre vs. Zim). DPV was used to quantify the analytes, the best DPV conditions were found using the simplex method, with the final aim to maximize the signal/noise ratio. DPVs were performed in phosphate 0.01 mol L^{-1} PB (pH 7.0), in a potential range of -0.15 to +0.35 V with a pulse width of 50 ms, and the final DPV pulse amplitude and scan rate were 20 mV and 50 mV s^{-1}, respectively. Before the use, the electrodes were pretreated with CVs (5 scans) in 0.1 mmol L^{-1} PB (pH 7) in 0.1 mol L^{-1} KCl, in the potential range of -0.30 V and +0.7 V (vs. pseudo-Ag), using a scan rate of 0.5 V s^{-1}. The latter procedure was also employed for the electrode surface regeneration, after the measurement of catechins standards or samples.

IV.2.7. Methods comparison

Data obtained with the proposed sensor have been compared with 3 conventional methods PPs evaluation: ABTS, F.C., and AuNPs. Epicatechin standard solutions were used as reference standard to calibrate the methods. For each method, the possible DMSO reactivity/perturbation has been evaluated, however, there were no significant changes with respect to the aqueous solvent (at the dilution employed for the sample analysis).

Folin-Ciocalteu procedure

20 µL of a properly diluted cocoa sample, extracted in the conventional way and with the DMSO strategy (section 2.3), was added to 20 µL of Folin-Ciocalteu reagent and stirred for 3 min. Then, 400 µL of sodium carbonate (Na_2CO_3, 7.5%) and deionized water were added up to the final volume of 1000 µL. The solution was stirred at room temperature for 60 min, in the dark, and the total PPs content was determined at 760 nm.

ABTS assay procedure

ABTS reagent stock solution was prepared according to Re et al. 1999 [61], the resulting radical $ABTS^{\cdot+}$ solution was diluted to reach an absorbance, reading at 734 nm, of 0.70 (±0.02). An appropriate diluted cocoa extract volume, extracted in the conventional way and with the DMSO strategy (section 2.3), was added to the ABTS reagent (final volume 2000 µL). Then the reaction mix was stored at room temperature for 5 min, in the dark, to evaluate the radical scavenging activity. The absorbance value at 734 nm was recorded and the sample mediated $ABTS^{\cdot+}$ shutdown was evaluated with respect to the blank/control, prepared without the sample addition (using the same amount and type of solvent used for extraction) with the following equation: absorbance decrease (%) = [(control absorbance value - sample absorbance value)/ control absorbance value]x100.

Gold nanoparticles assay procedure

AuNPs based colorimetric assay was used for the total PPs determination according to Della Pelle et al. 2015 [9]. For the AuNPs formation 30 µL of DMSO-cocoa powder extract, in the appropriate dilution, was mixed with 210 µL of DMSO and stirred for 1 min with an orbital shaker. Then, 25 µL of $HAuCl_4$ solution (2.0×10^{-2} mol L^{-1}) and 235 µL of phosphate buffer solution (pH 8.0; 1.0×10^{-2} mol $L^{-1)}$ were added (final volume 500 µL). The solution was mixed with an orbital shaker for 1 min and the reaction was started heating the reaction mix for 5 min at 45 °C in a water bath. Finally, the reaction was blocked at −20 °C for 5 min to allow measurements in series. The absorbance due to the AuNPs formation was recorded at 540 nm and evaluated after the blank subtraction (the blank was composed by reaction mix without sample).

IV.3. Results and discussion

IV.3.1. Electrochemical behavior of flavanols on hybrid CB/MoS2 transducers

In order to study the catechin (CT) electrochemical behavior 4 consecutive CVs have been carried out using a bare SPE and after each scan an EIS spectra has been recorded, as shown in **Figure IV-1**. The first cyclic voltammogram of CT performed using a bare SPE (**Figure IV-1A**, blue line), shows two anodic peaks, the potentials of the first (peak 1) and the second peak (peak 2) are 0.188 V and 0.481 V, respectively. A cathodic peak (peak 3) is observed at - 0.015 V; this reduction peak is related to the first oxidation peak which is a reversible reaction [25]. According to the literature, the oxidation mechanism proceeds in sequential steps, related with the catechol moiety (oxidation peak 1 and peak 3 reduction) and resorcinol group (peak 2) [25]. The first peak (catechol moiety) is higher compared with the current of resorcinol (peak 2) and remains in following scans; both behaviors are in agreement with the higher radical scavenging activity corresponding to ortho-diphenolic structures [25,53,62–64]. Noteworthy, in the following scans, the passivation process results evident, the oxidation product is not electroactive and passives more and more the electrode surface. This behavior is already reported by Brett group [25] onto a glassy carbon electrode. In fact, in this study is proved that the CT resorcinol group is irreversibly oxidized and the catechin moiety results strongly adsorbed on the electrode surface. The CT passivation [15,23,25] was also confirmed by EIS using $[Fe(CN)_6]^{4-/3-}$. Nyquist plots (**Figure IV-1B**) obtained by EIS exhibited a progressive increase of resistance to charge transfer (R_{ct}) scan by scan, in accordance with the CVs of CT. R_{ct} increased from 1.1 kΩ (before the first scan) to 41 kΩ (after 4 scans), clearly indicating a passivation process. Definitely, the CT strongly adsorbed on the SPE electrode surface and the final product is not electroactive and blocks the electrode surface.

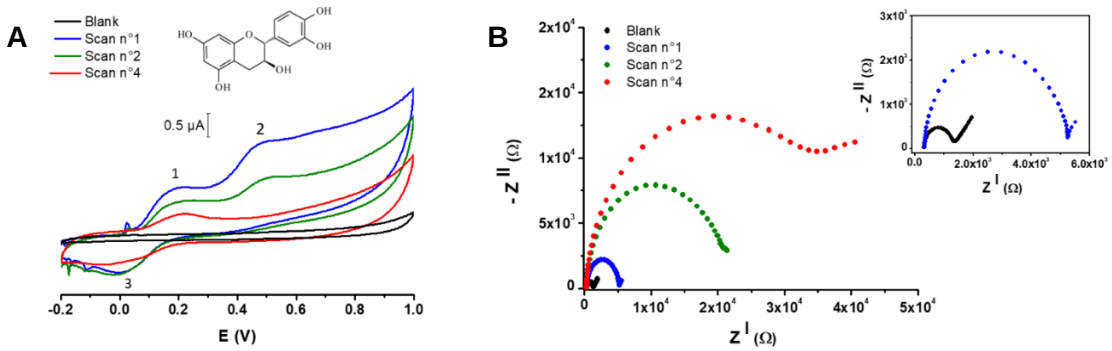

Figure IV-1: A) CVs of catechin (blue line) at 50 µmol L^{-1} performed with a bare SPE: 1st scan (blue line), 2nd scan (green line), 4th scan (red line), in black the scan performed before the catechin CV. CV performed in phosphate buffer 10 mmol L^{-1} + 0.1 mol L^{-1} KCl at pH 7.0 with a scan rate of 50 mV s^{-1}. B) Nyquist plots of 5 mmol L^{-1} $[Fe(CN)_6]^{4-/3-}$ in 0.1 KCl mol L^{-1} performed obtained with a bare SPE after the catechin CVs analysis reported in Figure 1A. After the1st scan (blue circles), 2nd scan (green circles), 4th scan (red circles), in black the Nyquist plot obtained before the catechin CV. In the inset a magnification of the Nyquist obtained before the CT CV (blank line) and after the 1st scan (blue line).

Once the electrochemistry in bare SPE was stated same study was carried on CB, MoS_2 and CB/MoS_2. Initially, cyclic voltammetry (CV) has been employed to study the electrochemical behavior of the SPE, SPE-CB, SPE-MoS_2 and SPE-CB/MoS_2 electrodes. The attention was focused on the first CT electron transfer reaction that occurs at very low positive potentials because is the relevant process for the radical scavenging activity [25,53,62–65]. In **Figure IV-2**, the CV curves obtained with 50 µmol L^{-1} of catechin in 0.01 mol L^{-1} PB (pH 7.0), at 50 mV s^{-1} scan rate, have been reported together with the relative blank (Phosphate Buffer), performed before and after the catechin scan. To confirm the irreversibility of the electrode passivation, the CT scan was followed by a mild surface regeneration (see section **IV.2.4**). Improved electrochemical performances, in term of peak intensity and reversibility, were obtained in all cases compared to bare SPE.

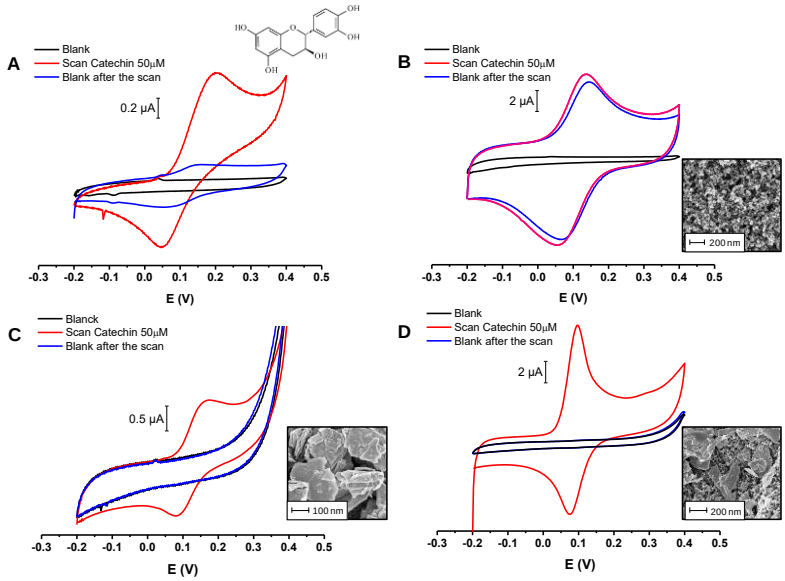

Figure IV-2: Cyclic voltammograms of the bare SPE A), SPE-CB B), SPE-MoS2 C), and SPE-CB/MoS2 D). Black line CV in 0.1 mmol L-1 PB (pH 7) + 0.1 mol L-1 KCl, before catechin CV. Red line CV of 50 µmol L-1 catechins (prepared in 0.1 mmol L-1 PB + 0.1 mol L-1 KCl, pH 7). Blue line CV in 0.1 mmol L^{-1} PB, pH 7 + 0.1 mol L^{-1} KCl, after catechins CV. CVs performed at a scan rate of 50 mV s^{-1}.

The bare SPE (**Figure IV-2A**) shows the worst response in term of oxidation currents ($i_{p,a}$ = 0.84 µA) and peak separation (ΔE_p = 147 mV) and an residual signal due to CT polymerization (blue line) after the scan and the regeneration step (5 CV scan in PB). These results are in accordance with literature [26], and the CV and EIS of **Figure IV-1** where catechin strongly adsorbs on the electrode surface hindering the electronic transfer. In **Figure IV-2B** is clearly showed that SPE-CB display a significant oxidation current increase ($i_{p,a}$ = 4.40 µA) lowering the oxidation potential of CT (SPE-CB $E_{p,a}$=142 mV vs .SPE $E_{p,a}$ =198mV) and showing a lower peak-to-peak separation (ΔE_p = 76 mV). However, in this case, the CT seems to remain attached to the electrode preserving the electroactivity and showing a residual current of the 97% (blue line). Similar behavior has been already reported for NMs, particularly with NMs with oxidized moieties [24] as in the case of CB [36,66]. Indeed, is reported that carboxyl and/or other oxygen-containing groups can behave as nucleophiles against the o-quinone ring (as Michael acceptor), leading to bond formation between flavanol and surface-active functional groups [24]. On the other hand, the SPE-MoS_2 (**Figure IV-2C**) displays just a slight increase of both oxidation peak ($i_{p,a}$ = 0.97 µA) and reversibility (ΔE_p= 88 mV) compared with the bare SPE, this because the MoS_2 has a low intrinsic

conductivity [44,46,57]. However, is noteworthy the total absence of residual signal (blue line) after the CT scan, this MoS_2 feature, at the best of our knowledge, has not been explored yet and could open new gates to MoS_2 application as an antifouling functional material. **Figure IV-2D** reports the SPE-CB/MoS_2 ability to merge the behavior of both materials. In fact, a significant enhancement of the analytical performance, compared to both the bare (SPE) and the single-NMs modified electrodes (SPE-CB and SPE-MoS_2) is showed. The ratio CB-MoS_2 75:25 (v/v) (from now this electrode will be named SPE-CB/MoS_2) was chosen, because higher amounts of MoS_2 (50 and 75 %, v/v) exhibited lower electrochemical improvements, as demonstrated in Chapter III, probably due to MoS_2 intrinsic low conductivity [44,46,57]. The SPE-CB/MoS_2 displays a significant increase in the oxidation current ($i_{p,a}$ = 9.7 µA) that occurs at lower potentials ($E_{p,a}$ = 98 mV). Moreover, a significant decrease in the ΔE_p (22 mV) was observed. Considering the obtained ΔE_p (near to 30 mV) the reaction involves two electrons that can be attributed to the 'catecholic ring' [25].

The pH effect was studied in **Figure IV-3** performing CV in a solution containing 25 µmol L^{-1} of CT. The peak intensities obtained at different pH catechin gave a straight line in the 4-8 pH range with a slope of 57 mV pH^{-1} unit. Considering these data, we can confirm a fast electron transfer with the same number of protons involved in the electrode reaction.

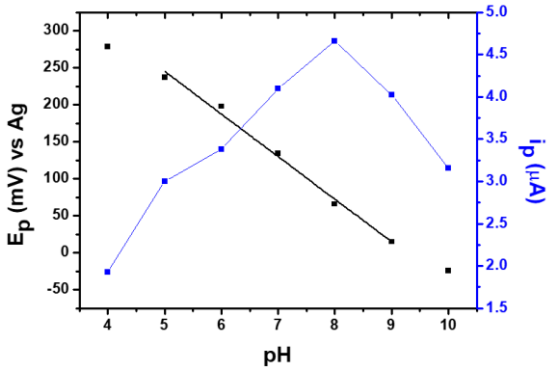

Figure IV-3: Influence of pH on anodic peak position and intensity for 25 µmol L^{-1} epicatechin. The cyclic voltammetry experiments were carried out in phosphate buffer at a scan rate of 25 mV/s.

The SPE-CB/MoS_2 modification performed with the 75% of CB and the 25 % of MoS_2 was able to totally prevent both the CT irreversible polymerization and the attachment onto the electrode surface. This behavior was confirmed in **Figure IV-4**, where the EIS of the SPE-CB/MoS_2 does not show any significant differences in the Nyquist plot after 4 consecutive scans of CT, confirming that the charge-transfer ability of the hybrid nanomaterial is not affected. In addition to the excellent electrochemical performance, a remarkable inter-electrode reproducibility was obtained in terms of $i_{p,a}$ and $E_{p,a}$ for the CT oxidation peak (RSD 1.2% and 3.5%, respectively, n=10).

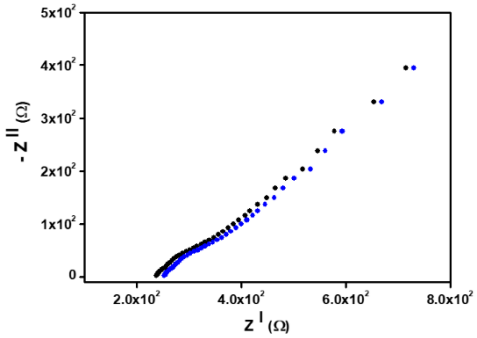

Figure IV-4: Nyquist plots of 5 mmol L^{-1} $Fe(CN)_6^{4-/3-}$ in 0.1 KCl mol L^{-1} obtained after (black circles) and before (blue circles) 4 consecutive 50 µmol L^{-1} catechin cyclic voltammetry scans, using the SPE-CB/MoS_2.

Figure IV-5 and **Figure IV-6** shows the SEM micrographs of the investigated electrodes. The SPE-MoS_2 is characterized by MoS_2 'crystals' with a broad size distribution centered around 870 ± 550 nm (see particle size distribution in **Figure IV-7**), composed by layers of stacked MoS_2 flakes, with the nanometric uniform side (SPE-MoS_2 magnification). In the micrograph of the SPE-CB (**Figure IV-6**) it is clearly visible the presence of CB primary units with a mean diameter of 20 ± 8 nm [67,68].

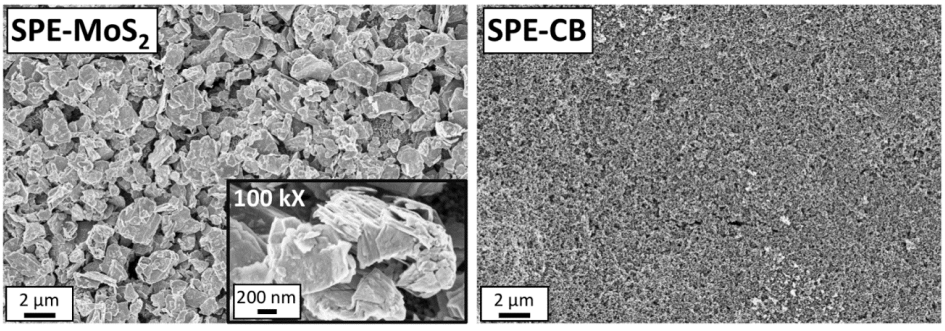

Figure IV-5: SEM micrographs of the SPE-MoS2 and SPE-CB.

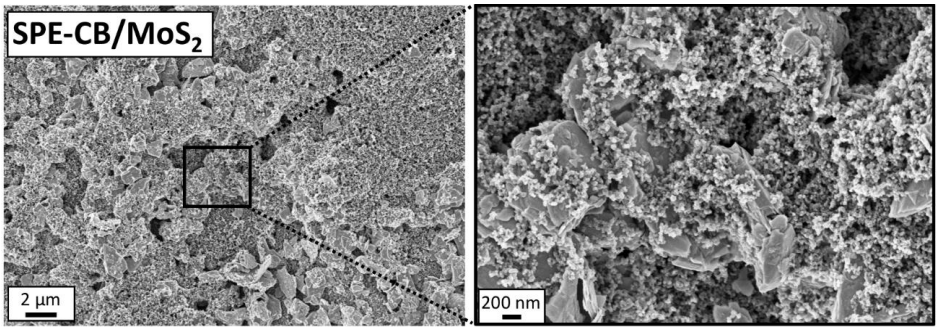

Figure IV-6: SEM micrograph and magnification of the SPE-CB/MoS_2.

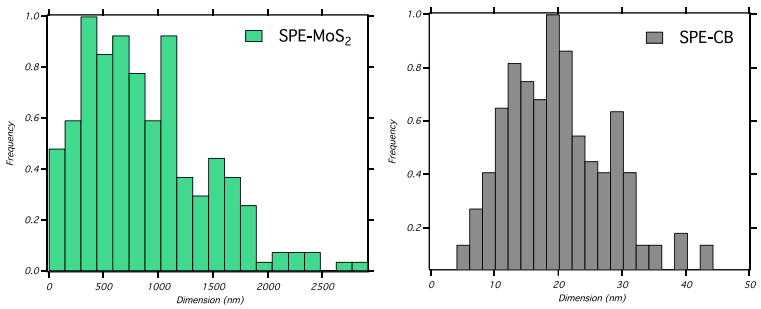

Figure IV-7: Particle size distributions obtained from the image analysis for the samples SPE-MoS_2 and SPE-CB. The distributions are calculated by measuring a consistent number of particles (more than 200 particles in the case of the sample SPE-MoS_2 and more than 400 for the SPE-CB sample).

The SPE-CB/MoS_2 shows the co-localization of MoS_2 crystals and carbon black primary particles; the two components interact but maintain their original morphology. The CB intercalation seems to reduce the MoS_2 natural tendency to restacking, with respect to the SPE-MoS_2, resulting in CB decorated MoS_2 flakes. In particular, the ~ 48% of the electrode surface is composed of MoS_2 'crystals' despite CB is added in a higher amount during the preparation of the electrode. This behaviour can be ascribed to the flakes-like conformation of MoS_2 that favours their floating to the surface.

The homogeneity of the obtained surfaces at the nanoscale was further evaluated by measuring the lacunarity of SEM micrographs. Lacunarity descriptor [69], which we calculated using the FracLac tool package [70] contained in ImageJ. The image lacunarity, Λ, is defined as the heterogeneity associated to an image: low values of lacunarity correspond to homogeneous systems.

Lacunarity can be calculated as follows:

$$\Lambda = \frac{\sum \lambda_g}{N_g}$$

where N_g is the number of orientations of the grid and λ_g is defined as:

$$\lambda_{\varepsilon,g} = \left(\frac{\sigma}{\mu}\right)^2_{\varepsilon,g}$$

where ε is the box dimension, g is the number of all possible orientations of the grid constituted by the different boxes, σ is the standard deviation of pixels per box and μ is the mean density of black pixels per box. Thus, there is a λ value for each ε in each series of grid size and for each g, in a set of grid orientations.

In our case, the lacunarity of the image was calculated by using the “Box Counting” algorithm with an ε value within 4 of the pixel size and a number of orientations, N_g, equal to 9. These parameters were adjusted in order to measure nanometric inhomogeneities. The calculation was performed on the micrographs with a magnification of 10 KX. The lacunarity values obtained for the different samples are 0.57, 0.23 and 0.37 for SPE-MoS_2, SPE-CB and SPE-CB/MoS_2, respectively.

As shown **Figure IV-8**, the SPE-CB electrode results in a more homogeneous surface at the nanometric level, while the lacunarity associated to the SPE-MoS_2 system is higher, in accordance with the broad size distribution of the MoS_2 crystals. Hence, as expected, the SPE-CB/MoS_2 presents an intermediate value of lacunarity with respect to the other two electrodes (SPE-CB and SPE-MoS_2), according to the co-presence of both CB and MoS_2 morphologies.

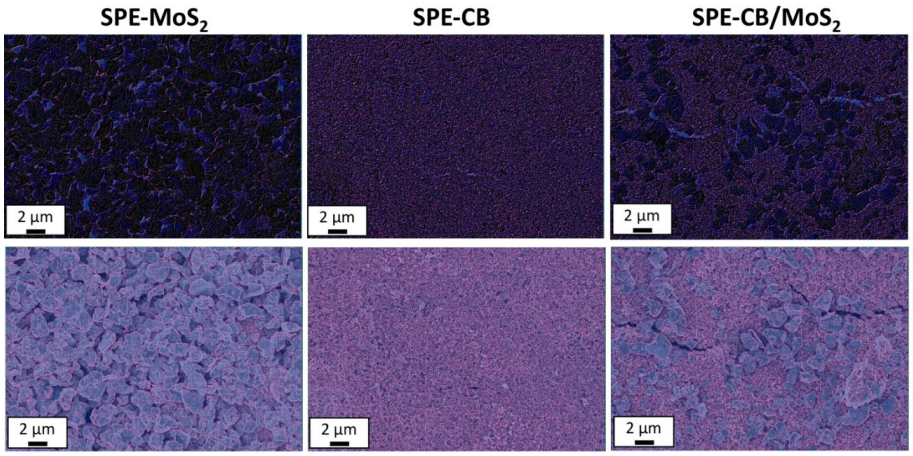

Figure IV-8: Top: Lacunarity grids obtained from the analysis of the SEM micrographs acquired on the different electrodes. Red corresponds to low values of lacunarity, blue indicates high lacunarity. Bottom: Overlay of lacunarity grids and SEM micrographs of all the investigated samples.

In order to assess the exploitability of the SPE-CB/MoS_2 for cocoa PPs analysis the proposed electrode has been tested against epicatechin (EP) and epigallocatechin (EG). These flavan-3-ols compounds, together with catechin, are the most abundant polyphenolic compounds of cocoa and chocolate and represent the monomers of the procyanidins [3,71].

The SPE-CB/MoS_2 again showed good electrochemical performance despite the EP and EG different chemical structure, resulting in different electrochemical behavior. In **Figure IV-9A** it is clearly noticed the EP increased oxidation current ($i_{p,a}$ = 10 µA) and the negative shift ($E_{p,a}$ = 88mV) in the oxidation potential with respect to the bare SPE ($i_{p,a}$ = 1.1 µA, $E_{p,a}$ = 198 mV). Moreover, in the case of EP, increased reversibility in terms of both peak intensity ratio and peak-to-peak separation was even recorded (ΔE_p = 19 mV). The CVs of EG (**Figure IV-9B**), despite the expected irreversible behaviour [72], allowed, also in this case, an $E_{p,a}$ negative shift (SPE-CB/MoS_2 $E_{p,a}$ = 69 mV vs SPE $E_{p,a}$ =120 mV) and a significantly improved anodic peak intensity ($i_{p,a}$ = 9.1 µA) compared to the bare SPE ($i_{p,a}$ = 1.6 µA). Even with EP and EG, the SPE-CB/MoS_2 totally prevent both the flavanols irreversible polymerization and the attachment to the electrode surface. In addition, despite the different structures of CT, EP and EG a very close oxidation current and oxidation potential have been obtained for all the compounds.

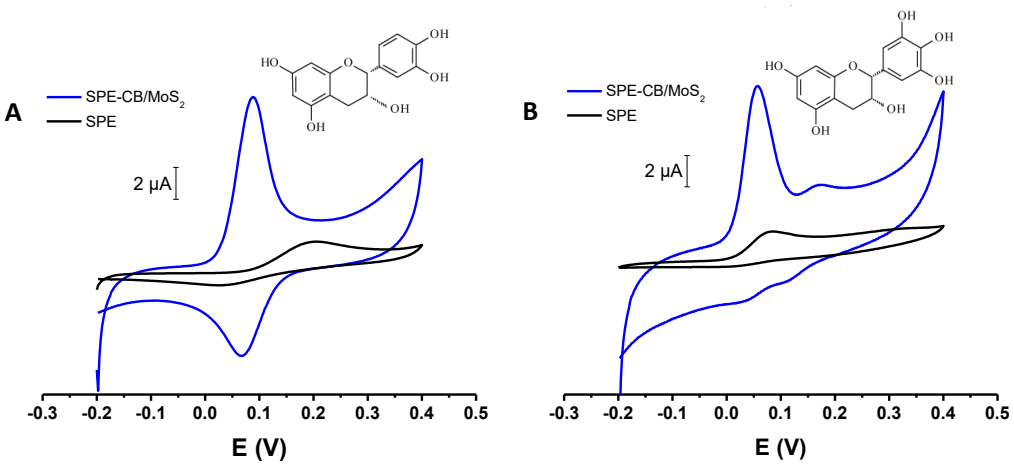

Figure IV-9: Cyclic voltammograms of the bare SPE (black line) and SPE-CB/MoS_2 (blue line) performed with 50 µmol L^{-1} epicatechin A) and epigallocatechin B) prepared in 0.1 mmol L^{-1} PB + 0.1 mol L^{-1} KCl (pH 7) at a scan rate of 50 mV s^{-1}.

IV.3.2. Analytical performance of hybrid CB/MoS_2 transducers for catechins determination

The analytical performance of the SPE-CB/MoS_2 sensor for quantitative analysis was carefully evaluated by studying the response toward CT, EP and EG using DPV under optimized parameters. **Figure IV-10** shows the voltammograms and the calibration curves obtained for the assayed concentrations of EP (A and D), CT (B and E) and EG (C and F) using the SPE-CB/MoS_2. Analytical figures of merit for the SPE-CB/MoS_2 towards CT, EP and EG detection are listed in **Table IV-1**.

Satisfactory linear range, sensitivity, and limit of detection were achieved in all the cases. Interestingly, all these analytical parameters are similar among them confirming the same anodic reactivity for the three analytes allowing the quantification of the flavanols index content with reliability. In addition, intra-electrode repeatability has been further confirmed by the RSD obtained with twenty different measurements performed with a solution containing 10 µmol L^{-1} epicatechin: $I_{p,a}$ < 1.1% and $E_{p,a}$ < 3.2%.

The poor linearity obtained for the bare SPE (R^2 = 0.9406 – 0.7316) is in accordance with the $E_{p,a}$ positive shift ($E_{p,a}$, average shift of 200 mV), that occurs for all the analytes, indicating an increase of the electrode surface passivation. Moreover, the lower

sensitivity (about 2 orders of magnitude vs SPE-CB/MoS_2) of the bare SPE towards all the analytes is evident.

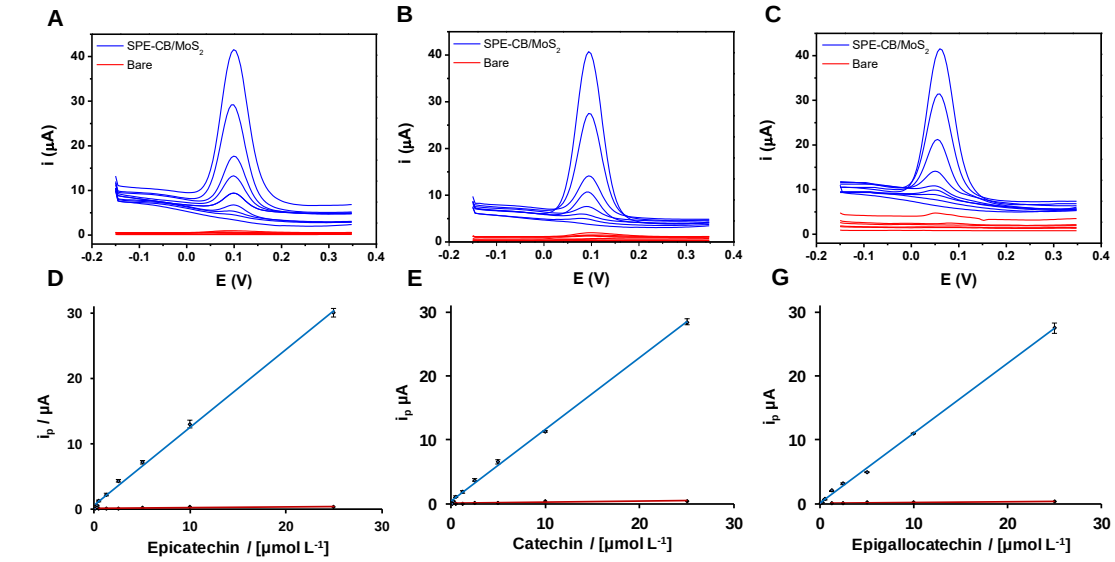

Figure IV-10: (A-C) DPV curves obtained using bare SPE (red line) and CB-SPE/MoS_2 (blue line) in presence of increasing concentrations of epicatechin (A), catechin (B) and epigallocatechin (C). (D-F) DPV calibration curves (mean value of three repetitions) obtained using bare SPE (red line) and CB-SPE/MoS_2 (blue line) in presence of increasing concentrations of epicatechin (D), catechin (E) and epigallocatechin (F). For each analyte, the calibration was performed in triplicate, the resulting linear equation (obtained with the mean values, n=3) and determination coefficient obtained for the SPE-CB/MoS_2 are reported in Table 1; while for the bare SPE: (CT) y = 0.0168x + 0.0798, R^2 = 0.7382; (EP) y = 0.0129x + 0.1256, R^2 = 0.7316; (EG) y = 0.0107x + 0.048, R^2 = 0.9406. (A-F) DPV conditions: pulse width 50 ms, pulse amplitude 20 mV. The standards were prepared in phosphate-buffered 0.01 mmol L^{-1} PB + 0.1 mol L^{-1} KCl (pH 7).

Table IV-1: Analytical characteristics of the SPE-CB/MoS_2 sensor employed for CT, EP, and EG detection.

Analyte	Equation (x=µmol L^{-1}; y=µA)	Linear Range (µmol L^{-1})	R^2	Sensitivity (µA L µmol^{-1})	LOD (µmol L^{-1})
CT	y = 1.122x + 0.413	0.1-25	0.998	8.93	0.18
EP	y = 1.185x + 0.762	0.1-25	0.998	9.43	0.17
EG	y = 1.092x + 0.090	0.1-25	0.998	8.69	0.18

[1]LODs were calculated as 3σ/slope ratio, where σ is the standard deviation of the mean value for 10 voltammograms of the blank. Analytical characteristics calculated using the mean value of three calibration curves.

The obtained LODs and linear ranges are comparable or better than those reported in the literature (see **Table IV-2**), even when applied to other food matrices. It should be emphasized that among the reported works for the analysis of catechin, this is the only case using screen-printed technology. Importantly, no one of the reported works pays attention to the fouling process, that is the principal drawback for the catechin detection. In this study, the attention has been paid not only to the proposed sensor performances but even to the success and the exploitability of the application in complex samples, using a significant number of samples and comparing the results with other well-established methods.

Table IV-2: Analytical characteristics and application of electrochemical sensors employed for catechins detection.

Electrode / Detection Mechanism	**Food Matrix (number of samples)**	**Sample Pre-treatment**	**Comparison methods**	**Linear Range** ($\mu mol\ L^{-1}$)	**LOD** ($\mu mol\ L^{-1}$)	**Ref.**
GCE/CV	Cocoa powder, chocolate (n=19)	Defatting/Liquid solid extraction	F.C., total flavonoid, DPPH, ABTS, FRAP	-	-	[38]
Pt-PEDOT/DPV	cocoa-based biscuit (n=3)	Stirring /filtration on Buchner	-	0.7-8.6 *	0.31*	[35]
GR- thermally reduced/DPV	Beer (n= 3)	Dilution	-	1.2-12.0**	-	[33]
GCE-N-doped graphene/DPV	Chinese green tea (n=4)	Dilution	-	1.0-30**	0.10**	[32]
SPE-CB/MoS_2/DPV	Cocoa powder (n=59)	DMSO solubilization	F.C., ABTS, AuNPs	0.1-25.0 *	0.17*	this work

*Epicatechin equivalents; ** Catechin equivalents.

Recovery (**Figure IV-11A**) and renewability (**Figure IV-11B**) studies were also evaluated using a representative mix of cocoa powder samples with different PPs content.

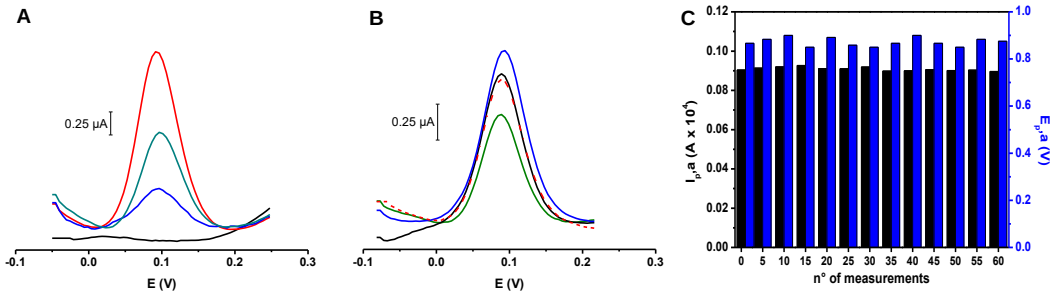

Figure IV-11: (**A**) DPV obtained analyzing a mix of cocoa samples (blue line), fortified with 0.25 µmol L^{-1}(green line) and 0.5 µmol L^{-1}(red line) of epicatechin. (**B**) DPV of three different samples with low (sample 12, green line), medium (sample 5, black line) and high (sample 1, blue line) polyphenols content. The dashed red line represents the sample 5 measurement repetition, performed after the measurement of the whole set of samples (n° 59). (**C**) DPV Oxidation currents and oxidation potentials obtained with 10 uM epicatechin, used to monitor the SPE-CB/MoS_2 response, during the samples analyzed. Each 5 samples analyzed the measurement has been performed.

The voltammograms obtained for the mix of samples (blue line), and the fortified samples (green and red lines), exhibited identical $E_{p,a}$, (90 ± 5 mV) and excellent RSD for $i_{p,a}$ ≤ 1.2%, (n=3) as well as quantitative recoveries with values ranging from 94% to 103% demonstrating the sensor exploitability for the catechins determination in complex samples.

Figure IV-11B shows the voltammograms obtained with cocoa samples with low (sample 12, green line), medium (sample 5, black line) and high (sample 1, blue line) PPs content (each diluted at the adequate dilution to fit the signal in the calibration plot). Noteworthy is the very high regenerability showed by the SPE-CB/MoS_2. This behavior was proven by monitoring the electrode state during the 59 sample measurements. The SPE-CB/MoS_2 regenerability is further underlined in **Figure IV-11B**, where the dashed red line represents the Sample 5 measured after measuring the whole set of samples, obtaining a signal recovery of 99%. These results are in accordance with previously discussed results (see section 3.1) and confirm the ability of the SPE-CB/MoS_2 to avoid the permanent catechins polymerization or attachment onto the electrode surface.

To prove the sensor surface regenerability, the whole set of samples (59 cocoa powders) has been measured on the same SPE-CB/MoS_2, and the electrode 'state' has been monitored measuring epicatechin standard (10 µmol L^{-1}) every 5 samples measured. Impressively, **Figure IV-11C**, shows a very stable response obtained that result in RSD of the signal obtained of 0.9 % and 5,2 % for the $I_{p,a}$ and $E_{p,a}$, respectively.

IV.3.3. Quantitative sample analysis of total catechins on hybrid CB/MoS_2 transducers

Then the applicability of the CB-SPE/MoS_2 for the determination of flavanols was rigorously carried out through the analysis of a wide set of cocoa samples (n=59). **Table IV-3** lists the quantitative analysis of cocoa samples by the proposed SPE-CB/MoS_2 sensor. In order to demonstrate analytical reliability of the proposed electrochemical sensor, cocoa powder samples were also analyzed by the classical F.C. (total PPs) and ABTS (antioxidant capacity) assays as well as by AuNPs-based free-extraction approach [59]. Particular attention was paid on the AuNPs method, which relies on the direct formation of AuNPs in organic solvent DMSO-aqueous medium, driven by endogenous PPs. This ‘extraction-free’ approach involves the use of DMSO acting as an organic solvent, able to ‘interact’, at the same time, with the fatty matrix and with the aqueous medium of measurement, making the cocoa PPs analysis

faster and easier. The effectiveness of this DMSO-based approach was tested with the set of 59 cocoa samples and compared both with a conventional liquid-liquid extraction (LL) methods which need a defatting step [59] (section 2.3) and with the well-established methods of Folin-Ciocalteu and ABTS. The effectiveness of the proposed DMSO-based approach was confirmed by the good correlations (**Figure IV-12:** Correlation curves between the data obtained (mean values, n=3), analyzing the 59 cocoa powder samples, extract with the proposed method based on DMSO and the conventional extraction (Conc.Ext.) method. Extracts analyzed using the Folin-Ciocalteu method (A) and ABTS assay (B). All the data are expressed in epicatechin equivalents.) obtained between DMSO-based and the LL conventional method (F-C: r=0.954 and ABTS: r=0.971, n=59) confirming the suitability of the DMSO-based extraction-free approach.

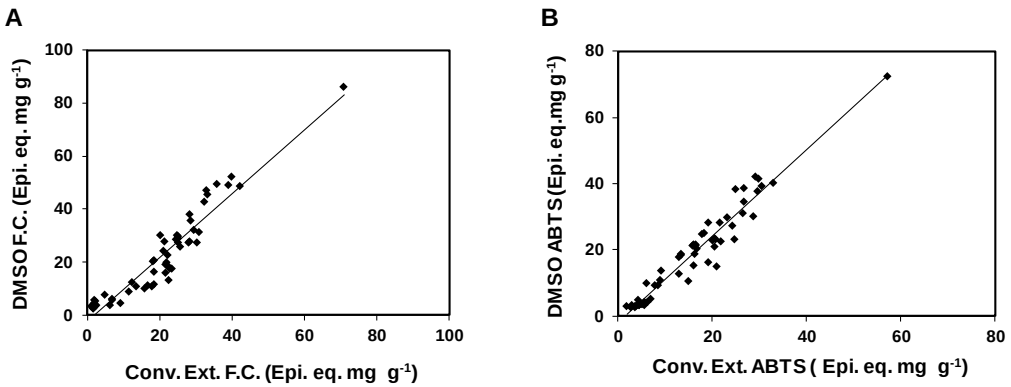

Figure IV-12: Correlation curves between the data obtained (mean values, n=3), analyzing the 59 cocoa powder samples, extract with the proposed method based on DMSO and the conventional extraction (Conc.Ext.) method. Extracts analyzed using the Folin-Ciocalteu method (A) and ABTS assay (B). All the data are expressed in epicatechin equivalents.

Furthermore, the DMSO-based approach requires a lower amount of sample (0.1 g vs. 8.0 g), a significant lower solvent consumption occurs (1.5 mL of DMSO vs. 150 mL of hexane and 5 mL of 5 mL of 70:29.5:0.5 acetone/water/acetic acid) as well as a reduction in waste generation; moreover, the procedure is not time-consuming (15' min vs. 8 h). Therefore, the DMSO-based free-extraction approach was selected for the quantitative determination of PPs in cocoa samples using the proposed SPE-CB/MoS_2 electrochemical sensor (**Table IV-3**). Despite heterogeneity of the samples, in terms of cocoa types, fat content (5.6-26.1%), color and PPs content, the data obtained with the SPE-CB/MoS_2 resulted highly correlated with all the well-established methods assays FC (r=0.972) and ABTS (r=0.966) as well as with the AuNPS-based (r=0.949).

Table IV-3: Analysis of cocoa samples by the SPE-CB/MoS_2 and the F.C, ABTS and AuNPs assays[1].

Sample	SPE-CB/MoS_2 (mg g^{-1})			Folin-Ciocalteu (mg g^{-1})			ABTS (mg g^{-1})			AuNPs (mg g^{-1})		
1	86.1	±	0.3	86.0	±	0.5	72.5	±	0.3	86.0	±	4.8
2	50.4	±	0.6	45.3	±	0.5	40.2	±	0.3	49.2	±	0.3
3	34.1	±	0.3	31.2	±	1.6	28.2	±	1.2	37.2	±	0.2
4	59.9	±	0.5	48.7	±	0.2	37.6	±	2.4	47.5	±	0.1
5	39.2	±	0.5	32.2	±	2.2	22.6	±	0.6	29.7	±	0.6
6	55.1	±	1.3	49.2	±	2.3	42.1	±	1.1	50.1	±	4.4
7	37.9	±	0.4	27.7	±	2.1	21.7	±	0.2	30.9	±	3.7
8	58.4	±	1.4	52.3	±	2.3	39.3	±	1.8	52.2	±	4.3
9	36.7	±	1.1	30.1	±	1.1	25.0	±	1.1	32.0	±	1.8
10	26.6	±	1.1	17.4	±	0.7	186	±	1.0	26.3	±	1.8
11	31.9	±	0.5	19.2	±	0.7	21.2	±	0.3	23.9	±	1.3
12	26.0	±	1.0	16.0	±	0.6	18.7	±	0.4	20.2	±	0.6
13	14.5	±	0.4	3.7	±	0.1	4.1	±	0.1	11.5	±	0.1
14	14.4	±	0.5	3.4	±	0.4	3.6	±	0.5	11.5	±	0.3
15	23.2	±	0.6	16.2	±	1.1	17.9	±	0.3	20.3	±	0.9
16	28.0	±	0.4	20.0	±	1.9	20.3	±	0.3	25.1	±	1.0
17	21.9	±	1.0	8.8	±	0.2	9.3	±	0.1	16.7	±	1.2
18	25.0	±	0.6	12.5	±	0.5	9.4	±	0.9	19.9	±	0.9
19	15.7	±	0.3	3.4	±	0.1	3.1	±	0.5	11.0	±	0.6
20	22.2	±	0.6	11.1	±	0.1	10.8	±	0.9	18.3	±	0.4
21	15.0	±	0.6	4.4	±	0.1	3.2	±	0.1	11.5	±	0.4
22	14.6	±	0.5	2.5	±	0.1	2.7	±	0.5	10.0	±	0.2
23	14.5	±	0.3	2.7	±	0.1	3.0	±	0.1	10.6	±	1.2
24	14.9	±	0.5	3.4	±	0.1	3.0	±	0.0	10.5	±	0.6
25	29.0	±	0.9	20.7	±	0.7	21.4	±	2.0	22.3	±	3.1
26	42.0	±	1.1	29.9	±	0.9	34.4	±	0.6	42.4	±	1.3
27	27.3	±	0.7	24.2	±	0.1	21.4	±	2.0	24.7	±	0.8
28	43.0	±	1.5	27.6	±	1.0	23.6	±	0.4	30.3	±	1.8
29	31.6	±	0.8	20.1	±	0.1	18.5	±	0.8	24.0	±	0.3
30	15.0	±	0.5	5.2	±	0.2	4.3	±	0.0	11.6	±	0.2
31	16.1	±	0.4	5.6	±	0.3	4.9	±	0.6	13.1	±	0.7
32	36.3	±	0.5	27.4	±	1.2	20.9	±	0.0	27.4	±	0.1
33	41.6	±	0.1	25.8	±	0.3	22.8	±	0.1	28.5	±	0.9
34	21.5	±	0.1	4.6	±	0.5	3.7	±	0.5	10.5	±	0.5
35	31.2	±	0.3	13.2	±	1.0	15.3	±	0.8	23.1	±	1.7
36	44.4	±	1.1	27.3	±	1.9	23.2	±	1.0	30.7	±	1.1
37	31.3	±	0.8	22.7	±	0.9	16.3	±	0.1	25.7	±	0.4
38	35.5	±	1.1	27.2	±	0.2	15.0	±	0.5	30.8	±	0.3
39	31.9	±	0.4	17.3	±	0.7	23.3	±	0.1	32.4	±	4.2
40	22.4	±	0.4	3.8	±	0.1	3.4	±	0.5	12.6	±	0.6
41	21.8	±	0.1	7.8	±	0.2	5.0	±	0.1	12.4	±	0.3
42	15.1	±	0.2	3.6	±	0.5	3.3	±	0.0	10.8	±	0.8
43	22.7	±	0.5	5.7	±	0.2	4.3	±	0.1	13.4	±	1.5
44	13.1	±	0.4	3.5	±	0.0	3.4	±	0.5	10.6	±	0.3
45	31.0	±	0.1	29.1	±	0.1	29.7	±	0.9	34.0	±	2.0
46	21.7	±	0.3	10.7	±	0.7	10.5	±	0.2	15.6	±	0.8
47	21.7	±	0.7	10.1	±	0.4	13.8	±	0.1	18.5	±	1.9
48	22.3	±	0.2	11.6	±	0.6	12.8	±	0.9	18.5	±	0.4
49	55.2	±	1.4	47.2	±	3.9	38.6	±	1.9	45.8	±	0.3
50	22.5	±	0.8	10.6	±	0.6	10.0	±	0.5	16.6	±	0.5
51	32.6	±	1.0	18.3	±	2.0	27.3	±	0.7	25.8	±	0.2
52	14.7	±	0.2	2.6	±	0.2	2.6	±	0.5	9.9	±	0.4
53	19.7	±	0.5	5.9	±	0.2	3.2	±	0.5	12.7	±	1.0
54	31.6	±	1.0	29.9	±	0.1	28.1	±	0.8	28.9	±	0.2
55	59.0	±	0.4	42.5	±	0.1	38.2	±	0.6	44.6	±	0.3
56	34.2	±	0.5	28.5	±	0.3	24.6	±	2.1	32.9	±	1.9
57	49.2	±	1.4	37.8	±	0.1	30.9	±	0.5	42.2	±	1.2
58	54.5	±	1.4	49.2	±	7.1	41.4	±	0.4	54.5	±	0.8
59	43.4	±	0.5	35.6	±	2.6	30.0	±	0.5	35.6	±	1.6

[1]The data are expressed as epicatechin equivalents as mean values ± SD, n=3. Calibration curves (performed with epicatechin; x = µmol L-1 and y = Abs.) showed both good linearity and coefficients of determination: F.C. $y = 0.1587x - 0.0032$, $R^2 = 0.9971$; ABTS $y = 69.682x + 0.7792$, $R^2 = 0.9925$; AuNPs $y = 0.0291x - 0.0753$, $R^2 = 0.9940$.

IV.4. Conclusions

An electrochemical sensor based on the synergic employment of MoS_2 and CB is successfully applied to catechins determination in complex cocoa samples. The SPE-CB/MoS_2 electrodes merge the CB ability to enhance the electrochemical response and the MoS_2 'antifouling' properties against catechins, drawbacks that occur to both conventional carbons and NMs-modified electrodes. The realized sensor showed an impressive stable and reproducible response, with low working potentials, excellent resistance to fouling with detection limits in the nanomolar range. Noteworthily, the whole set of 59 samples have been measured using a single SPE-CB/MoS_2, without loss of signal, proving it excellent ‘antifouling’ properties. Moreover, in order to speed up and simplify, the cocoa powder PPs analysis (that required 8 h), a fast (15 min) direct cocoa PPs DMSO-based solubilization extraction-free strategy is proposed. Definitely, the proposed approach is clearly intended for fast (total time 15' min, from sampling to analysis) evaluation of PPs in cocoa powder, the fast DMSO 'extraction' (15 min, without volatile solvents) together to the SPE-CB/MoS_2 (regenerable and portable) allows a real delocalization of the analysis and could be extended for the catechins analysis in other food matrices. The 'DMSO-based PPs approach results rapid, effective and eco-friendly (total working volume 1.5 mL), does not require evaporation steps (and volatile compounds) and can be coupled with cocoa PPs (and antioxidant capacity) content evaluation methods. The SPE-CB/MoS_2 showed an important synergistic effect and the combination of these nanomaterials can offer new opportunities to develop new devices and applications. In our case the proposed SPE-CB/MoS_2 overcome the proof of applicability, becoming an analytical tool able to overtake the classics catechins analytical drawbacks.

IV.5. References

[1] R. Tsao, Chemistry and biochemistry of dietary polyphenols, Nutrients. 2 (2010) 1231–1246. doi:10.3390/nu2121231.

[2] A. Belščak, D. Komes, D. Horžić, K.K. Ganić, D. Karlović, Comparative study of commercially available cocoa products in terms of their bioactive composition, Food Res. Int. 42 (2009) 707–716. doi:10.1016/j.foodres.2009.02.018.

[3] C. Di Mattia, G. Sacchetti, D. Mastrocola, M. Serafini, From cocoa to chocolate: The impact of processing on in vitro antioxidant activity and the effects of chocolate on antioxidant markers in vivo, Front. Immunol. 8 (2017) 1–7. doi:10.3389/fimmu.2017.01207.

[4] M.S. Beg, S. Ahmad, K. Jan, K. Bashir, Status, supply chain and processing of cocoa - A review, Trends Food Sci. Technol. 66 (2017) 108–116. doi:10.1016/j.tifs.2017.06.007.

[5] J.S. Bonvehi, F.V. Coil, Evaluation of bitterness and astringency of polyphenolic compounds in cocoa powder, 60 (1997) 365–370.

[6] C. Andres-Lacueva, M. Monagas, N. Khan, M. Izquterdo-Pulido, M. Urpi-Sarda, J. Permanyer, R.M. Lamuela-Raventós, Flavanol and flavonol contents of cocoa powder products: Influence of the manufacturing process, J. Agric. Food Chem. 56 (2008) 3111–3117. doi:10.1021/jf0728754.

[7] F. Ioannone, C.D. Di Mattia, M. De Gregorio, M. Sergi, M. Serafini, G. Sacchetti, Flavanols, proanthocyanidins and antioxidant activity changes during cocoa (Theobroma cacao L.) roasting as affected by temperature and time of processing, Food Chem. 174 (2015) 256–262. doi:10.1016/j.foodchem.2014.11.019.

[8] C. Di Mattia, M. Martuscelli, G. Sacchetti, I. Scheirlinck, B. Beheydt, D. Mastrocola, P. Pittia, Effect of Fermentation and Drying on Procyanidins, Antiradical Activity and Reducing Properties of Cocoa Beans, Food Bioprocess Technol. 6 (2013) 3420–3432. doi:10.1007/s11947-012-1028-x.

[9] F. Della Pelle,M.C. González, M. Sergi, M. Del Carlo, D. Compagnone, A. Escarpa, Gold Nanoparticles-based Extraction-Free Colorimetric Assay in Organic Media: An Optical Index for Determination of Total Polyphenols in Fat-Rich Samples, Anal. Chem. 87 (2015) 6905–6911. doi:10.1021/acs.analchem.5b01489.

[10] I. Ignat, I. Volf, V.I. Popa, A critical review of methods for characterisation of polyphenolic compounds in fruits and vegetables, Food Chem. 126 (2011) 1821–1835. doi:10.1016/J.FOODCHEM.2010.12.026.

[11] V. Ferrone, S. Genovese, M. Carlucci, M. Tiecco, R. Germani, F. Preziuso, F. Epifano, G. Carlucci, V.A. Taddeo, A green deep eutectic solvent dispersive liquid-liquid micro-extraction (DES-DLLME) for the UHPLC-PDA determination of oxyprenylated phenylpropanoids in olive, soy, peanuts, corn, and sunflower oil, Food Chem. 245 (2018) 578–585. doi:10.1016/j.foodchem.2017.10.135.

[12] R.V.S.S. Gottumukkala, N. Nadimpalli, K. Sukala, G. V Subbaraju, Determination of Catechin and Epicatechin Content in Chocolates by High-Performance Liquid Chromatography, 2014 (2014). doi:10.1155/2014/628196.

[13] T.H. Stanley, A.T. Smithson, A.P. Neilson, R.C. Anantheswaran, J.D. Lambert, Analysis of Cocoa Proanthocyanidins Using Reversed Phase High- Performance Liquid Chromatography and Electrochemical Detection: Application to Studies on the E ff ect of Alkaline Processing, (2015). doi:10.1021/acs.jafc.5b02661.

[14] F. Blasi, G. Rocchetti, D. Montesano, L. Lucini, G. Chiodelli, S. Ghisoni, G. Baccolo, M.S. Simonetti, L. Cossignani, Changes in extra-virgin olive oil added with Lycium barbarum L. carotenoids during frying: Chemical analyses and metabolomic approach, Food Res. Int. 105 (2018) 507–516. doi:10.1016/j.foodres.2017.11.061.

[15] F. Della Pelle, D. Compagnone, Nanomaterial-Based Sensing and Biosensing of Phenolic Compounds and Related Antioxidant Capacity in Food, Sensors. 18 (2018) 462. doi:10.3390/s18020462.

[16] J. Hoyos-arbeláez, M. Vázquez, J. Contreras-calderón, Electrochemical methods as a tool for determining the antioxidant capacity of food and beverages : A review, 221 (2017) 1371–1381. doi:10.1016/j.foodchem.2016.11.017.

[17] D.A. El-Hady, N. Abo El Maali, Determination of catechin isomers in human plasma subsequent to green tea ingestion using chiral capillary electrophoresis with a high-sensitivity cell, Talanta. 76 (2008) 138–145. doi:10.1016/j.talanta.2008.02.026.

[18] X. Huang, E. Teye, L.K. Sam-Amoah, F. Han, L. Yao, W. Tchabo, Rapid measurement of total polyphenols content in cocoa beans by data fusion of NIR spectroscopy and electronic tongue, Anal. Methods. 6 (2014) 5008–5015. doi:10.1039/c4ay00223g.

[19] Y. Hu, Z.J. Pan, W. Liao, J. Li, P. Gruget, D.D. Kitts, X. Lu, Determination of antioxidant capacity and phenolic content of chocolate by attenuated total reflectance-Fourier transformed-infrared spectroscopy, Food Chem. 202 (2016) 254–261. doi:10.1016/j.foodchem.2016.01.130.

[20] M.F. Barroso, C. Delerue-matos, M.B.P.P. Oliveira, Biosensors and Bioelectronics Towards a reliable technology for antioxidant capacity and oxidative damage evaluation : Electrochemical (bio) sensors, 30 (2011) 1–12. doi:10.1016/j.bios.2011.08.036.

[21] R. Prehn, J. Gonzalo-Ruiz, M. Cortina-Puig, Electrochemical detection of polyphenolic compounds in foods and beverages, Curr. Anal. Chem. 8 (2012) 472–484. doi:10.2174/157341112803216717.

[22] D. Rojas, F. Della Pelle, M. Del Carlo, E. Fratini, A. Escarpa, D. Compagnone, Nanohybrid carbon black-molybdenum disulfide transducers for preconcentration-free voltammetric detection of the olive oil o-diphenols hydroxytyrosol and oleuropein, Microchim. Acta. 186 (2019) 363. doi:10.1007/s00604-019-3418-5.

[23] T.A. Enache, A.M. Oliveira-brett, Phenol and para -substituted phenols electrochemical oxidation pathways, J. Electroanal. Chem. 655 (2011) 9–16. doi:10.1016/j.jelechem.2011.02.022.

[24] M. Amiri-Aref, J.B. Raoof, R. Ojani, A highly sensitive electrochemical sensor for simultaneous voltammetric determination of noradrenaline, acetaminophen, xanthine and caffeine based on a flavonoid nanostructured modified glassy carbon electrode, Sensors Actuators, B Chem. 192 (2014) 634–641. doi:10.1016/j.snb.2013.11.006.

[25] P. Janeiro, A.M. Oliveira Brett, Catechin electrochemical oxidation mechanisms, Anal. Chim. Acta. 518 (2004) 109–115. doi:10.1016/j.aca.2004.05.038.

[26] L. Blandón-Naranjo, F. Della Pelle, M. V. Vázquez, J. Gallego, A. Santamaría, M. Alzate-Tobón, D. Compagnone, Electrochemical Behaviour of Microwave-assisted Oxidized MWCNTs Based Disposable Electrodes: Proposal of a NADH Electrochemical Sensor, Electroanalysis. 30 (2018) 509–516. doi:10.1002/elan.201700674.

[27] F.S. Ligler, H.S. White, Nanomaterials in analytical chemistry, Anal. Chem. 85 (2013) 11161–11162. doi:10.1021/ac403331m.

[28] M. Pumera, A. Escarpa, Nanomaterials as electrochemical detectors in microfluidics and CE: Fundamentals, designs, and applications, Electrophoresis. 30 (2009) 3315–3323. doi:10.1002/elps.200900008.

[29] D. Capoferri, F. Della Pelle, M. Del Carlo, D. Compagnone, Affinity Sensing Strategies for the Detection of Pesticides in Food, Foods. 7 (2018) 148. doi:10.3390/foods7090148.

[30] F. Della Pelle, A. Scroccarello, S. Scarano, D. Compagnone, Silver nanoparticles-based plasmonic assay for the determination of sugar content in food matrices, Anal. Chim. Acta. (2018). doi: 10.1016/j.aca.2018.11.015.

[31] S. Masoum, M. Behpour, F. Azimi, M.H. Motaghedifard, Potentiality of chemometric approaches for the determination of (+)-catechin in green tea leaves at the surface of multiwalled carbon nanotube paste electrode, Sensors Actuators, B Chem. 193 (2014) 582–591. doi:10.1016/j.snb.2013.12.022.

[32] J. Pang, X. Wu, A. Li, X. Liu, M. Li, Detection of catechin in Chinese green teas at N-doped carbon-modified electrode, (2017). doi:10.1007/s11581-017-2006-0.

[33] C. Chu'Er, Z. Sofer, M. Pumera, A. Bonanni, Doped and undoped graphene platforms the influence of structural properties on the detection of polyphenols, Sci. Rep. 22 (2016) 3830–3834.

[34] V. Andrei, E. Sharpe, A. Vasilescu, S. Andreescu, A single use electrochemical sensor based on biomimetic nanoceria for the detection of wine antioxidants, Talanta. 156–157 (2016) 112–118. doi:10.1016/j.talanta.2016.04.067.

[35] L. Pigani, R. Seeber, A. Bedini, E. Dalcanale, M. Suman, Adsorptive-Stripping Voltammetry at PEDOT-Modified Electrodes. Determination of Epicatechin, Food Anal. Methods. 7 (2014) 754–760. doi:10.1007/s12161-013-9678-5.

[36] M. Gandhi, D. Rajagopal, S. Parthasarathy, S. Raja, S.T. Huang, A. Senthil Kumar, In Situ Immobilized Sesamol-Quinone/Carbon Nanoblack-Based Electrochemical Redox Platform for Efficient Bioelectrocatalytic and Immunosensor Applications, ACS Omega. 3 (2018) 10823–10835. doi:10.1021/acsomega.8b01296.

[37] G. Ziyatdinova, E. Kozlova, H. Budnikov, Polyquercetin/MWNT-modified Electrode for the Determination of Natural Phenolic Antioxidants, Electroanalysis. 29 (2017) 2610–2619. doi:10.1002/elan.201700440.

[38] J.M. Brcanović, A.N. Pavlović, S.S. Mitić, G.S. Stojanović, D.D. Manojlović, B.M. Kaličanin, J.N. Veljković, J.N. Veljkovi, S.S.M. Jelena M. Brcanovi, Aleksandra N. Pavlovi, G.S. Stojanovi, D.D. Manojlovi, B.M. Kalianin, Cyclic voltammetry determination of antioxidant capacity of cocoa powder, dark chocolate and milk chocolate samples: Correlation with spectrophotometric assays and individual phenolic compounds, Food Technol. Biotechnol. 51 (2013) 460–470. doi:10.1097/BTE.0000000000000074.

[39] M. Baccarin, F.A. Santos, F.C. Vicentini, V. Zucolotto, B.C. Janegitz, O. Fatibello-Filho, Electrochemical sensor based on reduced graphene oxide/carbon black/chitosan composite for the simultaneous determination of dopamine and paracetamol concentrations in urine samples, J. Electroanal. Chem. 799 (2017) 436–443. doi:10.1016/j.jelechem.2017.06.052.

[40] T.A. Silva, F.C. Moraes, B.C. Janegitz, O. Fatibello-Filho, Electrochemical Biosensors Based on Nanostructured Carbon Black: A Review, J. Nanomater. 2017 (2017) 1–14. doi:10.1155/2017/4571614.

[41] D. Rojas, F. Della Pelle, M. Del Carlo, M. D'Angelo, R. Dominguez-Benot, A. Cimini, A. Escarpa, D. Compagnone, Electrodeposited Prussian Blue on carbon black modified disposable electrodes for direct enzyme-free H_2O_2 sensing in a Parkinson's disease in vitro model, Sensors Actuators, B Chem. 275 (2018) 402–408. doi:10.1016/j.snb.2018.08.040.

[42] F. Della Pelle, M. Del Carlo, M. Sergi, D. Compagnone, A. Escarpa, Press-transferred carbon black nanoparticles on board of microfluidic chips for rapid and sensitive amperometric determination of phenyl carbamate pesticides in environmental samples, Microchim. Acta. 183 (2016) 3143–3149. doi:10.1007/s00604-016-1964-7.

[43] M. Pumera, A.H. Loo, Layered transition-metal dichalcogenides (MoS_2 and WS_2) for sensing and biosensing, TrAC - Trends Anal. Chem. 61 (2014) 49–53. doi:10.1016/j.trac.2014.05.009.

[44] M.A. Lukowski, A.S. Daniel, F. Meng, A. Forticaux, L. Li, S. Jin, Enhanced hydrogen evolution catalysis from chemically exfoliated metallic MoS_2 nanosheets, J. Am. Chem. Soc. 135 (2013) 10274–10277. doi:10.1021/ja404523s.

[45] Y. Lin, X. Chen, Y. Lin, Q. Zhou, D. Tang, Non-enzymatic sensing of hydrogen peroxide using a glassy carbon electrode modified with a nanocomposite made from carbon nanotubes and molybdenum disulfide, Microchim. Acta. 182 (2015) 1803–1809. doi:10.1007/s00604-015-1517-5.

[46] N. Lingappan, N.H. Van, S. Lee, D.J. Kang, Growth of three dimensional flower-like molybdenum disulfide hierarchical structures on graphene/carbon nanotube network: An advanced heterostructure for energy storage devices, J. Power Sources. 280 (2015) 39–46. doi:10.1016/j.jpowsour.2015.01.064.

[47] I. Song, C. Park, H.C. Choi, W. Zhang, P. Zhang, Z. Su, G. Wei, N.A. Kumar, M.A. Dar, R. Gul, J.B. Baek, M. Pumera, A.H. Loo, K.J. Huang, L.L.L. Wang, J.Z. Zhang, L.L.L. Wang, Y.P. Mo, G.W. Shi, Y.M. Liu, A.M. Van Der Zande, P.Y. Huang, D.A. Chenet, T.C. Berkelbach, Y. You, G.H. Lee, T.F. Heinz, D.R. Reichman, D.A. Muller, J.C. Hone, K. Lee, R. Gatensby, N. McEvoy, T. Hallam, G.S. Duesberg, K.G. Zhou, N.N. Mao, H.X. Wang, Y. Peng, H.L. Zhang, K. Lee, H.Y. Kim, M. Lotya, J.N. Coleman, G.T. Kim, G.S. Duesberg, Hydrothermal synthesis of molybdenum disulfide nanosheets as supercapacitors electrode material, Adv. Mater. 50 (2014) 554–561. doi:10.1002/adma.201101013.

[48] K.J. Huang, L. Wang, J.Z. Zhang, L.L. Wang, Y.P. Mo, One-step preparation of layered molybdenum disulfide/multi-walled carbon nanotube composites for enhanced performance supercapacitor, Energy. 67 (2014) 234–240. doi:10.1016/j.energy.2013.12.051.

[49] W. Zhang, P. Zhang, Z. Su, G. Wei, Synthesis and sensor applications of MoS_2 -based nanocomposites, Nanoscale. 7 (2015) 18364–18378. doi:10.1039/C5NR06121K.

[50] K.J. Huang, L. Wang, J. Li, Y.M. Liu, Electrochemical sensing based on layered MoS2-graphene composites, Sensors Actuators, B Chem. 178 (2013) 671–677. doi:10.1016/j.snb.2013.01.028.

[51] A. Sinha, Dhanjai, B. Tan, Y. Huang, H. Zhao, X. Dang, J. Chen, R. Jain, MoS_2 nanostructures for electrochemical sensing of multidisciplinary targets: A review, TrAC - Trends Anal. Chem. 102 (2018) 75–90. doi:10.1016/j.trac.2018.01.008.

[52] D. Talarico, F. Arduini, A. Constantino, M. Del Carlo, D. Compagnone, D. Moscone, G. Palleschi, Carbon black as successful screen-printed electrode modifier for phenolic compound detection, Electrochem. Commun. 60 (2015) 78–82. doi:10.1016/J.ELECOM.2015.08.010.

[53] F. Della, R. Di, L. Vázquez, F.J. Palomares, M. Del, M. Sergi, D. Compagnone, A. Escarpa, Press-transferred carbon black nanoparticles for class-selective antioxidant electrochemical detection, Appl. Mater. Today. 9 (2017) 29–36. doi:10.1016/j.apmt.2017.04.012.

[54] I. Vasilescu, S.A.V. Eremia, M. Kusko, A. Radoi, E. Vasile, G.-L. Radu, Molybdenum disulphide and graphene quantum dots as electrode modifiers for laccase biosensor, Biosens. Bioelectron. 75 (2016) 232–237. doi:10.1016/J.BIOS.2015.08.051.

[55] H. Huang, J. Zhang, M. Cheng, K. Liu, X. Wang, Amperometric sensing of hydroquinone using a glassy carbon electrode modified with a composite consisting of graphene and molybdenum disulfide, Microchim. Acta. 184 (2017) 4803–4808. doi:10.1007/s00604-017-2531-6.

[56] S. Ji, Z. Yang, C. Zhang, Y.E. Miao, W.W. Tjiu, J. Pan, T. Liu, Nonenzymatic sensor for glucose based on a glassy carbon electrode modified with $Ni(OH)_2$ nanoparticles grown on a film of molybdenum sulfide, Microchim. Acta. 180 (2013) 1127–1134. doi:10.1007/s00604-013-1035-2.

[57] V. Mani, M. Govindasamy, S.-M.M. Chen, R. Karthik, S.-T.T. Huang, Determination of dopamine using a glassy carbon electrode modified with a graphene and carbon nanotube hybrid decorated with molybdenum disulfide flowers, Microchim. Acta. 183 (2016) 2267–2275. doi:10.1007/s00604-016-1864-x.

[58] X. Li, X. Du, Molybdenum disulfide nanosheets supported Au-Pd bimetallic nanoparticles for non-enzymatic electrochemical sensing of hydrogen peroxide and glucose, Sensors Actuators, B Chem. 239 (2017) 536–543. doi:10.1016/j.snb.2016.08.048.

[59] L. Gu, S.E. House, X. Wu, B. Ou, R.L. Prior, Procyanidin and catechin contents and antioxidant capacity of cocoa and chocolate products, J. Agric. Food Chem. 54 (2006) 4057–4061. doi:10.1021/jf060360r.

[60] C.A. Schneider, W.S. Rasband, K.W. Eliceiri, NIH Image to ImageJ: 25 years of image analysis., Nat. Methods. 9 (2012) 671–675.

[61] R. Re, N. Pellegrini, A. Proteggente, A. Pannala, M. Yang, C. Rice-Evans, Antioxidant activity applying an improved ABTS radical cation decolorization assay, Free Radic. Biol. Med. 26 (1999) 1231–1237. doi:10.1016/S0891-5849(98)00315-3.

[62] M. Del Carlo, A. Amine, M. Haddam, F. Della Pelle, G.C. Fusella, D. Compagnone, Selective voltammetric analysis of o-diphenols from olive oil using Na2MoO4 as electrochemical mediator, Electroanalysis. 24 (2012) 889–896. doi:10.1002/elan.201100603.

[63] F. Della Pelle, A. Scroccarello, M. Sergi, M. Mascini, M. Del Carlo, D. Compagnone, Simple and rapid silver nanoparticles based antioxidant capacity assays: Reactivity study for phenolic compounds, Food Chem. 256 (2018) 342–349. doi:10.1016/j.foodchem.2018.02.141.

[64] F. Della Pelle, D. Vilela, M.C. González, C. Lo Sterzo, D. Compagnone, M. Del Carlo, A. Escarpa, Antioxidant capacity index based on gold nanoparticles formation. Application to extra virgin olive oil samples, Food Chem. 178 (2015) 70–75. doi:10.1016/j.foodchem.2015.01.045.

[65] A. Scroccarello, F. Della Pelle, L. Neri, P. Pittia, D. Compagnone, Silver and gold nanoparticles based colorimetric assays for the determination of sugars and polyphenols in apples, Food Res. Int. 119 (2019) 359–368. doi: 10.1016/j.foodres.2019.02.006.

[66] L. Blandón-Naranjo, J. Hoyos-Arbeláez, M. V. Vázquez, F. Della Pelle, D. Compagnone, NADH Oxidation onto different carbon-based sensors: Effect of structure and surface-oxygenated groups, J. Sensors. 2018 (2018). doi:10.1155/2018/6525919.

[67] F. Della Pelle, C. Angelini, M. Sergi, M. Del, A. Pepe, D. Compagnone, M. Del Carlo, A. Pepe, D. Compagnone, Nano carbon black-based screen printed sensor for carbofuran, isoprocarb, carbaryl and fenobucarb detection: application to grain samples, Talanta. 186 (2018) 389–396. doi:10.1016/j.talanta.2018.04.082.

[68] F. Della Pelle, L. Vázquez, M. Del Carlo, M. Sergi, D. Compagnone, A. Escarpa, Press-Printed Conductive Carbon Black Nanoparticle Films for Molecular Detection at the Microscale, Chem. - A Eur. J. 22 (2016) 12761–12766. doi:10.1002/chem.201601743.

[69] M.N. Barros Filho, F.J. Sobreira, Accuracy of lacunarity algorithms in Texture Classification of high spatial resolution images from urban areas, Int. Arch. Photogramm. Remote Senising Spat. Inf. Sci. 37 (2008) 417–422.

[70] A.L. Karperien, FracLac for ImageJ, Loop. (2013).

[71] Y. Li, Y. Feng, S. Zhu, C. Luo, J. Ma, F. Zhong, Journal of Food Composition and Analysis The effect of alkalization on the bioactive and flavor related components in commercial cocoa powder, J. Food Compos. Anal. 25 (2012) 17–23. doi:10.1016/j.jfca.2011.04.010.

[72] I. Novak, M. Šeruga, Š. Komorsky-Lovrić, Square-wave and cyclic voltammetry of epicatechin gallate on glassy carbon electrode, J. Electroanal. Chem. 631 (2009) 71–75. doi:10.1016/j.jelechem.2009.03.005Class-selective voltammetric determination of hydroxycinnamic acids structural analogs by using a WS_2/catechin-capped-AuNPs/carbon black-based nanocomposite sensor

V. Class-selective voltammetric determination of hydroxycinnamic acids structural analogs by using a WS2/catechin-capped-AuNPs/carbon black-based nanocomposite sensor

V.1. Introduction and objectives

PPs are secondary metabolites present in vegetables and fruits and derived foodstuff [1,2]. PPs belongs to a heterogeneous class of compounds, with important in vitro and in vivo activity [3,4], play a role in food manufacturing and conservation (markers of quality, process, and shelf-life, sensory perception, etc.), and represent an added value for marketing (e.g. functional foods, superfoods, etc.) [1,2]. Their hydrogen and electron-donating ability, as well as capacity to delocalize/stabilize phenoxyl radicals within their structure, are closely dependent on the chemical structure and, in particular, the hydroxyl function(s) arrangement [5]. The scientific community is still working to develop easy and rapid methodologies for the quali/quantitative determination and evaluation of the reactivity of PPs. However, because of the complexity of this matter, the PPs analysis still lacks official methods to rely on [2].

After the boost of graphene in the analytical and materials sciences, more recently other two-dimensional NMs started to be studied. In particular, TMDs have received great attention because of their chemistry, physical properties, and versatility [6–10]. However, their employment in the development of sensors for the analysis of real matrices needs to be further explored [7,11]. The main limitation of TMDs [9] is linked both to the intrinsic low conductivity and tendency to the restack, regardless of the type of synthesis and the resulting conformation of the sheets [13]. Nevertheless, TMDs have demonstrated to be elective building blocks for the development of hybrids nanomaterials, giving rise to improved and sometimes unexpected properties [8–11]. However, despite metal nanostructure-decorated MoS_2 nanocomposites, have been extensively studied [8], the use of WS_2 has been little explored [13,14] particularly in the sensors field [15].

The simultaneous determination of different PPs in food has been attempted using different nanocomposite-based sensors [16–18], commonly using a pre-concentration step (accumulation). In this regard, Puangjan et al. [16] reported a ZrO_2/Co_3O_4/reduced graphene oxide composite electrode to detect gallic, caffeic and protocatechuic acids in food samples, while multi-walled carbon nanotubes functionalized with AuNP-CT and p-aminothiophenol were used by Yola et al. [17] to assess quercetin and rutin content in fruit juices. Elçin et al. have exploited a ruthenium nanoparticle anchored calix[4]amidocrown-5 functionalized reduced graphene oxide electrode to simultaneously analyze quercetin, morin, and rutin in grape wine [18]. TMDs have been little explored in food PPs sensing [9,10].

The main objective in this chapter has been to develop a hybrid WS_2-based electrochemical sensor for the simultaneous analysis of hCNs as non-flavonoid phenols. For this kind of compunds, the redox potentials and the relative contents can be considered a good measure of antioxidant activity [5]. Indeed, the electrochemistry of hCNs-based antioxidants is governed by structure-property-activity relationships. Three hCNs structural analogs with different hydroxylic moieties have been selected as target compounds: caffeic acid (CF), sinapic acid (SP), and p-coumaric acid (CM). To the best of our knowledge, there are no reports about the simultaneous determination of these compounds in the literature, despite they are commonly found in food. This can be probably attributed to:

1. Strong passivating tendency of hCNs towards carbon-based sensors [2].
2. Poor electroactivity of SP and CM [20,21].
3. hCNs very similar structure that makes voltammetric discrimination challenging.

Therefore it is very interesting to study WS_2-based nanostructures due to being less explored and more conductive material in comparision with MoS_2. The SPE-CB-WS_2/AuNP-CT sensor developed here takes advantage of the combination of green-synthesized catechin-based gold nanoparticles coupled with WS_2 nanoflakes onto a highly electroactive CB network

V.2. Materials and methods

V.2.1. Reagents, stock solutions, and samples

Caffeic, sinapic, and *p*-coumaric acids were purchased from Sigma Aldrich (St Louis MO, USA). Potassium ferrocyanide, potassium ferricyanide, potassium chloride, sodium phosphate monobasic monohydrate ($NaH_2PO_4 \cdot H_2O$), sodium phosphate dibasic anhydrous (Na_2HPO_4), sodium citrate, sodium borohydride, N-N-dimethylformamide (DMF), methanol, cetyltrimethylammonium chloride (CTAC 25.0% in water), hydrogen tetrachloroaurate ($HAuCl_4 \cdot 3H_2O$, 99.9%), fructose, glucose, sucrose, citric acid, acetic acid, malic acid, succinic acid, tartaric acid, oxalic acid, quinic acid, and shikimic acid were purchased from Sigma Aldrich (St Louis MO, USA). Carbon black N220 was obtained from Cabot Corporation (Ravenna, Italy). WS_2 (99.8%, metals basis) was purchased from Alfa Aesar (Ward Hill, MA). PPs standards stock solutions were prepared in methanol at a concentration of 1.0×10^{-2} mol L^{-1} and stored at −18 °C in the dark. Milli-Q water (18.2 MΩ) was used for all the experiments. Rapeseed oil, apple puree, apple homogenized, and apple juice were purchased from a local market. Kalanchoe Crenata lyophilized leaves were purchased from a local market in Burundi.

V.2.2. Apparatus

CV, DPV, and EIS measures were performed by using a portable Palmsens 4 Potentiostat/Galvanostat/Impedance Analyzer (Palm Instruments BV, Houten, Netherlands) equipped with PS trace software. Screen-printed electrodes (SPE) with a three-electrode configuration (working and counter electrode of graphite, and Ag as pseudo-reference electrode) from EcoBioServices (Florence, Italy) were used. Absorbance measurements were obtained using a JENWAY 6400 Spectrophotometer from Barloworld Scientific (Staffordshire, UK). Scanning electron microscopy (SEM) and energy-dispersive X-ray spectroscopy (EDX) was performed with a ΣIGMA high-resolution scanning electron microscope (Carl Zeiss Microscopy GmbH, Germany).

V.2.3. Preparation of catechin-capped gold nanoparticles (AuNP-CT)

The AuNP-CT synthesis was carried out according to Della Pelle et al. [20,21] with some modifications (**Figure V-1**). The reaction mix containing 20 µL of CTAC (25.0% in water), 50 µL of $HAuCl_4$ 20 mmol L^{-1}, and 100 µL of catechin 1 mmol L^{-1} was prepared in 100 mmol L^{-1} phosphate buffer, (PB), at pH 8 in a final volume of 1 mL. The mixture was orbital stirred (at 300 rpm) for 2 minutes, treated with a hot bath at 45 °C for 10 minutes, and then placed in ice overnight to achieve the AuNP-CT precipitation (precipitated nanoparticles can be stored for 15 days at +4 °C). Afterward, the supernatant was removed, and the nanoparticles were recovered in 1 mL of H_2O. The absorbance of the obtained AuNP-CT was centered at 540 nm (LSPR maximum), and absorbance values between 2.0 ± 0.1 accepted.

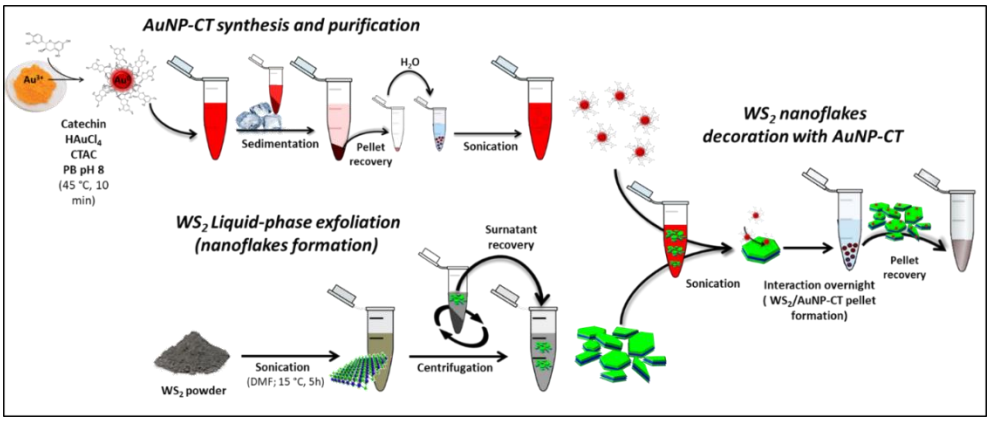

Figure V-1: Schematic representation of the AuNP-CT synthesis, WS_2 nanoflakes liquid-phase exfoliation, and of the WS_2 nanoflakes decoration with AuNP-CT

V.2.4. WS_2 decoration with AuNP-CT (WS_2/AuNP-CT)

For decoration of WS_2 flakes, a 2 mg mL^{-1} WS_2 dispersion was prepared in DMF, vortexed for 2 min, and treated with ultrasonic bath (3000683 Ultrasons Selecta, Barcelona, Spain) for 5 hours at low temperature (~15 °C). Afterward, the coarser part of the material was removed by centrifugation (300 g, 0.5 h). Then, 200 µL of WS_2 were mixed with 800 µL of AuNP-CT in an ultrasonic bath for 1 hour at room temperature (mixing each 20 min) and left to interact at 4 °C overnight. The obtained

WS_2 flakes decorated with AuNP-CT were centrifuged (700 g, 5 min), and the pellet resuspended in 200 µL of DMF.

V.2.5. Preparation of the CB-WS_2/AuNP-CT sensor

The WS_2/AuNP-CT was mixed with 200 µL of 1 mg mL^{-1} CB dispersion (previously prepared by 1 h of sonication in DMF:H_2O 1:1 according to Della Pelle et al.[9,22]). The SPE electrodes were modified via drop-casting of 6 µL of the nanohybrid suspension (by three different depositions of 2 µL, each deposition preceded by 1 min of sonication).

V.2.6. Microscopic and elemental analysis

Field Emission Scanning Electron Microscopy (FE-SEM) coupled with energy-dispersive X-ray spectroscopy (EDX) was performed with a ΣIGMA high-resolution scanning electron microscope (Carl Zeiss Microscopy GmbH, Germany). The electrodes' morphological characterization was assessed using an acceleration potential of 2 kV at a working distance of about 4 mm. Energy-dispersive X-ray analysis (EDX) was performed using a silicon drift detector (Oxford Instruments) coupled with SEM using a working distance of about 8.5 mm and an accelerating potential of 15 kV, analyzing a sampling area ranging from 0.06 to 0.09 mm^2.

V.2.7. Electrochemical measurements

All the materials and the obtained nanocomposites were investigated by cyclic voltammetry CV and EIS using a solution of 1 mmol L^{-1} $[Fe(CN)_6]^{3-/4-}$ and 0.1 mol L^{-1} KCl. CV was performed at a scan rate of 50 mV s^{-1}. EIS experiment was achieved using a sinusoidal wave of 5 mV amplitude in the 10^5 to 10^{-1} Hz frequency range, setting the potential at open circuit. Nyquist plots were fitted using the Randles modified equivalent circuit. CV and DPV were also employed to assess the electrochemical response of the sensors to the analytes (CF, SP, and CM). The measurements were carried out by depositing 100 µL of the analyte solution onto the working electrode surface. CVs of PPs was performed with a scan rate of 50 mV s^{-1}, in a potential window from -0.2 V to 0.8 V (vs. pseudo Ag/AgCl). DPVs of the analytes was performed individually and in mixture and the parameters were optimized to improve the

sensitivity and the resolution (potential range between -0.1 V and 0.65 V, pulse width 50 ms, modulation amplitude 50 mV, scan rate of 25 mV s^{-1}).

V.2.8. Samples preparation and analysis

The rapeseed oil extraction was performed according to Pirisi et al.[23], with some modifications. 6 g of rapeseed oil were dissolved in 3 mL of hexane and 6 mL of a MeOH: H_2O solution (60:40 v/v); then the sample was stirred for 1 min (with vortex) and centrifuged for 5 min at 3000 rpm. Thus, the polar fraction was collected, and the extraction procedure was repeated two times. Finally, the extract was washed with 6 mL of hexane and after centrifugation (3000 rpm, 5 min) the polar fraction was separated and dried by using rotavapor. The 'dried' polar fraction was recovered with 1.5 mL of MeOH:H_2O solution (60:40 v/v) and stored at -20 °C in the dark. 1.0 g of the apple puree, 1.0 g of apple homogenized, 0.15 g of lyophilized kalanchoe, and 2.0 g of apple juice were dissolved in a MeOH:H_2O solution (80:20 v/v) with a ratio of 1:5, 1:5, 1:33, and 1:2, respectively. The samples were treated with an ultrasonic bath for 5 minutes and stirred with an orbital shaker at 300 rpm, 30 min in the dark at room temperature. Afterward, the samples were centrifuged (700 g rpm, 5 min) and the supernatant was recovered and adjusted to the respective starting volume with MeOH:H_2O solution (80:20 v/v) and stored at -20 °C in the dark. The electrochemical measurements on the extracts were carried out using DPV (section 2.5). Before analysis, the samples were diluted in 0.01 mol L^{-1} (pH 7.0) phosphate buffer (to fit the calibration linear range) at the following ratios: 1:250 Rapeseed oil, Apple puree, Apple homogenized; 1:25 Apple juice; 1:400 Kalanchoe Crenata. As the PPs in samples are present in different ratios [24], the analysis of the samples has been conducted using the standard addition method. All samples were analyzed in triplicate.

V.3. Results and discussion

V.3.1. Sensor design

In order to develop an electrochemical sensor able to selectively measure hCNs and similar structural analogs, a pertinent nanomaterials-based configuration was employed. **Figure V-2** illustrates the SPE-CB-WS_2/AuNP-CT sensor architecture.

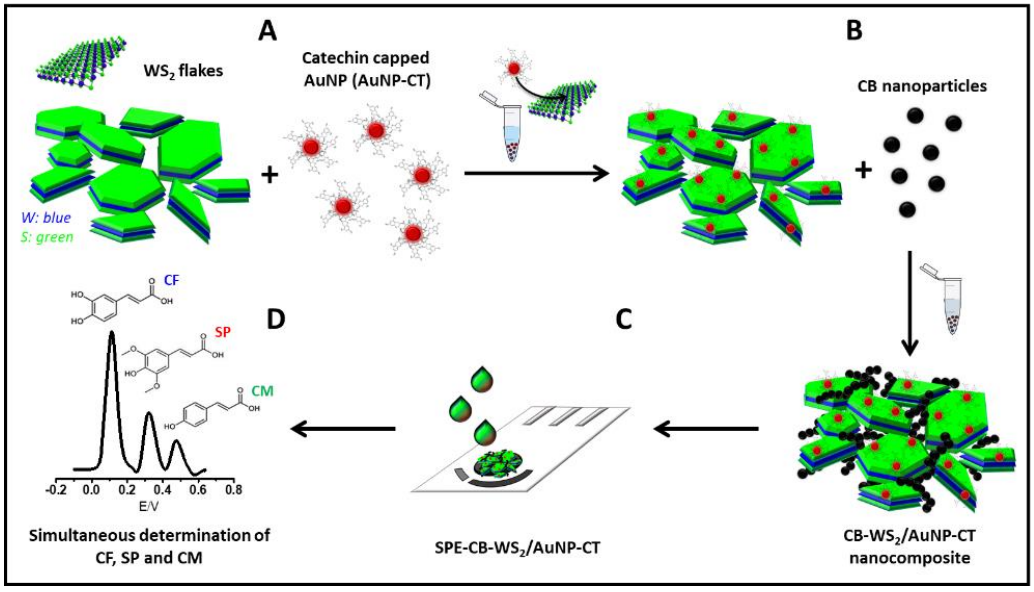

Figure V-2: Scheme of the SPE-CB-WS_2/AuNP-CT architecture for hydroxycinnamic acid structural analogs electrochemical sensing. A: WS_2 decoration with AuNP-CT B: assembly of WS_2/AuNP-CT into CB. C: SPE modification with the CB-WS_2/AuNP-CT nanocomposite. D: DPV simultaneous determination of CF, SP, and CM.

WS_2 flakes decoration with AuNP-CT was carried out using a sonochemical strategy to obtain a WS_2/AuNP-CT anti-fouling/conductive nanohybrid (**Figure V-1**). During WS_2/AuNP-CT decoration, the AuNP-CT solution (**Figure V-3**, red line), resulted completely decoloured, indicating that AuNP-CT were adsorbed on WS_2 flakes, and a well-deposited grey/rubin-red pellet formed by WS_2/AuNP-CT was obtained. The latter, after resuspension, gives a colloidal dispersion with an LSPR maximum at 540±7 nm (**Figure V-3**, blue line), definitely indicating the presence of the two nanomaterials. Finally, the decorated WS_2/AuNP-CT were assembled into a highly electroactive CB network to form the final nanocomposite, that was employed to modify the SPEs giving rise to the SPE-CB-WS_2/AuNP-CT electrochemical sensor.

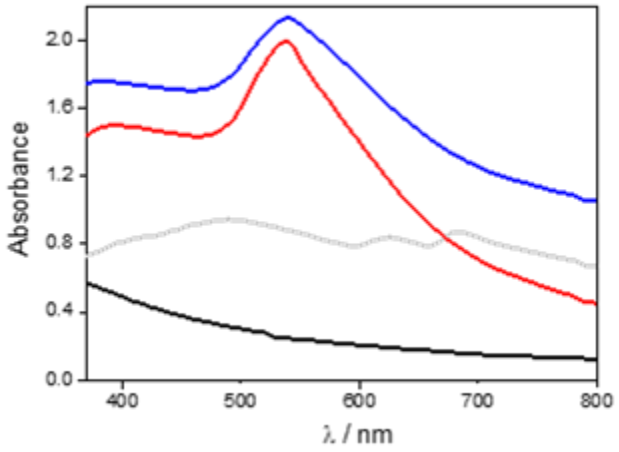

Figure V-3: UV-Vis absorption spectra: WS_2 dispersion diluted 1:5 (v/v) in 100 mmol L^{-1} phosphate buffer (pH 8.0) (grey line); AuNP-CT (red line); WS_2 decorated with AuNP (blue line); reaction mix without WS_2 and AuNP-CT (black line).

Despite the decoration of non-graphene 'layered' nanomaterials (e.g. MoS_2, $HxTiS_2$, etc.) with AuNPs has been attempted using different strategies [8,12,25], the decoration of WS_2 with AuNPs has been explored in lesser extension [13,14] particularly for the development of sensors [15]. In this work, the WS_2 decoration was attempted using AuNPs synthesized using catechin (AuNPs-CT), sodium citrate and sodium borohydride as mild reducing agent following the strategy shown on **Figure V-1**. Only AuNP-CT with their peculiar colloidal chemistry allowed an effective WS_2 nanoflakes decoration. On the other hand, both sodium citrate and sodium borohydride synthesized AuNPs failed to decorate the WS_2 flakes; this was evident by the persistence of the ruby-red colour, during the whole decoration process, indicating the failed interaction and the persistence of AuNPs in solution. This evidence points out the key role of the AuNP-CT colloidal chemistry, which allows a strong interaction with the WS_2 nanoflakes in the experimental conditions used. This behaviour is probably related to the catechin and catechin-related compounds shell around the gold metal core [20,21,26].

V.3.2. Morphological and electrochemical characterization

Figure V-4 reports SEM micrographs (A-C) acquired at different magnifications on the SPE-CB WS_2/AuNP-CT electrode, and EDX analysis (D).

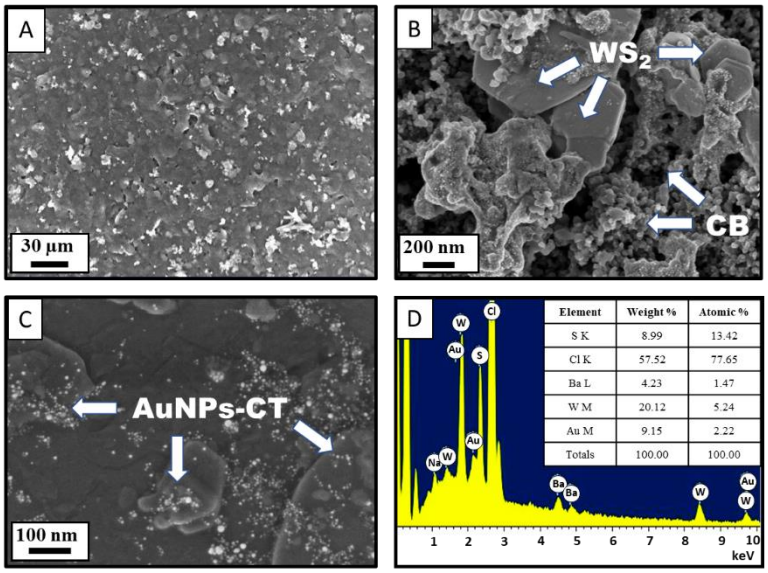

Figure V-4: SEM at different magnifications of the SPE-CB-WS_2/AuNP-CT: 1kX (**A**), 100 kX (**B**), 300 kX (**C**). EDX spectrum from SPE-CB-WS_2/AuNP-CT (**D**).

Figure V-4A depicts the uniform distribution of all the nanocomposite components and the total coverage of the electrode surface. Micrographs with higher magnification (**Figure V-4B**), it is possible to evidence the presence of WS_2 flakes with a broad size distribution centered at around 800 nm (calculated from more than 100 WS_2 flakes). CB primary particles are also visible in **Figure V-4B**, revealing the co-presence of the components and their interaction while their pristine morphology is fully retained. This behaviour can be attributed to the flakes-like conformation of WS_2 that favours their floating on the surface [9,10]. The presence of AuNP-CT with a size distribution centred at around 5±1 nm (see **Figure V-5B**) is further assessed by the micrograph at higher magnification (300 kX) in **Figure V-4C** and confirmed by EDX analysis (**Figure V-4D**); where the amount of Au with respect to W was found around 0.4/1.0. Additional SEM micrographs are reported in **Figure V-6** to better visualize the morphology of the obtained electrodes. The catechin ability to give rise to AuNPs stabilized by the same reacted-catechin (localized in the AuNPs shells) has also been proved [20,21,26], and the formation of a catechins layer on the surface of gold nanoparticles has been

demonstrated by Raman spectroscopy [27] and microscopic analysis [28]. In addition, the ability of catechins to interact with the WS_2 in solution, during the exfoliation phase, has been reported as well [29]. In this study, catechins acting as surfactants, demonstrated to assist the sonication-assisted aqueous exfoliation of TMDs enhancing the TMDs sheets water-dispersibility.

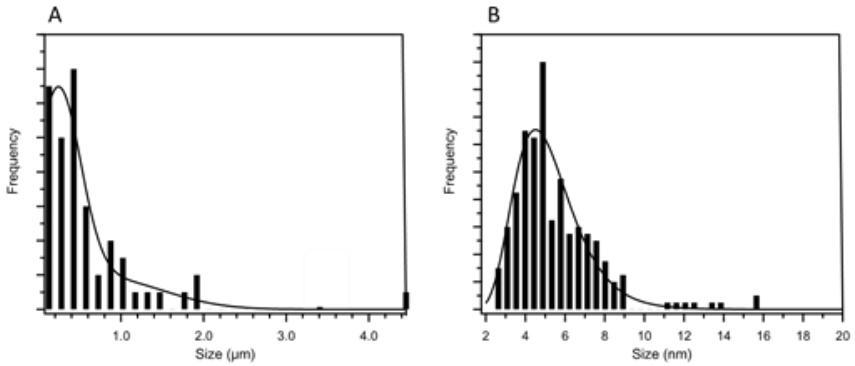

Figure V-5: Size distribution calculated on the SEM micrographs: A) WS2 flakes and B) gold nanoparticles.

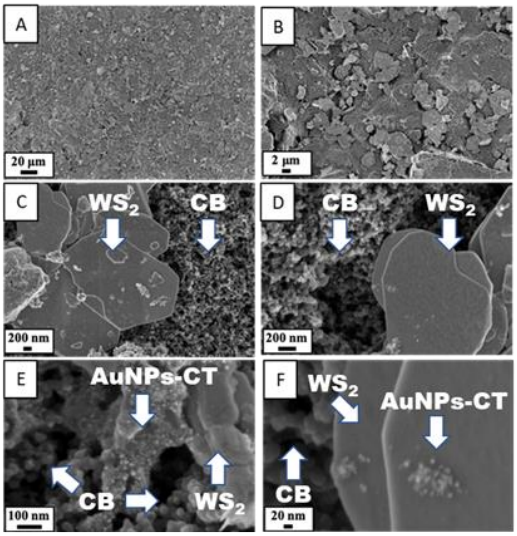

Figure V-6: SEM at different magnifications of the SPE-CB-WS_2/AuNP-CT: 1kX (**A**), 5 kX (**B**), 50 kX (**C**), 100 kX (**D**), 300 kX (**E**), 500 kX (**F**).

On the other hand, the electrochemical behaviour of the modified electrodes was investigated by cyclic voltammetry (CV). To better understand the contribution of each individual component on the final nanocomposite, the heterogeneous rate constant (k^0) was calculated in each electrode using the Nicholson method [30,31]. For a quasi-

reversible process, the relationship between k^0 and the dimensionless parameter (Ψ) is given by the **Eq.V.1**:

$$\Psi = k^0 \left(\frac{n\ \pi\ D_0\ F\ v}{RT} \right)^{-\frac{1}{2}} \qquad \text{Eq.V.1}$$

Where: k^0 is the heterogeneous rate constant (cm s^{-1}), D_O is the diffusion coefficient (cm^2 s^{-1}), v is the scan rate (V s^{-1}), R is the ideal gas constant (J mol^{-1} K^{-1}), n is the number of electrons, F is the Faraday's constant in (C mol^{-1}), T is the temperature (K), and Ψ is the Nicolson dimensionless number. The kinetic parameter Ψ is tabulated as a function of ΔE_P at a set temperature (298 K) for a one-step, one electron process with a transfer coefficient, α, equal to 0.5. The function of ψ (ΔE_P), which fits Nicholson's data, for practical usage is given by the **Eq.V.2** where $X = \Delta E_P$ (V).

$$\Psi = \left(\frac{-0.6288 + 0.0021X}{1 - 0.017X} \right) \qquad \text{Eq.V.2}$$

Therefore, a plot of Ψ vs $\left(\frac{\pi D_0 nvF}{RT}\right)^{-\frac{1}{2}}$ allows the k^0 to be readily determined by the slope. As an example, **Figure V-7A** shows the CVs experiments performed with the SPE-CB-WS_2/AuNP-CT at different scan rates (10, 25, 50, 75, 100, 150, 200 and 400 mV s^{-1}) used to obtain the ΔE_P values (employed to calculating k^0). **Figure V-7B** shows the Nicholson plot of the whole set of electrodes (k^0values obtained are listed in **Table V-1**).

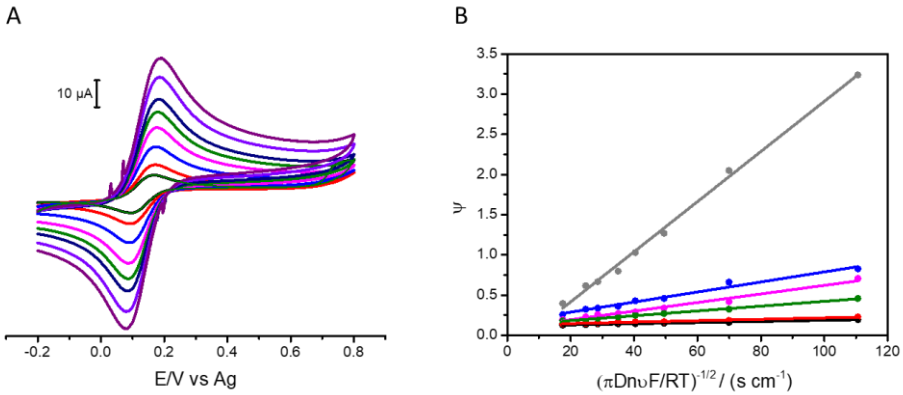

Figure V-7: (**A**) CVs of 1 mmol L^{-1} $[Fe(CN)_6]^{3-/4}$ solution in 0.1 M KCl of SPE-CB-WS_2/AuNP-CT. (**B**) SPE (black line), SPE-WS_2 (red line), SPE-CB (blue line), SPE-WS_2/AuNP-CT (violet line), SPE-CB-WS_2 (green line), SPE-CB-WS_2/AuNP-CT (grey line) Nicholson plots obtained with CVs performed at different scan rates in 1 mmol L^{-1} $[Fe(CN)_6]^{3-/4}$ solution in 0.1 M KCl.

Table V-1: Electrochemical characterization of the set of electrodes[a]

Electrode[a]	$i_{p,a}$ (µA)	$i_{p,c}$ (µA)	$E_{p,a}$ (mV)	$E_{p,c}$ (mV)	ΔE (mV)	$i_{p,a}/i_{p,c}$ (-)	Rct (kΩ)	k^0 (cm s^{-1})
SPE	6.5±0.3	-10.4±0.3	271±5	-29±1	300	0.624	16±1	$7.0\pm0.6\times10^{-4}$
SPE-WS_2	7.3±0.2	-11.1±0.1	264±3	8±1	256	0.660	9.2±0.4	$9.0\pm0.7\times10^{-4}$
SPE-CB	18.2±0.7	-19.6±0.5	183±7	88±2	95	0.928	0.98±0.05	$6.0\pm0.3\times10^{-3}$
SPE-WS_2/AuNP-CT	14.2±0.4	-17.0±0.5	181±5	83±1	98	0.835	2.3±0.2	$5.4\pm0.4\times10^{-3}$
SPE-CB-WS_2	15.4±0.6	-17.4±0.5	205±6	64±1	141	0.889	2.10±0.1	$3.2\pm0.2\times10^{-3}$
SPE-CB-WS_2/AuNP-CT	26.9±0.8	-27.1±0.5	165±2	95±1	70	0.994	2.80±0.01	$3.1\pm0.2\times10^{-2}$

[a] Data are expressed as mean values ± SD (n=3 electrodes)

Figure V-8 shows CVs of 1 mmol L^{-1} $[Fe(CN)_6]^{3-/4-}$ at bare SPE, SPE-WS_2, SPE-CB, SPE-WS_2/AuNP-CT, SPE-CB-WS_2, and SPE-CB-WS_2/AuNP-CT. The results clearly indicate higher electrocatalytic activity with faster electron-transfer (highest k^0) kinetics for the SPE-CB-WS_2/AuNP-CT. In particular, k^0 values follow this trend: SPE < SPE-WS_2 < SPE-CB-WS_2 < SPE-WS_2/AuNP-CT < SPE-CB < SPE-CB-WS_2/AuNP-CT, clearly indicating the contribution of both CB and AuNP-CT in the improvement of the final nanocomposite performance. In order to prove the enhanced properties of WS_2

decoration with AuNP-CT following the proposed sonochemical strategy, the WS_2 decoration has also been attempted via direct drop-casting of AuNP-CT. Nevertheless, worse electrochemical performances were obtained (see **Table V-2**).

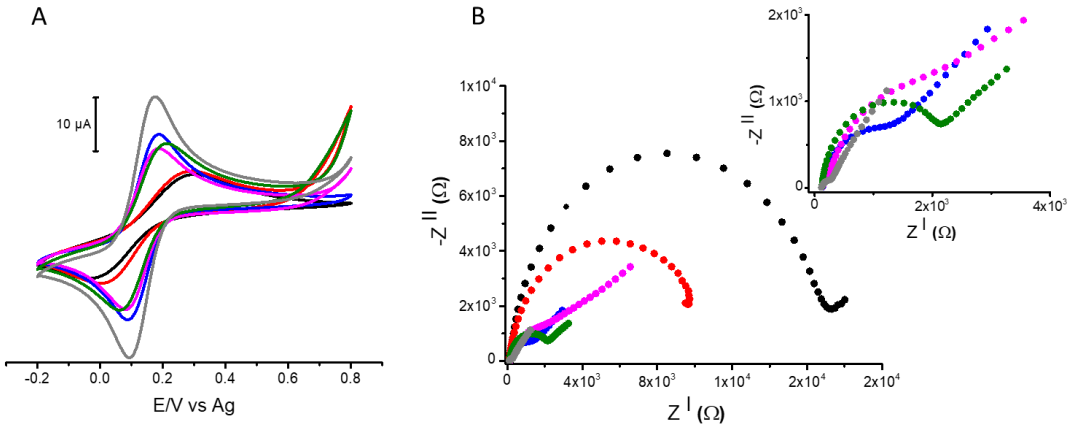

Figure V-8: Electrochemical characterization of the set of electrodes: (**A**) cyclic voltammograms at 50 mV s^{-1} and (**B**) EIS (inset reports the Nyquist plot magnification at low frequencies region). Conditions: 1 mmol L^{-1} $[Fe(CN)_6]^{3-/4-}$ redox probe in 0.1 mol L^{-1} KCl (pH 7.0). The code colour-based legend is as follows bare SPE (black), SPE-WS_2 (red), SPE-CB (blue), SPE-WS_2/AuNP-CT (violet), SPE-CB-WS_2 (green), and SPE-CB-WS_2/AuNP-CT (grey).

Table V-2: Comparison between the electrochemical response of the SPE-CB-WS_2/AuNP-CT sensor (AuNP-CT decoration via assembly approach), and SPE-CB-WS_2-AuNP-CT (AuNP-CT decoration via AuNP-CT drop-casting approach).

Electrode[a]	$i_{p,a}$ (µA)	$i_{p,c}$ (µA)	$E_{p,a}$ (mV)	$E_{p,c}$ (mV)	**ΔE** (mV)	$i_{p,a}$ /$i_{p,c}$ -
AuNP-casted						
SPE-CB-WS_2-AuNP-CT	20.5±2.4	-20.6±1.9	232±9	108±7	124	0.953
AuNP-assembled with WS_2						
SPE-CB-WS_2/AuNP-CT	26.9±0.8	-27.1±0.5	165±2	95±1	70	0.994

[a]Data are expressed as mean values ± SD (n=3 n=3 electrodes), 1 mM $[Fe(CN)_6]^{3-/4-}$ used as a redox probe.

Then, EIS was employed to further characterize the interfacial properties of the whole set of electrodes. The data have been fitted considering the Randless equivalent circuit (**Figure V-8**). As expected, the higher charge-transfer resistance (R_{ct}) was obtained with the bare SPE (R_{ct}=16 kΩ), followed by the SPE-WS_2 (R_{ct}= 9.2 kΩ). The latter little

R_{ct} decrease has been already reported for TMDs modified SPEs [7,8], while R_{ct} values of 2.3, 2.1, 0.98, and 0.28 kΩ were obtained with the SPE-CB-WS_2, SPE-WS_2/AuNP-CT, SPE-CB, and SPE-CB-WS_2/AuNP-CT, respectively. Interestingly, the final nanocomposite (CB-WS_2/AuNP-CT) significantly decreases R_{ct} even in comparison with CB-based electrodes, which are highly conductive transducers [32–35]. Therefore, the AuNP-CT decoration significantly improves the electrochemical performances of WS_2, and the combination of AuNP-CT and CB results in a synergistic effect that further promotes $[Fe(CN)_6]^{3-/4-}$ electron transfer.

V.3.3. Electrochemical behavior of cinnamic acid hydroxy derivatives

Figure V-9A-C reports the cyclic voltammograms obtained for the target hCNs, CF, SP, and CM.

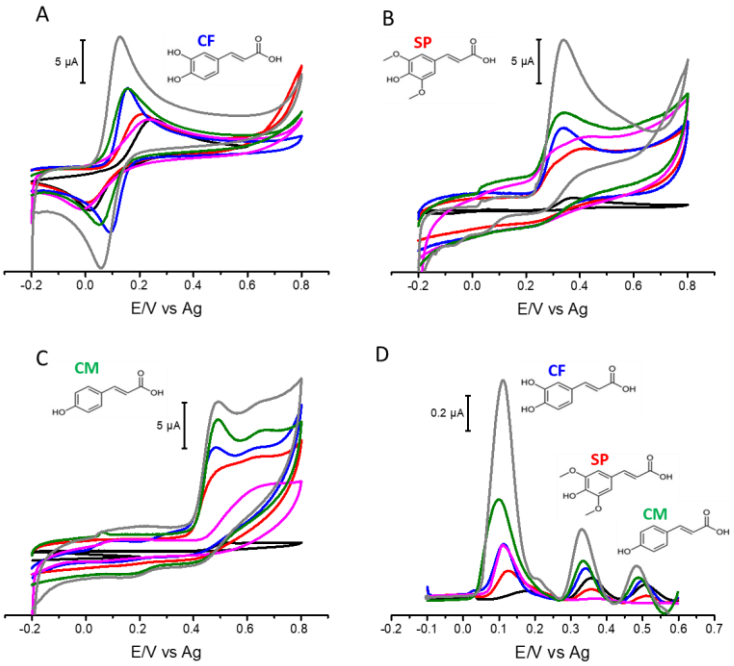

Figure V-9: Cyclic voltammograms at 50 mV s^{-1} of 0.1 mmol L^{-1} CF A), 0.2 mmol L^{-1} SP B) and 0.2 mmol L^{-1} CM C) in 0.1 mmol L^{-1} PB + 0.1 KCl (pH 7.0) at the set of modified electrodes. D) Differential pulse voltammograms (pulse width 50 ms, modulation amplitude 50 mV, scan rate of 25 mV s^{-1}) of a mixture containing CF, SP and CM 20 µmol L^{-1} each in 0.1 mmol L^{-1} PB + 0.1 KCl (pH 7.0) at the set of modified electrodes. The code colour-based legend is as follow: bare SPE (black line), SPE-WS_2 (red line), SPE-CB (blue line), SPE-WS2/AuNP-CT (violet line), SPE-CB-WS_2 (green line), and SPE-CB-WS_2/AuNP-CT (grey line).

CF reversibility improves using the SPE-CB-WS_2/AuNP-CT (ΔE_p=68mV vs. 220mV of the bare SPE) in comparison with the individual nanomaterials-modified electrodes. Noteworthy, the WS_2 itself (SPE-WS_2) gives rise to significantly higher oxidation peaks, compared to the bare electrode (SPE), in particular for the poorly reversible analytes SP and CM. This behaviour indicates a capacity of the WS_2 to interact with the target hCNs. However, WS_2 by itself returns broadened and little defined peaks, while more defined and higher oxidation peaks, occurring at lower potentials, can be detected for the hybrid CB-WS_2 sensor. This improvement is more pronounced in the presence of AuNP-CT (SPE-CB-WS_2/AuNP-CT), because of the higher conductivity of the hybrid nanocomposite.

The electrochemical behaviour of the whole set of electrodes was also evaluated after consecutive CVs (n=5) in the presence of 0.1 mmol L^{-1} CF and 0.2 mmol L^{-1} SP and CM. The voltammetric current retention (calculated comparing the first and the last scan) resulted to be ≥ 9% for SPE, ≥ 95% for SPE-WS_2, ≥ 49% in the case of SPE-CB, ≥ 93% for SPE-WS_2/AuNP-CT, ≥ 91% for SPE-CB-WS_2, and ≥ 94% for SPE-CB-WS_2/AuNP-CT. These data indicate the WS_2 ability to decrease permanent fouling of the sensor. Interestingly, this feature was also observed with mono-phenolic compounds (SP and CM), classically characterized by a very strong passivating tendency on carbon electrodes [2].

Once the electrochemical behaviour of individual hCys has been studied, mixtures of CF, CP and CM were analysed using DPV. **Figure V-9D** reports the DPVs of a mixture of CF, SP, and CM obtained using bare SPE, SPE-WS_2, SPE-CB, SPE-WS_2/AuNP-CT, SPE-CB-WS_2, and SPE-CB-WS_2/AuNP-CT. The SPE-CB-WS_2/AuNP-CT exhibits three sharp peaks at 110 mV, 330 mV, and 490 mV for CF, SP, and CM, respectively. Using the SPE-CB-WS_2/AuNP-CT, an impressive current intensity was obtained for CF, 24.0-fold higher than the bare electrode, 3.5-fold higher than SPE-CB, and 2.0-fold higher than SPE-CB/WS_2. Moreover, clear improvements were obtained even for SP (3.4-fold SPE, 2.3-fold SPE-CB, 1.8-fold SPE-CB/WS_2) and CM (3.0-fold SPE, 2.2-fold SPE-CB, 1.5-fold SPE-CB/WS_2).

These data demonstrate the synergistic effect of the CB-WS_2/AuNP-CT nanocomposite (in terms of selectivity, sensitivity, and fouling resistance) proving its capability for the simultaneous detection of CF, SP, and CM. As it was stated in the introduction section, the voltammetric simultaneous determination of CF, SP, and CM has been not reported in the literature and their determination is classically obtained with separative methods. Probably, this lack of electrochemical methods is related to the hCNs high passivating tendency.

V.3.4. Analytical performance of the SPE-CB-WS_2/AuNP-CT electrochemical sensor

Figure V-10 shows differential pulse voltammograms for the simultaneous calibration of CF (0.3-112 µmol L^{-1}), SP (1.2-125 µmol L^{-1}), and CM (1.3-125 µmol L^{-1}) at SPE-CB-WS_2/AuNP-CT sensor while the insets contains calibration plots for CF (blue line), SP (red line), and CM (green line). **Table V-3** lists the obtained analytical features. Very good linear concentration ranges and suitable LODs were obtained for the three hCNs. Noteworthy, the concomitant presence of the three targets hCNs had not severe influence on the whole calibration performance (the individual calibrations of the hCNs target are reported in **Figure V-11**).

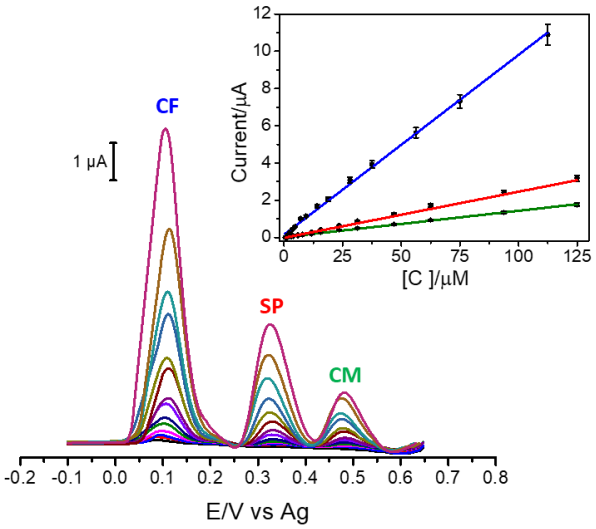

Figure V-10: Differential pulse voltammograms for the simultaneous calibration of CF (0.3-112.0 µmol L^{-1}), SP (1.2-125.0 µmol L^{-1}), and CM (1.3-125.0 µmol L^{-1}) at SPE-CB-WS_2/AuNP-CT sensor. Insets: calibration plots for CF (blue line), SP (red line), and CM (green line) (n=15 assayed concentrations, n=3 replicates each). Conditions: 0.1 mmol L^{-1} PB + 0.1 KCl, pH 7.0; pulse width 50 ms, modulation amplitude 50 mV, scan rate of 25 mV s^{-1}.

Table V-3: Calibration equations and analytical features for individual (top) and simultaneous (bottom) determination of the target hCNs at SPE-CB-WS2/AuNP-CT.

Analyte	Linear range (µmol L^{-1})	Linear equation (y= $i_{p,a}$/µA; x= [analyte]/µmol L^{-1})	R^2	LOD (µmol L^{-1})	LOQ (µmol L^{-1})
Caffeic acid[a]	0.3-200.0	y=0.0869x-0.0473	0.9998	0.10	0.30
Sinapic acid[a]	0.6-300.0	y=0.0309x-0.0458	0.9996	0.20	0.60
p-Coumaric acid[a]	0.9-175.0	y=0.0186x-0.0019	0.9990	0.30	0.90
Caffeic acid[b]	0.3-112.0	y=0.0945x+0.1564	0.9990	0.10	0.30
Sinapic acid[b]	1.2-125.0	y=0.0250x+0.0198	0.9990	0.40	1.20
p-Coumaric acid[b]	1.3-125.0	y=0.0141+0.0211	0.9990	0.40	1.30

[a]Data obtained increasing the concentration of one analyte, keeping constant the concentrations of the other two hCNs. [b]Data obtained increasing the three analytes concentrations simultaneously (n=3)

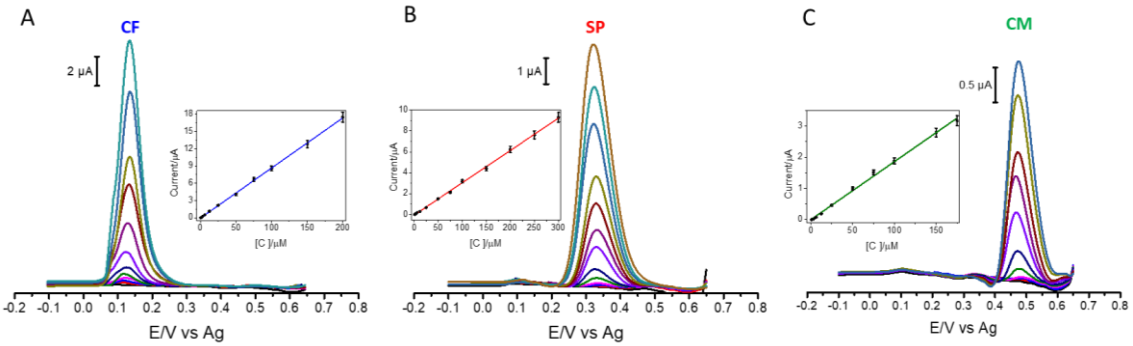

Figure V-11: Differential pulse voltammograms for the individual calibrations of CF, SP, and CM at SPE-CB-WS_2/AuNP-CT sensor. (**A**) CF at the concentration linear range of 0.3 to 200.0 µmol L^{-1} (n=12), in presence of fixed concentrations of SP and CP (at 3.0 µmol L^{-1} and 6.0 µmol L^{-1}, respectively); (**B**) SP at the concentration linear range of 0.6 to 300.0 µmol L^{-1} (n=13), in presence of fixed concentrations of CA and CM (at 0.8 µmol L^{-1} and 6.0 µmol L^{-1}, respectively); (**C**) CM at the concentration linear range of 0.9 to 175.0 µmol L^{-1} (n=11), in presence of fixed concentrations of CA and SP (at 0.8 µmol L^{-1} and 3.0 µmol L^{-1}, respectively); Insets: analytical curves for each compound (CF: blue line; SP red line; CM green line) obtained with the mean values of three repetitions. DPV Conditions: 0.1 mmol L^{-1} PB + 0.1 KCl mmol L^{-1} (pH 7.0), pulse width 50 ms, modulation amplitude 50 mV, scan rate of 25 mV s^{-1}.

Individual and simultaneous determination of SF, SP, and CM return repeatable results (RSD $i_{p,a}$ ≤ 3%, n=3) and a very good inter-electrodes precision (RSD $i_{p,a}$ ≤4%, n =10), indicating a reproducible and robust fabrication strategy. Long-term stability was also tested for 6 months (control every week), checking the DPVs responses of the sensor towards CF, SP, and CM assayed simultaneously. The responses of the SPE-CB/WS_2-AuNP-CT sensor slightly decrease in the first two months to 95% and remain stable for the following 4 months (up to 94%).

To further prove the SPE-CB-WS_2/AuNP-CT antifouling ability even in the case of simultaneous analysis of the studied hCNs, DPVs of the ternary mixture at fixed concentrations (CF, SP, and CM 20.0 µmol L^{-1} each) have been run before and after the whole set of measurements (n=15), as shown in **Figure V-12**. The signal retention obtained has been 98%, 97%, and 97% for CF, SP, and CM, respectively, confirming the electrode ability to avoid permanent passivation, commonly caused by these compounds.

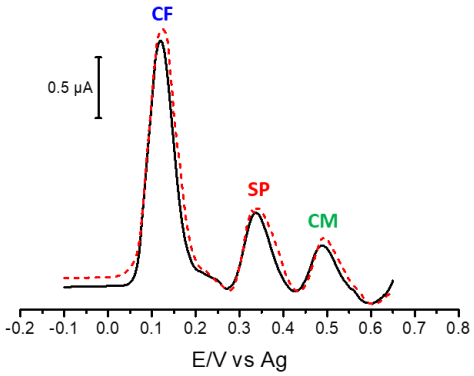

Figure V-12: Differential pulse voltammograms (pulse width 50 ms, modulation amplitude 50 mV, scan rate of 25 mV s^{-1}) of a mixture containing CF, SP, and CM 20 µmol L^{-1} each in 0.1 mmol L^{-1} PB + 0.1 KCl (pH 7.0) obtained using the same electrode before (black line) and after (red dashed line) the performing of calibration runs (n=15) as reported in Fig.4

V.3.5. Simultaneous determination of CF, SP, and CM in food samples

In order to prove the applicability of the SPE-CB-WS_2/AuNP-CT sensor, five commercial products: rapeseed oil, Kalanchoe Crenata, apple puree, apple homogenized, and apple juice were analyzed. **Figure V-13** shows the obtained voltammograms.

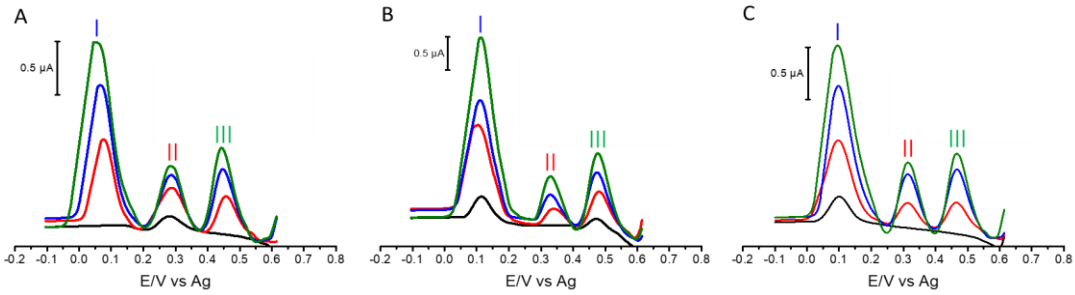

Figure V-13: Differential pulse voltammograms for sample analysis at SPE-CB-WS2/AuNP-CT sensor. Class-selective hCNs-based determination in food samples: rapeseed oil extract (A), kalanchoe Crenata (B) and apple juices (C); Peak I (CF equivalents), Peak II (SP equivalents), Peak III (CM equivalents). Samples spiked with three increasing concentrations of the mixture of CF, SP, and CM (unspiked samples: black line). Spiked samples, CF, SP, and CM concentration, respectively: 5, 10, and 15 µmol L^{-1} (red line); 10, 20, and 30 µmol L^{-1} (blue line); 15, 30 and 45 µmol L^{-1} (green line). Conditions: 0.1 mmol L^{-1} PB + 0.1 KCl, pH 7.0; pulse width 50 ms, modulation amplitude 50 mV, scan rate of 25 mV s^{-1}.

For the sake of clarity, we need to take into account that in nature PPs are never found as single compounds, but they are always present in complex mixtures in different

ratios. Therefore, the DPVs signals obtained have been assigned not only to the individual hCNs standard but also to the combined effect of other analogous structures (i.e. same hydroxyl moieties arrangement in the phenol structure) potentially present in the samples. Thus, this method should be considered as a class selective index, able to return information on the PPs structure and amount. In particular, with the proposed sensor an hCN-based triple index can be obtained, able to discriminate hCN with different hydroxylic functions arrangement and therefore different antioxidant capacity. Thus, the proposed indexes result able to simultaneously discriminate i) CF equivalents (Peak I), orto-diphenols structures that are oxidized at lowest oxidation potential ($E_{p,a}$ ~ 110 mV), possessing higher antioxidant capacity; ii) SP equivalents (Peak II), monophenols with a 4-hydroxy-3,5-dimethoxy structure, detected at an intermediate oxidation potential ($E_{p,a}$ ~ 330 mV), with intermediate antioxidant capacity; iii) SP equivalents (Peak III), monophenols, with higher oxidation potential ($E_{p,a}$ ~ 490 mV) and lower antioxidant capacity. This index results fully consistent with the literature, where the antioxidant capacity series of PPs follows the trend o-diphenols>methoxy-substituted monophenols>monophenols [20,21]. Thus, in this case, the oxidation potential and the peak intensity can return qualitative and quantitative information on the antioxidant capacity. For this reason, this approach may result particularly appealing for samples rich in cinnamic acids and PPs with similar structures but different antioxidant capacities. Therefore, as shown in **Figure V-13**, samples can be classified with the proposed indexes. **Table V-4** lists the hCNs-equivalents quantitative levels obtained for sample analysis.

Table V-4: Determination of hCNs equivalents in food samples[a].

Sample	Added (µmol L^{-1})			Found (µmol L^{-1})			Recovery (%)			RSD (%)		
	CF	SP	CM	CF	SP	CM	CF	SP	CM	CF	SP	CM
Rapeseed oil	-	-	-	3.3	6.3	<LOD	-	-	-	4	2	-
	5	10	15	8.7	16.6	15.2	108	103	101	3	4	1
	10	20	30	14.1	24.5	32.5	108	91	109	1	3	3
	15	30	45	18.9	32.2	43.7	104	87	97	1	2	5
Kalanchoe Crenata	-	-	-	5.3	<LOD	13.5	-	-	-	3	-	3
	5	10	15	10.0	10.4	29.4	94	104	106	4	4	3
	10	20	30	14.6	17.7	46.0	95	89	109	4	4	3
	15	30	45	18.6	29.6	59.0	86	99	101	1	3	2
Apple juice	-	-	-	3.5	<LOD	2.4	-	-	-	4	-	4
	5	10	15	8.6	9.3	16.0	102	93	91	2	3	4
	10	20	30	12.6	21.1	32.8	91	105	101	1	2	3
	15	30	45	16.9	27.8	42.3	89	93	87	1	4	4
Apple puree	-	-	-	8.2	<LOD	1.2	-	-	-	1	-	3
	5	10	15	13.1	8.7	15.4	98	87	94	1	3	4
	10	20	30	18.7	20.1	35.9	105	100	88	1	4	4
	15	30	45	24.2	26.0	42.4	109	87	94	1	4	3
Apple homogenized	-	-	-	5.3	<LOD	<LOD	-	-	-	2	-	-
	5	10	15	10.5	9.0	13.4	104	90	89	4	3	3
	10	20	30	14.2	17.3	27.3	90	87	88	2	4	4
	15	30	45	21.6	26.5	39.2	109	88	87	1	4	4

[a] Data expressed as mean value, n=3.

The results obtained in the present study compared to other nanomaterials-based electrodes demonstrate better or comparable performances in terms of LOD, linear range, and reusability (in terms of fouling resistance). However, no works regarding the simultaneous detection and determination of CF, SP, and CM have been found, and most of them concern the simultaneous determination only of two phenolic acid classes. Furthermore, even when individually analysed, little evidence is provided regarding the fouling resistance, which is the main analytical limitation for these compounds. In our opinion, the latter drawback is the main reason for the absence of electroanalytical approaches devoted to the simultaneous measurement of hCNs.

Definitely the electrochemical approach still remains attractive to study PPs 'antioxidant capacity'. Indeed, conceptually speaking, the electrochemical approach can return qualitative and quantitative information regarding antioxidant capacity, since phenols oxidation obtained at lowest potentials are inherently correlated with high antioxidant capacities [41,42]. This valuable information is not obtainable with classic spectrophotometric methods. On the other hand, despite the chromatographic methods enable to assess PPs composition and content, they are not able to evaluate the antioxidant capacity (neither total as well as of classes of compounds) [43].

Table V-5: Nanomaterial-based electrodes for simultaneous phenolics acid classes determination

Electrode	Technique	Sample	Analyte	Linear range	LOD	Fouling resistance	Ref.
				(µmol L^{-1})	(µmol L^{-1})	(ip,a decrease)	
CPE-NiTiO3	DPV	Peeling skin lotion	o-hydroxybenzoic acid,	10-90	0.38	5%, n =15	[38]
			p-hydroxybenzoic acids	10-90	0.10		
PTE-CB	DPV	Olive oil	Ortho-diphenols,	10-75	6.0	12%, n=26	[35]
			mono-phenols	10-75	20.0		
GCE-polyPCV/f-SWCNTs	DPV	Cognac and brandy	Gallic acid,	0.75-10	0.11	-	[39]
			ellagic acids	0.75-10	0.12		
GCE-rGO	SWV	Mango Juice	Gallic acid,	20-144	30.8	5%, n =10	[40]
			protocatechuic acids	20-166	10.2		
SPE-CB-WS2/AuNP-CT	DPV	Rapeseed oil, Kalanchoe Crenata, Apple juice, puree, and homogenized	Caffeic acid,	0.4-112	0.09,	3%, n = 15 (three analytes simultaneous determination)	This work
			sinapic acid,	0.7-125	0.36,		
			p-coumaric acid	1.4-93	0.39		

CPE-$NiTiO_3$: carbon paste electrode modified with nickel titanate nanoceramic; PTE-CB: Press-transferred carbon black electrode; GCE-polyPCV/f-SWCNTs: glassy carbon electrode modified with polyaminobenzene sulfonic acid functionalized single-walled carbon nanotubes; GCE-rGO: glassy carbon electrode modified with reduced graphene oxide.

V.4. Conclusions

A high-performance electrochemical sensor based on WS_2 decorated with AuNP-CT and supported in a CB network was successfully developed and applied to the simultaneous determination of a three hCNs-based polyphenolic-class index (accordingly to the hydroxyl moieties arrangement in the phenol structure) in food samples. The proposed sensor takes advantage of the AuNP-CT metallic properties, demonstrating electroactivity towards hydroxyl moieties through assembly in the WS_2 flakes that result in an enhanced conductivity with an exceptional antifouling activity due to WS_2. The final assembly of WS_2/AuNP-CT into CB network exhibited a further conductivity enhancement without loss of antifouling performance. The nanomaterial-based synergistic effect of the sensor results in enhanced selectivity, sensitivity, and reproducibility in the simultaneous determination of class-selective hCNs structural analogs in food samples. Given its excellent electrochemical performance, together with its low cost, disposability, and ease of use, this SPE-CB-WS_2/AuNP-CT nanocomposite-based sensor represents a powerful candidate for the development of electrochemical devices for the determination of (bio)compounds with high passivation tendency.

V.5. References

[1] H. El Gharras, Polyphenols: Food sources, properties and applications - A review, Int. J. Food Sci. Technol. 44 (2009) 2512–2518. doi:10.1111/j.1365-2621.2009.02077.x.

[2] F. Della Pelle, D. Compagnone, Nanomaterial-Based Sensing and Biosensing of Phenolic Compounds and Related Antioxidant Capacity in Food, Sensors. 18 (2018) 462. doi:10.3390/s18020462.

[3] D. Del Rio, A. Rodriguez-Mateos, J.P.E. Spencer, M. Tognolini, G. Borges, A. Crozier, Dietary (Poly)phenolics in Human Health: Structures, Bioavailability, and Evidence of Protective Effects Against Chronic Diseases, Antioxid. Redox Signal. 18 (2013) 1818–1892. doi:10.1089/ars.2012.4581.

[4] M. Serafini, I. Peluso, Functional Foods for Health: The Interrelated Antioxidant and Anti-Inflammatory Role of Fruits, Vegetables, Herbs, Spices and Cocoa in Humans., Curr. Pharm. Des. 22 (2016). doi:10.2174/1381612823666161123094235.

[5] J. Teixeira, A. Gaspar, E.M. Garrido, J. Garrido, F. Borges, Hydroxycinnamic acid antioxidants: An electrochemical overview, Biomed Res. Int. 2013 (2013). doi:10.1155/2013/251754.

[6] X. Huang, Z. Zeng, H. Zhang, Metal dichalcogenide nanosheets: Preparation, properties and applications, Chem. Soc. Rev. 42 (2013) 1934–1946. doi:10.1039/c2cs35387c.

[7] M. Pumera, A.H. Loo, Layered transition-metal dichalcogenides (MoS2and WS2) for sensing and biosensing, TrAC - Trends Anal. Chem. 61 (2014) 49–53. doi:10.1016/j.trac.2014.05.009.

[8] S. Su, Y. Xu, Q. Sun, X. Gu, L. Weng, L. Wang, Noble metal nanostructure-decorated molybdenum disulfide nanocomposites: synthesis and applications, J. Mater. Chem. B. 6 (2018) 5323–5334. doi:10.1039/c8tb01659c.

[9] F. Della Pelle, D. Rojas, A. Scroccarello, M. Del Carlo, G. Ferraro, C. Di Mattia, M. Martuscelli, A. Escarpa, D. Compagnone, High-performance carbon black/molybdenum disulfide nanohybrid sensor for cocoa catechins determination using an extraction-free approach, Sensors Actuators B Chem. 296 (2019) 126651. doi:10.1016/j.snb.2019.126651.

[10] D. Rojas, F. Della Pelle, M. Del Carlo, E. Fratini, A. Escarpa, D. Compagnone, Nanohybrid carbon black-molybdenum disulfide transducers for preconcentration-free voltammetric detection of the olive oil o-diphenols hydroxytyrosol and oleuropein, Microchim. Acta. 186 (2019) 363. doi:10.1007/s00604-019-3418-5.

[11] A. Aziz, M. Asif, G. Ashraf, M. Azeem, I. Majeed, M. Ajmal, J. Wang, H. Liu, Advancements in electrochemical sensing of hydrogen peroxide, glucose and dopamine by using 2D nanoarchitectures of layered double hydroxides or metal dichalcogenides. A review, Microchim. Acta. 186 (2019) 671. doi:10.1007/s00604-019-3776-z.

[12] Y. Shi, J.K. Huang, L. Jin, Y. Te Hsu, S.F. Yu, L.J. Li, H.Y. Yang, Selective decoration of Au nanoparticles on monolayer MoS2 single crystals, Sci. Rep. 3 (2013) 1839. doi:10.1038/srep01839.

[13] A.Y. Polyakov, L. Yadgarov, R. Popovitz-Biro, V.A. Lebedev, I. Pinkas, R. Rosentsveig, Y. Feldman, A.E. Goldt, E.A. Goodilin, R. Tenne, Decoration of WS_2 nanotubes and fullerene-like mos2 with gold nanoparticles, J. Phys. Chem. C. 118 (2014) 2161–2169. doi:10.1021/jp407388h.

[14] J.R. Dunklin, P. Lafargue, T.M. Higgins, G.T. Forcherio, M. Benamara, N. McEvoy, D.K. Roper, J.N. Coleman, Y. Vaynzof, C. Backes, Production of monolayer-rich gold-decorated 2H–WS_2 nanosheets by defect engineering, Npj 2D Mater. Appl. 1 (2017) 43. doi:10.1038/s41699-017-0045-z.

[15] Y. Wang, J. Ma, X. Ye, W.L. Wong, C. Li, K. Wu, Enhanced effects of ionic liquid and gold nanoballs on the photoelectrochemical sensing performance of WS_2 nanosheets towards 2,4,6-tribromophenol, Electrochim. Acta. 271 (2018) 551–559. doi:10.1016/j.electacta.2018.03.176.

[16] A. Puangjan, S. Chaiyasith, An efficient ZrO_2/Co_3O_4/reduced graphene oxide nanocomposite electrochemical sensor for simultaneous determination of gallic acid, caffeic acid and protocatechuic acid natural antioxidants, Electrochim. Acta. 211 (2016) 273–288. doi:10.1016/j.electacta.2016.04.185.

[17] M.L. Yola, N. Atar, A novel voltammetric sensor based on gold nanoparticles involved in p-aminothiophenol functionalized multi-walled carbon nanotubes: Application to the simultaneous determination of quercetin and rutin, Electrochim. Acta. 119 (2014) 24–31. doi:10.1016/j.electacta.2013.12.028.

[18] S. Elçin, M.L. Yola, T. Eren, B. Girgin, N. Atar, Highly Selective and Sensitive Voltammetric Sensor Based on Ruthenium Nanoparticle Anchored Calix[4]amidocrown-5 Functionalized Reduced Graphene Oxide: Simultaneous Determination of Quercetin, Morin and Rutin in Grape Wine, Electroanalysis. 28 (2016) 611–619. doi:10.1002/elan.201500495.

[19] D. Rojas, F. della Pelle, M. del Carlo, D. Compagnone, A. Escarpa, Group VI transition metal dichalcogenides as antifouling transducers for electrochemical oxidation of catechol-containing structures, Electrochem. Commun. (2020) 106718. doi:10.1016/J.ELECOM.2020.106718.

[20] F. Della Pelle, D. Vilela, M.C. González, C. Lo Sterzo, D. Compagnone, M. Del Carlo, A. Escarpa, Antioxidant capacity index based on gold nanoparticles formation. Application to extra virgin olive oil samples, Food Chem. 178 (2015) 70–75. doi:10.1016/j.foodchem.2015.01.045.

[21] F. Della Pelle, A. Scroccarello, M. Sergi, M. Mascini, M. Del Carlo, D. Compagnone, Simple and rapid silver nanoparticles based antioxidant capacity assays: Reactivity study for phenolic compounds, Food Chem. 256 (2018) 342–349. doi:10.1016/j.foodchem.2018.02.141.

[22] F. Della Pelle, C. Angelini, M. Sergi, M. Del, A. Pepe, D. Compagnone, M. Del Carlo, A. Pepe, D. Compagnone, Nano carbon black-based screen printed sensor for carbofuran, isoprocarb, carbaryl and fenobucarb detection: application to grain samples, Talanta. 186 (2018) 389–396. doi: 10.1016/j.talanta.2018.04.082.

[23] F.M. Pirisi, P. Cabras, C.F. Cao, M. Migliorini, M. Muggelli, Phenolic Compounds in Virgin Olive Oil. 2. Reappraisal of the Extraction, HPLC Separation, and Quantification Procedures, J. Agric. Food Chem. 48 (2000) 1191–1196. doi:10.1021/jf991137f.

[24] J.A. Rothwell, J. Perez-Jimenez, V. Neveu, A. Medina-Remón, N. M'Hiri, P. García-Lobato, C. Manach, C. Knox, R. Eisner, D.S. Wishart, A. Scalbert, Phenol-Explorer 3.0: A major update of the Phenol-Explorer database to incorporate data on the effects of food processing on polyphenol content, Database. (2013). doi:10.1093/database/bat070.

[25] X. Gan, H. Zhao, X. Quan, Y. Zhang, An Electrochemical Sensor based on p-aminothiophenol/Au Nanoparticle-Decorated HxTiS2 Nanosheets for Specific Detection of Picomolar Cu (II), Electrochim. Acta. 190 (2016) 480–489. doi:10.1016/j.electacta.2015.12.145.

[26] F. Della Pelle, M.C.M.C.M.C. González, M. Sergi, M. Del Carlo, D. Compagnone, A. Escarpa, Gold Nanoparticles-based Extraction-Free Colorimetric Assay in Organic Media: An Optical Index for Determination of Total Polyphenols in Fat-Rich Samples, Anal. Chem. 87 (2015) 6905–6911. doi:10.1021/acs.analchem.5b01489.

[27] A. Scroccarello, F. Della Pelle, E. Fratini, G. Ferraro, S. Scarano, P. Palladini, D. Compagnone, Colorimetric determination of polyphenols via gold nanoseeds decorated polydopamine film, Microchim. Acta. (2020). doi:10.1007/s00604-020-04228-4.

[28] Y. Choi, M.J. Choi, S.H. Cha, Y.S. Kim, S. Cho, Y. Park, Catechin-capped gold nanoparticles: Green synthesis, characterization, and catalytic activity toward 4-nitrophenol reduction, Nanoscale Res. Lett. 9 (2014) 1–8. doi:10.1186/1556-276X-9-103.

[29] C. Zhang, D.F. Hu, J.W. Xu, M.Q. Ma, H. Xing, K. Yao, J. Ji, Z.K. Xu, Polyphenol-Assisted Exfoliation of Transition Metal Dichalcogenides into Nanosheets as Photothermal Nanocarriers for Enhanced Antibiofilm Activity, ACS Nano. 12 (2018) 12347–12356. doi:10.1021/acsnano.8b06321.

[30] R.S. Nicholson, Theory and application of cyclic voltammetry for measurement of electrode reaction kinetics, Anal. Chem. 37 (1965) 1351–1355.

[31] I. Lavagnini, R. Antiochia, F. Magno, An Extended Method for the Practical Evaluation of the Standard Rate Constant from Cyclic Voltammetric Data, Electroanalysis. 16 (2004) 505–506. doi:10.1002/elan.200302851.

[32] F. Della Pelle, M. Del Carlo, M. Sergi, D. Compagnone, A. Escarpa, Press-transferred carbon black nanoparticles on board of microfluidic chips for rapid and sensitive amperometric determination of phenyl carbamate pesticides in environmental samples, Microchim. Acta. 183 (2016) 3143–3149. doi:10.1007/s00604-016-1964-7.

[33] V. Mazzaracchio, M.R. Tomei, I. Cacciotti, A. Chiodoni, C. Novara, M. Castellino, G. Scordo, A. Amine, D. Moscone, F. Arduini, Inside the different types of carbon black as nanomodifiers for screen-printed electrodes, Electrochim. Acta. 317 (2019) 673–683. doi: 10.1016/j.electacta.2019.05.117.

[34] F. Della Pelle, L. Vázquez, M. Del Carlo, M. Sergi, D. Compagnone, A. Escarpa, Press-Printed Conductive Carbon Black Nanoparticle Films for Molecular Detection at the Microscale, Chem. - A Eur. J. 22 (2016) 12761–12766. doi:10.1002/chem.201601743.

[35] F. Della, R. Di, L. Vázquez, F.J. Palomares, M. Del, M. Sergi, D. Compagnone, A. Escarpa, Press-transferred carbon black nanoparticles for class-selective antioxidant electrochemical detection, Appl. Mater. Today. 9 (2017) 29–36. doi: 10.1016/j.apmt.2017.04.012.

[36] A. Scroccarello, F. Della Pelle, L. Neri, P. Pittia, D. Compagnone, Silver and gold nanoparticles based colorimetric assays for the determination of sugars and polyphenols in apples, Food Res. Int. 119 (2019) 359–368. doi: 10.1016/j.foodres.2019.02.006.

[37] F. Della Pelle, A. Scroccarello, S. Scarano, D. Compagnone, Silver nanoparticles-based plasmonic assay for the determination of sugar content in food matrices, Anal. Chim. Acta. 1051 (2019) 129–137. doi: 10.1016/j.aca.2018.11.015.

[38] F.Z. Kashani, S.M. Ghoreishi, A. Khoobi, M. Enhessari, A carbon paste electrode modified with a nickel titanate nanoceramic for simultaneous voltammetric determination of ortho- and para-hydroxybenzoic acids, Microchim. Acta. 186 (2019) 2–9. doi:10.1007/s00604-018-3113-y.

[39] G. Ziyatdinova, E. Guss, E. Morozova, H. Budnikov, R. Davletshin, V. Vorobev, Y. Osin, Simultaneous voltammetric determination of gallic and ellagic acids in cognac and brandy using electrode modified with functionalized SWNT and poly(pyrocatechol violet), Food Anal. Methods. 12 (2019) 2250–2261. doi:10.1007/s12161-019-01585-6.

[40] R. Abdel-Hamid, A. Bakr, E.F. Newair, F. Garcia, Simultaneous Voltammetric Determination of Gallic and Protocatechuic Acids in Mango Juice Using a Reduced Graphene Oxide-Based Electrochemical Sensor, Beverages. 5 (2019) 17. doi:10.3390/beverages5010017.

[41] A.J. Blasco, M.C. González, A. Escarpa, Electrochemical approach for discriminating and measuring predominant flavonoids and phenolic acids using differential pulse voltammetry: Towards an electrochemical index of natural antioxidants, Anal. Chim. Acta. 511 (2004) 71–81. doi: 10.1016/j.aca.2004.01.038.

[42] A.J. Blasco, M.C. Rogerio, M.C. González, A. Escarpa, “Electrochemical index” as a screening method to determine “total polyphenolics” in foods: A proposal, Anal. Chim. Acta. 539 (2005) 237–244. doi: 10.1016/j.aca.2005.02.056.

[43] A. Escarpa, M.C. González, Approach to the content of total extractable phenolic compounds from different food samples by comparison of chromatographic and spectrophotometric methods, Anal. Chim. Acta. 427 (2001) 119–127. doi: 10.1016/S0003-2670(00)01188-0.

VI. Group VI transition metal dichalcogenides as antifouling transducers for electrochemical oxidation of catechol-containing structures

VI.1. Introduction and objectives

TMDs are a family of layered compounds with MX_2 formula, where M is a transition metal element, typically from group IV to VI and X is a chalcogen (S, Se or Te). These layers form an X–M–X structure where the atoms are strongly held together by covalent bonds, whereas among sheets weak Van der Waals (VdW) interactions occur. Disruption of VdW interactions and exfoliation of the layers can be achieved by employing different techniques as electrochemistry, intercalation chemistry and LPE [1–5]. Among these techniques, LPE stands as the most versatile technique able to produce large quantities of 2D nanosheets with sizes ranging from tenths to hundreds of nanometers, with few layers of thickness [6]. Due to their unique physical and chemical properties, TMDs nanosheets have recently attracted attention [7,8]. These materials have been employed for PPs detection taking advantage of their physical and electronic properties [9–14]. The latter phytochemicals compounds are interesting for their antioxidant properties, particularly those containing catechol moieties, which present the highest antioxidant activity [15,16]. However, the electrochemical detection of these compounds is especially challenging because the oxidation leads to electrode surface passivation [17].

While previous chapters are mainly focused on MoS_2 and WS_2 nanohybrids, in this Chapter the main objective is to carry out a systematic study of the electrochemical properties of four different Group VI TMDs (MoS_2, WS_s, $MoSe_2$ and WSe_2). The aim is to understand whether the properties already found in Chapters III to V for MoS_2 and WS_2 could be expanded to other TMDs. But also, deepen in their advantageous features for electrochemical oxidation of catechol containing flavonoids (CCF) compounds and in the mechanism behind their antifouling properties.

VI.2. Materials and methods

VI.2.1. Reagents and apparatus

MoS_2, WS_2, $MoSe_2$, and WSe_2 were purchased from Alfa Aesar (Germany). Catechin, disodium hydrogen phosphate anhydrous, sodium dihydrogen phosphate hydrate, potassium ferrocyanide, potassium ferricyanide, potassium chloride, and sodium cholate were purchased from Sigma Aldrich (St Louis, MO, USA). Electrochemical measurements were carried out in Autolab PGSTAT 12 potentiostat from Metrohm (Utrecht, Netherlands), Screen-Printed electrodes (SPE) were purchased from Dropsens S.L. (ref. DS110). Stock solutions of polyphenol standards were prepared in methanol at a concentration of 10^{-2} mol L^{-1} and stored at -20 ºC in the dark.

VI.2.2. TMDs-SPEs Preparation

TMDs exfoliation was carried out from solutions containing 10 mg mL^{-1} of the unexfoliated TMDs and 3 mg mL^{-1} of sodium cholate as surfactant. Solutions are first 'homogenized' in a bath sonicator (3000683 Ultrasons Selecta, Barcelona, Spain) for 15 min. Then, the solution was further sonicated in a tip sonicator for 3 h, keeping the temperature below 25 ºC using an ice bath. The sonication was carried out using a pulses program (2 s ON/ 1 s OFF and 60% amplitude) to minimize sample heating. Then, the TMD dispersion was centrifuged for 30 min at 500 RCF to eliminate unexfoliated material. The supernatant was collected and washed-centrifuged with water, ethanol, and isopropanol to eliminate the excess of surfactant; each washing step was repeated in triplicate. The washed TMDs were kept dry for further use. Electrode modification was carried out by drop-casting 5 µL of a 1 mg/mL dispersion of the washed TMDs

VI.2.3. Electrochemical Characterization

SPEs-TMDs were investigated using CV and EIS carried out in 5 mmol L^{-1} $[Fe(CN)_6]^{3-/4}$.EIS experiments were performed using a sinusoidal wave of 10 mV of amplitude in the 10^5 to 10^{-2} Hz frequency range at open circuit potential.

VI.2.4. Microstructure and elemental characterization

Raman spectra were recorded using an Alpha 300 AR (WITec, Ulm, Germany) confocal Raman microscope with laser wavelength set at 532 nm. Scanning electron microscopy (SEM) micrographs and were obtained with a JEOL 6335 F microscope (JEOL USA, Massachusetts, United States)) using an acceleration voltage of 5 kV. The TMDs flakes size distribution (performed on an average value of 50-100 'particles') were evaluated with ImageJ, v.1.49.p, the micrographs were converted into binary images by setting a threshold and then analyzed [18]

VI.3. Results and discussion

There is a lack of systematic studies about the electrocatalytic properties of TMDs, in particular towards PPs compounds. Therefore, electrocatalytic properties of group VI MX_2 (MoS_2, WS_2, $MoSe_2$, and WSe_2) towards CCF have been systematically evaluated in this work.

VI.3.1. MX_2 nanosheets exfoliation and characterization

LPE in water/sodium cholate solutions have been chosen in order to obtain MX_2 nanosheets. This approach has been previously reported to be able to produce a comparable degree of exfoliation among the different TMDs [19], which is hard to achieve employing organic solvents or other water/surfactant mixtures. [20].

To confirm the exfoliation process, scanning electron microscopy (SEM) and Raman Spectroscopy were performed. SEM images of bulk and exfoliated MX_2 are presented in **Figure VI-1**. In all cases, lateral size was extremely reduced compared to the bulk material confirming the formation of MX_2 nanosheets.

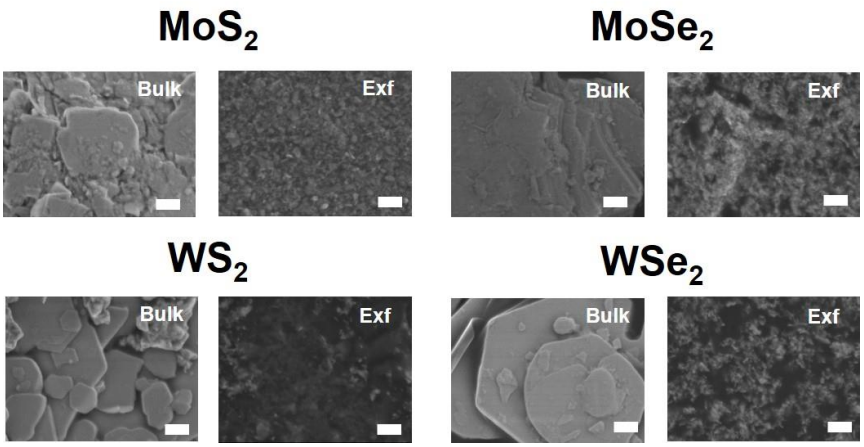

Figure VI-1: Scanning electron micrographs of bulk and exfoliated MX2. Scale bar: 1 µm.

Size distribution of exfoliated materials is shown in **Figure VI-2**. The mean size was 193±94,170±33, 173±26 and 164±54 nm for MoS_2, WS_2, $MoSe_2$ and WSe_2 respectively. Furthermore, nanosheets show rough surface and wrinkled edges compared to the smooth surface of bulk and defined edges of the bulk material that presumably has been incorporated during the exfoliation process [21].

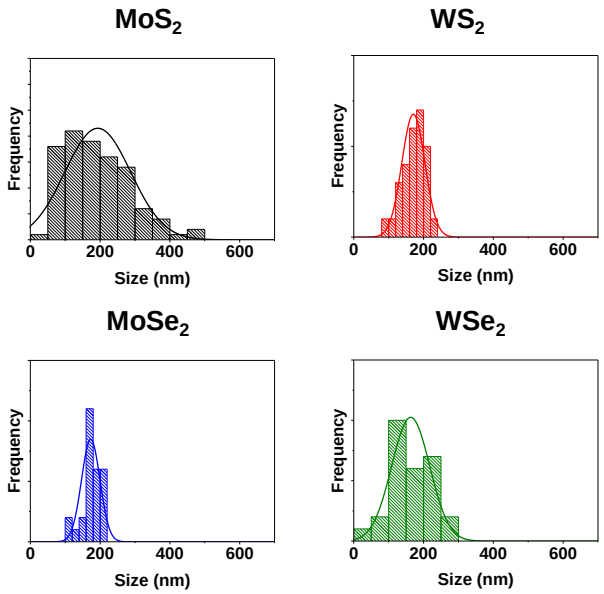

Figure VI-2: Size distributions of the exfoliated MX2 from the SEM images of **Figure VI-1**.

Raman spectroscopy is strongly related to layer thickness and crystalline structure of MX_2; therefore, it was employed to further characterize them. **Figure VI-3** reports Raman spectra of bulk and exfoliated MX_2. MoS_2 spectra consisted of two different bands, the in-plane (E^1_{2g}) and out-of-plane (A_{1g}) vibrations modes at around 380 and 405 cm^{-1}, respectively. Considering the data from the exfoliated material, softening and broadening (FWHM increase ~2 cm^{-1}) of both vibration modes are observed with respect to bulk material. $MoSe_2$ spectra show a well-defined peak at 250 cm^{-1} attributed to the A_{1g} vibration mode. In the case of the exfoliated material, similarly to MoS_2, the peak is slightly softened and notably broadened (FWHM from 9 to 17 cm^{-1}) compared to bulk material. These results indicate a decrease in the number of layers and lateral size suggesting the success of the exfoliation process [21,22]. In the case of WS_2, two peaks are recorded at 350 cm^{-1} and 420 cm^{-1} ascribed to E^1_{2g} and A_{1g}, respectively. In this case, no significant softening or broadening is observed. However, the ratio

between the intensity of the peak E^1_{2g} and A_{1g} is higher in the case of the exfoliated material (1.7 vs. 1); this is also considered an index of a successful exfoliation [23,24]. WSe_2 present both E^1_{2g} and A_{1g} modes overlapped and centered around 250 cm^{-1}. The Raman shift difference between E^1_{2g} and A_{1g} peak is related to the thickness and varies from 3 cm^{-1} to 11 cm^{-1} from bulk to monolayer respectively [25]. In the recorded spectra, a shoulder peak becomes more distinguishable in the case of the exfoliated material, indicating a higher separation of the vibration modes and hence a successful exfoliation.

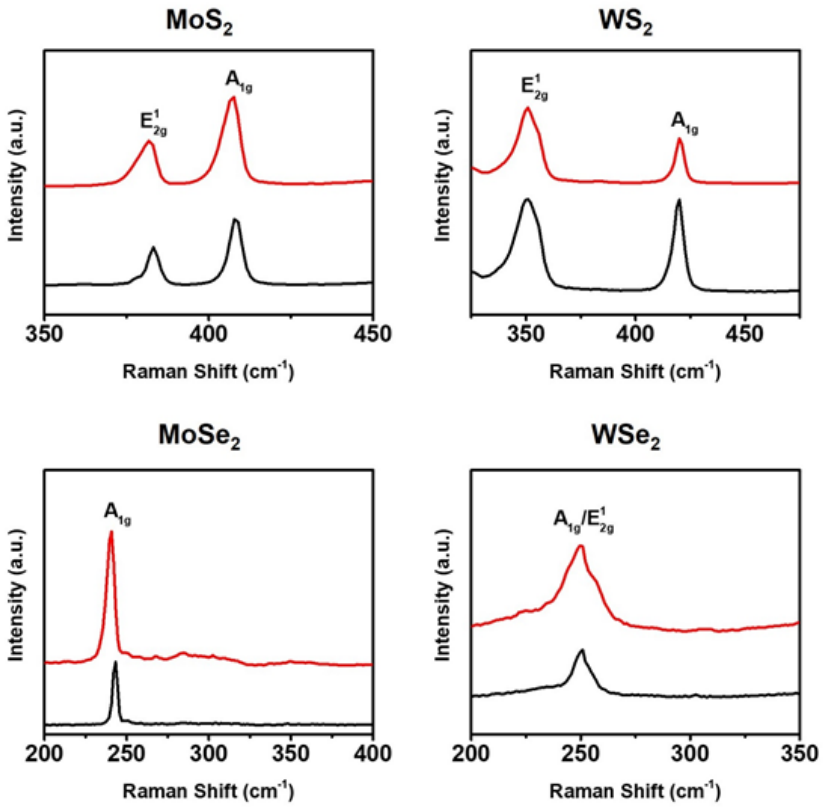

Figure VI-3: Raman spectra of exfoliated (red) and bulk (black) MX_2.

In order to further confirm the chemical composition of the sheets, the presence of MoO_3 (820 cm^{-1}) and WO_3 (697 cm^{-1}) vibrational modes have also been studied. In **Figure VI-4**, no peaks related to the oxides can be seen, except from WS_2, where a slight signal can be seen at 698 cm^{-1}. A signal of lower intensity is achieved in the case of the exfoliated material which can be attributed to the elimination of the oxides during the washing steps [26].

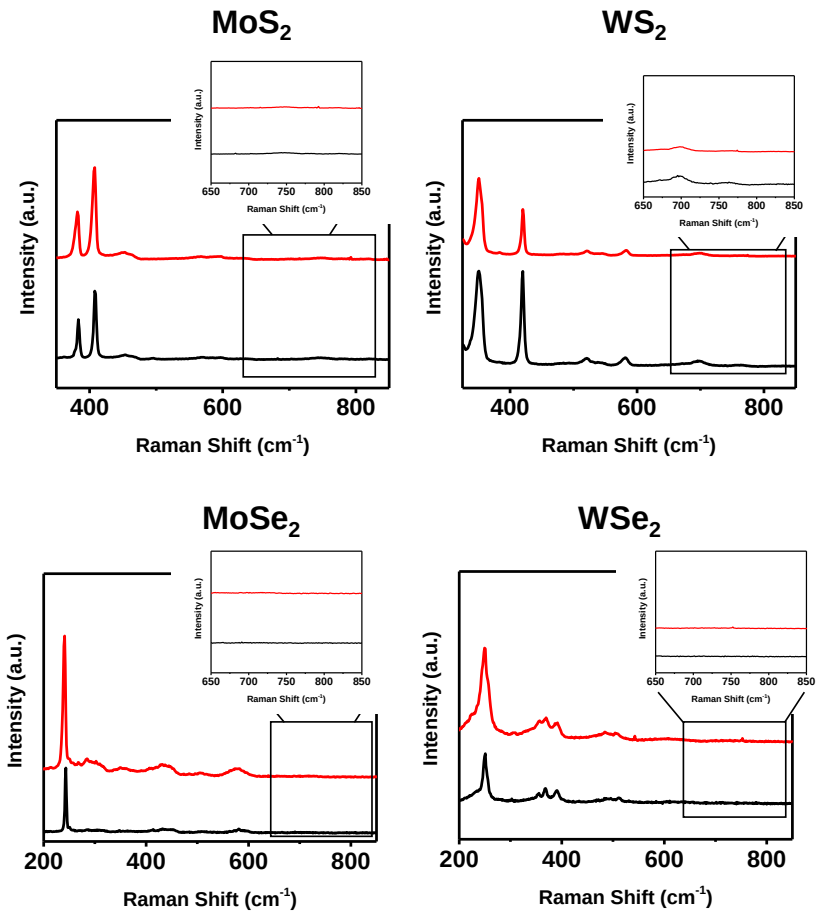

Figure VI-4: Raman spectra of bulk (black line) and exfoliated MX_2 (red line), inset shows a zoom of the Raman shift related to MoO_3 (820 cm^{-1}) and WO_3 (697 cm^{-1}).

VI.3.2. Electrochemical characterization

Electrode kinetics is a critical aspect in the development of new nanomaterials for sensing purposes, fast kinetics are desirable for their use as an electrochemical transducer for molecules of interest. Firstly; the possible influence of the surfactant was evaluated by CV in phosphate buffer recording the inherent electrochemistry of these materials (**Figure VI-5**). It can be seen that the anodic peak due to the oxidation of the metallic center of the MX_2 become more evident and sharper and a new cathodic peak appeared due to the oxygen reduction reaction (ORR) on the washed samples in comparison with those obtained in the just exfoliated ones. These results evidence that despite the great influence of the surfactant, the introduced washing steps enabled to obtain well-defined voltammograms due to the inherent electrochemistry of TMDs comparable to those reported in literature which employs exfoliation methods without the use of surfactant [27,28].

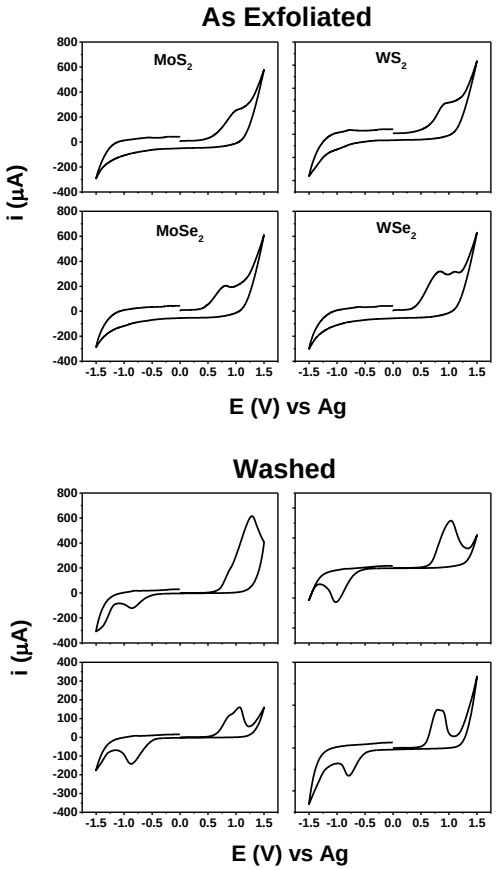

Figure VI-5: Cyclic voltammograms of SPE-modified with MX_2 as exfoliated and after the washing steps. CV recorded at 100 mV s^{-1} in phosphate buffer (pH=7).

Then, the electrochemical characterization of the selected Group VI MX_2 was performed employing CV and EIS using $[Fe(CN)_6]^{3-/4-}$, as inner-sphere redox probe. In each technique, the heterogeneous electron transfer rate (k^0) is inversely proportional to the peak separation (ΔEp) and the resistance to charge-transfer (R_{CT}), respectively. In fact, k^0 can be estimated from the ΔEp obtained at different scan rates following the Nicholson method [29] (See Chapter V for datails on the calculation). **Figure VI-6A** shows the CV performed using different MX_2 modified electrodes. As can be seen, the ΔEp values follow the trend: MoS_2 (275±19 mV)>WS_2 (203±13 mV) >WSe_2 (190±18 mV) >$MoSe_2$ (150±10 mV), showing the superior electrochemical performance of the selenides versus sulfides. By the application of the Nicholson method in the 5 to 100 mV/s scan rates range, k^0 values of $[(3.7\pm0.4) <(5.5\pm0.4) <(6.4\pm0.5) <(7.8\pm0.7)]\cdot10^{-4}$ cm s^{-1} are obtained for MoS_2, WS_2, WSe_2, and $MoSe_2$, respectively. In addition, EIS experiments were also carried out and the data were plotted in the Nyquist plot where the diameter of the semi-circle corresponds to the charge transfer resistance value and the linear part to the diffusion-controlled region. Impedance data were successfully fitted considering the Randles equivalent circuit ($\chi^2<0.025$), shown in the inset of **Figure VI-6B** where R_s, R_{CT}, C_{DL}, and Z_W represent solution resistance, charge-transfer resistance, double-layer capacitance and Warburg impedance, respectively. **Figure VI-6B** shows the impedance data obtained for each electrode. In the range of frequencies studied a mixed kinetic and diffusion control of the reaction is observed. By fitting the experimental data to the Randles equivalent circuit R_{CT} data can be extracted being 1170±50 Ω, 954±96 Ω, 727±115 Ω and 431±75 Ω for MoS_2, WS_2, WSe_2, and $MoSe_2$; thus, the trend was identical to ΔEp. These data are also in agreement with previously reported electrical conductivity of thin-films networks of MX_2 (WSe_2>$MoSe_2$> WS_2 > MoS_2) [30].

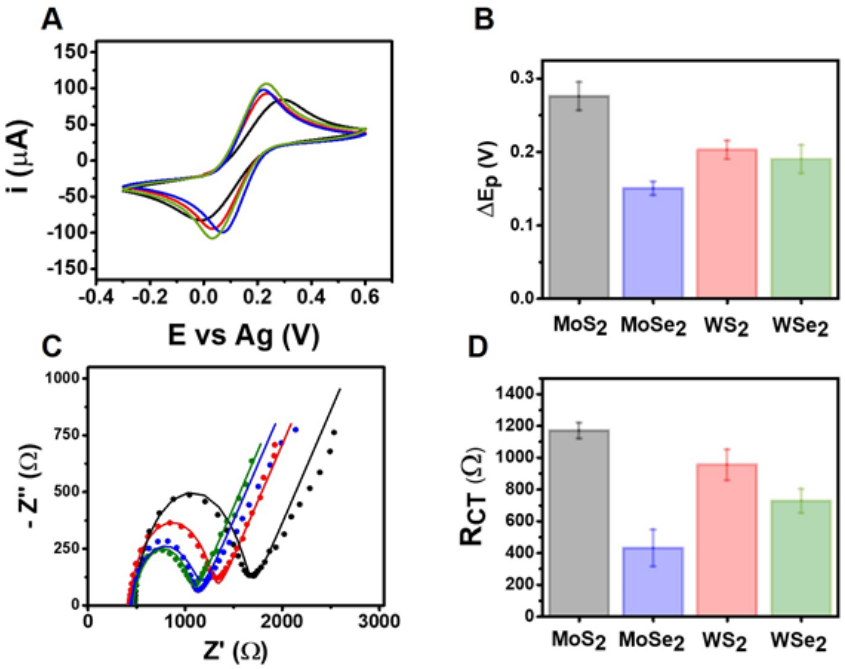

Figure VI-6: Electrochemical characterization employing 5 mM $[Fe(CN)_6]^{3-/4-}$ as redox probe employing A) CV and EIS. B) ΔEp and Rct were extracted for CV performed at 50 mV/s and EIS experiments respectively. Data taken from 5 different electrodes. Color code is maintained for each material in A and B panel.

VI.3.3. Electrochemical response towards CCF oxidation

The study in the electrochemical behaviour of MX_2 was extended to CCF oxidation employing catechin and rutin as representative compounds of flavonoid and glycosylated flavonoid, respectively. As can be seen from **Figure VI-7**, the superior electrochemical response towards catechin and rutin followed the same order for both CCF (WSe_2>$MoSe_2$>WS_2>MoS_2) exhibiting a quasi-reversible process. This result indicates the different electroactivity of MX_2, which in all cases resulted significantly improved (in terms of decreasing ΔEp and increasing ip_a) compared to the carbon-based screen-printed electrode. Noteworthy, the peak intensities due to flavonoids oxidation are in accordance with the intrinsic conductivity and electrochemical performance obtained with $[Fe(CN)_6]^{3-/4-}$. Furthermore, fouling effect of catechin and rutin was also evaluated (results are shown in **Figure VI-7B)**. The fouling resistance is increased in all TMDs in comparison with the bare carbon-based screen-printed electrode, as already reported by our group for MoS_2 [31,32].

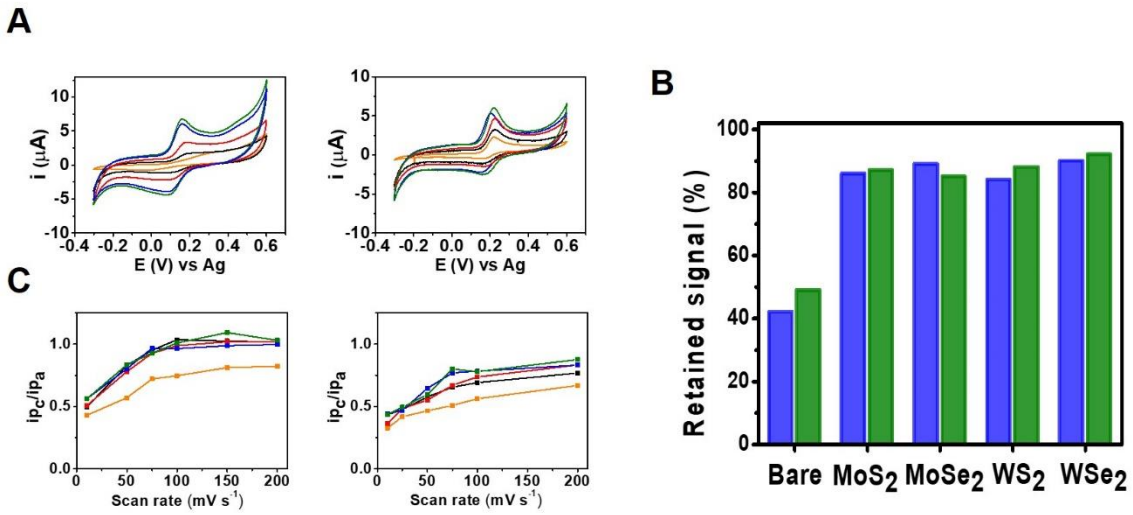

Figure VI-7: A) Cyclic voltammograms of 0.1 mM Catechin and Rutin on bare and MX2 modified electrodes recorded at 25 mV s-1 at pH=7. B) Retained signal after 10 measurements employing MX2-based electrodes for catechin (blue) and rutin (green). Bare electrode was added for comparison. C) Plot of the ipa/ipc ratio for each electrode obtained at different scan rates for Catechin and Rutin. Bare electrode (black) MoS2 (blue), WS2 (red), MoSe2 (blue) and WSe2 (green).

On top of that, as shown in **Figure VI-7C**, the ratio between the cathodic and anodic peaks differs from TMDs to bare electrode. If we compare the data at same scan rate, the ratio ip_c/ip_a is higher for MX_2 than for the carbon-based screen-printed electrode. As scan rate is increased, the ip_c/ip_a ratio increases indicating an electrochemical-chemical mechanism (EC), where an electrochemical reaction step (E) is followed by a coupled chemical reaction (C) [33]. CCFs have been described to follow this type of mechanism on glassy carbon electrodes; with the formation of a phenoxy radical intermediate [34]. The electrogenerated products in this reaction, CCF oligomers and polymers, have been demonstrated to be able to block the electrode surface causing the so-called electrode fouling [35–38]. In fact, we observed a notable electrode fouling in our experiments employing carbon-based screen-printed electrodes. Interestingly, this phenomenon is not observed on MX_2-based electrodes. An explanation for this observation is proposed according to the obtained results.

Figure VI-8 shows the proposed reaction scheme, once the phenoxy radical (R) is electrogenerated can follow two reactions pathways: (i) electrochemical oxidation to the quinone (Q) derivative of the corresponding CCF, (ii) chemically react to the corresponding CCF polymer/oligomer (P) able to block the electrode surface. It can be inferred from the ip_c/ip_a that the formation of Q is favored over P in the MX_2-based electrodes since ip_c/ip_a tends to 1, all R produced is converted to Q, that is detected in the reverse scan. On the other hand, in carbon-based electrode ip_c/ip_a is lower than in MX_2 for all scan rates studied suggesting that less Q is formed. The fouling effect is much higher in the case of carbon-based screen-printed electrode which further indicate a preferential formation of P compared to MX_2-based electrodes. These results suggest that MX_2 are able to drive preferentially the radical intermediate evolution towards the quinone product, avoiding PPs polymerization on the electrode surface with the subsequent fouling effect.

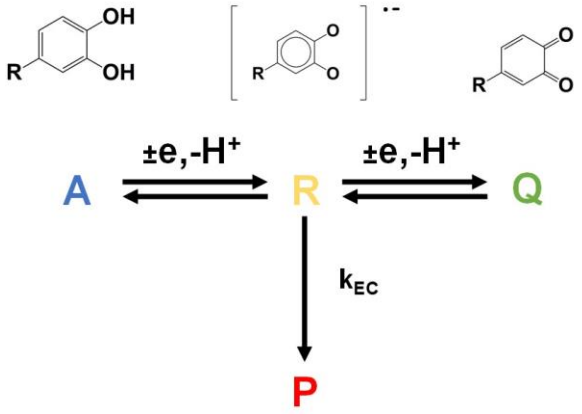

Figure VI-8: Proposed reaction scheme of CCF oxidation on MX_2-based electrodes

VI.4. Conclusions

Superior electrochemical performance of successfully exfoliated selenides compared with sulfides chalcogenides with higher k^0, lower Rct and higher electrocatalytic oxidation of CCF was found following the order: WSe_2>$MoSe_2$>WS_2>MoS_2. A dramatic enhancement in the antifouling properties for MX_2–based nanosheets compared to carbon-based electrodes was also found, revealing the key role of these materials. This behavior can be explained accordingly to an EC mechanism where MX_2 drives preferentially the oxidation of CCF towards the quinone product, avoiding PPs polymerization with the subsequent fouling effect. These findings confirm the outstanding antifouling properties of TMDs towards PPs and give an experimentally supported explanation to their antifouling properties. These results pave the way for a high-performance electrochemical analysis TMD-based in non-ideal samples.

VI.5. References

[1] X. Cai, Y. Luo, B. Liu, H.-M. Cheng, Preparation of 2D material dispersions and their applications, Chem. Soc. Rev. 47 (2018) 6224–6266. doi:10.1039/C8CS00254A.

[2] W. Choi, N. Choudhary, G.H. Han, J. Park, D. Akinwande, Y.H. Lee, Recent Development of Two--Dimensional Transition Metal Dichalcogenides and Their Applications, Mater. Today. 20 (2017) 116–130. doi:10.1016/j.mattod.2016.10.002.

[3] C. Backes, T.M. Higgins, A. Kelly, C. Boland, A. Harvey, D. Hanlon, J.N. Coleman, Guidelines for Exfoliation, Characterization and Processing of Layered Materials Produced by Liquid Exfoliation, Chem. Mater. 29 (2017) 243–255. doi:10.1021/acs.chemmater.6b03335.

[4] X. Chia, M. Pumera, Layered transition metal dichalcogenide electrochemistry: journey across the periodic table, Chem. Soc. Rev. 47 (2018) 5602–5613. doi:10.1039/C7CS00846E.

[5] A. Ambrosi, M. Pumera, Exfoliation of layered materials using electrochemistry, Chem. Soc. Rev. 47 (2018) 7213–7224. doi:10.1039/C7CS00811B.

[6] X. Zhang, Z. Lai, C. Tan, H. Zhang, Solution-Processed Two-Dimensional MoS_2 Nanosheets: Preparation, Hybridization, and Applications, Angew. Chemie Int. Ed. 55 (2016) 8816–8838. doi:10.1002/anie.201509933.

[7] A.T.E. Vilian, B. Dinesh, S.-M. Kang, U.M. Krishnan, Y.S. Huh, Y.-K. Han, Recent advances in molybdenum disulfide-based electrode materials for electroanalytical applications, Microchim. Acta. 186 (2019) 203. doi:10.1007/s00604-019-3287-y.

[8] A. Sinha, Dhanjai, B. Tan, Y. Huang, H. Zhao, X. Dang, J. Chen, R. Jain, MoS_2 nanostructures for electrochemical sensing of multidisciplinary targets: A review, TrAC Trends Anal. Chem. 102 (2018) 75–90. doi:10.1016/J.TRAC.2018.01.008.

[9] W. Zhang, L. Zong, G. Geng, Y. Li, Y. Zhang, Enhancing determination of quercetin in honey samples through electrochemical sensors based on highly porous polypyrrole coupled with nanohybrid modified GCE, Sensors Actuators B Chem. 257 (2018) 1099–1109. doi:10.1016/J.SNB.2017.11.059.

[10] B. Xu, B. Zhang, L. Yang, F. Zhao, B. Zeng, Electrochemical determination of luteolin using molecularly imprinted poly-carbazole on MoS_2/graphene-carbon nanotubes nanocomposite modified electrode, Electrochim. Acta. 258 (2017) 1413–1420. doi:10.1016/j.electacta.2017.12.004.

[11] Y. Zhang, Z. Liu, L. Zou, B. Ye, A new voltammetry sensor platform for eriocitrin based on CoS_2-MoS_2-PDDA-GR nanocomposite, Talanta. 189 (2018) 345–352. doi:10.1016/J.TALANTA.2018.07.004.

[12] B. Xu, L. Yang, F. Zhao, B. Zeng, A novel electrochemical quercetin sensor based on Pd/MoS_2-ionic liquid functionalized ordered mesoporous carbon, Electrochim. Acta. 247 (2017) 657–665. doi:10.1016/J.ELECTACTA.2017.06.130.

[13] H. Zhang, T. Wang, Y. Qiu, F. Fu, Y. Yu, Electrochemical behavior and determination of baicalin on a glassy carbon electrode modified with molybdenum disulfide nano-sheets, J. Electroanal. Chem. 775 (2016) 286–291. doi:10.1016/J.JELECHEM.2016.06.017.

[14] S. Su, W. Cao, C. Zhang, X. Han, H. Yu, D. Zhu, J. Chao, C. Fan, L. Wang, Improving performance of MoS_2 -based electrochemical sensors by decorating noble metallic nanoparticles on the surface of MoS_2 nanosheet, RSC Adv. 6 (2016) 76614–76620. doi:10.1039/C6RA12401A.

[15] F. Della Pelle, A. Scroccarello, M. Sergi, M. Mascini, M. Del Carlo, D. Compagnone, Simple and rapid silver nanoparticles based antioxidant capacity assays: Reactivity study for phenolic compounds, Food Chem. 256 (2018). doi:10.1016/j.foodchem.2018.02.141.

[16] J.M. Brcanović, A.N. Pavlović, S.S. Mitić, G.S. Stojanović, D.D. Manojlović, B.M. Kaličanin, J.N. Veljković, J.N. Veljkovi, S.S.M. Jelena M. Brcanovi, Aleksandra N. Pavlovi, G.S. Stojanovi, D.D. Manojlovi, B.M. Kalianin, Cyclic voltammetry determination of antioxidant capacity of cocoa powder, dark chocolate and milk chocolate samples: Correlation with spectrophotometric assays and individual phenolic compounds, Food Technol. Biotechnol. 51 (2013) 460–470. doi:10.1097/BTE.0000000000000074.

[17] X. Yang, J. Kirsch, J. Fergus, A. Simonian, Modeling analysis of electrode fouling during electrolysis of phenolic compounds, Electrochim. Acta. 94 (2013) 259–268. doi:10.1016/j.electacta.2013.01.019.

[18] C.A. Schneider, W.S. Rasband, K.W. Eliceiri, NIH Image to ImageJ: 25 years of image analysis, Nat. Methods. 9 (2012) 671–675. doi:10.1038/nmeth.2089.

[19] C. Backes, B.M. Szydłowska, A. Harvey, S. Yuan, V. Vega-Mayoral, B.R. Davies, P. Zhao, D. Hanlon, E.J.G. Santos, M.I. Katsnelson, W.J. Blau, C. Gadermaier, J.N. Coleman, Production of Highly Monolayer Enriched Dispersions of Liquid-Exfoliated Nanosheets by Liquid Cascade Centrifugation, ACS Nano. 10 (2016) 1589–1601. doi:10.1021/acsnano.5b07228.

[20] E.D. Grayfer, M.N. Kozlova, V.E. Fedorov, Colloidal 2D nanosheets of MoS2 and other transition metal dichalcogenides through liquid-phase exfoliation, Adv. Colloid Interface Sci. 245 (2017) 40–61. doi:10.1016/J.CIS.2017.04.014.

[21] A. Sajedi-Moghaddam, C.C. Mayorga-Martinez, E. Saievar-Iranizad, Z. Sofer, M. Pumera, Exfoliated transition metal dichalcogenide (MX_2; M = Mo, W; X = S, Se, Te) nanosheets and their composites with polyaniline nanofibers for electrochemical capacitors, Appl. Mater. Today. 16 (2019) 280–289. doi:10.1016/J.APMT.2019.06.002.

[22] H.S.S. Ramakrishna Matte, A. Gomathi, A.K. Manna, D.J. Late, R. Datta, S.K. Pati, C.N.R. Rao, MoS2 and WS2 Analogues of Graphene, Angew. Chemie Int. Ed. 49 (2010) 4059–4062. doi:10.1002/anie.201000009.

[23] A. Berkdemir, H.R. Gutiérrez, A.R. Botello-Méndez, N. Perea-López, A.L. Elías, C.I. Chia, B. Wang, V.H. Crespi, F. López-Urías, J.C. Charlier, H. Terrones, M. Terrones, Identification of individual and few layers of WS_2 using Raman Spectroscopy, Sci. Rep. 3 (2013). doi:10.1038/srep01755.

[24] E. Rahmanian, C.C. Mayorga-Martinez, R. Malekfar, J. Luxa, Z. Sofer, M. Pumera, 1T-Phase Tungsten Chalcogenides (WS_2, WSe_2, WTe_2) Decorated with TiO_2 Nanoplatelets with Enhanced Electron Transfer Activity for Biosensing Applications, ACS Appl. Nano Mater. 1 (2018) 7006–7015. doi:10.1021/acsanm.8b01796.

[25] H. Sahin, S. Tongay, S. Horzum, W. Fan, J. Zhou, J. Li, J. Wu, F.M. Peeters, Anomalous Raman spectra and thickness-dependent electronic properties of WSe_2, Phys. Rev. B - Condens. Matter Mater. Phys. 87 (2013) 165409. doi:10.1103/PhysRevB.87.165409.

[26] Z. Gholamvand, D. McAteer, C. Backes, N. McEvoy, A. Harvey, N.C. Berner, D. Hanlon, C. Bradley, I. Godwin, A. Rovetta, M.E.G. Lyons, G.S. Duesberg, J.N. Coleman, Comparison of liquid exfoliated transition metal dichalcogenides reveals MoSe 2 to be the most effective hydrogen evolution catalyst, Nanoscale. 8 (2016) 5737–5749. doi:10.1039/C5NR08553E.

[27] M. ZafirMohamadNasir, Z. Sofer, M. Pumera, Effect of Electrolyte pH on the Inherent Electrochemistry of Layered Transition-Metal Dichalcogenides (MoS_2, $MoSe_2$, WS_2, WSe_2), ChemElectroChem. 2 (2015) 1713–1718. doi:10.1002/celc.201500259.

[28] S.M. Tan, Z. Sofer, J. Luxa, M. Pumera, Aromatic-Exfoliated Transition Metal Dichalcogenides: Implications for Inherent Electrochemistry and Hydrogen Evolution, ACS Catal. 6 (2016) 4594–4607. doi:10.1021/acscatal.6b00761.

[29] R.S. Nicholson, Theory and Application of Cyclic Voltammetry for Measurement of Electrode Reaction Kinetics., Anal. Chem. 37 (1965) 1351–1355. doi:10.1021/ac60230a016.

[30] G. Cunningham, D. Hanlon, N. McEvoy, G.S. Duesberg, J.N. Coleman, Large variations in both dark- and photoconductivity in nanosheet networks as nanomaterial is varied from MoS_2 to WTe_2, Nanoscale. 7 (2015) 198–208. doi:10.1039/C4NR04951A.

[31] D. Rojas, F. Della Pelle, E. Del Carlo, Michele Fratini, D. Escarpa, Alberto Compagnone, M. Del Carlo, E. Fratini, A. Escarpa, D. Compagnone, Nanohybrid carbon black-molybdenum disulfide transducers for preconcentration-free voltammetric detection of the olive oil o-diphenols hydroxytyrosol and oleuropein, Microchim. Acta. 186 (2019) 363. doi:10.1007/s00604-019-3418-5.

[32] F. Della Pelle, D. Rojas, A. Scroccarello, M. Del Carlo, G. Ferraro, C. Di Mattia, M. Martuscelli, A. Escarpa, D. Compagnone, High-performance carbon black/molybdenum disulfide nanohybrid sensor for cocoa catechins determination using an extraction-free approach, Sensors Actuators B Chem. 296 (2019) 126651. doi:10.1016/j.snb.2019.126651.

[33] C. Sandford, M.A. Edwards, K.J. Klunder, D.P. Hickey, M. Li, K. Barman, M.S. Sigman, H.S. White, S.D. Minteer, A synthetic chemist's guide to electroanalytical tools for studying reaction mechanisms, Chem. Sci. 10 (2019) 6404–6422. doi:10.1039/c9sc01545k.

[34] H.P. Hendrickson, A.D. Kaufman, C.E. Lunte, Electrochemistry of catechol-containing flavonoids, J. Pharm. Biomed. Anal. 12 (1994) 325–334. doi:10.1016/0731-7085(94)90007-8.

[35] M. Polášek, I. Petriška, M. Pospíšilová, L. Jahodář, Use of molybdate as novel complex-forming selector in the analysis of polyhydric phenols by capillary zone electrophoresis, Talanta. 69 (2006) 192–198. doi:10.1016/J.TALANTA.2005.09.026.

[36] M. DelCarlo, A. Amine, M. Haddam, F. DellaPelle, G.C. Fusella, D. Compagnone, Selective Voltammetric Analysis of o-Diphenols from Olive Oil Using Na 2MoO 4 as Electrochemical Mediator, Electroanalysis. 24 (2012) 889–896. doi:10.1002/elan.201100603.

[37] M.-E. Ghica, A. Brett, Electrochemical Oxidation of Rutin, Electroanalysis. 17 (2005) 313–318. doi:10.1002/elan.200403100.

[38] P. Janeiro, A.M. Oliveira Brett, Catechin electrochemical oxidation mechanisms, Anal. Chim. Acta. 518 (2004) 109–115. doi:10.1016/j.aca.2004.05.038.

VII. Electrodeposited Prussian Blue on carbon black modified disposable electrodes for direct enzyme-free H_2O_2 sensing in a Parkinson's disease in vitro model

VII.1. Introduction and objectives

ROS are reduced forms of oxygen with important physiological functions and a critical role in redox regulation and oxidative stress development [1,2] The most relevant species are superoxide anion ($O_2^{\cdot-}$), hydroxyl radical ($OH^{\cdot}$) and hydrogen peroxide (H_2O_2) which are products of the normal metabolic consumption of oxygen. The main sources of ROS in aerobic cells can be related to membrane-bound NADPH oxidase and to incomplete oxygen reduction in mitochondria [3]. However, there are other pathways of generation of ROS such as ionizing radiation, Fenton and Haber-Weiss reaction of transition metal ions, drugs as antibiotics and chemotherapeutics [4]. Oxidative Stress (OS) is described as the imbalance between the production of oxidants (mainly ROS) and antioxidants defenses. Some situations may favor this imbalance, for instance, disfunction of antioxidant enzymes, exposure to some chemicals able to produce ROS, decrease in the levels or production of low molecular mass antioxidants and antioxidant enzymes [5]. This status can cause disruption in redox signaling and/or molecular damage. OS occurs when production of ROS/RNS is in excess with respect to the antioxidant protecting capacity; this causes irreversible damages to proteins, DNA and lipids. These biochemical alterations are implicated in several pathological processes such as cancer, Parkinson's and Alzheimer's disease, ischemia [6], atherosclerosis [7] and, in general, aging [8]. However, little amounts of ROS are necessary for the correct functioning of immunodefenses and redox signaling; the latter is denominated as a "oxidative eustress" [2]. Therefore, there is a need for analytical methods, possibly allowing continuous monitoring of ROS markers in cell cultures to evaluate the OS level in cells with respect to different treatments. Among the cellular produced ROS, H_2O_2 is the most representative in terms of amounts and half-life, and, therefore, the most studied.

Parkinson's disease involves an irreversible degeneration of the nigrostriatal dopaminergic pathway, resulting in an evident impairment of motor control. Although the etiology of Parkinson's disease remains unknown, recent studies have suggested that oxidative stress is an important mediator in this pathogenesis [9]. It is hypothesized that nigral dopaminergic neurons are exposed to high ROS levels, due to the metabolism of dopamine itself (both enzymatic and nonenzymatic) leading to the

generation of ROS, including superoxide anion, hydrogen peroxide (H_2O_2) and hydroxyl radicals. In fact, there are several indirect observations, such as the increased levels of the oxidation products of lipids, proteins, and nuclear acids in nigral cells, that are indicative of the role of oxidative stress in Parkinson's disease [10]. Hydroxydopamine (6-OHDA) is a selective catecholaminergic neurotoxin that has been widely used to produce Parkinson's disease models in vitro and in vivo; it induces a toxicity status that mimics the neuropathological and biochemical characteristics of Parkinson's disease [11]. It has been reported that 6-OHDA is oxidized rapidly by molecular oxygen to form the superoxide anion, hydrogen peroxide, and 2-hydroxy-5-(2-aminoethyl)-1,4-benzoquinone (p-quinone) as shown in Eq.VII.I [12]:

$$\text{6-OHDA} + O_2 \rightarrow \text{p-quinone} + H_2O_2 \qquad \text{Eq.VII.I}$$

It is well known that the ROS generated from 6-OHDA initiate cellular oxidative stress. On the other hand, it has been reported that p-quinone mediates 6-OHDA-induced cell death [13]. However, the exact mechanisms of ROS production and neurotoxicity induction, particularly in relation to caspase activation, are less clearly defined. Based on the above description, in this Chapter, we considered important the evaluation the H_2O_2 production after the exposure at 6-OHDA on the Parkinson's disease in vitro model; in this way, we can better understand the neurotoxic effect of this ROS at different timing.

Different analytical strategies have been proposed for H_2O_2 detection such as chemiluminescence,[14] fluorescence,[15,16] and electrochemical techniques [17]. Among these, electrochemical sensors are very appealing for their simplicity, speed, sensitivity, miniaturization and cost-effectiveness [18]. In the past two decades biosensors have dominated the sensors scenario even in the ROS detection field [17,19], while in the last decade nanomaterials have become alternative/ complementary sensor useful tools [20–24]. Indeed, nanostructured sensors allow to improve the sensitivity and selectivity providing larger surface area and faster electron transfers in comparison with their bulk counterparts [21,25,26]. Hence, the combination of nanomaterials and electrochemical sensors is very attractive. Direct sensing of H_2O_2 in classical metal electrodes such as platinum or gold is possible, however, it suffers

from poor selectivity due to the high overpotentials needed. The selection of a proper nanomaterial and catalyst can overcome this drawback. Prussian Blue (PB), also known as "artificial peroxidase" [27] is one of the most known and widely used electrocatalyst for H_2O_2 reduction. PB allows low potential and interference-free detection of H_2O_2 in oxygenated media; nonetheless, has some disadvantages such as poor stability at physiological pH and high crystallization rate which hinder the potential use in nanocomposites and application in biological media [28]. To overcome these shortcomings, electrode modification with soft or hard templates, polymers, carbonaceous materials or different metals have been used in different combinations to build specific analytical platforms for each application [19]. Carbon Black (CB) is a carbon nanomaterial widely used as reinforcing material and as filler in the preparation of rubber and plastic compounds and composites, made by petroleum products combustion so it is a very cheap carbonaceous nanomaterial (about 1€/Kg). It is characterized by a primary structure constituted of spherical particles with diameter between 30 and 100 nm and a secondary structure formed by aggregates having dimensions in the range of 100–600 nm [29]. CB dispersions after sonication, in appropriate solvents, appears as carbon nanoparticles. Recent data showed that modified electrodes based on CB present fast charge transfer and high electroactive area, comparable to carbon nanotubes and graphene [30]. These characteristics together with its lower price make CB a promising candidate for the design of electrochemical sensors and biosensors using an alternative nanomaterial to carbon nanotubes and graphene. For these reasons, in the last years several works have been reported on the CB dispersion for electrode modification, showing remarkable electrocatalytic properties towards several species of analytical interest [20,30–33], allowing the realization of new electrochemical devices devices [34–36]. In this Chapter 'nano CB' has been successfully used as electrode modifier for the controlled electrodeposition of PB and further applied for the monitoring of H_2O_2 in Parkinson's disease cellular model cultures.

VII.2. Materials and methods

VII.2.1. Materials

Experiments were carried out with MilliQ water from a Millipore MilliQ ((Millipore, Bedford, MA, USA), system. All inorganic salts, 6-OHDA, organic solvents and hydrogen peroxide (30% solution) were obtained at the highest purity from Sigma-Aldrich. SHSY5Y cells were obtained from Sigma (Sigma–Aldrich). Catalase from bovine liver powder, suitable for cell culture, 2,000-5,000 units/mg protein was purchased from Sigma-Aldrich (C1345). H2O2 concentration was periodically standardized by titration with KMnO4. Screen-Printed electrodes (SPE) were purchased from Dropsens S.L. (ref. DS110). DMEM, L-Glutamine, penicillin/streptomycin, trypsin and flask were purchased from Corning (Corning Life Sciences, Corning, NY).

VII.2.2. Instrumentation

All electrochemical measurements were carried out in Autolab PGSTAT 12 potentiostat from Metrohm (Utrecht, The Netherlands) connected to a personal computer. The software used was the Nova 2.1 (EcoChemie B.V.). The flow injection (FIA) system consisted of a Minipuls 3 (Gilson Inc., Middleton, WI, USA) peristaltic pump, flow-through cell (ref. FLWCL) (Dropsens, Spain). Sample volume was 50 µL, the working electrode potential chosen was -50 mV (vs internal reference). The running buffer solution in FIA experiments was 0.05 M phosphate buffer pH 7.4 containing 0.1 M KCl. High resolution scanning electron microscopy (HR-SEM) was carried out on the materials using a Zeiss Auriga HR- SEM. The scanning electron microscopy, Zeiss Auriga, High resolution FESEM was used to study the morphology of the prepared materials.

VII.2.3. Preparation of PB and CB-PB electrodes

A CBNPs dispersion of 1 mg/mL in water and dimethylformamide (DMF) (1:1 ratio). The dispersions were obtained using a bath sonicator for 30 min. Further, commercially screen-printed electrodes (DS110) were modified via drop-casting using different volumes (from 3.5 µL to 35 µL). The amount of CB was optimized checking the reversibility of $[Fe(CN)_6]^{3-/4-}$ couple using cyclic voltammetry and charge transfer resistance (Rct) in EIS. The selected optimum value was 10 µL drop-casted by 1 µL each time (**Figure VII-1**). Prussian Blue electrodeposition was carried out cycling the potentials between +400 and +800 mV (vs Ag) for different number of cycles in a solution containing solution containing 0.1 M KCl, 0.1 M HCl and 5 mM concentration of Fe^{3+} and $[Fe(CN)_6]^{3-}$. Electrodes were further modified with 2 µL of a Nafion ethanolic solution (0,5% v/v). Nafion is an ionic conductor that increase stability of PB modified electrodes, allowing the counterions transport to maintain the electroneutrality of PB film [37,38].

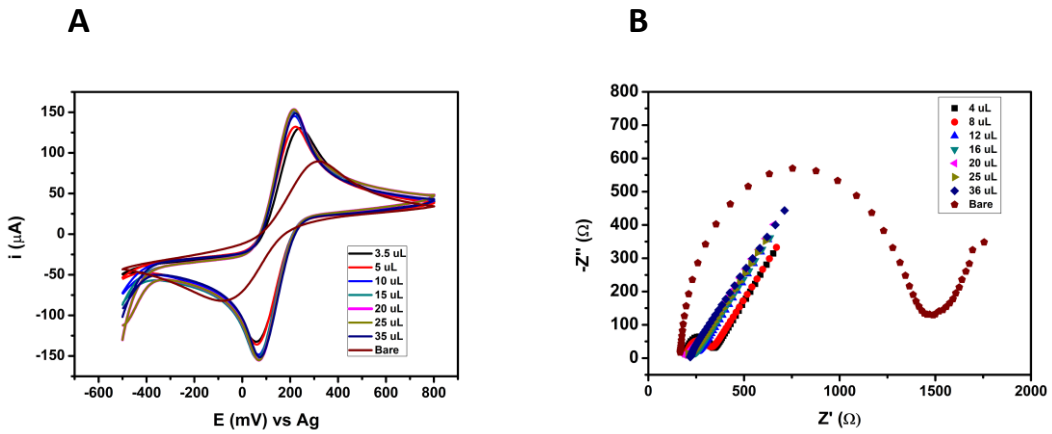

Figure VII-1:A) CV and B) EIS for bare SPE and SPE-CB with different quantities of CB

VII.2.4. Cell culture

The Neuroblastoma cell line SH-SY5Y were maintained at 37°C in a 5% CO_2 humidified atmosphere in DMEM medium supplemented with 10% heat-inactivated fetal bovine serum, 2 mM L-Glutamine, 0.2 mg/ml penicillin/streptomycin. The culture medium was changed every 2 days until cells reached approximately 70–80% confluency. Cells were harvested using 0.25% trypsin-0.53 mM EDTA solution and were seeded at approximately 4×10^4 cells/cm^2 in 75 cm^2-flasks, then treated with 6 OHDA (50µM) for different times.

VII.2.5. Cell viability

Cells were seeded (5.000 cells/well) in a 96 wells plate, the day after the cells were treated with 6 OHDA (50 µM) for 24 h while the control cells received only DMEM containing 10% of FBS, every treatment was performed in quintuplicate. The cells were incubated for different time and at expiration of incubation period cell viability was determined using Cell Titer One Solution Cell Proliferation Assay reading the absorbance at 492 nm, in a spectrophotometric microplate reader Infinite F200 (Tecan, Männedorf, Swiss). The results were expressed as absorbance recorded at 492 nm.

VII.3. Results and Discussion

VII.3.1. Preparation and characterization of CB-PBNPs electrodes

PB or ferric ferrocyanide is one of the oldest known coordination compounds with ferric ions coordinated to nitrogen and ferrous coordinated to carbon in a face centered cubic lattice. Usually, is electrochemically deposited using a mixture of Fe^{3+} and $[Fe(CN)_6]^{3-}$ where the ferric ions are reduced to form Prussian Blue. Particular attention has to be paid to the selection of the potential used for the electrodeposition; in fact, the concurrent reduction of both precursors leads to an irregular structure of the Prussian Blue layer onto the electrode surface [27]. As shown in the cyclic voltammogram of **F**igure **VII-2A**, the reduction peaks of Fe^{3+} and $[Fe(CN)_6]^{3-}$ are not resolved using bare SPE. Interestingly, in the case of CB-SPE the reduction peak potential of Fe^{3+} is anodically shifted 280 mV, and peak current is increased by a 1.5 factor confirming an electrocatalytic behaviour of CB toward Fe^{3+} reduction. On the other hand, for the reduction of $[Fe(CN)_6]^{3-}$, only a slight increase of peak intensity was observed, keeping the peak potential at the same value of unmodified SPE. Thus, the electrodeposition of PB was carried out using cycling voltammetry; the potential window and the sweep rate was selected according to the method developed by Karyakin et al [27,39]. Considering the reported electrochemical behaviour of the electrodes surface SPE were cycled from +400 mV to +800 mV (vs. Ag), allowing the selective reduction of Fe^{3+} keeping the $[Fe(CN)_6]^{3-}$ in its oxidized form. **F**igure **VII-2B** reports cyclic voltammograms in a solution containing 0.1M HCl and 0.1M KCl. An increase in the peak current and area was observed with number of electrodeposition cycles indicating a higher quantity of PB on the electrode surface. It is clearly noticeable the higher electrodeposited quantity at CB-modified electrodes compared to the bare SPE.

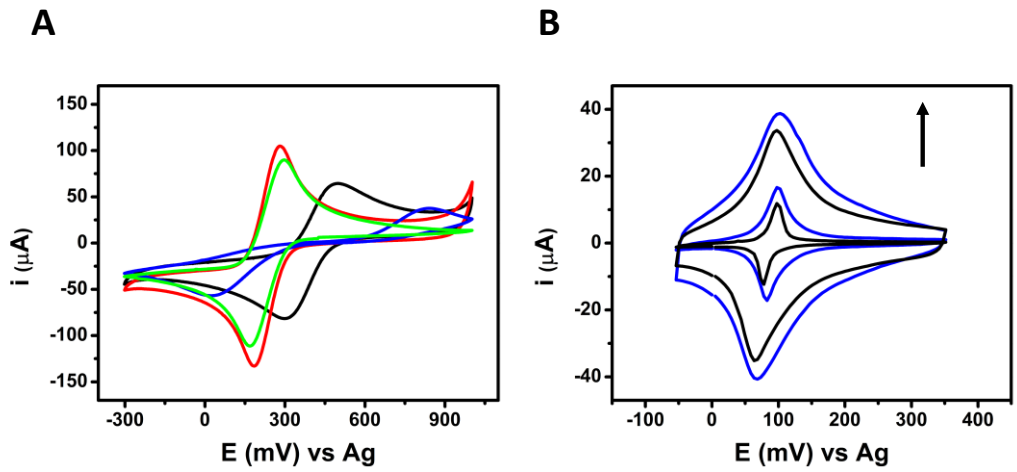

Figure VII-2: A) Cyclic Voltammetry of solutions containing, 5 mM Fe^{3+} and 5 mM $[Fe(CN)_6]^{3-}$ in a bare SPE (Blue and Green respectively) and SPE-CB (Black and Red respectively) recorded at 40 mV/s. B) Cyclic voltammograms electrodeposited PB on bare SPE (blue) and on SPE-CB (black) in 0.1M HCl and 0.1M KCl. Arrow indicate increasing number of growth cycles (5 and 20). Scan rate: 50 mV/s.

The electrocalitic activity of SPE-CB/PB was shown using different concentrations of H_2O_2 in **Figure VII-3A**, the combination of SPE-CB and PB allow a higher signal due to H_2O_2 reduction using amperometric detection compared to SPE-PB and SPE-CB as shown in **Figure VII-3B**. In carbon-based electrodes, the only available detection principle is H_2O_2 oxidation at high anodic potential, where easily oxidizable compounds usually presents in biological media causes appearance of parasitic signal due to it oxidation. In contrast, PB-based electrodes allow H_2O_2 detection by its reduction near 0V (vs Ag|AgCl), where other compounds rarely are electroactive.

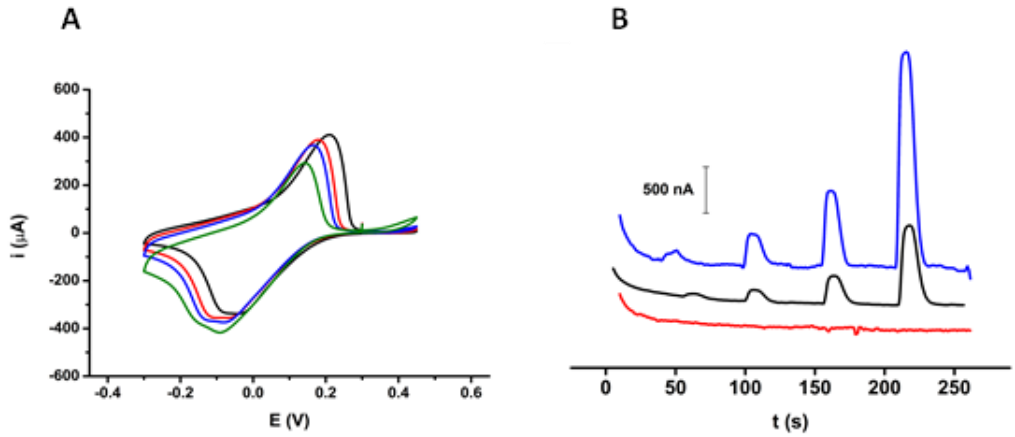

Figure VII-3: A) Cyclic voltammetry of SPE-CB/PB in Phosphate Buffer 50 mM, 0.1 KCl (black line) and in the same buffer containing 1 mM (red line), 2 mM (blue line) and 3 mM (green line) of H2O2. B) Amperometric signals in FIA for 5, 10, 20 and 50 μM of H_2O_2 in the same buffer using SPE-CB (red line), SPE-PB (black line) and SPE-CB/PB (blue line).

SEM micrographs confirmed the growth of PB onto the electrode surface. Increasing the number of electrodeposition cycles, the size of the PB nanoparticles increases. In addition, the amount of atomic iron, obtained from EDS spectra was found to be from 0 to 3.55% CB-SPE up to 20 cycles.

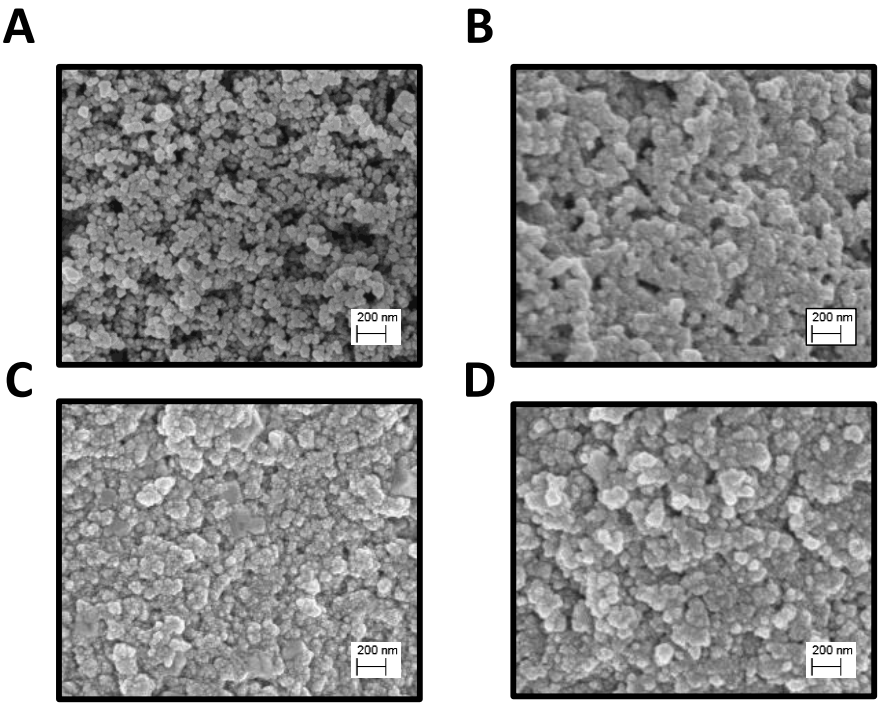

Figure VII-4: SEM images of A) CB modified SPE B) CB/PB 5 cycles C) CB/PB 10 cycles D) CB/PB 20 cycles modified SPE.

Table VII-1 list the surface coverage (Γ) of PB as well as $S \cdot t_{95\%}$ as sensor stability and sensitivity parameter. High stability and electrocatalytic activity are highly desirable to obtain. However, it is not trivial to find a compromise between the two characteristics. For this purpose, an accelerated degradation can be carried out [40]. Sensor's stability is evaluated by the time the measured current reaches the 95% of its initial value ($t_{95\%}$) under continuous flow of 500 µM H_2O_2 in Phosphate Buffer pH=7.4 using a wall-jet cell. Sensitivity (S) is estimated by the initial intensity divided by the concentration of H_2O_2.

As shown in **Table VII-1**, as we increased the surface coverage (Γ) of PB the parameter $S \cdot t_{95\%}$ raises from 5 to 10 cycles and slightly decreases from 10 to 20 cycles. Therefore, considering the values of $S \cdot t_{95\%}$ the compromise among sensitivity and stability of the sensor is found with 10 cycles of electrosynthesis.

Table VII-1: Optimization parameter for CB-PB electrodes

Electrode	Γ (nmol·cm^{-2})	$S \cdot t_{95\%}$ (A·min·M^{-1}·cm^{-2})
CB-PB- 5 cycles	0.85	1.83
CB-PB- 10 cycles	3.90	4.69
CB-PB- 20 cycles	6.40	4.59

VII.3.2. Analytical performance

The selected electrode was used for the electrochemical detection of H_2O_2 in a Flow Injection Analysis (FIA) system. FIA was chosen as a first approach for quantifying H_2O_2 in cell cultures, taking advantage of its high throughput, simplicity and possibility to automation. In order to find the optimal conditions for measuring, an optimization of the flow rate and potential employed in the analysis was carried out. **Figure VII-5A** shows the effect of the flow rate on the peak intensity of a solution containing 10 µM of H_2O_2. An increase in the flow rate increases the peak intensity until it reaches a constant value at a flow rate of 0.6 ml min^{-1} and above. Hydrodynamic voltammogram

of CB-PB electrodes in phosphate buffer and phosphate buffer containing 100 µM of H_2O_2 in aerated solution were also carried out. As shown in **Figure VII-5B** the current in presence of H_2O_2 reaches the limiting current at -50 mV. In addition, the selectivity of the electrodes in presence of oxygen, a common interferent using platinum or gold electrodes, is demonstrated as we have negligible current from the aerated buffer at the region of the limiting current for H_2O_2 reduction.

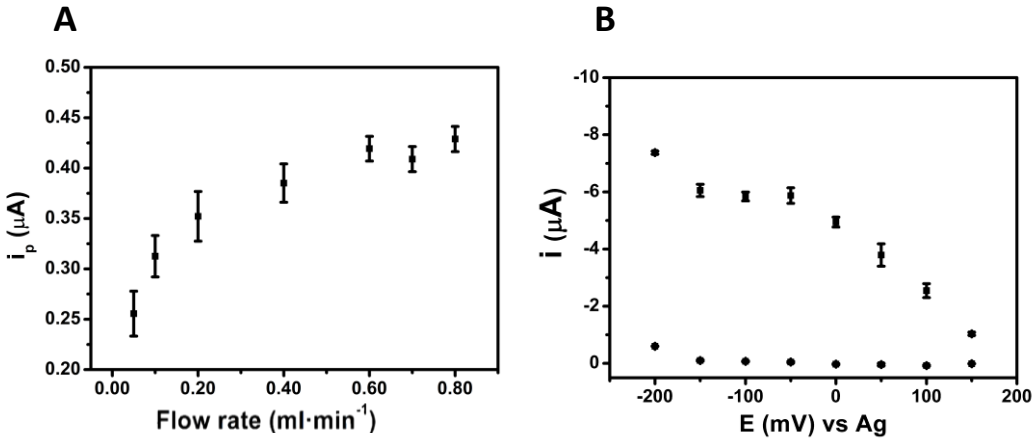

Figure VII-5: A) Peak current dependence with flow rate B) Hydrodynamic Voltamogramm (HDV) of a solution containing phosphate buffer (pH=7.4) (squares) and phosphate buffer (pH=7.4) and 10 µM of H_2O_2

The electrochemical performance of the electrodes was then tested in FIA analysis of hydrogen peroxide in hydrogen phosphate buffer pH = 7.4. Physiological pH is not the ideal pH for PB-based sensors; however, we obtained satisfactory data. **Figure VII-6A** reports the amperometric response of the developed sensor for the injection of different H_2O_2 concentrations ranging from 200 nM to 1 mM. Linearity was found over 4 orders of magnitude, as shown in **Figure VII-6B**. The equation of calibration curve was: i_p=0.039±0,007(µM)+0.66±0.01(A·M^{-1}·cm^{-2})[H_2O_2] with R^2= 0.999. The limit of detection calculated as 3σ/S, where σ is the standard deviation of 10 blank samples and S the sensitivity, was 10 nM. In addition, good intra-electrode repeatability and inter-electrode reproducibility were obtained RSD≤6% (n=3) and RSD≤10%(n=5), respectively.

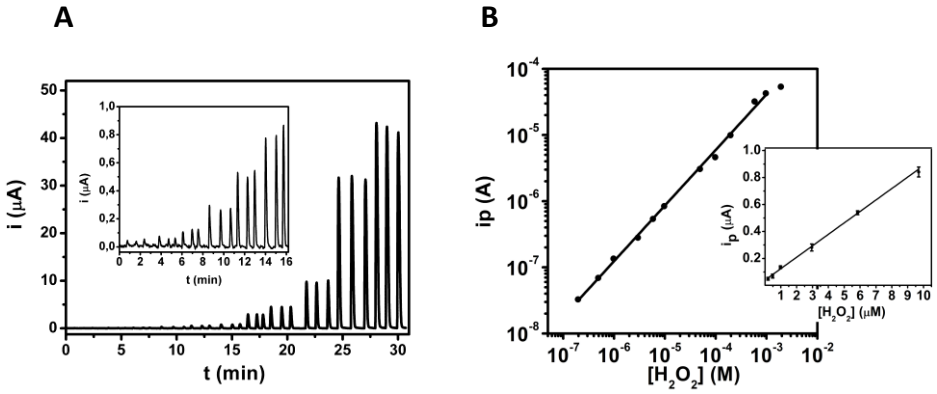

Figure VII-6: A) Signals in a FIA system to different concentrations of H_2O_2 B) Calibration plot for wide linear range. Inset: calibration plot for the lowest points. Measurements carried out in phosphate buffer (pH=7.4) flow rate 0.6 ml min^{-1}; E= -50 mV.

To the best of our knowledge, the combination of CB/PB and SPE to construct a H_2O_2 sensor has previously been used only by Cinti et al. [41]. In this Chapter, different combinations of CB/PB composites were synthetized producing different PB nanoparticles sizes; LODs were between 0.3 and 1.0 μM and sensitivities between 0.15-0.56 $A \cdot M^{-1} \cdot cm^{-2}$ using amperometry batch analysis. Our proposed electrode has a lower LOD and improved sensitivity (0.66 $A \cdot M^{-1} \cdot cm^{-2}$) and takes advantage of the measurement FIA system which allows a higher throughput (70 samples$\cdot h^{-1}$) and better repeatability. In addition, the SPE-CB/PB retained the analytical performance in terms of sensitivity (87% after 3 months at RT) demonstrating a good long-term stability.

VII.3.3. Application to H_2O_2 sensing in SHSY5Y differentiated in neurons cell culture

Cellular culture medium is a quite complex and challenging matrix since contains different organic compounds and proteins necessary for the cells. Matrix effect must be carefully assessed in order to produce reliable quantitative data. The sample matrix has been spiked with known amounts of H_2O_2 in the 5 -50 μmol L^{-1} concentration range. The recovery was in the whole range ≥96% with RSD≤4% (n=3). These data show that the procedure is suitable for H_2O_2 detection in cellular culture. Selectivity of the measurements was also evaluated vs. possible interferents found in the culture broth. To this aim the influence of Penicilin, Streptavidin, L-Glutamine and Fetal Bovine Serum have been studied. As reported in **Figure VII-7A** no significant interference was

observed. In addition, we have further tested the selectivity of our electrode against the H_2O_2 reduction in the complex matrix. As it is observed in **Figure VII-7B**, the signal due to the addition of 100 µM H_2O_2 in the cell culture media was completely suppressed by the addition of 0.2 mg of Catalase (100 µL 2 mg/ml). It should be also noticed that the sensor was able to measure in the DMEM cell culture for 1h maintaining the 80% of the initial signal in batch amperometry configuration, exhibiting an excellent stability in such complex media; this remarkable feature allows the use of such low-cost sensors as the modified SPE for a large number of measurements/experiments with cells.

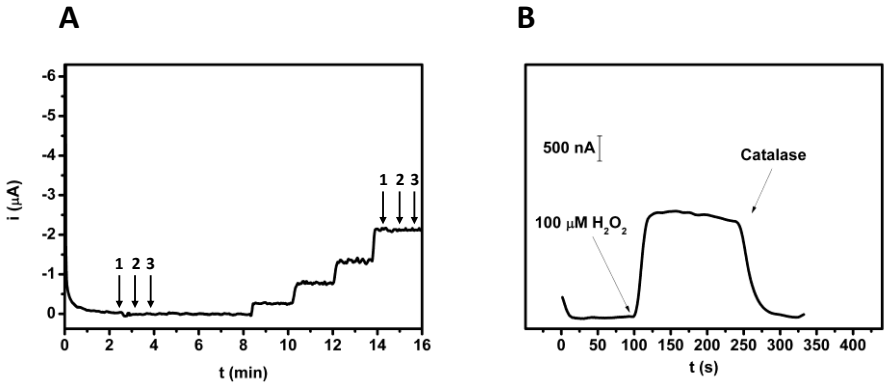

Figure VII-7: A) Amperometric signals due to the addition of FBS (1), L-Glu (2) and P/S (3) in DMEM medium B) Selectivity of the electrode towards 100 µM of H_2O_2 spiked in the cell culture without cells. E=-50 mV vs Ag.

Finally, the proposed strategy has been successfully applied to monitor in Parkinson's cellular culture H_2O_2 production (for 24 hours). Cells were stimulated by 6-OHDA, a selective catecholaminergic neurotoxin, which has been frequently used to create Parkinson's disease models. The toxic effect of 6-OHDA is mediated by its uptake into catecholaminergic nerve endings via the high-affinity catecholamine transporter system. Several works report that 6-OHDA triggers cell death through three main mechanisms: a) ROS generation through autoxidation, b) H_2O_2 generation following deamination by monoamine oxidase (MAO), c) direct inhibition of mitochondrial complexes I and IV [42]. However, many recent studies have reported that 6-OHDA does not induce toxicity either by direct mitochondrial inhibition or by enzymatic deamination by MAO, but through an extracellular mechanism [11,43]. The sample analysis was carried out in a flow injection system with the optimized Prussian Blue/

Carbon Black modified Screen Printed Electrode as detection system and using the following procedure: 1) injection of a known standard sample (triplicate) 2) Injection of sample (triplicate). The standard injections allow us to normalize the signal minimising, any matrix effect or change of the electrodes in the FIA setup. H_2O_2 amount found in the cell culture increases as a function of the incubation time, reaching a plateau-like region at 20h (**Figure VII-8)**. The concentration ranges were from 15.2 ± 0.8 µM at 15 min to 51.9 ± 0.3 µM at 24h, which are in accordance with values found in literature for the 6-OHDA model [11]. In this preliminary experiment, we demonstrate the relationship between an overproduction of H_2O_2 after 6-OHDA treatment with the high mortality evaluated with MTS viability assay (**Figure VII-8**). In fact, we observed an increase of cell mortality linked to H_2O_2 concentration.

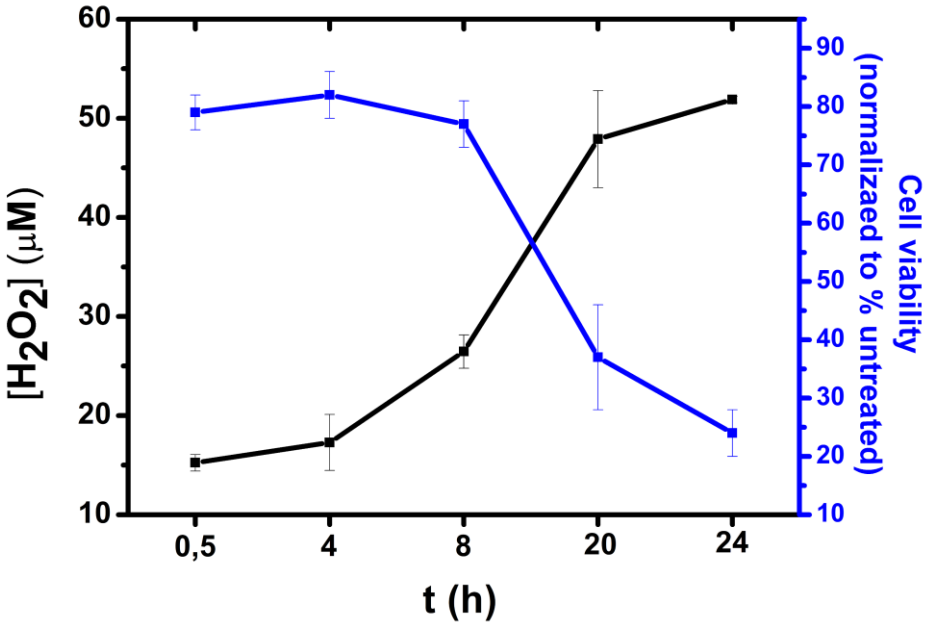

Figure VII-8: Hydrogen peroxide concentration (black) and cell viability (blue) in Parkinson's disease cellular model at different incubation time.

The analytical performance of other nanomaterials based electrochemical sensors used for measuring hydrogen peroxide in cell culture is reported in **Table VII-2**. The developed electrode showed better or comparable analytical performance compared with works found in the literature in terms of LOD and linear range, even compared with noble metals-based sensors. It is important to note that the developed electrode

consist in a SPE which show advantages compared to classic solid electrode such as disposability, easy to use without need of experienced personal and low sample consumption. When compared with other SPE (SPE-Cu-NWs), we found lower LOD, wider linear range and detection potential closer to 0 mV (vs Ag). In addition, to the best of our knowledge, this is the first time that H_2O_2 is measured and quantified in the 6-OHDA model for Parkinson's disease using electrochemical sensors.

Table VII-2: Comparison of analytical performance of hydrogen peroxide sensors applied to the determination of hydrogen peroxide released by cells

Electrode	Detection potential (mV)	LOD (M)	Linear range (M)	Application	Ref
Au-PB-PDA	+100 vs Ag/AgCl	$1.0x10^{-7}$	$1.0x10^{-6}$-$8.0x10^{-4}$	Hep G2 cells	[44]
SPE-Cu-NWs	-200 vs Ag	$4.0x10^{-7}$	$5.0x10^{-7}$-$8.0x10^{-4}$	Cisplatin-treated human renal HK-2 cells	[24]
g-CNTs/PB MCs	-50 vs Ag|AgCl, sat KCl	$1.3x10^{-8}$	$2.5x10^{-8}$-$1.6x10^{-3}$	RAW 264.7 cells	[45]
Pd/Au NWs	-50 vs Ag|AgCl, 3M KCl	$3.0x10^{-7}$	$1.0x10^{-6}$-$1.0x10^{-3}$	HL-1 cells	[46]
PtPb/Graphene	-200 vs Ag|AgCl	$2.0x10^{-9}$	$2.0x10^{-9}$-$2.5x10^{-3}$	Raw 264.7 cells	[47]
CuO@MnAl LDHs	-850 vs SCE	$1.3x10^{-7}$	$6.0x10^{-6}$-$2.2x10^{-3}$	Epithelial normal cells HBL100, breast cancer cells MCF-7 and glioma brain cancer cells U87	[48]
PdPt NCs@SGN/GCE	-0.1 vs SCE	$3.0x10^{-7}$	$3.0x10^{-6}$-$3.0x10^{-4}$	Hela cells	[49]
Ag NSs/GCE	-500 vs Ag|AgCl, sat KCl	$1.7x10^{-7}$	$5.0x10^{-6}$-$6.0x10^{-3}$	HeLa cells and SH-SY5Y cells	[50]
SPE-CB-PB-Nafion	-50 mV vs Ag	$1.0x10^{-8}$	$2.0x10^{-7}$-$1.0x10^{-3}$	Neuroblastoma SH-SY5Y cell line	This work

VII.4. Conclusions

An enzyme-free electrochemical sensing platform was successfully proposed for the quantification of H_2O_2 released by SHSY5Y cells. These cells challenged to 6-OHDA represent a model to study the Parkinson's disease, which is widely known to be affected by oxidative stress. To the best of our knowledge, this is the first time that an electrochemical PB/CB sensor is applied to sensing H_2O_2 directly in cell cultures. The described sensor showed detection limit in the nanomolar range and showed excellent selectivity in a complex environment such as the culture medium used, allowing the selective determination of very low amounts of H_2O_2 without interferences. In addition, in this Chapter H_2O_2 was quantified instead of following its almost instantaneous release from cells challenged to a stressor in contrast to [44] and [45]. These results could pave the way for a better understanding the neurotoxic effect of ROS using an in vitro model of Parkinson's disease.

VII.5. References

[1] H. Sies, C. Berndt, D.P. Jones, Oxidative Stress, Annu. Rev. Biochem. 86 (2017) 715–748. doi:10.1146/annurev-biochem-061516-045037.

[2] H. Sies, Hydrogen peroxide as a central redox signaling molecule in physiological oxidative stress: Oxidative eustress, Redox Biol. 11 (2017). doi:10.1016/j.redox.2016.12.035.

[3] C.R. Reczek, N.S. Chandel, The Two Faces of Reactive Oxygen Species in Cancer, Annu. Rev. Cancer Biol. 1 (2017) 79–98. doi:10.1146/annurev-cancerbio-041916-065808.

[4] A. Umeno, V. Biju, Y. Yoshida, In vivo ROS production and use of oxidative stress- derived biomarkers to detect the onset of diseases such as Alzheimer ' s disease , Parkinson ' s disease , and diabetes, Free Radic. Res. 5762 (2017). doi:10.1080/10715762.2017.1315114.

[5] V.I. Lushchak, Free radicals, reactive oxygen species, oxidative stress and its classification, Chem. Biol. Interact. 224 (2014) 164–175. doi:10.1016/j.cbi.2014.10.016.

[6] C. Espinosa-Diez, V. Miguel, D. Mennerich, T. Kietzmann, P. Sánchez-Pérez, S. Cadenas, S. Lamas, Antioxidant responses and cellular adjustments to oxidative stress, Redox Biol. 6 (2015) 183–197. doi:10.1016/J.REDOX.2015.07.008.

[7] A.J. Kattoor, N.V.K. Pothineni, D. Palagiri, J.L. Mehta, Oxidative Stress in Atherosclerosis, Curr. Atheroscler. Rep. 19 (2017). doi:10.1007/s11883-017-0678-6.

[8] S.I. Liochev, Reactive oxygen species and the free radical theory of aging, Free Radic. Biol. Med. 60 (2013) 1–4. doi:10.1016/j.freeradbiomed.2013.02.011.

[9] H. Sies, Oxidative stress: From basic research to clinical application, Am. J. Med. 91 (1991) S31–S38. doi:10.1016/0002-9343(91)90281-2.

[10] A. Miyama, Y. Saito, K. Yamanaka, K. Hayashi, T. Hamakubo, N. Noguchi, Oxidation of DJ-1 Induced by 6-Hydroxydopamine Decreasing Intracellular Glutathione, PLoS One. 6 (2011) e27883. doi:10.1371/journal.pone.0027883.

[11] Y. Saito, K. Nishio, Y. Ogawa, T. Kinumi, Y. Yoshida, Y. Masuo, E. Niki, Molecular mechanisms of 6-hydroxydopamine-induced cytotoxicity in PC12 cells : Involvement of hydrogen peroxide-dependent and -independent action, Free Radic. Biol. Med. 42 (2007) 675–685. doi:10.1016/j.freeradbiomed.2006.12.004.

[12] G. Cohen, R.E. Heikkila, Generation of Hydrogen-Peroxide, Superoxide Radical, and Hydroxyl Radical by 6-Hydroxydopamine, Dialuric Acid, and Related Cytotoxic Agents, J. Biol. Chem. 249 (1974) 2447–2452.

[13] Y. Izumi, H. Sawada, N. Sakka, N. Yamamoto, T. Kume, H. Katsuki, S. Shimohama, A. Akaike, p-quinone mediates 6-hydroxydopamine-induced dopaminergic neuronal death and ferrous iron accelerates the conversion ofp-quinone into melanin extracellularly, J. Neurosci. Res. 79 (2005) 849–860. doi:10.1002/jnr.20382.

[14] W. Vessey, A. Perez-Miranda, R. Macfarquhar, A. Agarwal, S. Homa, Reactive oxygen species in human semen: Validation and qualification of a chemiluminescence assay, Fertil. Steril. 102 (2014) 1576–1583. doi:10.1016/j.fertnstert.2014.09.009.

[15] A.-C. Ribou, Synthetic Sensors for Reactive Oxygen Species Detection and Quantification: A Critical Review of Current Methods, Antioxid. Redox Signal. 25 (2016) 520–533. doi:10.1089/ars.2016.6741.

[16] N. Burmistrova, O. Kolontaeva, A. Duerkop, New Nanomaterials and Luminescent Optical Sensors for Detection of Hydrogen Peroxide, Chemosensors. 3 (2015) 253–273. doi:10.3390/chemosensors3040253.

[17] H. Liu, L. Weng, C. Yang, A review on nanomaterial-based electrochemical sensors for H2O2, H2S and NO inside cells or released by cells, Microchim. Acta. 184 (2017) 1267–1283. doi:10.1007/s00604-017-2179-22.

[18] Z. Li, Y. Yu, Z. Li, T. Wu, J. Yin, The art of signal transforming: electrodes and their smart applications in electrochemical sensing, Anal. Methods. 7 (2015) 9732–9743. doi:10.1039/C5AY02373D.

[19] C. Calas-Blanchard, G. Catanante, T. Noguer, Electrochemical Sensor and Biosensor Strategies for ROS/RNS Detection in Biological Systems, Electroanalysis. 26 (2014) 1277–1286. doi:10.1002/elan.201400083.

[20] F. Della Pelle, D. Compagnone, Nanomaterial-Based Sensing and Biosensing of Phenolic Compounds and Related Antioxidant Capacity in Food, Sensors. 18 (2018) 462. doi:10.3390/s18020462.

[21] F.S. Ligler, H.S. White, Nanomaterials in analytical chemistry, Anal. Chem. 85 (2013) 11161–11162. doi:10.1021/ac403331m.

[22] J. Sun, H. Sun, Z. Liang, Nanomaterials in Electrochemiluminescence Sensors, ChemElectroChem. 4 (2017) 1651–1662. doi:10.1002/celc.201600920.

[23] G. Maduraiveeran, W. Jin, Nanomaterials based electrochemical sensor and biosensor platforms for environmental applications, Trends Environ. Anal. Chem. 13 (2017) 10–23. doi:10.1016/J.TEAC.2017.02.001.

[24] L. García-Carmona, M. Moreno-Guzmán, A. Martín, S. Benito Martínez, A.B. Fernández-Martínez, M.C. González, J. Lucio-Cazaña, A. Escarpa, Aligned copper nanowires as a cut-and-paste exclusive electrochemical transducer for free-enzyme highly selective quantification of intracellular hydrogen peroxide in cisplatin-treated cells, Biosens. Bioelectron. 96 (2017) 146–151. doi:10.1016/j.bios.2017.04.048.

[25] M. Pumera, A. Escarpa, Nanomaterials as electrochemical detectors in microfluidics and CE: Fundamentals, designs, and applications, Electrophoresis. 30 (2009) 3315–3323. doi:10.1002/elps.200900008.

[26] A. Escarpa, Lights and shadows on Food Microfluidics, Lab Chip. 14 (2014) 3213–3224. doi:10.1039/C4LC00172A.

[27] A.A. Karyakin, Advances of Prussian blue and its analogues in (bio)sensors, Curr. Opin. Electrochem. (2017). doi:10.1016/j.coelec.2017.07.006.

[28] Z. Chu, Y. Liu, W. Jin, Recent progress in Prussian blue films: Methods used to control regular nanostructures for electrochemical biosensing applications, Biosens. Bioelectron. 96 (2017) 17–25. doi:10.1016/j.bios.2017.04.036.

[29] F. Arduini, A. Amine, C. Majorani, F. Di Giorgio, D. De Felicis, F. Cataldo, D. Moscone, G. Palleschi, High performance electrochemical sensor based on modified screen-printed electrodes with cost-effective dispersion of nanostructured carbon black, Electrochem. Commun. 12 (2010) 346–350. doi:10.1016/j.elecom.2009.12.028.

[30] T.A. Silva, F.C. Moraes, B.C. Janegitz, O. Fatibello-Filho, Electrochemical Biosensors Based on Nanostructured Carbon Black: A Review, J. Nanomater. 2017 (2017) 1–14. doi:10.1155/2017/4571614.

[31] F. Della Pelle, M. Del Carlo, M. Sergi, D. Compagnone, A. Escarpa, Press-transferred carbon black nanoparticles on board of microfluidic chips for rapid and sensitive amperometric determination of phenyl carbamate pesticides in environmental samples, Microchim. Acta. 183 (2016) 3143–3149. doi:10.1007/s00604-016-1964-7.

[32] F. Arduini, S. Cinti, V. Scognamiglio, D. Moscone, Nanomaterials in electrochemical biosensors for pesticide detection: advances and challenges in food analysis, Microchim. Acta. 183 (2016) 2063–2083. doi:10.1007/s00604-016-1858-8.

[33] F. Della Pelle, C. Angelini, M. Sergi, M. Del, A. Pepe, D. Compagnone, M. Del Carlo, A. Pepe, D. Compagnone, Nano carbon black-based screen printed sensor for carbofuran, isoprocarb, carbaryl and fenobucarb detection: application to grain samples, Talanta. 186 (2018) 389–396. doi:10.1016/j.talanta.2018.04.082.

[34] S. Cinti, M. Basso, D. Moscone, F. Arduini, A paper-based nanomodified electrochemical biosensor for ethanol detection in beers, Anal. Chim. Acta. 960 (2017) 123–130. doi:10.1016/j.aca.2017.01.010.

[35] F. Della, R. Di, L. Vázquez, F.J. Palomares, M. Del, M. Sergi, D. Compagnone, A. Escarpa, Press-transferred carbon black nanoparticles for class-selective antioxidant electrochemical detection, Appl. Mater. Today. 9 (2017) 29–36. doi:10.1016/j.apmt.2017.04.012.

[36] F. Della Pelle, L. Vázquez, M. Del Carlo, M. Sergi, D. Compagnone, A. Escarpa, Press-Printed Conductive Carbon Black Nanoparticle Films for Molecular Detection at the Microscale, Chem. - A Eur. J. 22 (2016) 12761–12766. doi:10.1002/chem.201601743.

[37] F. Ricci, G. Palleschi, Sensor and biosensor preparation, optimisation and applications of Prussian Blue modified electrodes, Biosens. Bioelectron. 21 (2005) 389–407. doi:10.1016/j.bios.2004.12.001.

[38] J.J. García-Jareño, J. Navarro-Laboulais, F. Vicente, Electrochemical study of Nafion membranes/Prussian blue films on ITO electrodes, Electrochim. Acta. 41 (1996) 2675–2682. doi:10.1016/0013-4686(96)00121-1.

[39] A.A. Karyakin, E.A. Puganova, I.A. Budashov, I.N. Kurochkin, E.E. Karyakina, V.A. Levchenko, V.N. Matveyenko, S.D. Varfolomeyev, Prussian Blue Based Nanoelectrode Arrays for H 2 O 2 Detection, Anal. Chem. 76 (2004) 474–478. doi:10.1021/ac034859l.

[40] E. V. Karpova, E.E. Karyakina, A.A. Karyakin, Iron–nickel hexacyanoferrate bilayer as an advanced electrocatalyst for H 2 O 2 reduction, RSC Adv. 6 (2016) 103328–103331. doi:10.1039/C6RA24128J.

[41] S. Cinti, F. Arduini, G. Vellucci, I. Cacciotti, F. Nanni, D. Moscone, Carbon black assisted tailoring of Prussian Blue nanoparticles to tune sensitivity and detection limit towards H2O2 by using screen-printed electrode, Electrochem. Commun. 47 (2014) 63–66. doi:10.1016/J.ELECOM.2014.07.018.

[42] D. Blum, S. Torch, N. Lambeng, M.-F. Nissou, A.-L. Benabid, R. Sadoul, J.-M. Verna, Molecular pathways involved in the neurotoxicity of 6-OHDA, dopamine and MPTP: contribution to the apoptotic theory in Parkinson's disease, Prog. Neurobiol. 65 (2001) 135–172. doi:10.1016/S0301-0082(01)00003-X.

[43] K. Hanrott, L. Gudmunsen, M.J. O'Neill, S. Wonnacott, 6-Hydroxydopamine-induced Apoptosis Is Mediated via Extracellular Auto-oxidation and Caspase 3-dependent Activation of Protein Kinase Cδ, J. Biol. Chem. 281 (2006) 5373–5382. doi:10.1074/jbc.M511560200.

[44] R. Li, X. Liu, W. Qiu, M. Zhang, In Vivo Monitoring of H_2O_2 with Polydopamine and Prussian Blue-coated Microelectrode, Anal. Chem. 88 (2016) 7769–7776. doi:10.1021/acs.analchem.6b01765.

[45] T.S.T. Balamurugan, V. Mani, C.-C. Hsieh, S.-T. Huang, T.-K. Peng, H.-Y. Lin, Real-time tracking and quantification of endogenous hydrogen peroxide production in living cells using graphenated carbon nanotubes supported Prussian blue cubes, Sensors Actuators B Chem. 257 (2018) 220–227. doi:10.1016/J.SNB.2017.10.151.

[46] K.G. Nikolaev, V. Maybeck, E. Neumann, S.S. Ermakov, Y.E. Ermolenko, A. Offenhäusser, Y.G. Mourzina, Bimetallic nanowire sensors for extracellular electrochemical hydrogen peroxide detection in HL-1 cell culture, J. Solid State Electrochem. 22 (2018) 1023–1035. doi:10.1007/s10008-017-3829-3.

[47] Y. Sun, M. Luo, X. Meng, J. Xiang, L. Wang, Q. Ren, S. Guo, Graphene/Intermetallic PtPb Nanoplates Composites for Boosting Electrochemical Detection of H_2O_2 Released from Cells, Anal. Chem. 89 (2017) 3761–3767. doi:10.1021/acs.analchem.7b00248.

[48] M. Asif, W. Haitao, D. Shuang, A. Aziz, G. Zhang, F. Xiao, H. Liu, Metal oxide intercalated layered double hydroxide nanosphere: With enhanced electrocatalyic activity towards H2O2 for biological applications, Sensors Actuators B Chem. 239 (2017) 243–252. doi:10.1016/J.SNB.2016.08.010.

[49] Y. Fu, D. Huang, C. Li, L. Zou, B. Ye, Graphene blended with SnO2 and Pd-Pt nanocages for sensitive non-enzymatic electrochemical detection of H2O2 released from living cells, Anal. Chim. Acta. 1014 (2018) 10–18. doi:10.1016/J.ACA.2018.01.067.

[50] B. Ma, C. Kong, X. Hu, K. Liu, Q. Huang, J. Lv, W. Lu, X. Zhang, Z. Yang, S. Yang, A sensitive electrochemical nonenzymatic biosensor for the detection of H2O2 released from living cells based on ultrathin concave Ag nanosheets, Biosens. Bioelectron. 106 (2018) 29–36. doi:10.1016/J.BIOS.2018.01.041.

VIII. Oxidative Stress on-chip: Prussian blue-based electrode array for in situ detection of H_2O_2 from cell populations

VIII.1. Introduction and objectives

Redox homeostasis plays a key role in cell physiology, disruption of this status causes the so-called Oxidative Stress (OS). Investigations of responses linked to OS mechanism are fundamental for understanding physiological and pathological processes; in fact, OS has been related to several pathological conditions such as cancer, ischemia, atherosclerosis, Parkinson's and Alzheimer's disease [1–3]. Unraveling the complexity of the mechanisms of these pathologies represents an exciting area of research of cell biology. Despite classical biological investigations focused mainly on the determination of the protein-cascade initiated during oxidative stress, quantification, and kinetics of Reactive Oxygen Species (ROS) is also of high significance. Hence, appropriate analytical techniques able to perform the challenging task of in situ and real-time monitoring of the release of the short-lived ROS are required. Different approaches have been developed towards analytical miniaturization since these systems are able to place the transducers as close as possible to the production sites of ROS by cells.

Most of the classical methods are based on fluorescence, chemiluminescence, colorimetric assays, electron paramagnetic resonance (EPR) or electrochemistry [4]. Other approaches are based on the detection of oxidation products formed in the presence or ROS and RNS; however, this is not a direct measurement and makes real-time detection very challenging [5]. Luminescent and fluorescent probes are easy to use, able to cross cell membranes and the equipment required is usually readily available in biochemical labs, thus their use is widespread [6]. However, the specificity of these methods is still under discussion since most of the redox fluorescent molecules are able to react with different ROS. In addition, some molecules are able to form secondary species by redox cycling which can give artifacts or even toxic compounds [7]. EPR is recognized to be the most selective technique, however, the equipment is expensive and not user friendly; this hinders their use [8]. Electrochemical methods are easily suitable for ROS detection due to their different electroactivity and because the selectivity can be tuned by the selection of different electrode materials.

Moreover, electrochemistry stands out due to its inherent miniaturization, portability and low cost resulting very appropriate as detection system interfaced with

microsystems [9,10]. Moreover, the equipment needed is fully portable and straightforwardly coupled to the new technological advances in microelectronics in a cost-effective manner [11]. Usually, electrochemical analysis has been carried out in single cell analysis employing ultramicroelectrodes (UME). However, in this configuration, analysis of cell populations is tedious, time-consuming and requires specialized instrumentation [12]. On the other hand, the analysis of cell populations can give similar information for a whole population with simpler experimental setups and in a faster way.

Among ROS, H_2O_2 is considered a very powerful cytotoxic agent. The longer half-life compared with other ROS allows diffusion across the whole cell and extracellular space, with production of hydroxyl radical's through the Fenton Reaction (FR). Hydroxyl radicals are among the most powerful hydrogen acceptors, being able to damage cellular components.

Among the possible electrode materials that can selectively detect H_2O_2, Prussian Blue (PB) emerges as the most widely used electrocatalyst for non-enzymatic sensing. PB allows low potential and interference-free electrochemical reduction of H_2O_2 in oxygenated environment in contrast to metallic electrodes [13]. Metal-based electrodes (Pt, Au, Ag or Cu) suffer from interference from oxygen reduction and hence detects H_2O_2 by means of oxidation. In the latter case, the electrode suffers from the interferences of other electroactive species commonly found in biological media such as dopamine and ascorbic acid, among others. Hence, PB-based electrochemical sensors stand out as the best option for the electrochemical detection of H_2O_2 [14].

Most of the recently published devices able to culture and monitor ROS bursts from live cells have been fabricated using clean-room-based photolithographic fabrication methods [15–17]. While photolithography may still provide powerful research-scale solutions, in many clinical and biological applications the high-resolution obtained using photolithography are not needed and alternative low-cost fabrication methods are a real alternative [20]. The benefits of low-cost fabrication techniques (3D printing, laser cutting or xurography) and electrochemical detection create a powerful combination for the fabrication of ultra-low-cost disposable devices [21]. Alternative

methods for cell culturing have been recently reported by means of xurography and different laminated materials [22]. However, the incorporation of electrochemical sensor in this kind of devices remains unexplored.

In this work a PB-based array constituted by 8 electrodes is creatively used for cell culture and real time electrochemical hydrogen peroxide sensing. The concept of low-cost fabricated Prussian blue-based electrode array (PBEA) is exploited. The PBEA is composed by eight individual wells where cells can be directly cultured over the electrodes. The developed array was used for the detection of the hydrogen peroxide released from HeLa cells stimulated with N-formyl-L-methionyl-L-leucyl-L-phenylalanine (fMLP) and after endogenous pretreatment of the cells with cocoa polyphenols, that induced a decreased oxidative stress level.

VIII.2. Materials and methods

VIII.2.1. Materials and chemicals

Laminating pouches (Scotch, TP3854-100), self-adhesive vinyl (Arteza, ARTZ-8080), adhesive vinyl bumpers (Scotch, 3M), a thermal laminator (MATCC) were used for the fabrication and assembly of the chips. Prussian Blue-based Carbon (C2070424P2) and silver/silver chloride (C2130809D5) ink from Gwent Group were employed to fabricate the electrodes. A multi potentiostat/galvanostat µSTAT 8000 (DropSens, Oviedo, Spain), which incorporates "DropView 8400" software was employed for the electrochemical measurements.

Dulbecco's modified Eagle's medium (DMEM), Fetal Bovine Serum (FBS), penicillin/streptomycin, trypsin-EDTA, N-Formyl-L-methionyl-L-leucyl-L-phenylalanine (fMLP), Catalase from bovine liver (2,000–5,000 units/mg), Glucose, KCl, HCl, HEPES, $MgCl_2$, $NaHCO_3$, $CaCl_2$, H_2O_2 and DMSO were purchased from Sigma Aldrich.

A commercially available cocoa powder sample was employed, coming from Forastero cocoa beans subjected to an industrial fermentation, drying, and roasting process. Cocoa extracts were directly extracted in DMSO, according to [23]. Briefly, 0.1 g of cocoa powder were weighted and solubilized in 1.5 ml of DMSO. The dispersion was vortexed for 1 min and sonicated in an ultrasonic bath for 5 min at a temperature of 20 °C. Subsequently, the dispersion was centrifuged at 12,000 rpm for 5 min at a temperature of +4 °C for 10 min. The resulting supernatant was recovered and stored at –20 °C in the dark. Cocoa polyphenols concentration in the extract was determined using the Folin-Ciocalteau assay and expressed as gallic acid equivalents (GAE) [23]. The cocoa extract initial concentration was 47.6±0.2 g Kg^{-1} GAE. The extract was further conveniently diluted to the concentrations employed in the polyphenol treatment.

VIII.2.2. Electrode Microfabrication

Electrodes fabrication was based on the stencil-printing and thermal lamination of laminating pouches. Laminating pouches are PET (Polyethylene terephthalate) polymer films coated with EVA (Ethylene-vinyl acetate) thermo adhesive on one side

that allows the permanent bonding of the consisting layers upon heat and pressure applied through the rollers of a thermal laminator. Electrode design was sketched using AutoCAD 2018 (Autodesk, Student Version); a desktop cutting plotter (Silhouette Cameo 3, Silhouette) was used to cut. **Figure VIII-1** shows the schematics of the electrode design and fabrication.

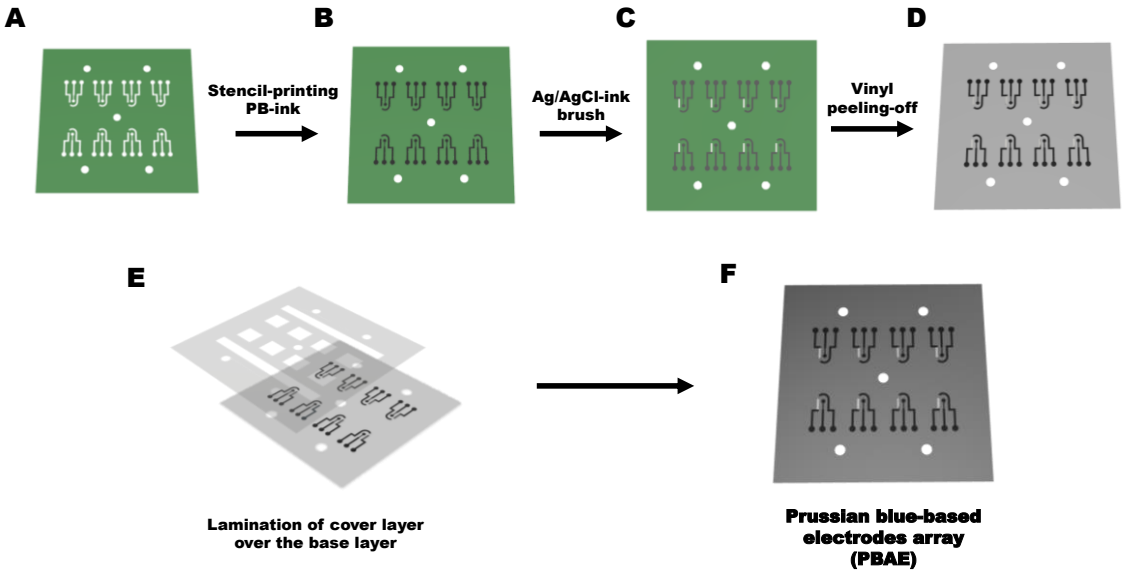

Figure VIII-1: Schematics of the fabrication process of the Prussian blue array-based electrodes (PBAE) electrochemical chips using benchtop equipment.

PBEA was constituted by two PET-EVA layers: a base layer, where the electrodes are patterned and a cover layer for electrical isolation. A stencil-printing approach was used for the fabrication of the electrodes. Briefly, a stencil with the electrode desired shape was cut in a self-adhesive vinyl sheet. This mask was then stuck onto the EVA-coated side of a laminating pouch (**Figure VIII-1A**). The PB-based ink was stencil-printed over the PET-EVA laminating pouch using a squeegee and it was cured for 30 minutes at 60°C (**Figure VIII-1B**). Then, the reference electrode was painted using silver/silver chloride ink and the whole set was allowed to cure for another 30 min (**Figure VIII-1C**).Finally, the vinyl stencil was peeled off obtaining the base layer (**Figure VIII-1D**). Then, the isolation layer is laminated for electrical isolation (**Figure VIII-1E**). The isolation layer is formed by PET-EVA cut using the desktop cutting machine. The design allows the electrochemical cell formation and the electrical contact for the connections. The assembled PBEA (**Figure VIII-1F**) is then placed

between two micromachined PMMA pieces that work as the holder and provide the electrical connections for the final device (see **Figure VIII-2A**). The PMMA (3 mm thick) holder is cut and holed using a bench saw and a milling bench. Holes of 8 mm diameter were milled for the well hole and 0.5 mm for the electrical contacts. For the electrical contacts, pogo pins (⌀=0.5mm, length = 16.35 mm) were used.

VIII.2.3. Cell Culture

HeLa cells were cultured in complete growth medium and incubated at 37ºC under 5% CO_2 atmosphere. Dulbecco's Modified Eagle's Medium (DMEM) was supplemented with 10% Fetal Bovine Serum (FBS) and 1% penicillin/streptomycin to make complete growth medium. Cells were routinely subcultured every 2-3 days at 70-80% cell confluence. They were detached using 0.05% trypsin-EDTA solution, centrifuged at 1000 rpm for 5 min and seeded on T75 flasks through 1:10 dilution. For the electrochemical experiments, confluent cells were harvested, centrifuged, and then homogenized in a certain volume to give a known concentration of suspended cells. Finally, 10 µL from the cell suspension was added to 190 µL of warm medium to give the final cell number in each well of the device. The prepared chips were placed inside the incubator (37ºC and 5% CO_2) for 12-16 h prior to electrochemical measurements to ensure cell adhesion. Before cell seeding, chips were washed with 70% ethanol-water solution and sterilized under UV light for 30 minutes.

VIII.2.4. Cytotoxicity determination of cocoa extracts

Non-toxic concentrations of cocoa extracts were determined using 3-(4,5-dimethylthiazol-2-yl)-2,5-diphenyltetrazolium bromide (MTT) cell viability assay. Cells were grown in 24-well plates at a density of 104 cells/well. After 24 h, the cells were washed with fresh medium and were treated with control medium or the medium supplemented with different concentrations of cocoa extracts. After incubation for 24 h, cells were rewashed, and 500 µL of MTT solution (1 mg/mL) was added and incubated for 4 h. Finally, 500 µL of DMSO was added to solubilize the formed formazan crystals, and the amount was determined by measuring the absorbance at 540 nm using a microplate reader. Cell viability was determined by the amount of MTT

converted into formazan crystal and quantified as a percentage compared to the control.

VIII.2.5. Electrochemical measurements on cell populations

Before electrochemical measurements, DMEM medium was replaced by Locke's buffer (pH=7.4, Glucose 5.6 mM, 154 mM NaCl, 5 mM KCl, 15 mM HEPES, 1.2 mM $MgCl_2$, 3.6 mM $NaHCO_3$ and 2.5 mM $CaCl_2$). Before cell stimulation the electrode was polarized at the working potential for 60 seconds to stabilize the background current. For the cocoa polyphenol treatment, cells were incubated for 24 h in DMEM supplemented with different GAE of cocoa polyphenols. After the treatment, the treatment media was removed and replaced by Locke's buffer. HeLa cells stimulation was triggered by the addition of 10 µL of the corresponding dilution of fMLP stock solution in Locke's buffer. The 10 mM stock solution of fMLP was prepared in DMSO and kept at -20ºC.

VIII.3. Results and Discussion

VIII.3.1. Design and electrochemical characterization of PB-based chips

The electrochemical device employed in this work is schematically presented in **Figure VIII-2**. **Figure VIII-2A** shows the exploded view of the components of the oxidative stress assessment device. The PB-based chip is composed of the PBEA and the PMMA holder including the electrochemical cell wells and the electrical connections. Interestingly, to increase the throughput several PBEA can be seeded with cells at the same time with no need of the chip holder during the incubation; PBEA can be later assembled on the holder on-demand before the electrochemical measurements. The hydrophobicity of the PET isolating layer allows to constrain cell-containing droplets right on top of the electrochemical cells of the flexible PBEA (see **Figure VIII-3A**). In this way, cells adhere in the very close vicinity of the working electrode. Photos of the device are reported in **Figure VIII-3**. This configuration allows detecting minute amounts of released molecules, since the local concentrations in the surroundings of the cells is higher compared to the bulk solution (see **Figure VIII-2B**, inset). In addition, this arrangement offers some advantages compared to the single-cell analysis usually carried out with ultramicroelectrodes (UME) as the electrochemical signals recorded represents the averaged responses for a cell population [18].

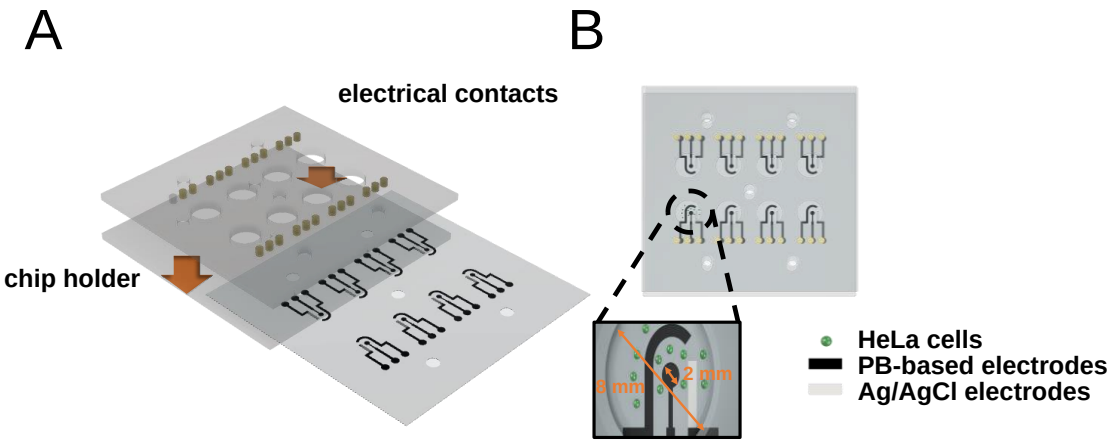

Figure VIII-2: A) Exploded view of the device showing all the components. B) Top view of the mounted device showing the PBAE containing the cell culture.

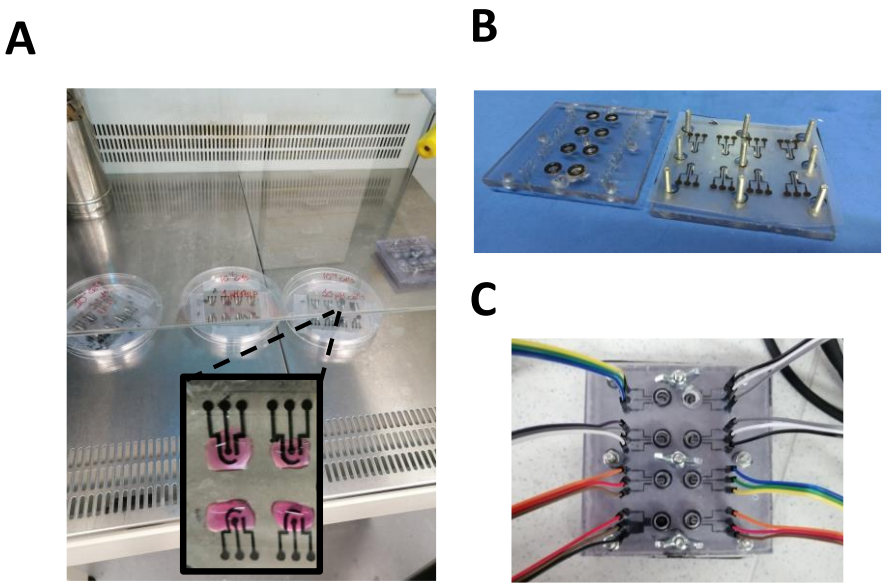

Figure VIII-3: A) Images of the electrochemical chips culturing HeLa cells before being placed on the chip holder. Inset: Zoom of the electrode wells showing the patterning of the cells over the electrochemical ells B) Electrochemical chips placed on the open holder C) Holder fully mounted and connected to potentiostat.

Electrochemical characterization of the developed electrodes was carried out by means of cyclic voltammetry (CV) and amperometry. CV of the obtained PB electrodes is presented in **Figure VIII-4A**. The voltammogram of the Prussian blue-based electrode arrays (PBEA) was characterized by two set of peaks. The first set of peaks corresponds to the conversion of Prussian Blue (PB) into Prussian White (PW). (**Eq.VIII.1**). The calculated half-wave potential $E_{1/2}$ of this set of peaks was ($E_{1/2}$ = ($E_{p,a}$+$E_{p,c}$)/2) +87±9 mV (n=8). This set of peaks is involved in the electrocatalytic reduction of hydrogen peroxide (**Eq.VIII.2**) as can be seen from the blue curve in **Figure VIII-4A**. The second set (**Eq.VIII.3**) is related to the oxidation of PB to Berlin Green (BG) with a $E_{1/2}$ of +0.770±12 mV (n=8). Additionally, PB quantity has been evaluated by integrating the oxidation peak of the PB/PW couple obtaining a charge of 3.4±0.3 µC (RSD=7%, (n=8)). This result indicates the high reproducibility of the fabrication method.

$$Fe_4^{III}[Fe^{II}(CN_6)_3] + 4e^- \leftrightarrow K_4Fe_4^{II}[Fe^{II}(CN_6)_3] \quad \textbf{Eq.VIII.1}$$

PB *PW*

$$H_2O_2 + 2e^- \rightarrow 2OH^- \quad \textbf{Eq.VIII.2}$$

$$Fe_4^{III}[Fe^{III}(CN_6)_3]A_3 + 3e^- \leftrightarrow Fe_4^{III}[Fe^{II}(CN_6)_3] + 3A^- \quad \textbf{Eq.VIII.3}$$

PB *BG*

CV was also performed at different scan rates ranging from 1 to 100 mV s^{-1}, where both the anodic and cathodic peak currents increased with the increase of the scan rate (**Figure VIII-5**). Peak currents varied with the square root of scan rate ($v^{1/2}$; **Figure VIII-4B)** , indicating a diffusion-controlled process due to the insertion and release process of cations in solution [25,26]. Good linearity was achieved (R^2>0.990) with regression equations of $I_{p,a}$ (µA) = (-2.8±0.7) + (6.1±0.1) [$v^{1/2}$] (mV s)$^{1/2}$ and $I_{p,c}$ (µA) = (-4±1) + (-6.4±0.1) [$v^{1/2}$] (mV s)$^{1/2}$ for the anodic and cathodic process, respectively.

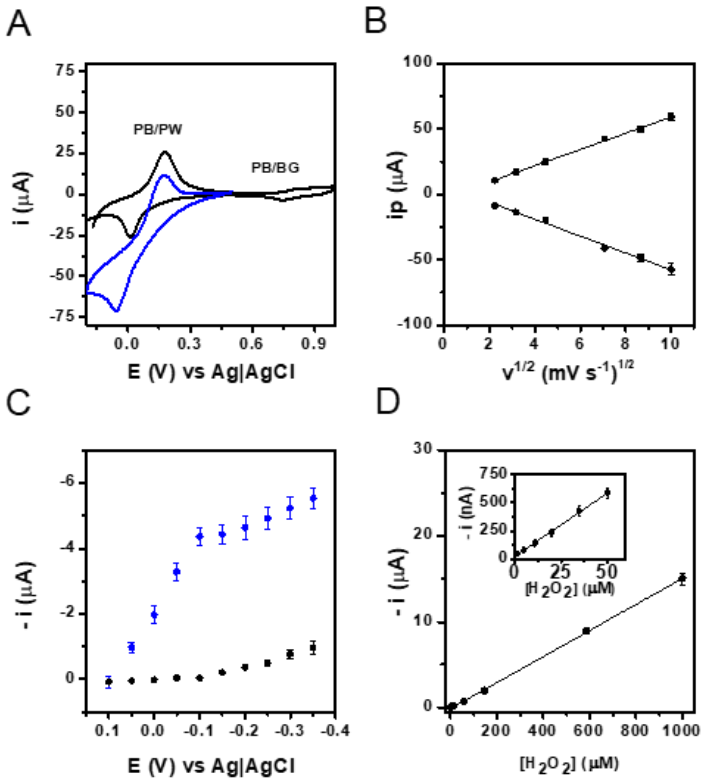

Figure VIII-4: A) Cyclic voltammogram obtained at 5 mV s^{-1} in HCl/KCl buffer (Black line) and in presence of 2.5 mM of H_2O_2 (Blue line). B) Plot of anodic and cathodic peaks extracted from the cyclic voltammograms at different scan rates. C) Amperometric response at different potentials in Locke's Buffer and in presence of 0.1 mM H_2O_2. D) Calibration plots obtained in Locke's Buffer for the whole linear range using amperometry at -0.1 V vs Ag|AgCl. Inset shows the calibration in the lower concentration range. Results are expressed as mean ± SD with n = 6.

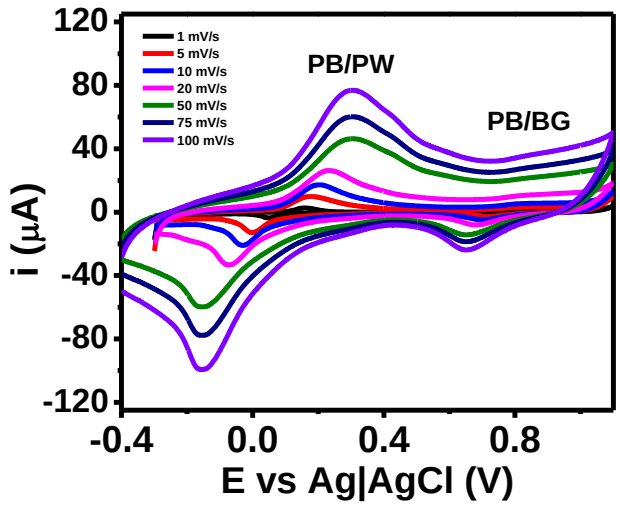

Figure VIII-5: Cyclic voltammograms of the developed chips carried out in 0.1 M HCl/KCl at scan rates from 1 to 100 mV s^{-1}.

In order to determine the optimal potential for the determination of H_2O_2 in the presence of oxygen, constant potential amperometry was carried out at different applied potentials ranging from +0.10 to -0.35 V vs Ag|AgCl. **Figure VIII-4C** reports current values at each potential for the buffer (black points) and a solution containing 0.1 mM of H_2O_2 (blue points). For the solution containing H_2O_2 the expected sigmoidal curve was obtained, with a limiting current -4.3±0.3 µA at -0.10 V. For subsequent experiments -0.1 V was chosen as the sensing potential. At around -0.20 V a second, voltammetric wave starts rising in both buffer and H_2O_2 solutions. This is ascribed to O_2 reduction. Thus, it can be clearly seen that H_2O_2 can be selectively detected in the presence of O_2 in contrast to metal-based electrodes. Calibration was carefully studied using amperometry at the optimum potential (-0.10 V) to determine the sensitivity, linearity, and limit of detection (LOD) towards H_2O_2. As shown in **Figure VIII-4D** the sensor exhibited good linearity (R^2=0.997) in the 5-1000 µM concentration range with a regression equation i (µA) = (-0.10±0.06) + (0.0152±0.0001) [H_2O_2] (µM). The sensitivity of the method was evaluated in the lower concentration interval of 5-50 µM i (µA) = (0.025±0.007) + (0.0112±0.0003) [H_2O_2] (µM) shown in the inset. The LOD was calculated as LOD=3σ/S where σ is the standard deviation of the intercept and S is the slope of the calibration plot. The calculated LOD was 1.9 µM. The obtained figure of merits is comparable to some reported in literature as shown in **Table VIII-1**. However, the main contribution of the developed PBEA is the easiness of fabrication with low-cost equipment but maintaining a well-enough performance. Operational stability of the sensor was also evaluated in a solution containing 0.1 mM of H_2O_2. As reported in **Figure VIII-6** the signal remained stable with at least 90% retained signal for 1 hour under operation in Locke's buffer demonstrating the high performance of the developed sensors.

Table VIII-1: Prussian Blue-based electrodes reported in literature fabricated by different approaches.

Electrode	LOD (µM)	Linear range (µM)	Fabrication method	Remarks	Ref
g-CNTs/PB MCs	0.013	0.025-1598	Drop casting	Application to cell culture	[1]
Graphene oxide/PB	0.8	5-1000	Dip coating	Application to cell culture	[2]
PBNPs	20	0.02–0.7	Inkjet printing	Easy fabrication	[3]
PBNPs (15 nm)-SPE	0.2	0.001–4.5	Inkjet printing	Easy fabrication Low-cost fabrication	[4]
Pad-printed carbon	0.41	0.41-200	PAD printing	Easy fabrication Application to cell culture	[5]
PBEA	**1.9**	**5-1000**	**Benchtop stencil printing**	**Easy fabrication Application to cell culture Multiplexed detection**	**This work**

g-CNTs/PB MCs: Prussian blue microcubes decorated graphenated carbon nanotubes. PBNPs: Prussian Blue nanoparticles. PBEA: Prussian blue-based electrode arrays.

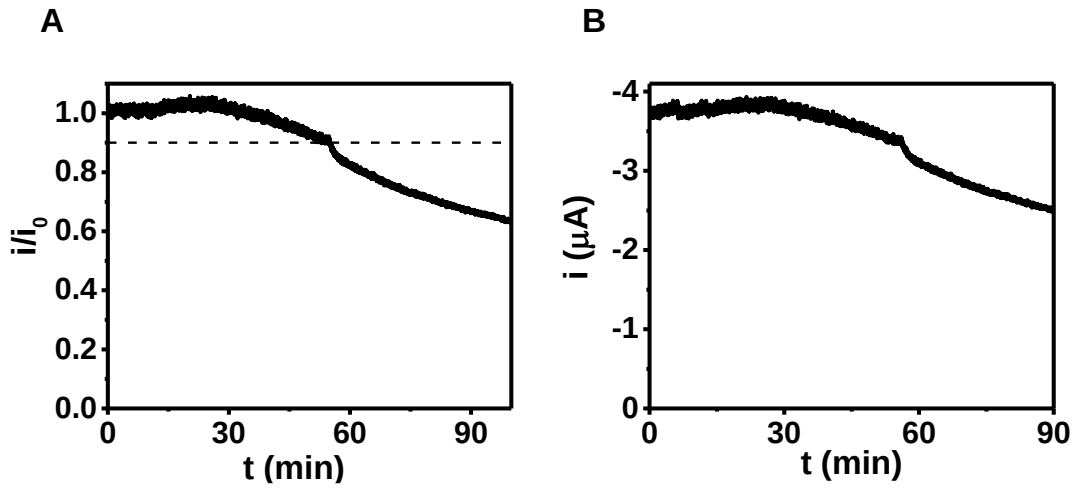

Figure VIII-6: Operational stability of the sensor performed in batch amperometry conditions in Locke's Buffer containing 0.1 mM H_2O_2 A) Signal normalized to initial signal. Dashed lines represent the 90% of the initial signal B) Raw signal expressed as current.

VIII.3.2. Real-time electrochemical detection of H_2O_2 released by HeLa cells

As above mentioned, the PBEA allows to measure simultaneously eight channels. A typical simultaneous measurement on the 8 electrodes PBEA is shown in **Figure VIII-7**, where the response of HeLa cells to different stimulation conditions was recorded. Cells were stimulated with 100µM fMLP in all channels except from 7, which was used as control well. When cells were stimulated with fMLP, an instantaneous increase in the electrochemical signal due to release of H_2O_2 by the cells (CH 1 to 6) occurred. As it can be seen no signal is obtained from the cells over the electrode without any stimulation (CH7). Furthermore, when catalase (CAT) was added in the well, no change in the signal was recorded either, since the H_2O_2 released by cells was consumed by CAT (CH 8). As an additional control, the response towards the addition of 100 µM of fMLP in well without cells was also recorded (see **Figure VIII-8A**). No signal is observed upon the addition of fMLP, confirming that no electrochemical signal is produced due to fMLP. As further selectivity control, CAT was added during H_2O_2 release revealing that as the CAT was added the signal switched-off (see **Figure VIII-8B**). These results clearly indicate the selectivity of the sensor towards H_2O_2.

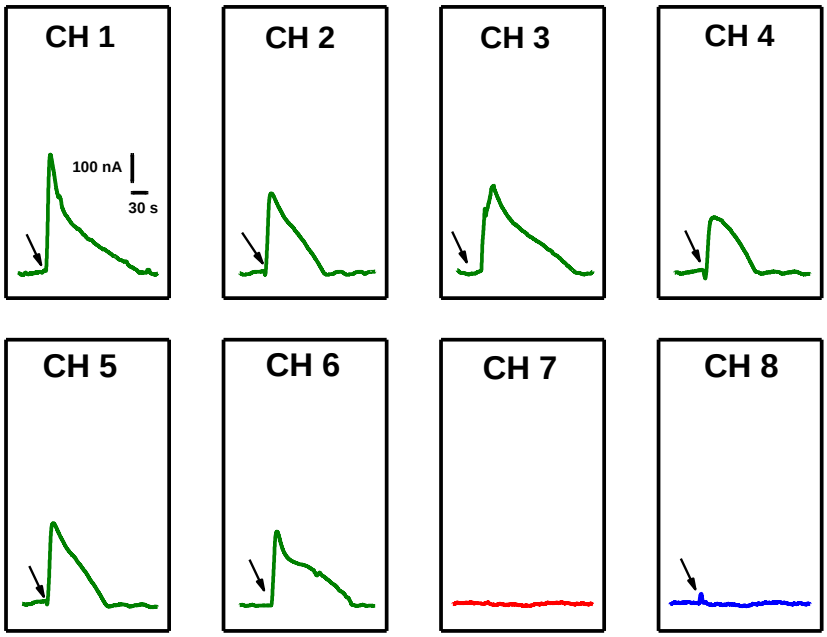

Figure VIII-7: Constant voltage amperometry simultaneous signals in the PBEA. CH 1 – 6 shows typical responses for oxidative stress responses. CH 7 shows the signal from non-stimulated HeLa cells. CH 8 shows the signal in presence of 0.1 mg mL^{-1} CAT. Arrows indicate the addition of 100 µM of fMLP. Each well contained 10^4 cells. Working potential (E=-100 mV vs Ag/AgCl). X and Y scales are shown in CH 1 and are maintained in the rest of the channels.

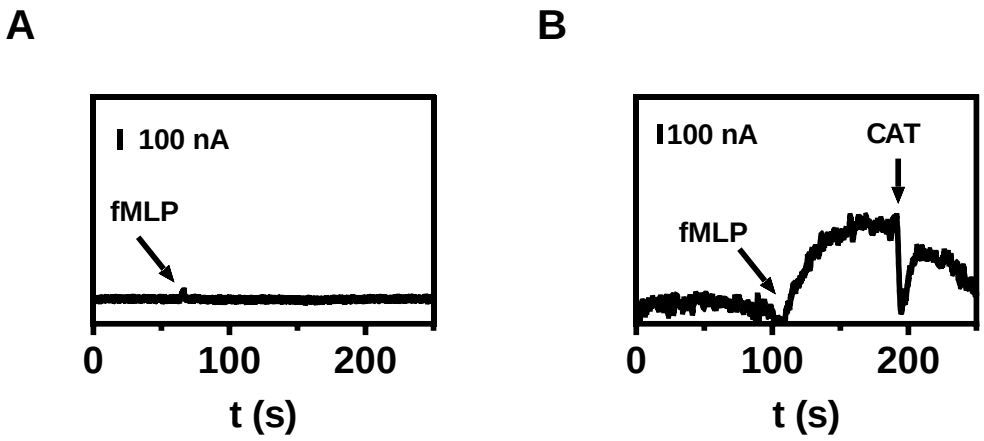

Figure VIII-8: Additional selectivity tests A) Addition of 1 µM of fMLP on the electrochemical cells without not containing HeLa cells B) Selectivity test over a raising signal of HeLa cells stimulated with 1 µM of fMLP arrows indicate the addition of 10 µL Catalase 0.1 mg/mL to the media.

To transform the obtained signals into quantitative results, the area under the obtained curve is integrated to calculate the charge ($\boldsymbol{Q_p}$). In this way we obtain the full information of the stimulation process rather than instantaneous concentrations on the electrode surface. $\boldsymbol{Q_p}$ is transformed in the molar quantities of H_2O_2 ($\boldsymbol{N_{H_2O_2}}$) employing Faraday's equation (**Eq.VIII.4**) considering that the reduction of H_2O_2 involves two electrons ($n=2e^-$) [27].

$$\boldsymbol{N_{H_2O_2} = \frac{Q_p}{nF}} \qquad \textbf{Eq.VIII.4}$$

The dependence of the charge recorded on the cell load from 10^3 to $2 \cdot 10^5$ cells per well is studied in **Figure VIII-9A**. An increase in the charge recorded on the electrode is observed with the increase in the cell number. According to these results, 10^4 cells per well were employed for subsequent experiments as a compromise between cell density and a significant electrochemical signal. Different concentrations of fMLP were also tested and the results are presented in Error! Reference source not found. **Figure VIII-9B**. Increasing concentrations of fMLP give increasing signals from the cells from 0.1 to 10 µM while from 10 to 100 µM no significant increase is observed. The obtained results follow a dose-response relationship with a maximum at 10 µM.

After demonstrating the ability of the PBEA to detect the H_2O_2 released by HeLa cell populations, the effect on food polyphenols on them was also evaluated. As proof of the concept HeLa cells were treated with different concentrations of cocoa extracts to study the protective role of these compounds in the oxidative stress process. Firstly, the cytotoxicity of the cocoa extracts has been evaluated using the MTT assay. As shown in **Figure VIII-10**, the cocoa extracts do not have cytotoxic effect in the range of 0.1 to 100 µg mL^{-1} GAE.

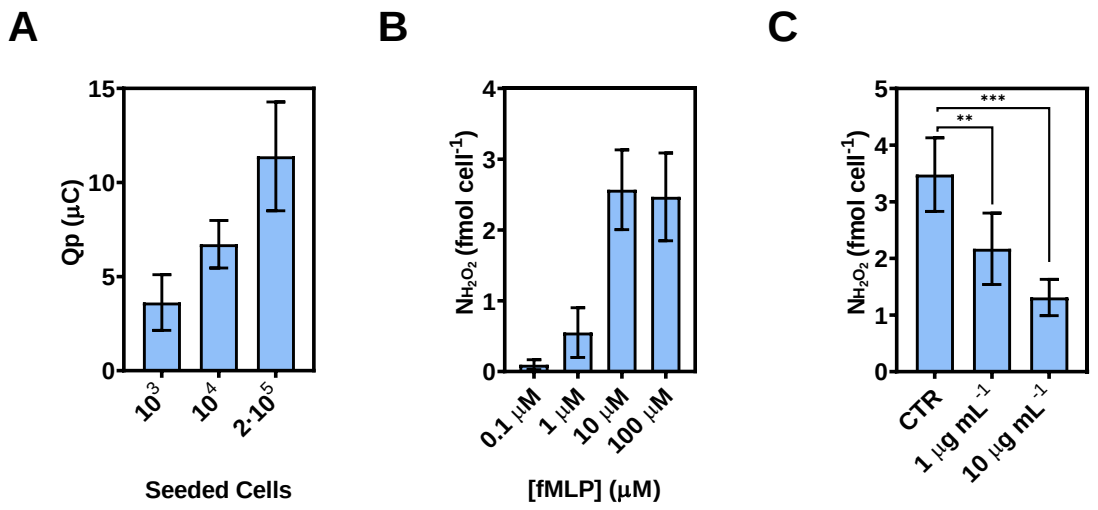

Figure VIII-9: A) Mean charge recorded with different number of cells seeded in the chip (n=6) B) Mean H_2O_2 production per cell for different concentrations of fMLP C) Comparison of H_2O_2 production for untreated and treated cells with different concentrations of cocoa extracts. Results are expressed as mean ± SD with n = 6. Significance of the difference between control and fMLP stimulated ** p<0.01, *** p<0.001.

Consequently, HeLa cells cultured over the electrode were treated for 24 h using 1 and 10 µg mL^{-1} of cocoa extracts. After treatment, the media containing the polyphenols was replaced and the electrochemical signal recorded. **Figure VIII-9C** shows the recorded signals for untreated cells (CTR) and cells treated using two levels of cocoa extract 1 and 10 µg mL^{1}. A significant decrease in the H_2O_2 production after the stress with the addition 10 µM of fMLP is observed for both the concentrations tested. Differences between means were compared using the Student's t-test for independent (unpaired) samples being statically significant different $p<0.01$ and $p<0.001$ for the 1 and 10 µg mL^{-1} , respectively, confirming the ability of the cocoa extracts to decrease the H_2O_2 production in dose-dependent way. These results were in agreement with previous studies where flavonoids, the main family of polyphenols present in cocoa extracts, were demonstrated to decrease the oxidative burst of mammalian cells which is usually due to an inhibition of the NADPH oxidase and myeloperoxidase [28]. Other works found in literature also demonstrated the ability of polyphenols to reduce the oxidative burst from immune cells employing fMLP and other stimulants able to trigger ROS production [29-31].

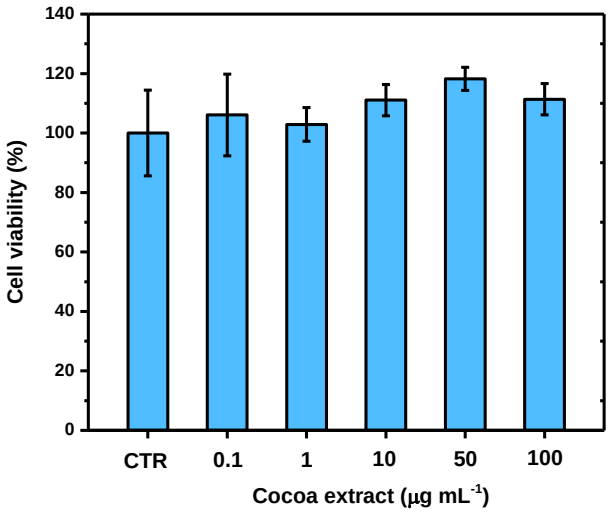

Figure VIII-10: Cytotoxicity of cocoa extracts for 24 h on HeLa cells assessed by the MTT assay. Cell viability was expressed as percentage of untreated control cells.

VIII.4. Conclusions

PBAE was successfully integrated into a multichambered chip for real-time detection of H_2O_2 released from live cells. The produced electrodes retained electrochemical properties of PB and exhibited a good analytical sensitivity (LOD=1.9 μM).

The electrochemical chip-containing array of 8 electrochemical sensors allowed high-throughput cell analysis, enabling to monitor the real-time release of H_2O_2 by HeLa cells in just 5 minutes with excellent selectivity. These results can pave the way for the high-throughput screenings of the oxidative stress state of cell populations upon chemical stress from target molecules and highlights the protective role of different compounds as food antioxidants using inexpensive miniaturized on-chip technologies.

VIII.5. References

[1] A.J. Kattoor, N.V.K. Pothineni, D. Palagiri, J.L. Mehta, Oxidative Stress in Atherosclerosis, Curr. Atheroscler. Rep. 19 (2017). doi:10.1007/s11883-017-0678-6.

[2] S.I. Liochev, Reactive oxygen species and the free radical theory of aging, Free Radic. Biol. Med. 60 (2013) 1–4. doi:10.1016/j.freeradbiomed.2013.02.011.

[3] H. Sies, C. Berndt, D.P. Jones, Oxidative Stress, Annu. Rev. Biochem. 86 (2017) 715–748. doi:10.1146/annurev-biochem-061516-045037.

[4] Y. Zhang, M. Dai, Z. Yuan, Methods for the detection of reactive oxygen species, Anal. Methods. 10 (2018) 4625–4638. doi:10.1039/c8ay01339j.

[5] A.-C. Ribou, Synthetic Sensors for Reactive Oxygen Species Detection and Quantification: A Critical Review of Current Methods, Antioxid. Redox Signal. 25 (2016) 520–533. doi:10.1089/ars.2016.6741.

[6] X. Jiao, Y. Li, J. Niu, X. Xie, X. Wang, B. Tang, Small-Molecule Fluorescent Probes for Imaging and Detection of Reactive Oxygen, Nitrogen, and Sulfur Species in Biological Systems, Anal. Chem. (2017) acs.analchem.7b04234. doi:10.1021/acs.analchem.7b04234.

[7] P. Wardman, Fluorescent and luminescent probes for measurement of oxidative and nitrosative species in cells and tissues: Progress, pitfalls, and prospects, Free Radic. Biol. Med. 43 (2007) 995–1022. doi:10.1016/j.freeradbiomed.2007.06.026.

[8] M. Kopáni, P. Celec, L. Danišovič, P. Michalka, C. Biró, Oxidative stress and electron spin resonance, Clin. Chim. Acta. 364 (2006) 61–66. doi:10.1016/J.CCA.2005.05.016.

[9] A. Rios, A. Escarpa, B. Simonet, Miniaturization of Analytical Systems: Principles, Designs and Applications, Wiley, 2009. doi:10.1002/9780470748091.

[10] D.G. Rackus, M.H. Shamsi, A.R. Wheeler, Electrochemistry, biosensors and microfluidics: a convergence of fields, Chem. Soc. Rev. 44 (2015) 5320–5340. doi:10.1039/c4cs00369a.

[11] A. Ainla, M.P.S. Mousavi, M.-N. Tsaloglou, J. Redston, J.G. Bell, M.T. Fernández-Abedul, G.M. Whitesides, Open-Source Potentiostat for Wireless Electrochemical Detection with Smartphones, Anal. Chem. 90 (2018) 6240–6246. doi:10.1021/acs.analchem.8b00850.

[12] M. Malferrari, M. Becconi, S. Rapino, Electrochemical monitoring of reactive oxygen/nitrogen species and redox balance in living cells, Anal. Bioanal. Chem. 411 (2019) 4365–4374. doi:10.1007/s00216-019-01734-0.

[13] D. Rojas, F. Della Pelle, M. Del Carlo, M. d'Angelo, R. Dominguez-Benot, A. Cimini, A. Escarpa, D. Compagnone, Electrodeposited Prussian Blue on carbon black modified disposable electrodes for direct enzyme-free H2O2 sensing in a Parkinson's disease in vitro model, Sensors Actuators B Chem. 275 (2018) 402–408. doi:10.1016/J.SNB.2018.08.040.

[14] A.A. Karyakin, Advances of Prussian blue and its analogues in (bio)sensors, Curr. Opin. Electrochem. (2017). doi:10.1016/j.coelec.2017.07.006.

[15] Y. Li, C. Sella, F. Lemaître, M. Guille-Collignon, C. Amatore, L. Thouin, Downstream Simultaneous Electrochemical Detection of Primary Reactive Oxygen and Nitrogen Species Released by Cell Populations in an Integrated Microfluidic Device, Anal. Chem. 90 (2018) 9386–9394. doi:10.1021/acs.analchem.8b02039.

[16] Z.-M. Lyu, X.-L. Zhou, X.-N. Wang, P. Li, L. Xu, E.-H. Liu, Miniaturized electrochemiluminescent biochip prepared on gold nanoparticles-loaded mesoporous silica film for visual detection of hydrogen peroxide released from living cells, Sensors Actuators B Chem. 284 (2019) 437–443. doi:10.1016/J.SNB.2018.12.149.

[17] S. V Sridharan, J.F. Rivera, J.K. Nolan, M.A. Alam, J.L. Rickus, D.B. Janes, On-chip microelectrode array and in situ transient calibration for measurement of

transient concentration gradients near surfaces of 2D cell cultures, Sensors Actuators, B Chem. 260 (2018) 519–528. doi:10.1016/j.snb.2017.12.194.

[18] Y. Li, A. Meunier, R. Fulcrand, C. Sella, C. Amatore, L. Thouin, F. Lemaître, M. Guille-Collignon, Multi-chambers Microsystem for Simultaneous and Direct Electrochemical Detection of Reactive Oxygen and Nitrogen Species Released by Cell Populations, Electroanalysis. 28 (2016) 1865–1872. doi:10.1002/elan.201501157.

[19] S. V. Sridharan, J.F. Rivera, J.K. Nolan, M.A. Alam, J.L. Rickus, D.B. Janes, On-chip microelectrode array and in situ transient calibration for measurement of transient concentration gradients near surfaces of 2D cell cultures, Sensors Actuators B Chem. 260 (2018) 519–528. doi:10.1016/J.SNB.2017.12.194.

[20] D.I. Walsh, D.S. Kong, S.K. Murthy, P.A. Carr, Enabling Microfluidics: from Clean Rooms to Makerspaces, Trends Biotechnol. 35 (2017) 383–392. doi:10.1016/j.tibtech.2017.01.001.

[21] J.F. Hernández-Rodríguez, D. Rojas, A. Escarpa, Rapid and cost-effective benchtop microfabrication of disposable carbon-based electrochemical microfluidic devices, Sensors Actuators B Chem. 324 (2020) 128679. doi:10.1016/j.snb.2020.128679.

[22] L.E. Stallcop, Y.R. Álvarez-García, A.M. Reyes-Ramos, K.P. Ramos-Cruz, M.M. Morgan, Y. Shi, L. Li, D.J. Beebe, M. Domenech, J.W. Warrick, Razor-printed sticker microdevices for cell-based applications, Lab Chip. 18 (2018) 451–462. doi:10.1039/c7lc00724h.

[23] F. Della Pelle, D. Rojas, A. Scroccarello, M. Del Carlo, G. Ferraro, C. Di Mattia, M. Martuscelli, A. Escarpa, D. Compagnone, High-performance carbon black/molybdenum disulfide nanohybrid sensor for cocoa catechins determination using an extraction-free approach, Sensors Actuators B Chem. 296 (2019) 126651. doi:10.1016/j.snb.2019.126651.

[24] A. Karyakin, E. Karyakina, L. Gorton, Prussian-Blue-based amperometric biosensors in flow-injection analysis, Talanta. 43 (1996) 1597–1606. doi:10.1016/0039-9140(96)01909-1.

[25] M.A. Malik, P.J. Kulesza, R. Marassi, F. Nobili, K. Miecznikowski, S. Zamponi, Countercation intercalation and kinetics of charge transport during redox reactions of nickel hexacyanoferrate, Electrochim. Acta. 49 (2004) 4253–4258. doi:10.1016/j.electacta.2004.04.021.

[26] A.A. Karyakin, E.A. Kuritsyna, E.E. Karyakina, V.L. Sukhanov, Diffusion controlled analytical performances of hydrogen peroxide sensors: Towards the sensor with the largest dynamic range, Electrochim. Acta. 54 (2009) 5048–5052. doi:10.1016/j.electacta.2008.11.049.

[27] A.A. Karyakin, E.E. Karyakina, L. Gorton, The electrocatalytic activity of Prussian blue in hydrogen peroxide reduction studied using a wall - jet electrode with continuous flow, J. Electroanal. Chem. 456 (1998) 97–104. doi:10.1016/S0022-0728(98)00202-2.

[28] E. Middleton, C. Kandaswami, T.C. Theoharides, The effects of plant flavonoids on mammalian cells: implications for inflammation, heart disease, and cancer., Pharmacol. Rev. 52 (2000) 673–751.

[29] P.J. Nowak, A. Zasowska-Nowak, P. Bialasiewicz, J. de Graft-Johnson, D. Nowak, M. Nowicki, Inhibitory effect of plant phenolics on fMLP-induced intracellular calcium rise and chemiluminescence of human polymorphonuclear leukocytes and their chemotactic activity *in vitro*, Pharm. Biol. 53 (2015) 1661–1670. doi:10.3109/13880209.2014.1001403.

[30] S. Suri, M.A. Taylor, A. Verity, S. Tribolo, P.W. Needs, P.A. Kroon, D.A. Hughes, V.G. Wilson, A comparative study of the effects of quercetin and its glucuronide and sulfate metabolites on human neutrophil function in vitro, Biochem. Pharmacol. 76 (2008) 645–653. doi:10.1016/j.bcp.2008.06.010.

[31] F. Ioannone, G. Sacchetti, M. Serafini, Effect of Dark Chocolate Extracts on Phorbol 12-Myristate 13-Acetate-Induced Oxidative Burst in Leukocytes Isolated by Normo-Weight and Overweight/Obese Subjects, Front. Nutr. 4 (2017) 23. doi:10.3389/fnut.2017.00023.

IX. General Conclusions

IX. General Conclusions

The main and transversal conclusion of this Doctoral Thesis is the demonstration of the potential of miniaturized nanomaterial-based electrochemistry in two sensing relevant applications: the potential of TMD in the analysis of relevant PPs in food samples together with the ability of PB-based sensors to detect and quantify oxidative stress in different cell lines. Hence, the main conclusions derived from this Doctoral Thesis are:

1. The incorporation of TMD to other nanomaterials in electrochemical sensor technology has been demonstrated to be highly relevant, resulting in a synergistic approach that combines the unique physical and chemical properties of TMD with the intrinsic benefits of carbon nanomaterials.

Even though the relatively low intrinsic conductivity and narrow electrochemical window of TMD, their hybridization with other nanomaterials has allowed improving their inherent properties. Two enhanced properties have been identified:

- Apparent electrocatalysis towards catechol-containing PPs.
- Impressive antifouling properties during the oxidation of the aforementioned catechol-containing PPs compounds.

These findings have also been demonstrated for the other compounds of the group VI TMDs; $MoSe_2$ and WSe_2. The mechanism underlying their antifouling properties has also been proposed for the first time.

2. PB-based sensors have demonstrated its potential in the evaluation of oxidative stress in cell lines. The incorporation of PB-based sensors in LoC devices have permitted the culturing of cells and direct *in-situ* evaluation of their oxidative stress status and the effect of food functional PPs on it.

- PB-based electrochemical sensors have enabled a reliable detection of oxidative stress (OS) in living cells towards hydrogen peroxide monitorization in two different cell cultures SH-SY5Y and HeLa.

- The sensors have been PB-based electrochemical sensors integrated in a LoC device have enabled the detection of the produced H_2O_2 in the culturing of HeLa cells. The device was able to effectively detect a decrease in the H_2O_2 production response of HeLa cells treated with cocoa extracts in a dose-dependent-way.

X. Annexes

X.1. List of Figures

X.2. List of Tables

X.3. List of Acronyms

6-OHDA: Hydroxydopamine

AA: Antioxidant activity

ABTS: 2,2'-azino-bis(3-ethylbenzothiazoline-6-sulfonic acid)

AuNPs: Gold nanoparticles

BDE: Boron doped electrode

BG: Berlin green

CB: Carbon black

CCF: Catechol containing flavonoids

CE: Counter electrode

CF: Caffeic acid

CM: p-coumaric acid

CNTs: Carbon nanotubes

CT: Catechin

CUPRAC: Cupric reducing antioxidant capacity

CV: Cyclic voltammetry

CVD: Chemical vapor deposition

DCFH: Diclorofluorescein

DCFH-DA: Diclorofluorescein diacetate

DPPH: 2,2-diphenyl-1-picrylhydrazyl

DPV: Differential pulse voltammetry

EDS: Energy-dispersive X-ray spectroscopy

EIS: Electrochemical impedance spectroscopy

EP: Epicatechin

EPG: Epigallocatechin

EVA: ethylene-vinyl acetate

EVOO: Extra virgin olive oil

FC: Folin Ciocalteau

FE-SEM: Field-emission scanning microscopy

fMLP: N-Formyl-L-methionyl-L-leucyl-L-phenylalanine

FR: Fenton reaction

FRAP: Ferric reducing antioxidant power

FT-IR: Fourier-transform infrared spectroscopy

GCE: Glassy carbon electrode

hCNs: Hydroxycinnamic acids

HER: Hydrogen evolution reaction

HET: Heterogeneous electron transfer rate

HYT: Hydroxytyrosol

LPE: Liquid phase exfoliation

LSV: Linear sweep voltammetry

MAO: Monoamine oxidase

MOF: Metallorganic framework

MTT: 3-(4,5-dimethylthiazol-2-yl)-2,5-diphenyltetrazolium bromide

MWCNTs: Multiwall carbon nanotubes

NIR: Near infrared spectroscopy

NM: Nanomaterial

OCP: Open circuit potential

OLEU: Oleuropein

ORAC: Oxygen radical absorbance capacity

OS: Oxidative stress

PB: Prussian blue

PBAE: Prussian blue array-based electrodes

PET: Polyethylene terephthalate

PMMA: Poly(methyl methacrylate)

PPs: Polyphenols

PW: Prussian white

RCF: Relative centrifugal force

RE: Reference electrode

RNS: Reactive nitrogen species

ROS: Reactive oxygen species

SEM: Scanning electron microscopy

SOD: Superoxide dismutase

SP: Sinapic acid

SPE: Screen-printed electrode

SWV: Square wave voltammetry

TMDs: Transition metal dichalcogenides

tRGO: Thermally reduced graphene oxide

UME: Ultramicroelectrode

WE: Working electrode

X.4. Dissemination activities

X.4.1. List of publications

1. **D. Rojas**, F. Della Pelle, M. Del Carlo, M. d'Angelo, R. Dominguez-Benot, A. Cimini, A. Escarpa, D. Compagnone, Electrodeposited Prussian Blue on carbon black modified disposable electrodes for direct enzyme-free H_2O_2 sensing in a Parkinson's disease in vitro model, Sensors Actuators B Chem. 275 (2018) 402–408. doi:10.1016/J.SNB.2018.08.040.
2. **D. Rojas**, F. Della Pelle, M. Del Carlo, E. Fratini, A. Escarpa, D. Compagnone, Nanohybrid carbon black-molybdenum disulfide transducers for preconcentration-free voltammetric detection of the olive oil o-diphenols hydroxytyrosol and oleuropein, Microchim. Acta. 186 (2019) 363. doi:10.1007/s00604-019-3418-5.
3. F. Della Pelle, **D. Rojas**, A. Scroccarello, M. Del Carlo, G. Ferraro, C. Di Mattia, M. Martuscelli, A. Escarpa, D. Compagnone, High-performance carbon black/molybdenum disulfide nanohybrid sensor for cocoa catechins determination using an extraction-free approach, Sensors Actuators B Chem. 296 (2019) 126651. doi:10.1016/j.snb.2019.126651.
4. **D. Rojas**, F. Della Pelle, M. Del Carlo, D. Compagnone, A. Escarpa, Group VI transition metal dichalcogenides as antifouling transducers for electrochemical oxidation of catechol-containing structures, Electrochem. Commun. 115 (2020) 106718. doi:10.1016/j.elecom.2020.106718.
5. F. Della Pelle, **D. Rojas**, F. Silveri, G. Ferraro, E. Fratini, A. Scroccarello, A. Escarpa, D. Compagnone, Class-selective voltammetric determination of hydroxycinnamic acids structural analogs using a WS_2/catechin-capped AuNPs/carbon black–based nanocomposite sensor, Microchim. Acta. 187 (2020) 296. doi:10.1007/s00604-020-04281-z.
6. **D. Rojas**, J.F. Hernández-Rodríguez, F. Della Pelle, M. del Carlo, D. Compagnone, A. Escarpa. Oxidative Stress on-chip: Prussian blue-based electrode array for in situ detection of H_2O_2 from cell populations, Biosensors and Bioelectronics. (In press)

X.4.2. Oral communications

1. 4º Convegno Nazionale di Sensori (CNS), **Daniel Rojas***, Flavio Della Pelle, Michele Del Carlo, Dario Compagnone, "*Nanostructured screen-printed electrodes for hydrogen peroxide sensing in cell cultures"*, Catania (Italy), 21-23/02/2018. *National.*

2. XXVII Congresso Nazionale della Divisione di Chimica Analitica, **Daniel Rojas***, Flavio Della Pelle, Michele Del Carlo, Dario Compagnone, *"Carbon Black -MoS_2 nanocomposite as novel screen-printed electrodes modifier"*, Bologna (Italy), 16-20/09/2018. *National.*

3. IX International Congress on Analytical Nanoscience and Nanotechnology (NyNA), **Daniel Rojas***, Flavio Della Pelle, Michele Del Carlo, Dario Compagnone, *"Carbon black-molybdenum disulfide nanohybrids as electrochemical transducers",* Zaragoza (Spain), 2-7/07/2019. *International.*

4. XXVIII Congresso Nazionale della Divisione di Chimica Analitica, Flavio Della Pelle*, **Daniel Rojas**, Michele Del Carlo, Mattia Diodato, Alberto Escarpa, Dario Compagnone, "*Nanomaterial-based sensors and food polyphenols: An analytical challenge and a source of useful electrochemical compounds",* Bari (Italy), 22-26/09/2019. *National.*

5. 25th Latin-American Symposium on Biotechnology, Biomedical, Biopharmaceutical, and Industrial Applications of Capillary Electrophoresis and Microchip Technology, Flavio Della Pelle*, **Daniel Rojas**, Michele Del Carlo, Luis Vázquez, Dario Compagnone, Alberto Escarpa, "*Carbon Black based electrochemical transducers for microfluidic detection",* Alcalá de Henares (Spain), 29/09/2019-02/10/2019. *International.*

6. 9th International workshop on biosensors, Dario Compagnone*, Flavio Della Pelle, **Daniel Rojas**, Michele Del Carlo, Alberto Escarpa, "*Transition metal dichalcogenides based nanohybrid sensors as useful devices in food polyphenols analysis"*, Erfoud (Morocco), 9-11/10/2019. *International.*

* Indicate speaker.

X.4.3. Poster presentations

1. 25th Latin-American Symposium on Biotechnology, Biomedical, Biopharmaceutical, and Industrial Applications of Capillary Electrophoresis and Microchip Technology, Juan F. Hernández-Rodríguez, **Daniel Rojas**, Alberto Escarpa, "*Low-cost and accessible rapid-prototyping of microfluidic devices",* Alcalá de Henares (Spain), September 2019. *International.*

2. SelectBio conference - Lab-on-a-chip, microfluidics, organ-on-a-chip, point-of-care diagnostics conference*,* **Daniel Rojas**, Juan F. Hernández-Rodríguez, Flavio Della Pelle, Michele Del Carlo, Alberto Escarpa, Dario Compagnone, *"Microfluidic devices for cell culturing and electrochemical sensing of hydrogen peroxide and nitrite",* Rotterdam (Netherlands), June 2019. *International.*

3. 2nd European Biosensor Symposium (EBS), *"Nanomaterial-based electrochemical sensing strategies for cell lines oxidative stress evaluation and for bio-compounds detection in food"* **Daniel Rojas**, Flavio Della Pelle, Michele Del Carlo, Alberto Escarpa, Dario Compagnone, Florence (Italy), February 2019. *International.*

4. XXVII Congresso Divisione di Chimica Analitica, **Daniel Rojas**, Flavio Della Pelle, Michele Del Carlo, Dario Compagnone, *"Electrodeposited Prussian Blue on carbon black modified disposable electrodes for direct enzyme-free H_2O_2 sensing in a Parkinson's disease model",* Bologna (Italy), September 2018. National.

5. 64th Congress of the Italian Embryological Group (GEI) **Daniel Rojas**, Flavio Della Pelle, Michele Del Carlo, Dario Compagnone, *"Disposable electrodes for direct enzyme-free H_2O_2 sensing in a Parkinson's disease in-vitro model",* L'Aquila (Italy), June 2018. *National.*

6. Annual meeting of cellular and molecular biotechnologies doctoral programmes, **Daniel Rojas**, *"Novel nanomaterials for lab on a chip devices development: application to environmental stressors in food system and their effect on the oxidative stress in select cell"*, L'Aquila (Italy), February 2018. *National*